Massive corrections in scattering amplitudes at higher orders for LHC phenomenology

Federico Coro

Thesis submitted for the Degree of Doctor in Physics

Director: Leandro Javier Cieri

Departament de Física Teòrica

IFIC, Universitat de València

Programa de Doctorat en Física - 3126

València, Noviembre, 2024

Title:
Massive corrections in scattering amplitudes at higher orders for LHC phenomenology

Author:
Federico Coro
Department de Física Teòrica
Instituto de Física Corpuscular (IFIC)
Universitat de València, Spain

Supervisor:
Leandro Javier Cieri
Department de Física Teòrica
Instituto de Física Corpuscular (IFIC)
Universitat de València, Spain

This thesis has been typeset by LaTeX and the Sapthesis class.

Prof. Leandro Javier CIERI, Contratado Investigador Distinguido (CIDEGENT),

CERTIFICA,

Que la presente memoria, titulada ”**Massive corrections in scattering amplitudes at higher orders for LHC phenomenology**”, corresponde al trabajo realizado bajo su dirección por **Federico Coro**, para su presentación como Tesis Doctoral en el Programa de Doctorado en Física de la Universitat de València.

Y para que conste firma el presente certificado en Paterna, el 7 de Noviembre de 2024.

Leandro Javier Cieri

Las firmas están en el archivo de la Escuela de Doctorat.

Abstract

In this PhD thesis we discuss, within the framework of the Standard Model (SM) of particle physics, the scattering amplitudes relevant for phenomenology at the Large Hadron Collider (LHC). Scattering amplitudes are an essential element for the comparison of theoretical predictions with experimental data. The amplitudes are calculated by a perturbative expansion of the couplings that define the nature of the interaction. The precision achieved with the new LHC runs allows the measurement of physical observables at the $\mathcal{O}(\%)$ threshold. To obtain a theoretical comparison, it is therefore necessary to calculate higher-order corrections in the perturbative expansion. This is important for two reasons: to check the parameters of the SM and to search for deviations between theoretical predictions and experimental data in the search for new physics.

The general structure of the amplitude is studied in detail, breaking down the different contributions that arise from Feynman integrals, which graphically represent the various orders contributing to the scattering process. Particular emphasis is placed on the methods currently used for a complete calculation of the partonic cross sections. In particular, a detailed study is conducted on the calculation of scalar integrals for multi-loop and multi-leg processes. The study of integrals is crucial, as a fast numerical evaluation in phase space is necessary to carry out a phenomenological analysis. Furthermore, it is possible to study the function space that defines the Feynman integrals. These functions, which can be more or less complex depending on the process, establish a connection with different active research fields in mathematics. Especially when masses are involved, the mathematical structures required to reach an analytical form of the amplitude become very intricate.

The methods described are used to compute massive corrections for different processes relevant to the LHC. The first process to be studied is the production of two photons in the quark-annihilation channel $q\bar{q} \to \gamma\gamma$ in perturbative quantum chromodynamics (QCD). This work subsequently led to a phenomenological study of the production of two photons, including for the first time the massive corrections, given by the top quark, up to the next-to-next-to leading order (NNLO) in QCD. The work in this way includes a complete amplitude calculation, from the construction of the form factors to their phenomenological use. For the first part, the canonical basis of the master integrals (MIs) is written, except for some of the non-planar topology for which a maximal cut study is carried out. Furthermore, the contribution of real emission corrections is included to make a complete study with all the massive corrections up to NNLO.

Massive corrections for diphoton production have been studied at two-loop level, also in the gluon-fusion channel $gg \to \gamma\gamma$. In this case, a detailed analysis of the geometry associated with the integrals is carried out. In this way, an epsilon-factorized form is reached for the system of differential equations satisfied by the MIs. The MIs are expressed in terms of iterated integrals, thereby revealing the significant simplifications this brings both at the amplitude level and for the integrals themselves.

Acknowledgments

During this challenging journey, which has lasted almost three years, there are many people who deserve to be thanked. First and foremost, I would like to thank my advisor, Leandro Cieri, for believing in me and in the project from the very beginning. Despite the difficulties, he has always tried to instill a sense of calm and to help me understand that everything would be okay. A special thanks goes to Roberto Bonciani, as he has been a constant presence from my Master's thesis through to the completion of this PhD, through ongoing work and continuous conversations. Equally important, I thank Matteo Becchetti for his continuous support and for helping me understand what I truly want to pursue in physics. Leandro, Roberto, and Matteo have been essential figures far beyond the purely academic level.

Furthermore, for sharing work, conference rooms, and hours upon hours of work discussions with me for nearly four years now, I thank Federico Ripani.

I would like to express my gratitude to my collaborators Lorenzo Tancredi, Christoph Nega, and Fabian J. Wagner. Working with them has greatly enriched my knowledge, and thanks to their enthusiasm, a wonderful collaboration was established.

I would like to thank Donato Bini for being the first to inspire my passion for physics and mathematics, as well as for the stimulating discussions that continue to this day.

I would like to thank those who started out as colleagues and have now become true friends, Simone and Guido. The years spent with them have been an essential time in my life, a chapter I will always look back on with affection. Simone continues to be a constant presence, an endless source of memes and trashy songs; his notes on the Compton effect remain the best I've ever seen, almost as iconic as the font for his PhD thesis. Guido may only reach out through memes, but the power of friendship that binds us is too strong.

I want to thank Colomba Brancaccio because, even though we've known each other for a short time, there was an immediate connection both in work and in friendship.

I would like to thank Giada for all the unforgettable moments we spent together and for her constant care toward me. She can truly be called a good friend.

I would like to thank Davide and Fabricio for making my days in Valencia more carefree, being a constant source of support for me.

I would like to thank Emanuela, Lorenzo, Andrea, Baibhab, and Juliana for sharing this PhD journey at IFIC with me and for undoubtedly enhancing my experience there.

My most important acknowledgment goes to my family. Their presence has been essential at every step of my journey. My parents, Anna Rita and Alfredo, have always done everything possible to support me and make me feel well, despite my personality. I know that dealing with me is sometimes challenging. My grandparents, Giulia and Ugo, have always supported every choice I made, taking on the roles of second parents without ever asking for anything in return. From them, I learned that sometimes you shouldn't take life too seriously. My brother Francesco has been fundamental to me for as long as I can remember. Words alone cannot express the gratitude I feel for him and my family. The only place I can truly call home is wherever they are.

This PhD thesis was supported by Generalitat Valenciana GenT Excellence Programme (CIDEGENT/2020/011) and ILINK22045.

List of Publications

This PhD thesis is based on the following publications:

Papers

- [1] M. Becchetti, R. Bonciani, L. Cieri, F. Coro, F. Ripani, *Full top-quark mass dependence in diphoton production at NNLO in QCD*, Phys. Lett. B 848 (2024) 138362, arXiv:2308.10885,
- [2] M. Becchetti, R. Bonciani, L. Cieri, F. Coro, F. Ripani, *Two-loop form factors for diphoton production in quark annihilation channel with heavy quark mass dependence*, JHEP 12 (2023) 105, arXiv:2308.11412,
- M. Becchetti, F. Coro, C. Nega, L. Tancredi, F.J. Wagner, *Analytic two-loop amplitudes for $q\bar{q} \to \gamma\gamma$ and $gg \to \gamma\gamma$ mediated by a heavy-quark loop*, to appear on arXiv soon,

Proceedings

- [3] F. Coro, *Full NNLO QCD corrections to diphoton production*, PoS EPS-HEP2023 (2024) 263, arXiv:2310.10458,
- [4] F. Coro, *Photon pair production: full NNLO corrections in QCD with heavy quark mass dependence*, PoS LL2024 (2024) 041.

Contents

List of Abbreviations xiv

List of Figures xv

List of Tables xviii

1 Introduction 1

2 Advanced computational methods for scattering amplitudes in the Standard Model 6

2.1 Scattering amplitudes . . . 6
2.1.1 Dimensional regularization . . . 8
2.2 Structure of scattering amplitudes . . . 9
2.2.1 Colour structure . . . 9
2.2.2 Lorentz tensor structure . . . 10
2.3 Tensor decomposition . . . 10
2.4 Spinor-helicity formalism . . . 12
2.5 Multi-loop multi-leg Feynman integrals . . . 17
2.6 Integration-by-part identities . . . 19
2.7 Lorentz invariance identities . . . 22
2.8 Laporta algorithm . . . 23
2.9 Differential equations method for Feynman integrals . . . 24
2.10 ϵ-factorised form . . . 26
2.11 Multiple polylogarithms . . . 29
2.11.1 MPLs and pure functions . . . 31
2.12 Canonical logarithmic form . . . 32
2.13 Integration kernels and geometry - MPLs case . . . 32
2.14 Elliptic curves . . . 34
2.15 Elliptic multiple polylogarithms . . . 40
2.16 ϵ-factorised differential equations beyond MPLs . . . 41
2.16.1 ϵ-factorised form for the elliptic triangle . . . 42
2.17 Cuts of Feynman integrals . . . 46
2.18 Baikov representation . . . 49
2.19 Maximal cut . . . 52
2.19.1 Maximal cut of one-loop bubble diagram . . . 54
2.19.2 Maximal cut of the sunrise integral . . . 56
2.20 Generalised power series expansion . . . 60
2.20.1 Generalise power series - ϵ-factorised form and coupled sectors . . . 63

3 Universality of transverse-momentum cross sections and hard factors 66
3.1 The transverse momentum subtraction method . . . 66
3.2 Transverse momentum resummation . . . 69
3.2.1 The resummed component . . . 71
3.3 The fixed order expansion . . . 73
3.4 Hard-virtual coefficients and their universal structure . . . 77
3.4.1 Preliminary considerations and notation . . . 77
3.4.2 Hard-virtual amplitude and subtraction operators . . . 78

4 Two-loop form factors for diphoton production in quark annihilation channel with heavy quark mass dependence 81
4.1 Amplitude structure . . . 82
4.2 Scalar integral families and MIs computation . . . 84
4.2.1 MIs . . . 87
4.3 renormalisation . . . 88
4.3.1 Hard-virtual function . . . 89
4.4 DEs & canonical basis . . . 90
4.4.1 Planar family PLA . . . 90
4.4.2 Planar family PLB . . . 91
4.4.3 Non-planar family NPL . . . 92
4.4.4 Maximal Cut . . . 94
4.5 Semi-Analytic solution with Generalised power series . . . 97

5 Analytic evaluation of the helicity amplitudes for diphoton production in gluon fusion with heavy quark mass dependence 102
5.1 Analytic scattering amplitude for $gg \to \gamma\gamma$ . . . 102
5.1.1 Scalar integral families and MIs computation . . . 105
5.2 DEs and evaluation in terms of iterated integrals . . . 108
5.2.1 Alphabet for the system of DEs . . . 110
5.2.2 Boundary conditions . . . 111
5.2.3 Iterated integrals . . . 111
5.2.4 UV renormalisation . . . 112
5.2.5 IR subtraction . . . 113
5.3 Helicity amplitudes in terms of iterated integrals . . . 113

6 Diphoton production at the LHC 115
6.1 Standard isolation criterion . . . 116
6.2 Frixione isolation criterion . . . 117
6.3 Phenomenological setup . . . 118
6.4 Massive contributions to the NNLO cross section . . . 119
6.5 Full NNLO results with top quark mass dependence . . . 120
6.5.1 Two-loop contribution and comparison with the one-loop box . . . 120
6.5.2 Massive Double-Real corrections . . . 122
6.5.3 Massive Real-Virtual corrections . . . 122
6.5.4 NNLO invariant mass distribution with full top quark mass dependence 123
6.5.5 Ratios of each massive contributions . . . 125

7 Conclusions and outlooks 126

8 Resumen de la tesis **128**
8.1 Introducción . . . 128
8.2 Objetivos Alcanzados . . . 129
8.3 Metodología . . . 130
8.3.1 Amplitudes y correcciones de orden superior. . . . 130
8.3.2 Estructuras de Lorentz tensoriales . . . 131
8.3.3 Integrales de Feynman de múltiples bucles y múltiples patas . . . 131
8.3.4 Reducción integral . . . 132
8.3.5 Método de ecuaciones diferenciales . . . 133
8.3.6 Núcleos de integración y geometría . . . 133
8.3.7 Forma factorizada en ϵ más allá de los MPLs . . . 135
8.3.8 Corte máximo . . . 136
8.3.9 Expansión en serie de potencias generalizada . . . 136
8.3.10 Método de sustracción en momento transverso y resumación . . . 137
8.4 Resultados y conclusiones . . . 137
8.4.1 Factores de forma masivos a dos bucles para $q\bar{q} \to \gamma\gamma$ . . . 137
8.4.2 Evaluación analítica de las amplitudes de helicidad masivas a dos bucles para $gg \to \gamma\gamma$ . . . 139
8.4.3 Dependencia completa de la masa del quark top en la producción de dos fotones a NNLO en QCD . . . 140

A One-forms and wedge product **143**

B MIs for $q\bar{q} \to \gamma\gamma$ **145**
B.1 MIs . . . 145
B.2 Crossings . . . 146

C Canonical MIs for $q\bar{q} \to \gamma\gamma$ **147**
C.1 PLA canonical MIs . . . 147
C.2 NPL canonical MIs . . . 148

D RV - RR contributions to diphoton production **150**
D.0.1 Real-Virtual contributions to diphoton production . . . 150
D.0.2 Double-Real contributions to diphoton production . . . 151

E MIs for $gg \to \gamma\gamma$ **153**

F Letters **157**
F.1 Algebraic letters . . . 157
F.2 Rational letters . . . 159
F.3 Modular letters . . . 159
F.4 Elliptic letters . . . 160

List of Abbreviations

Definition	Abbreviation
Standard Model	SM
Quantum Field Theory	QFT
Quantum Electrodynamics	QED
Quantum Chromodynamics	QCD
Dimensional Regularization	DR
't Hooft-Veltman scheme	tHV
Leading Order	LO
Next-To-Leading Order	NLO
Next-To-Next-To-Leading Order	NNLO
Leading Logarithmic	LL
Next-To-Leading Logarithmic	NLL
Next-To-Next-To-Leading Logarithmic	NNLL
Ultraviolet	UV
Infrared	IR
Integration-By-Parts Identities	IBPs
Lorentz Invariance Identities	LIs
Irreducible Scalar Products	ISPs
Master Integrals	MIs
Differential Equations	DEs
Multiple Polylogarithms	MPLs
Elliptic Multiple Polylogarithms	eMPLs
Uniformal Transcendental Weight	UT
Counter-Terms	CT
Effective Field Theory	EFT
Kinoshita-Lee-Nauenberg (theorem)	KLN
Dokshitzer-Gribov-Lipatov-Altarelli-Parisi (equation)	DGLAP
Double-Virtual (contribution)	DV
Real-Virtual (contribution)	RV
Double-Real (contribution)	RR
Beyond The Standard Model	BSM
Common Dimensional Regularisation	CDR

List of Figures

2.4.1 Number of terms in the different steps of the amplitude and cross section computation. . . . 12

2.5.2 Graph defined in terms of vertices, internal and external edges. 18

2.10.3 Three curves γ_1 (blue), γ_2 (red) and γ_3 (green) connecting the point $\underline{x}_0$, in which we compute the boundary conditions, with the point $\underline{x}$. 28

2.13.4 Genus 0, genus 1 and genus 2 Riemann surfaces. 33

2.13.5 Punctured Riemann sphere. The red dots represent the singularities of the integration kernels. 34

2.14.6 Elliptic curve $y^2 = x^3 - 5x + 3$ for real values of x and y. 36

2.14.7 Real Riemann surface of genus one. 37

2.14.8 The two independent cycles of the torus, γ_1 and γ_2. 39

2.16.9 Non-planar triangle with massive loop. The thick lines in the loop represent the massive propagator, while the external thick line represents the off-shell momentum p_{12}. 43

2.17.10 Result in terms of cutted diagrams. 48

2.19.11 Three integration contour obtained for positive sign of the polynomial under the square roots. 58

2.19.12 Integration contour obtained for negative sign of the polynomial under the square roots. 59

2.20.13 Parametrised contour connecting the boundary point $\underline{x}_0$ to another point $\underline{x}$. 61

2.20.14 Example of matching between expanded solutions around different points. 62

3.1.1 LO cross section initiated by the sub-process $c\,\bar{c} \to F$, with $c = q, g$, for F colourless. 69

3.1.2 Different contributions at NLO and NNLO for the following sub-processes $c\,\bar{c} \to F$, with $c = q, g$. 69

4.2.1 Representative set of two-loop diagrams with internal heavy quark loops. 86

4.2.2 Representative set of diagrams associated with the PLC topology, which do not contribute to the helicity amplitudes. 86

4.2.3 Master integral basis for PLA, PLB and NPL topologies. The figure does not show the MIs defined by a permutation of the external moments. 87

4.2.4 New set of MIs coming from the NPL integral family 87

4.4.5 Diagrams representing the two elliptic sectors in the non planar topology NPL. Thin lines represent massless particles, while thick lines massive particles. 94

4.4.6 Elliptic curve in Weierstrass form for $m_t^2 = 1$ and $s = \frac{1}{400}$. 98

4.5.7 Schematic representation of the procedure exploited to optimise the grid construction within `DiffExp`. Red dots represents the points in which the MIs are evaluated and the blue dashed lines connect the sequential evaluations. 99

4.5.8 Numerical checks for the non-planar double box MIs $\mathcal{J}_{39}, \mathcal{J}_{40}, \mathcal{J}_{41}$ and $\mathcal{J}_{42}$. The plots show the order $\mathcal{O}(\epsilon^0)$ of the masters. The red and blue lines represent the numerical values of the real and imaginary parts of the MIs obtained with `DiffExp`. The crossed dots represent the numerical values obtained with `AMFlow`. The evaluations are performed for different values of $\sqrt{s}$ at a fixed angle θ (in this case $\cos\theta = 0.3$). . 100

4.5.9 NNLO hard function grid in the physical phase-space region between 8 GeV and 2.2 TeV. 101

4.5.10 Schematic representation of the procedure exploited to build the two grids with DiffExp. The dots represents the points in which the MIs are evaluated and the dashed lined connect two sequential evaluations. 101

5.1.1 Representative set of two-loop diagrams with internal heavy-quark loops associated to the relevant scalar integral families. 107

6.1.1 Cone centred on the direction of the photon. 116

6.2.2 Cone centred around the photon's direction. R is the radius of the cone and r is the distance between the photon and the parton (a quark or a gluon) inside the cone. 117

6.2.3 Plot of $\chi(r; R)$ for various values of n. 118

6.4.4 Representative diagram for the one-loop box contribution. 119

6.4.5 Representative diagram for the Double-Virtual contribution. 119

6.4.6 Representative diagram for the Real-Virtual contribution. 119

6.4.7 Representative diagram for the Double-Real contribution. 120

6.5.8 Ratios of different massive corrections to the massless case. In the top panel we show the ratio of our two-loop massive form factors for $q\bar{q} \to \gamma\gamma$ to the massless one. In the lower panel we show the ratio of the massive one-loop box $gg \to \gamma\gamma$ to the massless one. 121

6.5.9 Invariant mass distribution of the double-real contribution to the NNLO fully massive result and comparison between the different channels with respect to the total double-real contributions. 122

6.5.10 Invariant mass distribution of the one-loop diphoton production in association with the emission of one jet. We show the different partonic channels and a comparison with the size of the Double-Real corrections. 123

6.5.11 NNLO invariant mass distribution with full top quark mass dependence. 124

6.5.12 Ratios of each massive contributions with respect to the NNLO massless cross section as a function of the invariant mass. 125

8.3.1 Ejemplos de superficies de Riemann con diferentes géneros. 134

8.3.2 Esfera de Riemann perforada. Los puntos rojos son los polos de los núcleos de integración. 134

8.3.3 Curva paramétrica que conecta el punto de frontera con un nuevo punto. 136

8.4.4 Conjunto representativo de diagramas de dos bucles con bucle de quarks pesados internos, que contribuyen a las correcciones de QCD a NNLO para la producción de dos fotones en el canal de aniquilación de quarks. Las líneas negras delgadas representan quarks ligeros, las líneas negras gruesas quarks pesados, las líneas rizadas gluones y las líneas onduladas fotones. 138

8.4.5 Nuevas MIs provenientes de la topología NPL. 138

8.4.6 Cuadrícula de la función virtual dura desde 8 GeV hasta 2.2 TeV. . . . 139

8.4.7 Diferentes topologías para los diagramas de dos bucles con bucle de quarks pesados internos. 139

8.4.8 Proporción de correcciones masivas de dos bucles para $q\bar{q}$ respecto al caso sin masa (panel superior) y proporción del cuadro de un bucle $gg \to \gamma\gamma$ respecto al caso sin masa (panel inferior). 141

8.4.9 Distribución de masa invariante a NNLO con dependencia completa de la masa del quark top. 141

8.4.10 Proporciones de cada contribución masiva respecto a la sección eficaz sin masa a NNLO. 142

D.0.1 One-loop diagrams for $q\bar{q} \to \gamma\gamma g$ with top quark loop. 150

D.0.2 Tree-level diagrams for $q\bar{q} \to \gamma\gamma g$. 150

D.0.3 Diagrams for $q\bar{q} \to \gamma\gamma t\bar{t}$. 152

D.0.4 Diagrams for $gg \to \gamma\gamma t\bar{t}$. 152

List of Tables

2.4.1 Number of Feynman diagrams for scattering amplitudes involving only gluons at 0, 1 and 2 loops. 13
2.4.2 Correspondance between Dirac and Weyl notation with their respective spinors. 14

4.5.1 Numerical comparison between `DiffExp` and `AMFlow` for the order ϵ^0 of the non-planar MI $\mathcal{J}_{42}$. The centre of mass energy and the photon scattering angle are respectively $\sqrt{s} = 52.1615\,\mathrm{GeV}$ and $\cos\theta = -0.99$. The two independent numerical solutions are equal up to 200 digits, of which only 60 are shown. 101

5.3.1 Simplifications at the integrand and amplitude levels for the finite remainder of the helicity amplitudes, rewritten in terms of iterated integrals. 114

8.4.1 Simplificaciones obtenidas al escribir las amplitudes de helicidad en términos de integrales iteradas. 140

Chapter 1

Introduction

The study of fundamental interactions in nature relies heavily on quantum field theory (QFT), a comprehensive mathematical framework that combines the principles of special relativity and quantum mechanics. These two theories have revolutionised our understanding of physics, despite their seemingly contradictory foundations. QFT describes particles as excitations of quantum fields that permeate space-time, providing a unified description of particles and their interactions. This approach led to the development of the Standard Model (SM) of particle physics in the 1970s.

Within the SM, particles and their interactions are defined, in a consistent mathematical framework, through gauge symmetries. All the forces, except gravity, are described by the symmetry group $SU(3)_c \otimes SU(2)_L \otimes U(1)_Y$. This group has $8 + 3 + 1 = 12$ generators with a non-trivial commutator algebra, due to its non-abelian nature. The theory of strong interactions, i.e. QCD, is based on the exact symmetry of the $SU(3)_c$ group, whose gauge bosons (force-carrying particles) are 8 massless particles named gluons. The electro-weak force is instead described by the $SU(2)_L \otimes U(1)_Y$ symmetry, which is spontaneously broken via the Higgs mechanism [5, 6, 7] to $U(1)_{em}$. The 3 gauge bosons of the electro-weak force, W^+, W^- and Z, acquire mass through the Higgs mechanism, while the one of $U(1)_{em}$ remains massless, namely the photon γ.

Since its formulation, the SM has achieved remarkable success, explaining a vast array of experimental results with high precision. The discovery of the W and Z bosons in 1983 validated the unification of the electroweak theory. Over the years, there have been numerous experimental confirmations and new particles discovered, including the top quark [8], predicted by the Standard Model as a member of one of the three generations of quarks. Technological advancements in new accelerators led to the discovery in 2012, by the LHC, of the only scalar field predicted by the theory, the Higgs boson [9, 10].

2012 marked a major victory with the discovery of the boson responsible for mass in the SM, but it also marked the end, for now, of major discoveries in particle physics. Although the necessary energy range has been reached for the discovery of some particles predicted by different theories, progress has stalled. The SM remains the best framework for understanding the microscopic structure of the universe, but it has long been clear that this is not the end of the story. As mentioned above, it includes three of the four fundamental forces of nature, excluding gravity, and it does not explain the existence of dark matter and dark energy, the mass of neutrinos, among other unresolved issues.

We have entered the so-called *precision era*, in which the LHC continues to be the fundamental tool for theoretical particle physicists to test the SM and simultaneously search for signs of new physics. In particular, there has been a shift from the discovery phase to the precision phase, where we search for discrepancies between theoretical predictions and experimental data. To achieve this, it is essential that theoretical predictions match the measured values of physical observables within the experimentally achieved uncertainty threshold.

Significant experimental progress has led to a significant reduction in uncertainties, which are already at the percentage level. Theoretical models and computational tools must therefore be able to make predictions within the experimental limits.

On the theoretical side, the precision required for comparison with experimental data can be achieved through higher order corrections. These are essential to bring theoretical predictions into line with the remarkable precision achieved by experiments at colliders. These corrections are the main focus of this work. In the calculation of physical observables, the S-matrix can be perturbatively expanded in the form of so-called Feynman diagrams. Each diagram corresponds to a term in the perturbative expansion in powers of the interaction coupling. Depending on the required precision, different types of contributions are introduced. In particular, one can include loop diagrams, which represent virtual corrections, and emissions, where an extra particle is added to the final state, which represent real corrections.

In QFT, the couplings of the theory depend on the energy of the process. This phenomenon, known as the 'running' of coupling, is a fundamental aspect for understanding interactions in high-energy particle physics. In Quantum Electrodynamics (QED), The electromagnetic coupling α_{em} describes the strength of the electromagnetic force. Its value increases as the energy increases. For example, we observe the difference for a momentum transfer equal to 0 and equal to the mass of the Z boson $m_Z \approx 91.18\,\text{GeV}$:

$$\alpha_{em}(0) \approx \frac{1}{137} \approx 0.0073, \qquad \alpha_{em}(m_Z) \approx \frac{1}{128} \approx 0.0078. \tag{0.1}$$

In both cases $\alpha_{em} \ll 1$ (this holds for the energy scales involved at LHC), enabling the perturbative expansion in powers of α_{em} for processes at colliders involving the electromagnetic interactions.

The situation is different in the case of QCD. The strong coupling constant is defined as $\alpha_s = g^2/4\pi$, where g is the coupling of the basic interaction between quarks and gluons. The 'running' of coupling constant in this case is a direct consequence of the renormalisation. For a renormalisation scale μ_R, the running is provided by the renormalisation group equations:

$$\frac{d\alpha_s(\mu_R^2)}{d\log\mu_R^2} = \beta(\alpha_s)\,, \tag{0.2}$$

in terms of the QCD beta function $\beta(\alpha_s)$. The beta function admits an expansion in powers of α_s:

$$\beta(\alpha_s) = -\beta_0\,\alpha_s^2 - \beta_1\,\alpha_s^3 - \beta_2\,\alpha_s^4 - \cdots\,. \tag{0.3}$$

At one-loop (the leading order term), the solution of eq. (0.2) gives:

$$\alpha_s(\mu_R^2) = \frac{2\pi}{\beta_0}\frac{1}{\log\left(\frac{\mu_R}{\Lambda_{QCD}}\right)}, \tag{0.4}$$

where $\Lambda_{QCD} \approx 200 - 300\,\text{MeV}$. When the renormalisation scale μ_R approaches to Λ_{QCD}, the reliability of the perturbative character of QCD is spoiled. Unlike the coupling constant in QED, the value of α_s decreases at high energies and becomes large at low energies. This is a well-known property of QCD, i.e. asymptotic freedom [11, 12, 13, 14, 15]. At low energies, it is not possible to use perturbative techniques, and non-perturbative methods are required. However, at the energy levels relevant to LHC physics, perturbative expansion can be considered. In fact, if we take the Z boson mass as the relevant scale:

$$\alpha_s(m_z^2) \approx 0.118\,, \tag{0.5}$$

consequently, perturbation theory can be applied in the case of QCD at high energy scales.

In the perturbative expansion framework, the physical quantity that allows a comparison between theoretical predictions and experimental data is the cross section. In QCD it is possible to compute the scattering between two hadrons based on the factorisation theorem [16]. It states that the cross section can be calculated as the convolution of two different components, i.e. the parton distribution functions (PDFs) [17, 18] $f_{i/h}(x, \mu_F)$ and the partonic cross section $\widehat{\sigma}_{a\,b}$, which are the long- and short-range interaction factors respectively. We have introduced the factorisation scale μ_F, which is necessary for the calculation of cross sections in QCD, since there are generally soft and collinear divergences when considering the partonic contribution, and changing the factorisation scale alters the distribution of divergences between the partonic cross section and the PDFs. Given two hadrons h_1 and h_2 we can then calculate the cross section as:

$$\sigma_{h_1\,h_2}(s) = \sum_{a,b} \int dx_1\, f_{a/h_1}(x_1,\, \mu_F) \int dx_2\, f_{b/h_2}(x_2,\, \mu_F)\, \widehat{\sigma}_{a\,b}(\widehat{s},\, \mu_R,\, \mu_F), \tag{0.6}$$

where s is the hadronic energy scale of the process and we defined $\widehat{s} = x_1\, x_2\, s$ (as the partonic centre of mass energy) and $\widehat{\sigma}_{a\,b}(\widehat{s},\, \mu_R,\, \mu_F)$ is the partonic cross section . The PDF's depend on the factorisation scale μ_F. From a given PDF value at a fixed scale μ_F the evolution of the PDFs is unambiguously determined by the Dokshitzer-Gribov-Lipatov-Altarelli-Parisi (DGLAP) equation [19, 20, 21]:

$$\frac{\partial}{\partial \log \mu_F^2} f_{i/h}(x, \mu_F) = \int_x^1 \frac{dz}{z} \sum_j P_{ij}(\alpha_s(\mu_F), z)\, f_{j/h}(x/z, \mu_F), \tag{0.7}$$

where the P-functions are the so-called splitting functions. The latter admit a perturbative expansion in the strong coupling:

$$P_{ij}(\alpha_s(\mu_F), z) \;=\; \sum_{l=1}^{\infty} \left(\frac{\alpha_s(\mu_F)}{2\,\pi} \right)^l \, P_{ij}^{(l)}(z)\,. \tag{0.8}$$

In a general computation of the hadronic cross section, there are several components of the interactions: PDFs, partonic cross section, parton showers and hadronization. We mainly focus on the computation of scattering amplitudes as they are the essential elements which serve to compute the partonic cross section. The description in terms of Feynman integrals leads to virtual contributions and real-emission contributions. In this thesis, the main focus is to compute massive higher orders corrections to scattering amplitudes, considering all the different types of contributions, in order to obtain numbers to perform a phenomenological analysis. Massive corrections means that we consider Feynman diagrams with a loop of heavy quark.

We begin this thesis by discussing the state-of-the-art techniques used to compute multi-loop and multi-leg scattering amplitudes. The general structure of the amplitudes includes integrals associated with Feynman diagrams. In QFT, for a renormalisable theory such as the SM, these integrals are divergent in strictly $d_0 = 4$ space-time dimensions. We work with dimensionally regulated integrals, in a generic dimension $d = d_0 - 2\epsilon$. All divergences, although of different kinds, are expressed as poles in the dimensional regulator ϵ. In this context, the amplitude consists of a colour structure, a tensor part and scalar integrals. The techniques discussed allow us to work both at the level of the amplitude and at the level of the integrals. In particular, once the colour structure has been extracted, the amplitude can be expressed in terms of Lorentz-invariant tensors and scalar form factors. The tensor parts encode the dependencies of external momenta, metric tensor, Dirac gamma matrices and polarisation vectors, while the scalar form factors are obtained by applying projection operators to the amplitude written as sums of Feynman diagrams. The choice of variables to express the amplitude can be a crucial step in the calculation, as a good choice can lead to significant simplifications. We introduce the spinor-helicity formalism to compute the so-called helicity amplitudes, where external momenta and polarisation vectors are expressed in terms of spinors and spinor products for specific helicity states.

For multi-loop and multi-leg processes, at the integrand level, we have to compute integrals for any undetermined internal virtual momentum and integrals must depend on a set of variables called scales. The number of external legs and internal mass affects directly the number of scales. The presence of multiple scales constitutes a bottleneck in scattering amplitude computations. Nowadays, on the wish list of two-loop processes to study, there are several $2 \to 3$ processes [22]. After years of effort, progress has been made in this direction [23, 24, 25, 26, 27, 28, 29, 30, 31, 32, 33, 34, 35, 36, 37, 38, 39, 40, 41]. Difficulties arise both from a computational and an analytical point of view. Even modern software can struggle with the vast quantity of memory required to compute and simply such big expressions. On the other side, the presence of a high number of scales is strictly connected with the problem of finding an analytic closed expression for the integrals that characterize the amplitude.

To reach the precision level of the LHC experimental measurements, it is fundamental to consider massive corrections. Heavy particles in the loop affect not only the phenomenological predictions, but also the mathematical structure of scattering amplitudes. The mass dependence in Feynman integrals leads to an analytic representation of the integrals in terms of functions of increasing complexity. In recent years, a close connection between precision physics and mathematics has become evident. Identifying the classes of functions that arise from the evaluation of Feynman integrals is fundamental to a better understanding of their analytical properties. Special functions beyond polylogarithms have been observed for many physical processes, as well as integrals over higher-dimensional surfaces. This establishes an intersection with active research fields in mathematics, such as algebraic geometry and complex geometry.

To understand which geometry is associated to the integrals, we define the so-called maximal cut, based on the concept of generalised cut, which play a key role not only for this purpose but also for the analytic evaluation of the integrals.

To compute dimensionally regulated Feynman integrals we rely on the definition of *Master Integrals* (MIs). These scalar integrals form a basis and any integral of a generic scattering amplitude can be written as a linear combination of these MIs. As the number of loops and legs increases, the number of Feynman diagrams increases drastically, then we need to find this basis in order to deal with the smallest possible set of scalar integrals. Once we have expressed the amplitude in terms of the MIs, we need to calculate them, either analytically or numerically. In both cases we use the *differential equations method*. The MIs satisfy a system of first-order linear differential equations with respect to the kinematic invariants involved in the process. This approach is the most widely used in this field of research and several software packages implement this method. The system can be cast into a special form in which the dependencies on the ϵ regulator are factorised out of the matrix of differential equations. In this case, a solution of the MIs in terms of Chen iterated integrals is allowed.

In chapter 2 we describe the state-of-the-art techniques for computing scattering amplitudes, with particular emphasis on the computation of the scalar integrals. We also focus on the richness of the algebraic structures involved. We use all the machinery introduced to explain how to evaluate the integrals analytically and semi-analytically, by *generalised power series expansion*, order by order in the expansion in ϵ.

In chapter 3 we discuss the method of transverse momentum subtraction. Subtraction methods are needed to remove divergences that arise in the intermediate stages of the calculations. The method presented in this chapter is fundamental to carry out a phenomenological study based on Monte Carlo numerical codes. This allows us to provide a complete amplitude calculation, from the construction of the form factors to their phenomenological use.

In chapter 4 we apply the method described above to calculate the massive two-loop form factors and helicity amplitudes for diphoton production in the quark annihilation channel. The MIs are evaluated by means of the differential equations and a specific form, the so-called *canonical logarithmic form*, is obtained for all MIs except those whose analytic structure involves elliptic functions.

In chapter 5 we study the two-loop helicity amplitudes for diphoton production in gluon fusion with a heavy quark loop. We use a procedure to obtain a ϵ-factorised form for the complete system of MIs, including those defined over an elliptic curve. Specifically, the elliptic sector is the same one studied in chapter 4. This procedure introduces new transcendental functions. We write the MIs in terms of iterated integrals over four different kinds of integration kernels. We show the simplifications at amplitude and integrand level that our calculation implies for the finite remainder of the helicity amplitudes.

In chapter 6 we use the result presented in chapter 4 to perform a phenomenological study of the production of two photons, including for the first time all the massive corrections given by the top quark up to NNLO. Virtual corrections and real emission corrections are included to provide a complete NNLO study of the process.

Chapter 2

Advanced computational methods for scattering amplitudes in the Standard Model

In this chapter we describe the methods and the techniques used to compute, analytically and numerically, the Feynman integrals that appear in the perturbative computation of scattering amplitudes.
A generic amplitude can be written as a product of tensor structures, which depend on the process, and a large number of scalar integrals. This large number of integrals can be reduced, through reduction methods that we will analyze in detail, to a minimal set, the so-called master integrals (MIs). In this way, to evaluate a scattering amplitude, it will be necessary to compute these MIs. There are different methods used in the literature, and we will discuss the method of differential equations, which in some cases allows for an analytical evaluation. However, this is not always possible and generally depends on the function space that defines the integrals. Therefore, we will discuss an alternative method for a semi-analytical evaluation that allows for a numerical result at any point in the phase space, regardless of the mathematical structure.

2.1 Scattering amplitudes

In quantum field theory (QFT), the physical observable that allows a comparison between the theoretical predictions and the experiments is the hadronic cross section. As we discussed before, through eq. (0.6) we factorize the process-dependent partonic cross section from the PDFs part. For a scattering process between two initial partons, with momenta p_a, p_b and energy E_a, E_b, producing n partons as final state with momenta $\{p_f\}_{f=1,\cdots,n}$ and energies $\{E_f\}_{f=1,\cdots,n}$ the cross section is defined by:

$$d\sigma = \frac{1}{\mathcal{F}}\, d\phi_f \,|A_{ab\to f}|^2, \tag{1.1}$$

where the flux $\mathcal{F}$ represents the number of particles passing through a unit area per unit time:

$$\mathcal{F} = 2\,E_a\,2\,E_b\,|v_a\,-\,v_b|, \tag{1.2}$$

defined in terms of the relative velocity of the beams $|v_a\,-\,v_b|$ and of the energies of the initial partons E_a, E_b. $d\phi_f$ represents the phase-space for a scattering process with n particles in the final state. It is defined as the momenta space of the final particles with the constraints imposed by momenta conservation:

$$d\phi_f = \prod_{f=1}^{n} \frac{d^3 p_f}{(2\pi)^2\, 2\, E_f}\, (2\pi)^4\, \delta^4 \left(p_a + p_b - \sum_{f=1}^{n} p_f \right). \tag{1.3}$$

Finally, the last missing term in eq. (1.1), i.e. $\mathcal{A}_{ab\to f}$, is the *scattering amplitude*, which describes the evolution of the system from an initial state to a final state during the scattering process and it is a measure of the scattering probability.
From eq. (1.3) we can obtain the total cross section integrating over the phase-space of the final state the flux factor (a constant) times the square modulus of the scattering amplitude. If we rename the integration measure as:

$$d\Phi_f = \frac{d\phi_f}{\mathcal{F}}, \tag{1.4}$$

the total partonic cross section is given by:

$$\sigma = \int d\Phi_f |\mathcal{A}_{ab\to f}|^2. \tag{1.5}$$

The analytic computation of the cross section through the integration of the scattering amplitude, in terms of the S-matrix, is a challenging task. In order to obtain theoretical predictions, the perturbative expansion becomes a fundamental tool and, consequently, the cross section can be expanded in powers of the strong coupling α_s:

$$\sigma = \sigma_{\mathrm{LO}} + \left(\frac{\alpha_s}{2\pi}\right) \sigma_{\mathrm{NLO}} + \left(\frac{\alpha_s}{2\pi}\right)^2 \sigma_{\mathrm{NNLO}} + \cdots, \tag{1.6}$$

where the choice of the expansion in $\left(\frac{\alpha_s}{2\pi}\right)$ is a convention related to the standard normalization of the loop integrals. LO represents the *Leading Order*, NLO the *Next-to-Leading Order* and NNLO the *Next-to-Next-to-Leading Order*. The dots in eq. (1.6) represent the possible addition of more terms in the α_s expansion. One must consider different contributions related to real radiation emission in the final state or the presence of loops due to radiation where the partons become virtuals. In general, the cross sections in eq. (1.6) reads:

$$\begin{aligned}
\sigma_{\mathrm{LO}} &= \int d\Phi_f |\mathcal{A}^{(0)}_{ab\to f}|^2, \\
\sigma_{\mathrm{NLO}} &= \int d\Phi_f\, 2\,\mathfrak{Re}\left(\mathcal{A}^{(0)\star}_{ab\to f}\, \mathcal{A}^{(1)}_{ab\to f}\right) + \int d\Phi_{f+j} |\mathcal{A}^{(0)}_{ab\to f+j}|^2, \\
\sigma_{\mathrm{NNLO}} &= \int d\Phi_f\, 2\,\mathfrak{Re}\left(\mathcal{A}^{(0)\star}_{ab\to f}\, \mathcal{A}^{(2)}_{ab\to f}\right) + \int d\Phi_{f+j}\, 2\,\mathfrak{Re}\left(\mathcal{A}^{(0)\star}_{ab\to f+j}\, \mathcal{A}^{(1)}_{ab\to f+j}\right) \\
&\quad + \int d\Phi_{f+2j} |\mathcal{A}^{(0)}_{ab\to f+2j}|^2,
\end{aligned} \tag{1.7}$$

where at NLO and NNLO we consider this extra real radiation in the final state increasing the phase-space from f to $f+j$ or $f+2j$. We consider also the loop corrections, due to the extra virtual partons, represented as $\mathcal{A}^{(l)}$, where l is the number of loops. A detailed description of the different contributions for the cross section at NLO and NNLO will be given in section 3.1.
In this general framework, we are interested in the calculation of scattering amplitudes for an arbitrary number of loops and external legs. In the context of perturbation theory, the amplitude can be expanded in powers of α_s:

$$\mathcal{A} = \sum_{l=0}^{\infty} \left(\frac{\alpha_s}{2\pi}\right)^l \mathcal{A}^{(l)}, \tag{1.8}$$

where $\mathcal{A}^{(l)}$ can be expressed as a sum of Feynman diagrams that provide the corresponding $\mathcal{O}(\alpha_s)$. The first term in the expansion $\mathcal{A}^{(0)}$ corresponds to *tree-level diagrams*, i.e. diagrams without loops. $\mathcal{A}^{(1)}$ corresponds to *one-loop diagrams* and can be written as the sum of diagrams with one closed loop of virtual particles. For each loop there is an internal momentum k^μ undetermined by external constraints, so we need to integrate over the momentum space of the loop momentum. For $l \geq 2$ the number of loops is increased and there is an internal momentum for each loops to be integrated.

2.1.1 Dimensional regularization

In Quantum field theory (QFT) the integrals are performed in d_0 space-time dimensions, with $d_0 \in \mathbb{Z}$. The SM is formulated in $d_0 = 4$ space-time dimensions, i.e. 3 spatial dimensions and 1 time dimension. It is well known that loop integrals diverge for $d_0 = 4$, leading to ultraviolet (UV) and infrared (IR) divergences. We need to introduce a regularization scheme to obtain a systematic and mathematically consistent way to treat these divergent expressions. There are several possibilities, but the method of dimensional regularization [42, 43] has become a standard in scattering amplitude calculations. DR works by analytically continuing $d_0 = 4$ to a general $d = d_0 - 2\epsilon$, that can be not integer or even complex, where ϵ is a small parameter known as dimensional regulator. The physical limit is recovered by $\epsilon \to 0$. Within DR the four-dimensional integral over loop momentum is replaced by a d-dimensional integral:

$$\int \mathcal{D}k\big|_{d_0=4} \longrightarrow \int \mathcal{D}k\big|_{d=4-2\epsilon}, \tag{1.9}$$

where $\mathcal{D}k$ represents a general integration measure. During the thesis we will use $\mathcal{D}k$ to represents the integration measure in DR. In order to preserve the correct dimensionality of the couplings in the SM Lagrangian, we need to multiply the couplings by μ^ϵ, where μ is an arbitrary parameter of mass dimension 1. This ensures that the coupling constants remain dimensionless.
The d-dimensional integrals satisfy well defined integration properties. Given an arbitrary function $f(k)$ of the loop momentum, $\alpha, \beta \in \mathbb{C}$, $\Lambda \in SO(1,\, d-1)$ (element of the Lorentz group) and a d-dimensional momentum p^μ, the integrals satisfies:

- **Additivity and linearity**

$$\int \mathcal{D}k\, \left(\alpha\, f(k) \,+\, \beta\, f(k)\right) \,=\, \alpha \int \mathcal{D}k\, f(k) \,+\, \beta \int \mathcal{D}k\, f(k), \tag{1.10}$$

- **Scaling:**

$$\int \mathcal{D}k\, f(\alpha\, k) \,=\, \alpha^{-d} \int \mathcal{D}k\, f(k), \tag{1.11}$$

- **Translation invariance:**

$$\int \mathcal{D}k\, f(k\,+\,p) \,=\, \int \mathcal{D}k\, f(k), \tag{1.12}$$

- **Rotation invariance:**

$$\int \mathcal{D}k\, f(\Lambda\, k) \,=\, \int \mathcal{D}k\, f(k). \tag{1.13}$$

DR is important for different reasons. Firstly, it preserves gauge symmetry and Poincaré invariance. This is crucial in a QFT like the SM for the consistency and renormalizability of the theory. Furthermore, DR allows for a systematic treatment of divergences. UV and IR divergences are not removed through dimensional regularization, but are reorganized into poles in the dimensional regulator. When considering the physical dimensions, i.e. $\epsilon \to 0$, these types of divergences appear as terms of the form $\frac{1}{\epsilon^n}$, where n represents the order of the poles. Once the UV and IR poles have been identified, different techniques can be used to remove these singularities and obtain the finite remainder of the amplitude. The UV divergences will be dealt with through renormalisation. There are different renormalisation schemes, and especially for corrections involving internal masses in loops, mixed schemes are adopted, as will be explicitly shown in the production of two photons. The IR divergences, on the other hand, will be handled through subtraction methods due to the universality of these types of poles. The nature of these singularities arises from the presence of massless particles, particularly in processes involving soft or collinear emissions of massless particles. Through the Kinoshita-Lee-Nauenberg (KLN) theorem [44, 45], we know that at the level of the cross-section, there must be a cancellation of the IR divergences when summing all real and virtual contributions. However, if we consider the intermediate steps, the amplitude will have these poles, which need to be removed through subtraction method [46, 47, 48, 49, 50, 51, 52, 53, 54].

2.2 Structure of scattering amplitudes

Previously, we discussed how the amplitude can be described through a sum of Feynman diagrams contributing to the process at the perturbative order we are interested in. Considering the particles involved in the process under study, the amplitude can be factored into three main contributions:

$$\mathcal{A} = \mathcal{C} \times T \times I, \tag{2.1}$$

where $\mathcal{C}$ is a set of colour factors, T encodes the dependency for the Lorentz tensors and I represents the scalar integrals associated to the loop structure of the amplitude. Each part corresponds to a different aspect of the interaction in the scattering process. These three parts are independent and, in practice, they can be calculated separately. The part related to the integrals associated with Feynman diagrams will be discussed in depth from section 2.5 until the end of the chapter. We will now briefly discuss the colour structures and the tensor structures allowed to maintain Lorentz and gauge invariance.

2.2.1 Colour structure

In QCD, the amplitude $\mathcal{A}$ can be rewritten as a linear combination of colour factors and so-called colour-ordered amplitudes. The color factors come from the group theory associated to the gauge symmetry $SU(N_c)$, where N_c is the number of colours. The Lie algebra of $SU(N_c)$ is defined by:

$$\begin{aligned} &[T^a, T^b] = i f^{abc} T^c, \\ &f^{abk} f^{cdk} + f^{bck} f^{adk} + f^{cak} f^{bdk} = 0, \end{aligned} \tag{2.2}$$

where f^{abc} are the structure constants of the Lie algebra of $SU(N_c)$. The set of indices $\{a, b, c, d, k\}$ are defined in the adjoint representation of $SU(N_c)$ and goes from 1 to $N_c^2 - 1$. The structure constants appear naturally in the computation of the amplitude through interactions between 3 and 4 gluons. In order to separate the color structures from the colour-ordered amplitudes, the structure constants are replaced by the Gell-Mann matrices throught the following relation:

$$f^{abc} = -2i\,\mathrm{Tr}\left([T^a, T^b]T^c\right). \tag{2.3}$$

Subsequently, the sums over equal indices is carried out using the Fierz identity:

$$T^a_{ij}\, T^a_{kl} = \frac{1}{2}\left(\delta_{il}\,\delta_{jk} - \frac{1}{N_c}\delta_{ij}\,\delta_{kl}\right), \tag{2.4}$$

where the set of indices $\{i, j\}$ are defined in the fundamental representation of $SU(N_c)$ and goes from 1 to N_c. In light of Schur's lemma, the Casimir of the fundamental and adjoint representations of $SU(N_c)$ are defined through:

$$\begin{aligned} T^a_{ij}\, T^a_{jk} &= C_F\, \delta_{ij}, \\ f^{abc}\, f^{abd} &= C_A\, \delta^{cd}, \end{aligned} \tag{2.5}$$

whose values are $C_F = \frac{N_c^2-1}{2N_c}$ and $C_A = N_c$.

In this way it is possible to obtain the amplitude in terms of colour factors and colour-ordered amplitudes which encode the dependencies from the kinematic of the process. The gauge invariance of the amplitude $\mathcal{A}$ ensures the gauge invariance of each colour-ordered amplitudes separately. For a detailed review of color decomposition see Ref. [55, 56].

2.2.2 Lorentz tensor structure

Once the colour factors have been extracted from the amplitude, the next piece to be analyzed is the tensor structure. Lorentz and gauge invariance are fundamental to understanding how the tensor structure is composed and, specifically, how momenta, polarization vectors, and spinors combine in the amplitude. The allowed terms must include Lorentz covariant quantities as momenta, metric tensor and spinor bilinears composed by Dirac γ-matrices and spinors. If the process involves external bosons, the polarization vectors of the latter must be included.

2.3 Tensor decomposition

Thus far, we have discussed the structure of the amplitude and its factorisation into a color part, a tensor part, and finally the part consisting of scalar integrals. In order to compare with experimental data, increasingly complex processes from a computational perspective are required. At one loop, various methods have been implemented and optimized [57, 58, 59, 60, 61, 62, 63, 64, 65, 66, 67, 68, 69, 70, 71, 72] to deal with the full calculation. In the multi-loop and multi-leg scenario, the complexity increases significantly. Generally, the amplitude is expressed in terms of Feynman diagrams, and consequently the entire tensor structure characterizing the diagram is present. Thanks to a series of techniques, that will be described in detail later, it is preferable to compute scalar integrals. Consequently, different algebraic manipulations are used to factorize the tensor structure from the integrals. The most widely used modern technique for the decomposition of any scattering amplitude, regardless of the number of loops and the presence of internal masses, is the *projector method* [73, 74]. The symmetries of the problem, including Poincaré invariance and gauge invariance, are used to parametrize the scattering amplitude in terms of Lorentz tensors and scalar form factors. In this way it is possible to obtain the so-called projection operators which, when applied to the amplitude (written in terms of Feynman diagrams), produce the scalar form factors.

To illustrate the general method we work in perturbative QCD and suppose that through the symmetries of the problem we have written the amplitude as a linear combination of Lorentz tensors T_i and scalar form factors F_i:

$$\mathcal{A}(p_1, \cdots, p_n) = \sum_{i=1}^{n} F_i(p_1, \cdots, p_n)\, T_i. \tag{3.1}$$

The number of tensors in d-dimension is process-dependent, since the latter are built from the external momenta, polarisation vectors and metric tensor. For example, in the $gg \to \gamma\gamma$ [75] process there are in total 2^4 independent tensors due to the presence of four polarisation vectors $\epsilon^\mu, \epsilon^\nu, \epsilon^\rho, \epsilon^\sigma$.

The projection operators are defined such that when applied to the amplitude after summing over the polarisations they give the scalar form factors:

$$\sum_{pol} \mathcal{P}_j \mathcal{A}(p_1, \cdots, p_n) = F_j(p_1, \cdots, p_n). \tag{3.2}$$

It is possible to define them as a linear combination of the Hermitian conjugate basis tensors:

$$\mathcal{P}_j = \sum_{i=1}^{N} \left(M^{-1}\right)_{ij} T_i^\dagger, \tag{3.3}$$

where the matrix M is defined as:

$$M_{ij} = \sum_{pol} T_i^\dagger T_j. \tag{3.4}$$

From eq. (3.1) it is possible to compute the so-called helicity amplitudes:

$$\mathcal{A}_{\lambda_1, \cdots, \lambda_n}(p_1, \cdots, p_n) = \sum_{i=1}^{N} F_i(p_1, \cdots, p_n)\, T_{i\ \lambda_1, \cdots, \lambda_n}, \tag{3.5}$$

obtained by fixing the helicities of all the external particles in all the possible ways. In doing this there is a change of scheme [76] to the 't Hooft-Veltman scheme (tHV). In the tHV scheme we work with d-dimensional internal states, but 4-dimensional external states. Put the external momenta and polarisation vectors in 4-dimension has direct consequences on tensors, since it is shown that a subsystem of the tensors in d-dimensions spans the entire space and it is possible to rewrite the remaining tensors through an orthogonalization process so as to force them to live in the -2ϵ subspace. The fundamental observation is that the matrix M in eq. (3.4) has null determinant in d=4. Then, in d=4, $rank(M) = Q \leq N$. It is always possible to swap the basis tensors such that the new independent ones are the first Q. It is possible then to define a new full rank matrix:

$$M_{ij}^{Q\times Q} = \sum_{pol} \overline{T}_i^\dagger \overline{T}_j \quad i, j = 1, \cdots, Q, \tag{3.6}$$

and consequently the new projector operators:

$$\mathcal{P}_j^{Q\times Q} = \sum_{i=1}^{Q} \left(\left(M^{Q\times Q}\right)^{-1}\right)_{ij} \overline{T}_i^\dagger \quad j = 1, \cdots, Q. \tag{3.7}$$

As anticipated, we can rewrite the remaining tensors from those obtained with d-dimensional external states removing their projections along the new basis tensors T_i with $i = 1, \cdots, Q$:

$$\overline{T}_i = T_i - \sum_{j=1}^{Q} \left(\mathcal{P}_j^{Q\times Q} T_i\right) \overline{T}_j \quad i = Q+1, \cdots, N, \tag{3.8}$$

where $\mathcal{P}_j^{Q\times Q}$ are defined such that:

$$\sum_{pol} \mathcal{P}_j^{Q\times Q}\overline{T}_k = \delta_{jk}. \tag{3.9}$$

We stress that the sum over the polarisations and the projections are made in d-dimension.

Of course, it is possible to redefine in this way the amplitude in eq. (3.5) in terms of the new tensors basis:

$$\mathcal{A}_{\lambda_1,\cdots,\lambda_n}(p_1,\cdots,p_n) = \sum_{i=1}^{Q} \overline{F}_i(p_1,\cdots,p_n)\,\overline{T}_{i\;\lambda_1,\cdots,\lambda_n}, \tag{3.10}$$

where the sum now has an upper limit of Q. We reorganized the basis such that the first Q tensors span the full process dependent tensor space, while the $N-Q$ remaining tensors vanishes in 4-dimension. Then we just have to compute the form factors $\overline{F}_i$ from a small number of independent tensors (in 4-dimensional external states).

2.4 Spinor-helicity formalism

The scattering amplitudes are the main target of the calculation as they are essential for determining the partonic cross-section, as shown in eq. (1.5). However, the difficulty of the calculation increases significantly as the number of loops and external legs grows. In Table 2.4.1 it is presented the general scheme for the terms involved in the calculation of a scattering amplitude and subsequently its squared modulus, from an initial set of Feynman diagrams. Specifically, we start with n Feynman diagrams, and thus n separate terms, but after calculating the traces and summing over polarizations, m terms with $m < n$ contribute. However, when we proceed to calculate the squared modulus, these m terms become m^2.

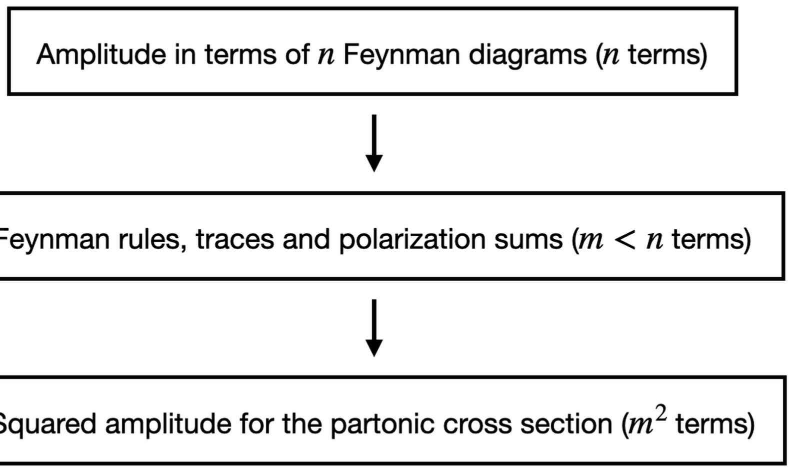

Figure 2.4.1. Number of terms in the different steps of the amplitude and cross section computation.

Computing the amplitude in this way can become complicated due to the large number of terms. In Table 2.4.2, the number of diagrams for the process $gg \to gg$ is shown, where only interactions between gluons are included, and the number increases significantly as the number of external gluons and/or the number of loops increases [77].

Here we introduce the spinor-helicity formalism [56, 78], where instead of defining the amplitude in terms of the four-momenta and polarization vectors, spinors and helicities are used. This simplifies the calculation, since we compute the amplitude for a specific helicity configuration and different configurations are computed separately since they do not interfere among themselves.

Number of external gluons	Number of diagrams at 0 loops	Number of diagrams at 1 loops	Number of diagrams at 2 loops
4	4	39	529
5	25	437	8210
6	220	5800	142335
7	2485	90450	2784565

Table 2.4.1. Number of Feynman diagrams for scattering amplitudes involving only gluons at 0, 1 and 2 loops.

Furthermore, in the traditional approach we have gauge redundancies due to the freedom of adding a term proportional to the momentum of a gauge boson p^μ to the polarization vector:

$$\epsilon^\mu \to \epsilon^\mu + \beta\, p^\mu, \tag{4.1}$$

where β is a constant. This gauge transformation leaves the amplitude invariant, but there is not unique choice to fix the polarizations with the constraint imposed by the transversality with the boson momentum $p_\mu\, \epsilon^\mu = 0$. In the spinor-helicity formalism, instead, we have different configurations with positive and negative helicities and there are no terms that need to be canceled through gauge fixing.

As stated in [56, 78], it is possible to use the local isomorphism of the Lorentz group to $SU(2) \otimes SU(2)$ in order to use the spinor representation, which consists of the Weyl spinor for massless vectors. Then, we can use generally the finite-dimensional irreducible representations of the latter given by $\left(\frac{m}{2}, \frac{n}{2}\right),\ m, n \in \mathbb{Z}$.

In terms of chirality, we have the positive-chirality spinor representation $\left(\frac{1}{2}, 0\right)$ and the negative-chirality spinor representation $\left(0, \frac{1}{2}\right)$. We represent with λ_a the two-component positive-chirality spinor and with $\tilde{\lambda}_{\dot{a}}$ the negative one, where in both cases $a = 1, 2$.

In the computation of scattering amplitudes it's a common practice to use four momenta p_i^μ as kinematic variables, and in particular their Lorentz-invariant products $s_{ij} = (p_i + p_j)^2$. However, by choosing better kinematic variables it is possible to reduce all redundancies between momenta and polarization vectors and at the same time explicitly consider the spin of the particles, since in the Standard Model all but the Higgs boson have spin.
Given $u(p_i)$ as the positive-energy solution of the Dirac equation, we can define the positive and negative chirality spinor by applying to the solution, respectively, the positive and negative chirality projector operators:

$$\begin{aligned} \mathbb{P}_+ &= \frac{1+\gamma_5}{2}, \\ \mathbb{P}_- &= \frac{1-\gamma_5}{2}, \end{aligned} \tag{4.2}$$

such that:

$$\begin{aligned} u_+(p_i) &= \mathbb{P}_+\, u(p_i), \\ u_-(p_i) &= \mathbb{P}_-\, u(p_i), \end{aligned} \tag{4.3}$$

where γ_5 is the matrix defined by the four Dirac gamma matrices as $\gamma_5 \equiv i\,\gamma^0\,\gamma^1\,\gamma^2\,\gamma^3\,\gamma^4$. In the Weyl basis the γ-matrices are defined by:

$$\gamma^\mu = \begin{pmatrix} 0 & \sigma^\mu \\ \underline{\sigma}^\mu & 0 \end{pmatrix}, \tag{4.4}$$

where $\sigma^\mu = (\mathbb{1}, \overline{\sigma})$ and $\underline{\sigma}^\mu = (\mathbb{1}, -\overline{\sigma})$ and $\overline{\sigma}$ is the vector of Pauli matrices:

$$\sigma_1 = \begin{pmatrix} 0 & 1 \\ 1 & 0 \end{pmatrix}, \quad \sigma_2 = \begin{pmatrix} 0 & -i \\ i & 0 \end{pmatrix}, \quad \sigma_3 = \begin{pmatrix} 1 & 0 \\ 0 & -1 \end{pmatrix}. \tag{4.5}$$

The spinors in eq. (4.3) correspond to the positive-energy solution of the Dirac equation. In the massless case, knowing the positive solutions is enough to have the entire system of solutions as $v_\pm(p_i)$, i.e. the negative-energy solutions, correspond to $u_\mp(p_i)$.

Given a four-momentum p_μ, we can define a 2×2 matrix by contracting the momentum with the σ^μ:

$$p_{a\dot{a}} = \sigma^\mu_{a\dot{a}} p_\mu = p_0 + \overline{\sigma}\cdot\overline{p} = \begin{pmatrix} p_0 + p_3 & p_1 - i\,p_2 \\ p_1 + i\,p_2 & p_0 - p_3 \end{pmatrix} = \lambda_a\,\tilde{\lambda}_{\dot{a}}, \tag{4.6}$$

where the last equality holds in the massless case and the chain of equality gives us the explicit expression of λ_a and $\tilde{\lambda}_{\dot{a}}$ up to a phase.

Table 2.4.2 shows the correspondence between the Dirac and Weyl notations and in particular the representation by spinors in both cases.

Weyl state	Dirac state	Weyl spinor	Dirac spinor
$\|i\rangle$	$\|i^+\rangle$	$\lambda_a(p_i)$	$u_+(p_i)$
$\|i]$	$\|i^-\rangle$	$\tilde{\lambda}^{\dot{a}}(p_i)$	$u_-(p_i)$
$\langle i\|$	$\langle i^-\|$	$\lambda^a(p_i)$	$u_-^\dagger(p_i)\,\gamma^0$
$[i\|$	$\langle i^+\|$	$\tilde{\lambda}_{\dot{a}}(p_i)$	$u_+^\dagger(p_i)\,\gamma^0$

Table 2.4.2. Correspondance between Dirac and Weyl notation with their respective spinors.

Finally, we can define some important Lorentz-invariant quantities and identities in the spinor representation. The product between spinors uses the Levi-Civita tensor in $SU(2)$, i.e. ϵ^{ab} and $\epsilon^{\dot{a}\dot{b}}$. Then, we can define the products:

$$\begin{aligned} \langle i\,j\rangle &= \epsilon^{ab}\,\lambda_a(p_i)\lambda_b(p_j) = -\langle j\,i\rangle, \\ [i\,j] &= \epsilon^{\dot{a}\dot{b}}\,\tilde{\lambda}_{\dot{a}}(p_i)\,\tilde{\lambda}_{\dot{b}}(p_j) = -\,[j\,i]. \end{aligned} \tag{4.7}$$

For a massless particle $p_i^\mu\,p_{i\,\mu} = 0$, then it follows directly from eq. (4.6) that the determinant of the matrix should vanish:

$$\det(p_{a\dot{a}}) = \det(\lambda_a\,\tilde{\lambda}_{\dot{a}}) = 0. \tag{4.8}$$

As a consequence of the anti-symmetry:

$$\langle i\,i\rangle = [i\,i] = 0. \tag{4.9}$$

It's useful to note the following properties:

$$\begin{aligned} [i|\gamma^\mu|j\rangle &= \langle j|\gamma^\mu|i], \\ [i|\gamma^\mu|j\rangle^\star &= [j|\gamma^\mu|i\rangle. \end{aligned} \tag{4.10}$$

Using the 2×2 matrix that define a four-momenta in terms of the spinors, it is possible to define the Mandelstam invariants, or generally the scalar products, in the new formalism:

$$\begin{aligned} p_i \cdot p_j &= \frac{1}{2}\,\epsilon^{ab}\,\epsilon^{\dot{a}\dot{b}}\,p_{i\;a\dot{a}}\,p_{j\;b\dot{b}} = \frac{1}{2}\,\epsilon^{ab}\,\epsilon^{\dot{a}\dot{b}}\,\lambda_a\,\tilde{\lambda}_{\dot{a}}\,\lambda_b\,\tilde{\lambda}_{\dot{b}} \\ &= \frac{1}{4}\tilde{\lambda}_{\dot{a}}(p_i)\,\sigma^{\mu\;\dot{a}a}\,\sigma_a(p_i)\,\tilde{\lambda}_{\dot{b}}(p_j)\,\sigma_\mu^{\dot{b}b}\,\lambda_b(p_j), \end{aligned} \tag{4.11}$$

where we used the relation between the σ-matrices and the ϵ-tensors:

$$\epsilon^{ab}\,\epsilon^{\dot{a}\dot{b}} = \frac{1}{2}\sigma^{\mu\;a\dot{a}}\sigma_\mu^{b\dot{b}}, \tag{4.12}$$

together with the Fierz identity:

$$\sigma^{\mu\;a\dot{a}}\sigma_\mu^{b\dot{b}} = 2\,\delta^{ab}\,\delta^{\dot{a}\dot{b}}. \tag{4.13}$$

This allow us to write the scalar products as:

$$s_{ij} = (p_i + p_j)^2 = 2\,p_i\,p_j = \langle i\,j\rangle[j\,i]. \tag{4.14}$$

For real momenta different chirality spinors λ_a and $\tilde{\lambda}_{\dot{a}}$ are connected through complex conjugation:

$$\lambda_a(p_i) = \left(\tilde{\lambda}_{\dot{a}}(p_i)\right)^\star, \tag{4.15}$$

then the product between positive-chirality and the negative-chirality spinors is connected by:

$$[i\,j] = \langle i\,j\rangle^\star. \tag{4.16}$$

The contraction with γ-matrices can be written in Weyl basis as:

$$\gamma^\mu\,p_{i\;\mu} = \begin{pmatrix} 0 & \lambda_a(p_i)\,\tilde{\lambda}_{\dot{a}}(p_i) \\ \lambda^a(p_i)\,\tilde{\lambda}^{\dot{a}}(p_i) & 0 \end{pmatrix} = |i\rangle[i| + |i]\langle i|. \tag{4.17}$$

From eq. (4.14) and eq. (4.16) it follows that we can rewrite the spinor products as:

$$\begin{aligned} \langle i\,j\rangle &= \sqrt{s_{ij}}e^{i\,\phi_{ij}}, \\ [i\,j] &= \sqrt{s_{ij}}e^{-i\,\phi_{ij}}, \end{aligned} \tag{4.18}$$

where ϕ_{ij} is a generic phase. Each spinor $\lambda_a(p_i)$ and $\tilde{\lambda}_{\dot{a}}(p_i)$ could be written in polar coordinates including the phase. For two spinors $\lambda_a(p_i)$ and $\lambda_a(p_j)$ in polar coordinates:

$$\begin{aligned} \lambda_a(p_i) &= |\lambda_a(p_i)|\,e^{i\theta_i}, \\ \lambda_a(p_j) &= |\lambda_a(p_j)|\,e^{i\theta_j}, \end{aligned} \tag{4.19}$$

such that the phase ϕ_{ij} correspond to the phase difference among the two spinors:

$$\phi_{ij} = arg(\langle i\,j\rangle) = \theta_i - \theta_j. \tag{4.20}$$

A common used property in computations is the momentum conservation $\sum_{i=1}^n p_{i\;\mu} = 0$ (with all the particles incoming). For any p_i and p_j the momentum conservation reads:

$$\sum_{k=1}^n \langle i\,k\rangle[k\,j] = 0. \tag{4.21}$$

Eq. (4.21) could be very useful in order to find relations between spinor products. Suppose to have a generic l-loop process with four external legs with associated momenta p_1, p_2, p_3, p_4, if we choose i=1,j=2:

$$\sum_{m=1}^{4} \langle 1\, m\rangle [m\, 2] = \langle 1\, 1\rangle [1\, 2] \,+\, \langle 1\, 2\rangle [2\, 2] \,+\, \langle 1\, 3\rangle [3\, 2] \,+\, \langle 1\, 4\rangle [4\, 2] = 0, \tag{4.22}$$

where we know that $\langle 1\, 1\rangle = [2\, 2] = 0$ from eq. (4.9). Consequently:

$$\langle 1\, 3\rangle [3\, 2] = -\langle 1\, 4\rangle [4\, 2]. \tag{4.23}$$

Another important property that allows to greatly simplify the calculations in scattering amplitudes is the Schouten identity. The Schouten identity is a consequence of the fact that we are in a 2-dimensional space and any linear combination of three spinors must be linearly dependent. Given a set of spinors, since the space is 2-dimensional any linear combinations of three spinor products as sum of three terms, which is zero due to the linear dependence:

$$\langle i\, j\rangle \langle k\, l\rangle \,+\, \langle i\, k\rangle \langle l\, j\rangle \,+\, \langle i\, l\rangle \langle j\, k\rangle = 0. \tag{4.24}$$

Since throughout the thesis we are dealing with massive internal states but with photons and gluons in the final and initial states, we need to define the polarisation vectors in this formalism. Consider a massless spin-1 particle with momentum p_i whose associated spinors are λ_a and $\tilde{\lambda}_a$. To define the polarisation vectors we need another vector q called reference vector and the associated reference spinors μ_a and $\tilde{\mu}_a$. Then, the polarisation vectors for definite helicities could be defined as:

$$\epsilon^{+}_{\mu}(p_i, q) = \frac{1}{\sqrt{2}} \frac{\langle q|\gamma_\mu|i]}{\langle q\, i\rangle} \qquad \epsilon^{-}_{\mu}(p_i, q) = -\frac{1}{\sqrt{2}} \frac{[q|\gamma_\mu|i\rangle}{[q\, i]}, \tag{4.25}$$

or in terms of two-components spinors:

$$\epsilon^{+}_{a\dot{a}} = \sqrt{2}\, \frac{\mu_a\, \tilde{\lambda}_{\dot{a}}}{\langle \lambda \mu\rangle} \qquad \epsilon^{-}_{a\dot{a}} = -\sqrt{2}\, \frac{\lambda_a\, \tilde{\mu}_{\dot{a}}}{[\tilde{\lambda}\, \tilde{\mu}]}. \tag{4.26}$$

It's relevant to notice that the choice of the reference vector (and spinors) correspond to a gauge freedom. Polarisation vectors must satisfy the transverse condition:

$$\epsilon^{\pm}_{\mu}(p_i, q)\, p_i^{\mu} = 0, \tag{4.27}$$

that holds also for the reference vector, since by definitions the polarisation vectors are proportional to the spinors. Furthermore:

$$\epsilon^{\mu\, -}(p_i, q)\, \epsilon^{+}_{\mu}(p_i, q) = \frac{1}{2} \frac{\langle q|\gamma^\mu|i]}{\langle q\, i\rangle} \frac{\langle i|\gamma_\mu|q]}{[i\, q]} = \frac{\langle i\, q\rangle\, [i\, q]}{\langle q\, i\rangle\, [i\, q]} = -1, \tag{4.28}$$

where we used the following relation:

$$\langle i|\gamma^\mu|q] = [q|\gamma^\mu|i\rangle, \tag{4.29}$$

together with the Fierz identity:

$$\langle q|\gamma^\mu|i]\, \langle j|\gamma_\mu|k] = 2\, \langle q\, j\rangle\, [i\, k] \qquad \forall\, p_q, p_i, p_j, p_k. \tag{4.30}$$

As a last well-known property of polarisation vectors, we can easily check that:

$$\epsilon^{\mu\, +}(p_i, q)\, \epsilon^{+}_{\mu} = \frac{1}{2} \frac{\langle q|\gamma^\mu|i]}{\langle q\, i\rangle} \frac{\langle q|\gamma_\mu|i]}{\langle q\, i\rangle} = \frac{\langle q\, q\rangle [i\, i]}{\langle q\, i\rangle\, \langle q\, i\rangle} = 0, \tag{4.31}$$

where we used again eq. (4.30) and the same result is found in the case of negative helicity.

2.5 Multi-loop multi-leg Feynman integrals

Previously, we discussed how the amplitude can be written in terms of Feynman diagrams. In this section, we describe in detail the Feynman integrals associated with these diagrams, which, through projection operators applied to the amplitude, appear in the scalar form factors. These integrals provide an essential computational framework to compute higher-order terms in the perturbative expansion of scattering amplitudes. In dimensional regularization in a d-dimensional space-time, we can define a generic l-loop Feynman integral with n external legs as:

$$I(a_1, \cdots, a_m) = \int \prod_{i=1}^{l} \mathcal{D}k_i \frac{\mathcal{N}\left(\{k_i \cdot q_j\}\right)}{\prod_{s=1}^{m} D_s^{a_s}}. \tag{5.1}$$

Here we associate a momentum p_i to each external leg defining the set $\{p_i\}_{i=1,\cdots,n}$, which satisfy the momentum conservation:

$$\sum_{i=1}^{n} p_i = 0, \tag{5.2}$$

where, in eq. (5.2), we assumed, without loss of generality, that all the momenta are incoming. $\mathcal{D}k_i$ is the integration measure for the i-th loop momentum k_i, which we will assume, unless otherwise specified in the thesis, to be:

$$\mathcal{D}k_i = \frac{d^d k_i}{i\pi^{d/2}}. \tag{5.3}$$

$\mathcal{N}\left(\{k_i \cdot q_j\}\right)$ is a polynomial in the products between loop momenta k_i and q_j, involving always at least one loop momentum, with $q_j \in \{k_1, \cdots, k_l, p_1, \cdots, p_n\}$.

The denominators $\{D_s\}_{s=1,\cdots,m}$ are called *propagators* and for a generic massive particles are defined by:

$$D_s = (v_s^2 - m_s^2), \tag{5.4}$$

where the momentum v_k can be written as a linear combination of loop momenta and external momenta:

$$v_s = \sum_{i=1}^{l} A_{si}\, k_i + \sum_{i=1}^{n-1} B_{si}\, p_i, \tag{5.5}$$

and A_{si} and B_{si}, elements of two matrices $\mathbb{A}$ and $\mathbb{B}$, can take values on the set $\{-1, 0, +1\}$. It's important to notice that the sum over the external momenta is up to $n-1$ and this is due to the fact that from eq. (5.2) not all the external momenta are independents and we can always express one of them as a linear combination of the others.

The exponents of the propagators can be gathered in $a = (a_1, \cdots, a_m) \in \mathbb{Z}^m$ such that $|a| = \sum_{i=1}^{m} a_i$.

Each l-loop Feynman integral is associated to a graph called Feynman diagram which consists of vertices, internal and external edges [79], as represented in Fig. 2.5.2.

Internal edges represent propagating particles and, following our notations, we can associate to them a momentum v_i, a mass m_i and an integer a_i. External edges are the legs of a Feynman diagrams and we associate an external momentum to each of them. The vertices connect the edges and at each vertex the conservation of moments must hold.

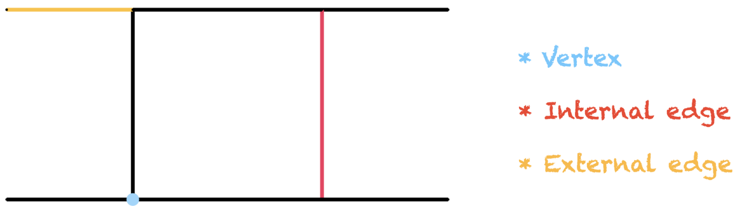

Figure 2.5.2. Graph defined in terms of vertices, internal and external edges.

The Feynman integral in eq. (5.1) is a function of the external momenta and the masses. We can condense the information contained in the scalar products of the four-momenta in the so-called Mandelstam invariants s_{ij}. Assuming all the external momenta incoming, we define:

$$s_{ij} = (p_i + p_j)^2 \qquad i, j = 1, \cdots, n. \tag{5.6}$$

In a process with n external momenta, there are in total $\binom{n}{2} = \frac{n(n-1)}{2}$ Mandelstam invariants, but the momentum conservation and the on-shell conditions reduce the number of independent invariants to:

$$N_{s_{ij}} = \frac{n(n-1)}{2} - (n-1). \tag{5.7}$$

We will discuss in details the Lorentz invariance of Feynman integrals and the relations that this invariance generates in section 2.7. Here, we shall confine ourselves to stating that by Lorentz invariance the Feynman integrals must depends only on the products of external momenta and on the internal masses squared. We can group the variables on which the Feynman integrals depend into a single vector, referring to its components as *scales*:

$$\underline{x} = \left(\{s_{ij}\}_{i,j=1,\cdots,n-1},\, \{m_s^2\}_{s=1,\cdots,m}\right), \tag{5.8}$$

where the products in s_{ij} are between the $(n-1)$ independent external momenta and potentially the presence of external masses is due to the squared external momenta. The number of internal masses is up to the number of propagators, i.e. the number of internal edges.

From scales dependence it follows that performing a shift on the external momenta and masses of a parameter $\lambda \in \mathbb{R} \setminus 0$, the scales transform as $\underline{x} \to \lambda^2\, \underline{x}$. We want to use this information to obtain the *mass dimension* of a generic Feynman integral, i.e. the power with which the mass appears in the expression. For a physical quantity χ, we denote its mass dimension as $[\chi]$. Let us consider individually the different pieces that appear in the Feynam integral in eq. (5.1). Each integration measure has mass dimension $[\mathcal{D}k] = \mathrm{d}$, then, in the l-loop case, $\prod_{i=1}^{l} \mathcal{D}k_i$ contributes with a factor $l\, d$. Each propagator $D_s^{a_s}$ has mass dimension $-2\, a_s$, then the product $\prod_{s=1}^{m} D_s^{a_s}$ contributes with a factor $-2\,|a|$. Then, if we represent with $[\mathcal{N}(\{k_i\, q_j\})]$ the mass dimension of the polynomial, the mass dimension of an l-loop Feynman integrals is:

$$[I(a_1, \cdots, a_m)] = l\, d - 2\,|a| + [\mathcal{N}(\{k_i\, q_j\})]. \tag{5.9}$$

Given a set of n external momenta $\{p_i\}_{i=1,\cdots,n}$, which satisfy the conservation rule in eq. (5.2) and a set of loop momenta $\{k_i\}_{i=1,\cdots,l}$ for a l-loop Feynman integral, the number of scalar products between them is given by:

$$N_{sp} = \frac{1}{2}\, l\,(l+1) + l\,(n-1). \tag{5.10}$$

For a generic multi-loop multi-leg Feynman integral the scalar products obtainable from the m propagators, whose total number is N_m, are not enough to describe the full set of N_{sp} and we need to introduce new scalar products, the so-called *irreducible scalar products* (ISPs) such that:

$$N_{SP} = N_{ISP} + N_m. \tag{5.11}$$

We can apply tensor decomposition method in order to reduce the polynomial at the numerator $\mathcal{N}(\{k_i\, q_j\})$ to ISP adding a set of denominators $\{S_h\}_{h=1,\cdots,N_{ISP}}$.

Therefore, we define the scalar l-loop Feynman integral with n external legs as:

$$I(a_1, \cdots, a_m, b_1, \cdots, b_{N_{ISP}}) = \int \prod_{i=1}^{l} \mathcal{D}k_i \frac{\prod_{h=1}^{N_{ISP}} S_h^{b_h}}{\prod_{s=1}^{m} D_s^{a_s}}, \quad a_s,\, b_h \in \mathbb{Z}. \tag{5.12}$$

In eq. (5.12) we have inserted auxiliary scalar products in the form $S_h^{b_h}$ corresponding to D_{m+h}, with $h = 1, \cdots, N_{ISP}$. Then, we have a set of denominators $\{D_j^{a_j}\}_{j=1,\cdots,N_{sp}}$ with $a_j \in \mathbb{Z}$, that allows us to write the l-loop Feynman integral as:

$$I(a_1, \cdots, a_{N_{sp}}) = \int \prod_{i=1}^{l} \mathcal{D}k_i \frac{1}{\prod_{j=1}^{N_{sp}} D_j^{a_j}}, \quad a_j \in \mathbb{Z}. \tag{5.13}$$

We refer to integrals of this form as *scalar integral families* or *topologies*.

Given the correspondence between Feynman diagrams and integrals, we will associate scalar integrals, regardless of the spinor structure and color, with the same denominators but with different indices $a = (a_1, \cdots, a_{N_{sp}})$ to the same topology.

We refer to *sub-topologies* as the set of integrals with the same denominators as the reference topology but with indices $a_j = 0$ for $j = 1, \cdots, N_{sp}$. For a set of indices $a = (a_1, \cdots, a_{N_{sp}})$ we can define $\theta(a) = \left(\Theta\left(a_1 - \frac{1}{2}\right), \cdots, \Theta\left(a_{N_{sp}} - \frac{1}{2}\right)\right)$, where $\Theta(x)$ denotes the Heaviside step function and we subtract $\frac{1}{2}$ in order to avoid problem for $\Theta(x = 0)$:

$$\Theta(x) = \begin{cases} 0 & \text{se } x < 0 \\ 1 & \text{se } x > 0 \end{cases} \longrightarrow \Theta\left(x - \frac{1}{2}\right) = \begin{cases} 0 & \text{se } x < \frac{1}{2} \\ 1 & \text{se } x \geq \frac{1}{2}. \end{cases} \tag{5.14}$$

We define a *sector* as the set of integrals of a family that share a subset of propagators raised to positive powers. Given an integral family $I(a_1, \cdots, a_{N_{sp}})$, we say that two integrals within the same family belong to the same sector if we could define two set of indices A_1 and A_2 such that $\theta(A_1) = \theta(A_2)$. For a detailed review on multi-loop and multi-leg Feynman integrals see Ref. [80, 79, 81]

2.6 Integration-by-part identities

We have seen that Feynman integrals satisfy important properties in dimensional regularization. This allows us to greatly simplify the calculations of scattering amplitudes involving a large number of integrals depending on the number of scales and the number of loops.

Tkachov and Chetyrkin [82] were the first to find relations between integrals belonging to the same topology that allow to express such scalar integrals in terms of linear combinations of a finite basis of the so-called *master integrals* (MIs). The proof that the number of MIs is always finite took place many years later [83, 84]. It is important to stress that the choice of the basis is not unique and different choices are possible, however a correct choice involves notable simplifications in the computation of such integrals, as we will see later.

The crucial observation that allows us to derive the linear relations between the Feynman integrals is their invariance under linear shift of loop momenta:

$$k_i \to A_{ij}\, k_j \,+\, B_{im}\, p_m, \quad i,j = 1,\cdots,l,\;\; m = 1,\cdots,n, \tag{6.1}$$

where $\{k_i\}_{i=1,\cdots,l}$ are the loop momenta, $\{p_i\}_{i=1,\cdots,n}$ are the external momenta, A_{ij} are the elements of a $l\times l$ invertible matrix $\mathbb{A}$ with $|det(\mathbb{A})| = 1$ and B_{ij} are the elements of a $l \times n$ matrix $\mathbb{B}$.

For an infinitesimal transformation:

$$k_i \to k_i' = k_i + b_{ij}\, q_j, \qquad q_j \in \{k_1,\cdots,k_l,p_1,\cdots,p_n\}, \tag{6.2}$$

the generic l-loop integral transform in the following way:

$$\int \prod_{i=1}^{l} \mathcal{D}k_i \, \frac{\prod_{h=1}^{n_{ISP}} S_h^{b_h}}{\prod_{s=1}^{m} D_s^{a_s}} \to \int \prod_{i=1}^{l} \mathcal{D}k_i \left(1 \,+\, b_{ij}\left(\frac{\partial}{\partial k_i}\, q_j\right)\right) \frac{\prod_{h=1}^{n_{ISP}} S_h^{b_h}}{\prod_{s=1}^{m} D_s^{a_s}}. \tag{6.3}$$

It is possible in that way consider a set of operators [85]:

$$O_{ij} = \frac{\partial}{\partial k_i}\, q_j, \tag{6.4}$$

that form a closed algebra, i.e. the set of these operators under the operations defined within the algebra remains within the same algebra. These operators satisfy the commutation relation:

$$[O_{ij}, O_{kl}] = \delta_{il}\, O_{kj} \,-\, \delta_{kj}\, O_{il}. \tag{6.5}$$

Based on this symmetry observations and on the fact that the integrand vanish at the boundary of the manifold spanned by loop momenta and then the total derivative of any Feynman integrand must vanish as a generalization of the Gauss theorem in dimensional regularisation, we may define the general form of the so-called integration-by-part identities (IBPs):

$$\int \prod_{i=1}^{l} \mathcal{D}k_i \, O_{ij}\, \frac{\prod_{h=1}^{n_{ISP}} S_h^{b_h}}{\prod_{s=1}^{m} D_s^{a_s}} = 0. \tag{6.6}$$

Every Feynman integral within a topology satisfy a set of IBPs. The derivatives do not introduce any new denominator, so the relations are between integrals belonging to the same topology.

If we consider all the possible operators O_{ij} we have a total of IBPs given by:

$$N_{IBPs} = l(l+n), \tag{6.7}$$

where l is the number of loops and n in the number of independent external momenta. As example, we consider the massive one-loop bubble with different masses:

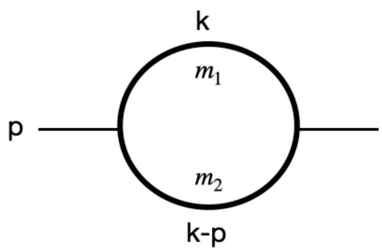

$$\longrightarrow\; I(a_1,a_2) \;=\; \int \mathcal{D}k\, \frac{1}{(k^2-m_1^2)^{a_1}\,((k-p)^2-m_2^2)^{a_2}}. \tag{6.8}$$

According to eq. (6.7), we can derive two IBPs obtained from:

$$\int \mathcal{D}k \, \frac{\partial}{\partial k} \left(k \, \frac{1}{(k^2 - m_1^2)^{a_1} \, ((k-p)^2 - m_2^2)^{a_2}} \right) = 0, \tag{6.9}$$

$$\int \mathcal{D}k \, p \, \frac{\partial}{\partial k} \left(\frac{1}{(k^2 - m_1^2)^{a_1} \, ((k-p)^2 - m_2^2)^{a_2}} \right) = 0. \tag{6.10}$$

From eq. (6.9) we obtain:

$$\begin{aligned}
&\int \mathcal{D}k \, \frac{\partial}{\partial k} \left(k \, \frac{1}{(k^2 - m_1^2)^{a_1} \, ((k-p)^2 - m_2^2)^{a_2}} \right) = d \int \mathcal{D}k \frac{1}{(k^2 - m_1^2)^{a_1} \, ((k-p)^2 - m_2^2)^{a_2}} \\
&- 2\, a_1 \int \mathcal{D}k \frac{k^2}{(k^2 - m_1^2)^{a_1+1} \, ((k-p)^2 - m_2^2)^{a_2}} \; - \; 2\, a_2 \int \mathcal{D}k \frac{k \cdot (k-p)}{(k^2 - m_1^2)^{a_1} \, ((k-p)^2 - m_2^2)^{a_2+1}} \\
&= d \int \mathcal{D}k \frac{1}{(k^2 - m_1^2)^{a_1} \, ((k-p)^2 - m_2^2)^{a_2}} \; - \; 2\, a_1 \int \mathcal{D}k \frac{1}{(k^2 - m_1^2)^{a_1} \, ((k-p)^2 - m_2^2)^{a_2}} \\
&- 2\, a_1 \int \mathcal{D}k \, \frac{m_1^2}{(k^2 - m_1^2)^{a_1+1} \, ((k-p)^2 - m_2^2)^{a_2}} \; - \; a_2 \int \mathcal{D}k \frac{1}{(k^2 - m_1^2)^{a_1-1} \, ((k-p)^2 - m_2^2)^{a_2+1}} \\
&- \; a_2 \int \mathcal{D}k \frac{1}{(k^2 - m_1^2)^{a_1} \, ((k-p)^2 - m_2^2)^{a_2}} \; - \; a_2 \int \mathcal{D}k \frac{m_1^2 \, + \, m_2^2}{(k^2 - m_1^2)^{a_1} \, ((k-p)^2 - m_2^2)^{a_2+1}} = 0,
\end{aligned} \tag{6.11}$$

and from eq. (6.10):

$$\begin{aligned}
&\int \mathcal{D}k \, p \, \frac{\partial}{\partial k} \left(\frac{1}{(k^2 - m_1^2)^{a_1} \, ((k-p)^2 - m_2^2)^{a_2}} \right) = -\, 2\, a_1 \int \mathcal{D}k \frac{p \cdot k}{(k^2 - m_1^2)^{a_1+1} \, ((k-p)^2 - m_2^2)^{a_2}} \\
&- \; 2\, a_2 \int \mathcal{D}k \frac{p \cdot (k-p)}{(k^2 - m_1^2)^{a_1} \, ((k-p)^2 - m_2^2)^{a_2+1}} = -\, a_1 \int \mathcal{D}k \frac{(m_2^2 \, - \, m_1^2)}{(k^2 - m_1^2)^{a_1+1} \, ((k-p)^2 - m_2^2)^{a_2}} \\
&- \; a_1 \int \mathcal{D}k \frac{1}{(k^2 - m_1^2)^{a_1} \, ((k-p)^2 - m_2^2)^{a_2}} \; + \; a_1 \int \mathcal{D}k \frac{1}{(k^2 - m_1^2)^{a_1+1} \, ((k-p)^2 - m_2^2)^{a_2-1}} \\
&- \; a_2 \int \mathcal{D}k \frac{(m_2^2 \, - \, m_1^2)}{(k^2 - m_1^2)^{a_1} \, ((k-p)^2 - m_2^2)^{a_2+1}} \; - \; a_2 \int \mathcal{D}k \frac{1}{(k^2 - m_1^2)^{a_1-1} \, ((k-p)^2 - m_2^2)^{a_2+1}} \\
&+ \; a_2 \int \mathcal{D}k \frac{1}{(k^2 - m_1^2)^{a_1} \, ((k-p)^2 - m_2^2)^{a_2}} = 0,
\end{aligned} \tag{6.12}$$

where we used the following relations to rewrite the scalar products at the numerators in terms of denominators:

$$\begin{aligned}
&2\, k \cdot (k-p) \; = \; (k^2 \, - \, m_1^2) \, + \, ((k-p)^2 \, - \, m_2^2) \, + \, m_1^2 \, + \, m_2^2, \\
&2\, p \cdot k = (m_2^2 \, - \, m_1^2) \, + \, (k^2 \, - \, m_1^2) \, - \, ((k-p)^2 \, - \, m_2^2), \\
&2\, p \cdot (k \, - \, p) = (m_2^2 \, - \, m_1^2) \, + \, (k^2 \, - \, m_1^2) \, - \, ((k-p)^2 \, - \, m_2^2).
\end{aligned} \tag{6.13}$$

Then, for the one-loop bubble integral with different masses we have the following IBPs:

- **First IBP:**

$$\begin{aligned}
&(d \, - \, 2\, a_1 \, - \, a_2) \, I(a_1, a_2) \; - \; 2\, a_1 \, m_1^2 \, I(a_1 + 1, a_2) \; - \; a_2 \, I(a_1 - 1, a_2 + 1) \\
&- \; a_2 \, (m_1^2 \, + \, m_2^2) \, I(a_1, a_2 + 1) = 0,
\end{aligned} \tag{6.14}$$

- **Second IBP:**

$$
\begin{aligned}
&(a_2 - a_1)\, I(a_1, a_2) - a_1\, (m_2^2 - m_1^2)\, I(a_1+1, a_2) + a_1\, I(a_1+1, a_2-1) \\
&- a_2\, (m_2^2 - m_1^2)\, I(a_1, a_2+1) - a_2\, I(a_1-1, a_2+1) = 0.
\end{aligned}
\tag{6.15}
$$

By solving these two equations we obtain the minimum set of MIs with which we can express any integral of the form (a) as a linear combination of them.

It's important to stress that, in general, the coefficients of the linear combinations are rational function that depend on the scales and on the dimensional regulator.

2.7 Lorentz invariance identities

In QFT the physical observables must be Lorentz invariants. This implies that they don't depend on the reference system choice, but on the intrinsic properties of the system. Since we are dealing with scattering amplitudes composed by Feynman integrals, the latter must be Lorentz invariants. This implies a further set of relations [86], that are used in order to perform the reduction to a finite set of integrals.

Consider an infinitesimal Lorentz transformation:

$$\Lambda^\mu_\nu = \delta^\mu_\nu + \delta\omega^\mu_\nu, \tag{7.1}$$

where δ^μ_ν is an infinitesimal antisymmetric tensor:

$$\delta\omega^\mu_\nu = -\delta\omega^\nu_\mu. \tag{7.2}$$

We can apply a Lorentz transformation to one of the external momenta p_i^μ, where $i = 1, \cdots, n$ being n the number of independent external momenta. This introduce a transformed momentum $p_i^{\mu\,\prime}$:

$$p_i^{\mu\,\prime} = \Lambda^\mu_\nu\, p_i^\nu = p_i^\mu + \delta\omega^\mu_\nu\, p_i^\nu. \tag{7.3}$$

At the integral level:

$$I(p_i) = I(p_i^{'}) = I(p_i) + \delta\omega^\mu_\nu \sum_{i=1}^{n} p_i^\nu \frac{\partial}{\partial p_i^\mu} I(p_i). \tag{7.4}$$

eq. (7.2) implies that:

$$\sum_{i=1}^{n} \left(p_i^\nu \frac{\partial}{\partial p_i^\mu} - p_i^\mu \frac{\partial}{\partial p_i^\nu} \right) I(p_i) = 0. \tag{7.5}$$

LIs can be found by contracting eq. (7.5) with the antisymmetric tensor $\omega^{\mu\nu}$ obtained from antisymmetric combinations of external momenta. The number of LIs between Feynman integrals is given by:

$$N_{LIs} = \frac{1}{2}\, n(n-1), \tag{7.6}$$

connected to the number of independent scalar products $p_i\, p_j$ with $i \neq j,\ i, j = 1, \cdots, n$.

As examples we can consider the massive bubble and the massive triangle integrals.

- **Massive bubble**

  From eq. (7.6) it is clear that the number of LIs depend on the number of external independent momenta. In this case there is only one external momenta p, then the number of LIs is zero:

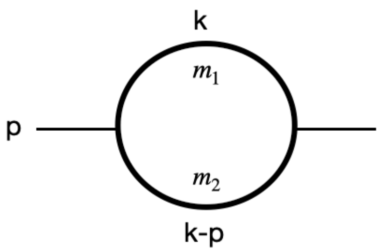

$$\longrightarrow \quad N_{LIs} = 0. \tag{7.7}$$

- **Massive triangle**

  In the case of a three-point integral the situation is different. It's important to notice that the LIs depend only on the external momenta and no on the other scales as masses. Then, the result is equal to the massless case:

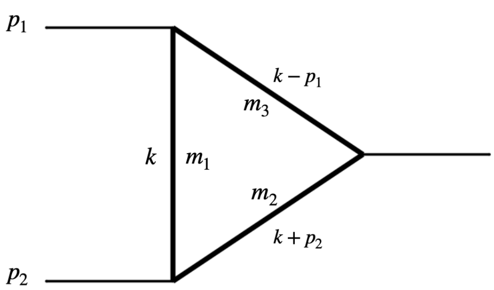

$$\longrightarrow \quad N_{LIs} = 1, \tag{7.8}$$

  because there are two independent external momenta p_1^μ and p_2^μ. In this case the LIs reads:

$$(p_1^\mu p_2^\nu - p_1^\nu p_2^\mu) \sum_{i=1}^{2} \left(p_i^\nu \frac{\partial}{\partial p_i^\mu} - p_i^\mu \frac{\partial}{\partial p_i^\nu} \right) I(p_i) = 0. \tag{7.9}$$

Derivatives of the Feynman integrals with respect to external momenta (and also loop momenta) does not introduce new denominators, then it is always possible to obtain as a result a linear combination of IBPs [85].

The LIs introduce important relations between scalar integrals that can be used to simplify the reduction process to MIs. For this reason, the LIs are implemented in different softwares.

2.8 Laporta algorithm

Solving IBPs to find the minimal set of MIs is a challenging task and it is often still a bottleneck in scattering amplitudes computations. The number of IBPs according to eq. (6.7) depends on the number of loops and independent external momenta and if we consider the IBPs for a system containing all the integrals in a given family we might have to deal with an excessive number of relations to solve. Furthermore, for processes involving a high number of scales, and consequently of scalar products, the complexity of the coefficients in the IBPs represents a problem also from the computational point of view that is not

always solvable. A procedure for finding MIs is the Laporta algorithm [87], which is based on ordering the integrals and selecting those with less complexity, according to certain criteria, so as to be able to write a simplified system of IBPs and subsequently solve it using linear algebra methods such as Gaussian elimination.
In eq. (5.13) we defined the l-loop Feynman integral $I(a_1, \cdots, a_{N_{sp}})$ with a set of denominators $\{D_j^{a_j}\}_{j=1,\cdots,N_{sp}}$ with $a_j \in \mathbb{Z}$. Following the definition of sector and the map from $a = (a_1, \cdots, a_{N_{sp}})$ to $\theta(a) = \left(\Theta\left(a_1 - \frac{1}{2}\right), \cdots, \Theta\left(a_{N_{sp}} - \frac{1}{2}\right)\right)$, we can label different sectors assigning them a sector identity, i.e. a number between 0 and $2^{N_{sp}} - 1$:

$$S_{id} = \sum_{j=1}^{N_{sp}} 2^{j-1}\, \Theta\left(a_j - \frac{1}{2}\right). \tag{8.1}$$

In order to separate the set with only positive powers from the negative, we start by counting the number of different propagators of integrals within a sector:

$$t = \sum_{j=1}^{N_{sp}} \Theta\left(a_j - \frac{1}{2}\right). \tag{8.2}$$

Then, we can define the variable r as the sum of the positive indices to which the propagators are raised:

$$r = \sum_{j=1}^{N_{sp}} a_j\, \Theta\left(a_j - \frac{1}{2}\right), \tag{8.3}$$

and the variable s similarly for negative powers of the propagators:

$$s = \sum_{j=1}^{N_{sp}} |a_j|\, \Theta\left(-a_j + \frac{1}{2}\right). \tag{8.4}$$

To assign to each integral an order of complexity we can represent them as a list of integers $(t, S_{id}, r, s, \cdots)$ and then ordered lexicographically with respect to this tuple. We identify as simpler the integrals with a smaller t, then we consider in the set with equal t the integrals with smaller S_{id} and so on also for r and s, and eventually for other variables denoted by the dots.
After sorting the integrals and thus selecting only the simplest ones, according to the criteria previously established, a set of linear equations is obtained through IBPs and LIs, which is significantly simplified compared to the full system. At this point, it is possible to use the Gaussian elimination method, which allows for solving the system thus obtained. In this way, it is possible to find the solution of the integrals in terms of the minimal set of MIs. For a detailed review see Ref. [79]. The algorithm is implemented in many programs and packages as `Kira` [88, 89], `LiteRed` [90, 91], `Reduze` [92, 93], `FIRE` [94, 95].

2.9 Differential equations method for Feynman integrals

Dimensionally regulated Feynman integrals can be reduced, through IBPs, to a minimal set of integrals, the so-called master integrals (MIs). Once the basis has been found, a method to evaluate them must be determined. One possibility is the direct integration, for example, using Feynman parametrization to express the integrand in terms of Symanzik polynomials. In this section we introduce the method of differential equations (DEs) for computing Feynman integrals. MIs satisfies a system of first-order linear DEs with

respect to the kinematic invariants. By solving this system, we may derive an analytic expression for the integrals basis. We discuss how, with a rotation of the initial basis, it is possible to obtain an ϵ-factorised form for the system of DEs, where the dimensional regulator ϵ is factored out from the kinematics. If this form is reached, the system could be solved as an expansion for small values of ϵ in terms of Chen iterated integrals [96]. We introduce the canonical basis for the integrals, which fulfil a particular case of this ϵ-factorised form. Several methods have been developed to express the MIs in canonical form. When possible, an analytical solution can be found, order-by-order in ϵ, in terms of Goncharov polylogarithms [97, 98, 99]. There is no general algorithm that guarantees obtaining such a form in all cases. The situation becomes extremely complex when the integrals are defined over elliptic curves or even more complicated varieties. It is therefore crucial to understand the mathematical structure of Feynman integrals, and this, as we will see, is directly related to the computation of the DEs.
The DEs method was introduced for the first time by Kotikov [100], where the Feynman integrals were differentiated with respect to the internal masses, and subsequently the generalization with respect to the external invariants was introduced by Remiddi [101] and Gehrmann and Remiddi [86].
To illustrate the method, we begin by considering the derivatives with respect to an internal mass squared m_s^2. Consider a set of N MIs $\underline{\mathcal{J}}(\underline{x},\epsilon) = \{\mathcal{J}_n(\underline{x},\epsilon)\}_{n=1,\cdots,N}$ for the scalar integral families involved in the computation of a scattering amplitude. The MIs depend on the set of scales $\underline{x}$, defined in eq. (5.8), and on the dimensional regulator ϵ. Considering one MI from the basis, the derivative with rspect to an internal mass squared m_s^2 becomes:

$$\partial_{m_s^2}\mathcal{J}_n(\underline{x},\epsilon) = \int \prod_{i=1}^{l} \mathcal{D}k_i\, \partial_{m_s^2} \frac{1}{\prod_{j=1}^{N_{sp}} D_j^{a_j}}. \tag{9.1}$$

The general structures of the denominators is given in eq. (5.4), being v_s a linear combination of loop and external momenta. If we assume that the internal mass m_s appears only in the s-th denominator:

$$\begin{aligned}\partial_{m_s^2}\mathcal{J}_n(\underline{x},\epsilon) &= \int \prod_{i=1}^{l} \mathcal{D}k_i\, \frac{1}{D_1^{a_1}} \cdots \partial_{m_s^2} \frac{1}{(v_s^2\, -\, m_s^2)^{a_s}} \cdots \frac{1}{D_{N_{sp}}^{a_{N_{sp}}}} \\ &= a_s \int \prod_{i=1}^{l} \mathcal{D}k_i\, \frac{1}{D_1^{a_1}} \cdots \frac{1}{(v_s^2\, -\, m_s^2)^{a_{s+1}}} \cdots \frac{1}{D_{N_{sp}}^{a_{N_{sp}}}}\end{aligned} \tag{9.2}$$

Through IBPs, LIs, and the symmetries of the problem, we are able to express a MI in terms of a linear combination of MIs within the same topology. Consequently, the derivatives of the MIs are linear combinations of the MIs, and the coefficients are generally rational functions that depend on the scales and on the dimensional regulator. In the internal mass case, the general structure of the differential equation for the basis of MIs is:

$$\partial_{m_k^2}\, \underline{\mathcal{J}}(\underline{x},\epsilon) = \mathbb{A}(\underline{x},\epsilon)\, \underline{\mathcal{J}}(\underline{x},\epsilon), \tag{9.3}$$

where, if the basis $\underline{\mathcal{J}}$ has length N, $\mathbb{A}$ is a $N \times N$ matrix.
Now, we can generalise in terms of all the scales from which the MIs depend [80]. As in the internal mass case, we can use IBPs in order to obtain a closed system of linear differential equations:

$$d\underline{\mathcal{J}}(\underline{x},\epsilon) = \mathbb{A}(\underline{x},\epsilon)\, \underline{\mathcal{J}}(\underline{x},\epsilon). \tag{9.4}$$

Here, d is the total differential, i.e. given the set of scales $\underline{x} = \{x_i\}$, it is given by:

$$d = \sum_{i=1} dx_i \, \partial_{x_i}. \tag{9.5}$$

$\mathbb{A}(\underline{x}, \epsilon)$ is the matrix of one-forms, and it should be stress that since the entries are obtained from IBPs they should be rational functions of $\underline{x}$ and ϵ. A detailed mathematical definition of one-forms and the wedge product is provided in Appendix A, as a foundation for what will follow in this section.
From the anti-symmetry of the wedge product it is clear that the total differential squared vanish:

$$\sum_{i=1} dx_i \, \partial_{x_i} \wedge \sum_{i=1} dx_i \, \partial_{x_i} = \sum_{i=1} \partial^2_{x_i} \left(dx_i \wedge dx_i \right) = 0. \tag{9.6}$$

Then, from eq. (9.4) and eq. (9.6), it follows that:

$$\begin{aligned} d^2 \underline{\mathcal{J}}(\underline{x}, \epsilon) \; = \; 0 \; = \; d(\mathbb{A}(\underline{x}, \epsilon) \, \underline{\mathcal{J}}(\underline{x}, \epsilon)) &= (d\mathbb{A}(\underline{x}, \epsilon)) \, \underline{\mathcal{J}}(\underline{x}, \epsilon) \; - \; \mathbb{A}(\underline{x}, \epsilon) \wedge d\underline{\mathcal{J}}(\underline{x}, \epsilon) \\ &= (d\mathbb{A}(\underline{x}, \epsilon)) \underline{\mathcal{J}}(\underline{x}, \epsilon) \; - \; \mathbb{A}(\underline{x}, \epsilon) \wedge \mathbb{A}(\underline{x}, \epsilon) \, \underline{\mathcal{J}}(\underline{x}, \epsilon), \end{aligned} \tag{9.7}$$

from which we obtain the so-called *integrability condition*:

$$d\mathbb{A}(\underline{x}, \epsilon) \; - \; \mathbb{A}(\underline{x}, \epsilon) \wedge \mathbb{A}(\underline{x}, \epsilon) = 0. \tag{9.8}$$

It is very important to stress that the choice of the MIs basis is not unique, and we can perform a rotation in order to pass from a basis to another one. If our starting basis is $\underline{\mathcal{J}} = \{\mathcal{J}_n\}_{n=1,\cdots,N}$ we can define a new basis $\underline{f} = \{f_n\}_{n=1,\cdots,N}$ defined by:

$$\underline{\mathcal{J}}(\underline{x}, \epsilon) = \mathbb{B}(\underline{x}, \epsilon) \, \underline{f}(\underline{x}, \epsilon), \tag{9.9}$$

where we refer to $\mathbb{B}(\underline{x}, \epsilon)$ as a rotation matrix. Then, we define a new system of linear differential equations:

$$d\underline{f}(\underline{x}, \epsilon) = \mathbb{A}^{'}(\underline{x}, \epsilon) \, \underline{f}(\underline{x}, \epsilon) \tag{9.10}$$

where the matrix $\mathbb{A}(\underline{x}, \epsilon)$ transforms as:

$$\mathbb{A}^{'}(\underline{x}, \epsilon) = \mathbb{B}^{-1}(\underline{x}, \epsilon) \, \mathbb{A}(\underline{x}, \epsilon) \, \mathbb{B}(\underline{x}, \epsilon) \; - \; \mathbb{B}^{-1}(\underline{x}, \epsilon) \, d\mathbb{B}(\underline{x}, \epsilon). \tag{9.11}$$

2.10 ϵ-factorised form

In the previous section, we saw that given a set of MIs, it is possible to derive a closed set of first-order linear differential equations. Once the system is written, a method is needed to solve it and obtain an analytical solution for the MIs. The general solution is very complicated and often constitutes the most difficult part of the calculations due to the presence of complex mathematical structures. The choice of the initial basis of MIs is very important, and it is possible to perform a rotation to work with a different basis. In this section, we will see that if it is possible to find a rotation that allows factoring out the dimensional regulator from the matrix of differential equations, a simpler form is obtained, and in such a case, an analytical solution can be achieved in terms of Chen iterated integrals.

Henn [102, 103] showed that through a change of basis with algebraic coefficients, it is possible to find a transformation of the form in eq. (9.11) such that the dependence on ϵ is factorised out:

$$\mathbb{A}^{'}(\underline{x}, \epsilon) = \epsilon\, \tilde{\mathbb{A}}(\underline{x}). \tag{10.1}$$

Through this rotation, we obtain a new system of MIs, and the system of differential equations takes on a simplified form, the so-called *ϵ-factorised form*:

$$d\underline{f}(\underline{x}, \epsilon) = \epsilon\, \tilde{\mathbb{A}}(\underline{x})\, \underline{f}(\underline{x}, \epsilon). \tag{10.2}$$

In this case it is possible to obtain a formal solution in terms of Chen iterated integrals:

$$\underline{f}(\underline{x}, \epsilon) = \mathbb{P}\, \exp\left(\epsilon \int_{\underline{x}_0}^{\underline{x}} \tilde{\mathbb{A}}(\underline{x}^{'})\right) \underline{f}(\underline{x}_0, \epsilon), \tag{10.3}$$

where $\mathbb{P}$ stands for the path-ordered exponential, $\underline{f}(\underline{x}_0, \epsilon)$ is the initial conditions vector, i.e. the MIs are evaluated in a boundary point $\underline{x}_0$ and the value in that point it is assumed to be know. The integral is between a path γ connecting the boundary point with another one.

We can notice that the structure of eq. (9.4) is similar to the equation of the parallel transport for a vector $V = V^{\mu}\, \partial_{\mu}$:

$$dV^{\mu} + \omega^{\mu}_{\nu}\, V^{\nu} = 0, \tag{10.4}$$

where ω^{μ}_{ν} are the one-forms of the gauge connection matrix. Consequently, we can interpret $\mathbb{A}$ as a gauge connection and we can relate the integrability condition to the curvature two-form:

$$F = d\mathbb{A} - \mathbb{A} \wedge \mathbb{A}. \tag{10.5}$$

Through eq. (9.8) we notice that the space is flat, and consequently, through the connection with parallel transport, we have homotopy invariance, meaning the integral depends only on the initial and final points and not on the specific curve connecting the two points. In Fig. 2.10.3 we can see different path connecting the boundary point $\underline{x}_0$ and the point $\underline{x}$, but we have the invariance with respect to the path.

The formal solution in terms of Chen iterated integrals in eq. (10.3) is usefuls for the computation of the MIs. The integration kernels are given by the entries of the matrix $\tilde{\mathbb{A}}$, then a simplified choice of the initial basis can simplify the problem. The solution can be obtained by expanding the MIs in a Laurent series around $\epsilon = 0$. Since we are working in DR, we are only interested in the first few Laurent coefficients and do not need the full dependence on the dimensional regulator. We have seen that in DR the singularities are expressed in terms of poles in ϵ, thus if k_m is the degree of divergence, i.e. $\underline{f}^{k_m}(\underline{x})$ is the leading pole, we can express the MIs as a Laurent series:

$$\underline{f}(\underline{x}, \epsilon) = \sum_{k=k_m}^{\infty} \underline{f}^{k}(\underline{x})\, \epsilon^{k}, \tag{10.6}$$

where the vector of coefficients $\underline{f}^{k}(\underline{x})$ of the ϵ-expansion at the order k is said to have weight k.

We can always multiply out the highest pole in ϵ or generally choose a normalization such that the MIs becomes finite in the limit $\epsilon \to 0$. We pass from a Laurent series to a Taylor series around $\epsilon = 0$:

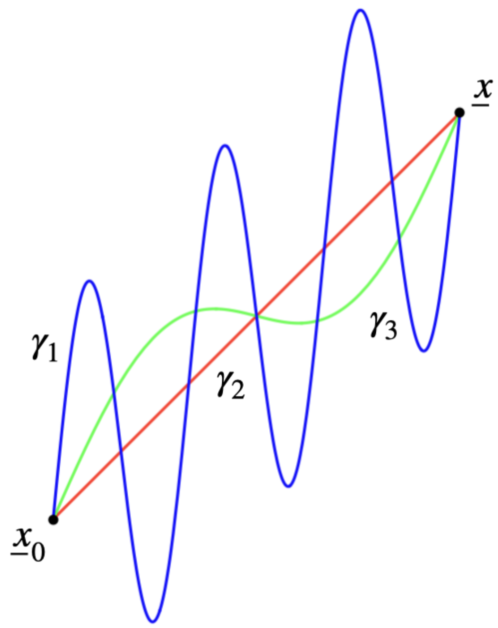

Figure 2.10.3. Three curves γ_1 (blue), γ_2 (red) and γ_3 (green) connecting the point $\underline{x}_0$, in which we compute the boundary conditions, with the point $\underline{x}$.

$$\underline{f}(\underline{x},\epsilon) = \sum_{k=k_m}^{\infty} \underline{f}^k(\underline{x})\,\epsilon^k \quad\longrightarrow\quad \underline{f}(\underline{x},\epsilon) = \sum_{k=0}^{\infty} \underline{f}^k(\underline{x})\,\epsilon^k. \tag{10.7}$$

As a consequence of the homotopy invariance, we are free to choose the path. We can parametrize the curve γ:

$$\gamma(\lambda)\;:\lambda\in[0,\,1]\quad \lambda\mapsto\{x_1(\lambda),...,x_n(\lambda)\},\quad \text{with}\quad \begin{cases}\gamma(0)=\underline{x}_0\\ \gamma(1)=\underline{x}\end{cases} \tag{10.8}$$

Plugging the Taylor expansion in eq. (10.3) we obtain:

$$\begin{aligned}\underline{f}(\underline{x},\epsilon) &= \underline{f}\,(\gamma(0)) + \sum_{k=1}^{\infty}\epsilon^k\sum_{i=1}^{k}\int_0^1\gamma^\star\left(d\tilde{\mathbb{A}}(\lambda_1)\right)\int_0^{\lambda_1}\gamma^\star\left(d\tilde{\mathbb{A}}(\lambda_2)\right)\cdots\int_0^{\lambda_{i-1}}\gamma^\star\left(d\tilde{\mathbb{A}}(\lambda_i)\right)\\ &\times\underline{f}^{k-i}\,(\gamma(0)) \;=\; \underline{f}\,(\gamma(0)) + \sum_{k=1}^{\infty}\epsilon^k\sum_{i=1}^{k}\int_0^1\gamma^\star\omega_1\int_0^{\lambda_1}\gamma^\star\,\omega_2\cdots\int_0^{\lambda_{i-1}}\gamma^\star\omega_i\\ &\times\underline{f}^{k-i}\,(\gamma(0))\,,\end{aligned} \tag{10.9}$$

where $\gamma(0)$ corresponds to the boundary point $\underline{x}_0$ and $\{\omega_i\}_{i=1,\cdots,N}$ is the set of differential one-forms defined by eq. (0.5). We denoted by $\gamma^\star\omega_i$ the pull-back of ω_i along the curve γ:

$$\gamma^\star\omega_i = \omega(\gamma(\lambda_i))\left(\frac{d\gamma(\lambda_i)}{d\lambda_i}\right), \tag{10.10}$$

and by $\gamma^\star\,(d\mathbb{A}(\lambda_i))$ the pull-back of the matrix $\mathbb{A}$ along the curve γ, i.e. the pull-back is applied to each entry of the matrix individually.

2.11 Multiple polylogarithms

In the computation of Feynman integrals, in dimensional regularisation, a vast array of different functions can appear in their analytical expression. The integral defined in eq. (5.13) is a meromorphic function of ϵ, i.e. it has at most poles in ϵ but no branch cuts. In general, we are interested in the Laurent expansion of $I(a_1, \cdots, a_{N_{sp}})$ around $\epsilon = 0$. The mathematical structure of the Laurent series coefficients is extensive and complex and it involves different kind of functions.
It's easy to see that also in the easiest Feynman integral, i.e. the one-loop two-point integral, the analytic expression involves different functions:

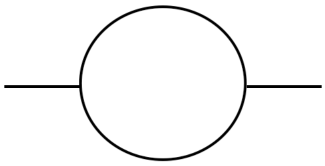

$$= \int e^{\epsilon\gamma_E} \frac{d^d k}{i\pi^{d/2}} \frac{1}{k^2(k+p)^2} = \frac{1}{\epsilon} + 2 - \log(-p^2)$$
$$+ \epsilon\left(\frac{1}{2}\log^2(-p^2) - 2\log(-p^2) - \frac{1}{2}\zeta(2) + 4\right) + \mathcal{O}(\epsilon^2), \tag{11.1}$$

since there are logarithms and $\zeta(2) = \frac{\pi^2}{6}$, i.e. the Riemann ζ function:

$$\zeta(s) = \sum_{n\geq 1} \frac{1}{n^s}. \tag{11.2}$$

Already going to the three-point integral there is a new function, the classical polylogarithm [104], defined for $s \geq 2$ as:

$$Li_s(z) = \int_0^z Li_{s-1}(t)\frac{dt}{t} = \int_0^z \frac{dt_1}{t_1} \cdots \int_0^{t_{s-2}} \frac{dt_{s-1}}{t_{s-1}} \int_0^{t_{s-1}} \frac{dt_s}{1-t_s}, \tag{11.3}$$

where each integral is taken along a path within the unit circle, extending from the lower limit of integration to the upper limit and the recursion start with the ordinary logarithm:

$$Li_1(z) = -\log(1-z). \tag{11.4}$$

For $\underline{s} = \{s_i\}_{i=1,\cdots,k}$ we can define the differential forms:

$$\omega_{\underline{s}}(t) = \omega_0^{s-1}(t)\,\omega_1(t)\,\cdots\,\omega_0^{s_k-1}(t)\,\omega_1(t), \tag{11.5}$$

where:

$$\begin{aligned} \omega_0(t) &= \frac{dt}{t}, \\ \omega_1(t) &= \frac{dt}{1-t}. \end{aligned} \tag{11.6}$$

Then:

$$Li_{\underline{s}}(z) = \int_0^z \omega_{\underline{s}}. \tag{11.7}$$

In multi-loop and multi-leg computations there are further generalisations of the classical polylogarithms, defined in eq.(11.3), and even much more complicated structures [105].
Multiple polylogarithms in several variables are defined by:

$$Li_{(s_1,\cdots,s_k)}(z_1,\cdots,z_k)=\sum_{n_1>n_2>\cdots>n_k\geq 1}\frac{z_1^{n_1}\cdots z_k^{n_k}}{n_1^{s_1}\cdots n_k^{s_k}}, \tag{11.8}$$

for $s_i \geq 1$ and $\mid z_i \mid< 1$, $i=1,\cdots,k$. For a detailed review, see Ref. [106].
Feynman integrals involving loops and Feynman diagrams often lead to expressions involving multiple polylogarithms with variables that depend on the masses of the particles and their configurations. In particular, Goncharov polylogarithms are defined as multiple polylogarithms (MPLs) [97, 98] defined recursively in terms of Chen iterated integrals for $n \geq 0$

$$G(a_1,\cdots,a_n;z)=\int_0^z \frac{dt}{t-a_1}G(a_2,\cdots,a_n;t), \tag{11.9}$$

where $a_i \in \mathbb{C}$ for $i=1,\cdots,n$, $z\in\mathbb{C}$ and the recursion start with $G(z)=G(;z)=1$. The vector $\underline{a}=(a_1,\cdots,a_n)$ is called the weight vector and its elements are called indices, while z is the argument of the MPLs. The number n of indices, which coincides with the number of iterated integrals, is called the weight of the MPLs, but it is also often referred to as a degree of transcendentality.
If all the indices are equal to zero, we define a regularised version of the MPLs:

$$G(\underline{0}_n;z)=\frac{1}{n!}\log^n z, \tag{11.10}$$

by regularising the logarithm:

$$\log z=\int_1^z \frac{dt}{t}. \tag{11.11}$$

The definitions of MPLs in eq.(11.8) and in eq.(11.9) are related by:

$$Li_{(s_1,\cdots,s_k)}(z_1,\cdots,z_k)=(-1)^k\,G(\underline{0}_{n_k-1},\frac{1}{x_k},\cdots,\underline{0}_{n_1-1},\frac{1}{z_1\cdots z_k};1). \tag{11.12}$$

In the special case in which all the indices are the same, grouped for simplicity in the vector $\underline{a}_n$, we have:

$$G(\underline{a}_n;z)=\frac{1}{n!}\log^n\left(1-\frac{z}{a}\right). \tag{11.13}$$

These cases show how MPLs are related to ordinary logarithms and multiple polylogarithms written in terms of nested sums. For a detailed review of MPLs, see Ref. [107, 108, 105]. MPLs satisfy very important properties, among these the relavant ones are:

- **Invariance under rescaling**

  For $\{a_i\}_{i=1,\cdots,n}$ with $a_n\neq 0$ and for $k\in\mathbb{C}$:

$$G(k\,a_1,\cdots,k\,a_n;k\,z)=G(a_1,\cdots,a_n;z). \tag{11.14}$$

- **Hölder convolution**

  For $a_1\neq 1$ and $a_n\neq 0$, $\forall\,p\in\mathbb{C}$:

$$G(a_1,\cdots,a_n;1)=\sum_{k=0}^{n}(-1)^k G\left(1-a_k,\cdots,1-a_1;1-\frac{1}{p}\right)G\left(a_{k+1},\cdots,a_n;\frac{1}{p}\right). \tag{11.15}$$

- **Shuffle relations**

  MPLs form a shuffle algebra, which allows us to express the product of two MPLs defined with the same integration limits in terms of linear combination of MPLs:

$$G(\underline{a}_1; z)\, G(\underline{a}_2; z) = \sum_{\underline{a}=\underline{a}_1 \sqcup\!\sqcup\, \underline{a}_2} G(\underline{a}; z), \tag{11.16}$$

  where the sum runs over all the shuffles of $\underline{a}_1$ and $\underline{a}_2$, being the shuffles defined as the permutations that preserve the relative orderings. As an example we consider the product of two MPLs of length two:

$$\begin{aligned} G(a,b;z)\, G(c,d;z) = & \, G(a,b,c,d;z) + G(a,c,b,d;z) + G(c,a,b,d;z) \\ & + G(a,c,d,b;z) + G(c,a,d,b;z) + G(c,d,a,b;z). \end{aligned} \tag{11.17}$$

  This property is fundamental for MPLs, since define a shuffle algebra, i.e. a vector space whose multiplication rule is defined by the shuffle product. Moreover, this algebra is graded, since the shuffle product preserves the weight of the MPLs. Then, if we denote with $\mathcal{A}$ the algebra generated by the MPLs, it can be written as a direct sum:

$$\mathcal{A} = \bigoplus_{k=0}^{\infty} \mathcal{A}_k, \tag{11.18}$$

  such that:

$$\mathcal{A}_h \sqcup\!\sqcup\, \mathcal{A}_g \subseteq \mathcal{A}_{h+g}, \tag{11.19}$$

  for non negative integers h and g.

- **Weight drop under differentiation**

  The algebra $\mathcal{A}$ for MPLs is closed under differentiation and integration. In particular, it is well known that MPLs satisfy a differential equation of the form:

$$dG(a_1, \cdots, a_n; z) = \sum_{k=1}^{n} G(a_1, \cdots, a_{k-1}, a_{k+1}, \cdots, a_n; z)\, d\log\left(\frac{a_{k-1} - a_k}{a_{k+1} - a_k}\right), \tag{11.20}$$

  where $a_{n+1} = z$ and the weigth drop is due to the lack of a_k inside the MPL. This is very important, since any MPLs up to weight three can be always written in terms of classical polylogarithms. Then, after differentiation the computation of MPLs become simpler and after differentiating iteratively a sufficient number of times we obtain rational functions.

2.11.1 MPLs and pure functions

MPLs are defined as iterated integrals of rational functions, with at most simple poles, over the punctured Riemann sphere. From eq. (11.9) it follows immediately that we have an n-fold integral:

$$G(a_1, \cdots, a_n; z) = \int_0^z \frac{dt_1}{t_1 - a_1} \int_0^{t_1} \frac{dt_2}{t_2 - a_2} \cdots \int_0^{t_{n-1}} \frac{dt_n}{t_n - a_n}. \tag{11.21}$$

We have already discussed the transcendental weight of MPLs, which coincides with the number of integrations. Thanks to eq. (11.20), we have that MPLs satisfy inhomogeneous unipotent DEs, where the transcendetal weight is decreased by one. MPLs are the perfect example of *pure functions* [109]. In particular we can define a pure integral as an integral with all non-vanishing residues equals up to a sign. A pure function of weight n is defined such that its total differential can be written in terms of other pure functions but witht transcendetal weight reduced by one. From how MPLs have been defined, it is evident that they are pure functions. For a review of pure functions in the context of scattering amplitudes see Ref. [110, 111].

2.12 Canonical logarithmic form

It has been conjectured [102] that there exists a rotation as in eq. (9.9) such that a particular form of the differential equations is obtained, in which ϵ is factored out from the matrix of one-forms. A particular form is reached if these one-forms have at most logarithmic singularities, i.e., the entries of the connection matrix can be written as a $\mathbb{Q}$-linear combination of logarithms:

$$\tilde{\mathbb{A}}(\underline{x}) = \sum_i \tilde{A}_i \, d\log\left(\alpha_i(\underline{x})\right), \tag{12.1}$$

where $\tilde{A}_i$ are constant matrices with $\mathbb{Q}$-coefficients and $\alpha_i(\underline{x})$ are algebraic functions of the scales called *letters*. The set $\{\alpha_i\}$ of letters is called *alphabet*. We refer to this case as *canonical logarithmic form*.

In this case the system of DEs can be written as:

$$d\underline{f}(\underline{x}, \epsilon) = \epsilon \sum_i \tilde{A}_i \frac{\sum_j dx_j}{\sum_j x_j - a_{ij}} \underline{f}(\underline{x}, \epsilon). \tag{12.2}$$

2.13 Integration kernels and geometry - MPLs case

In this section we want to discuss the deep connection and the relations between the one-forms and the space of functions on which the Feynman integrals are defined. The complexity of Feynman integrals is strictly connected to the geometry of the underlying Feynman diagrams. The Landau equations, that characterize the singularities of Feynman integrals, could define the associated algebraic varieties interpreted as Riemann surfaces with a genus. Generally, for a connected, compact with no boundary surface S, the genus g is a non-negative integer defined in terms of the Euler characteristic $\chi(S)$:

$$g = 1 - \frac{1}{2}\chi(S), \tag{13.1}$$

where $\chi(S) = V - E + F$ is expressed in terms of the number of vertices, edges and faces of any polygonal decomposition of the surface. In Fig. 2.13.4 we show the sphere, the torus and the double-torus as example, respectively, of genus 0, genus 1 and genus 2 surfaces.

For a DEs system in ϵ-factorised form, through eq. (10.3), it is possible to find a solution for MIs in terms of iterated integrals. The structure of the iterated integrals depends on the integration kernels and specifically on the one-forms that characterize the DEs matrix.

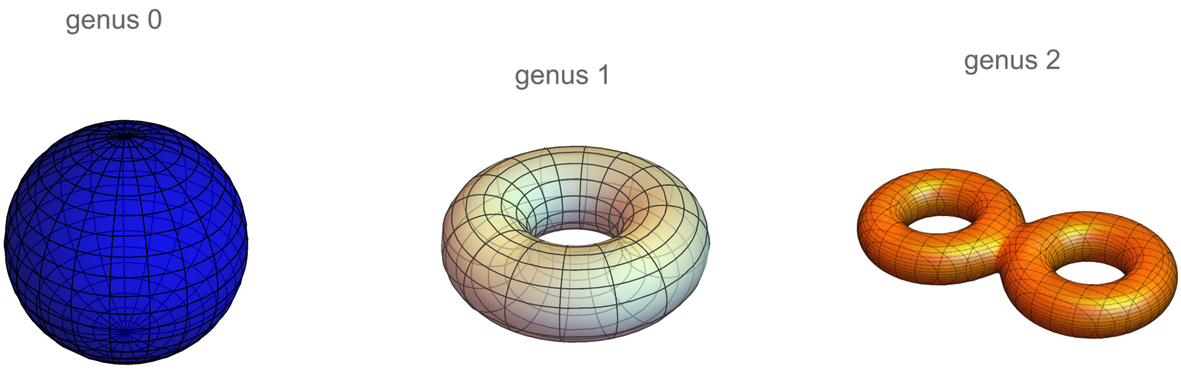

Figure 2.13.4. Genus 0, genus 1 and genus 2 Riemann surfaces.

Given a complex manifold M and a set of one-forms $\omega_1, \cdots, \omega_n \in \mathcal{A}^1(M)$, where $\mathcal{A}^1(M)$ is a $\mathbb{C}$-vector space of one-forms on M, the iterated integral of $\{\omega_i\}_{i=1,\cdots,n}$ along a path $\gamma : [0, 1] \to M$ is defined by:

$$\int_\gamma \omega_1 \cdots \omega_n = \int_{0 \leq t_1 \leq \cdots \leq t_n \leq 1} \gamma^\star \omega_1(t_1) \cdots \gamma^\star \omega_n(t_n). \tag{13.2}$$

For classical polylogarithms defined in eq. (11.3), we already discussed the integration kernels structures in terms of two possible holomorphic differentials. We want now to understand on which geometry MPLs are defined. MPLs given in eq. (11.9) are defined in terms of integration kernels $\frac{dt}{t-a_i}$ which are meromorphic functions with simple poles at $t = a_i$. For DEs in canonical logarithmic form, the DEs matrix is defined in eq. (12.1) in terms of dlog-forms. If we consider the differential one-forms:

$$\omega \in \{d\log(\alpha_i(x))\}, \tag{13.3}$$

the pull-back of ω in eq. 13.2 leads to exactly the same one-forms that define MPLs. These meromorphic functions are naturally defined over the simplest genus 0 Riemann surface, i.e. the Riemann sphere $\mathbb{C} \cup \{\infty\}$, specifically over the punctured Riemann sphere shown in Fig. 2.13.5.

Given the system of DEs satisfied by the MIs, whose analytical structure involves MPLs, the Laurent series expansion with respect to ϵ has an important property. In the canonical logarithmic case, eq. (10.3) reads:

$$\underline{f}(\underline{x}, \epsilon) = \mathbb{P}\mathrm{exp}\left(\epsilon \int_\gamma \sum_i \tilde{A}_i d\log(\alpha_i(\underline{x}'))\right) \underline{f}(\underline{x}_0, \epsilon), \tag{13.4}$$

where γ is any path connecting an initial point x_0 to another point x in which we want to compute the integrals. We can expand the MIs in Taylor series around $\epsilon = 0$ as in eq. (10.7). From the MPLs definition if the system satisfy a canonical logarithmic system of DEs, it follows that the expansion coefficients $\underline{f}^{(k)}(\underline{x})$ can be written as a linear combination of MPLs of transcendental weight k. In this case $\underline{f}(\underline{x}, \epsilon)$ is said to be pure and of *uniformal transcendental weight* (UT) [112, 102, 103].

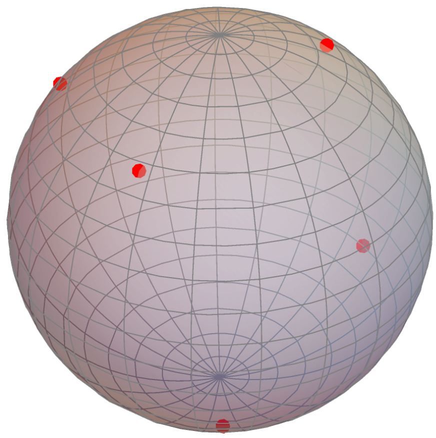

Figure 2.13.5. Punctured Riemann sphere. The red dots represent the singularities of the integration kernels.

2.14 Elliptic curves

We have discussed the presence of functions, beyond simple rational functions, that appear in the analytical calculations of Feynman integrals and that define their mathematical structure. In particular, we have seen that the mathematical structure is contained in the coefficients of the Laurent series for the MIs. We started from the simple one-loop calculation of the bubble integral in order to show the presence of the Riemann ζ-function toghether with logs, showing that adding just one more leg we obtain generalizations of logarithms, namely classical polylogarithms. Increasing the number of loops or external legs the situation becomes much more complicated. Of great importance in physics are the MPLs, since the calculation by iterated integrals is strictly connected to the one-forms obtainable from the differential equations system of the MIs. However, the story is not over because there is a vast array of more complicated structures involving much more complex geometries than the Riemann sphere on which MPLs are defined. There are plenty of examples of MIs whose analytic structures involves function beyond the MPLs. In this section we want to briefly introduce elliptic curves and the natural generalization of multiple polylogarithms in this case. For a review on elliptic curves and projective space see Ref. [79, 113].
In order to introduce the elliptic curves we need first to define projective spaces and algebraic curves.

- **Projective space:**

  Let V be a vector space over a field $\mathbb{K}$. The projective space of V is defined as $\mathbb{P}(V)$, that is the equivalence classes group of $V \setminus \{0\}$ with respect to the equivalence relation $\sim$ defined via $a \sim b$ that holds if and only if $a = \lambda\, b$ for some $\lambda \in \mathbb{K}^\star$, where $\mathbb{K}^\star$ is formally defined as $\mathbb{K}^\star = \mathbb{K} \setminus \{0\}$. This means that $\mathbb{P}(V)$ is the set of one-dimensional subspaces of V. Given $\mathbb{C}^{n+1}$, we can define the n-dimensional complex projective space $\mathbb{P}(\mathbb{C}^{n+1})$ as $\mathbb{P}^n(\mathbb{C})$. If $x = (x^0, \cdots, x^n) \in \mathbb{C}^{n+1} \setminus \{0\}$, we represents the projection

$[x] \in \mathbb{P}^n(\mathbb{C})$ with $[x^0 : \cdots : x^n]$. By definition in terms of equivalence classes:

$$[\lambda\, x^0 : \cdots : \lambda\, x^n] = [x^0 : \cdots : x^n] \qquad \forall\, \lambda \in \mathbb{C}^\star, \forall\, [x] \in \mathbb{P}^n(\mathbb{C}). \tag{14.1}$$

It's important to stress that $\mathbb{P}^n(\mathbb{C})$ is an n-dimensional manifold, so it's possible to define smooth functions between the local charts.

- **Algebraic curves:**

  We start by considering a polynomial function of degree d in the projective space $\mathbb{P}^n(\mathbb{C})$:

$$P(x_0, \cdots, x_n) = \sum_{i_0+\cdots+i_n=d} a_{i_0} \cdots a_{i_n}\, x_0^{i_0} \cdots x_n^{i_n}, \tag{14.2}$$

  and due to eq. (14.1):

$$P(\lambda\, x_0, \cdots, \lambda\, x_n) = \sum_{i_0+\cdots+i_n=d} a_{i_0} \cdots a_{i_n}\, \lambda^d\, x_0^{i_0} \cdots x_n^{i_n} \qquad \forall \lambda \in \mathbb{C}^\star. \tag{14.3}$$

  Then, for any polynomial $P \in \mathbb{P}^n(\mathbb{C})$ its zero locus is well defined :

$$V(S) = \{\underline{x} \in \mathbb{P}^n(\mathbb{C}) \,:\, P(\underline{x}) = 0\; \forall\, P \in S\} \subset \mathbb{P}^n(\mathbb{C}). \tag{14.4}$$

  Subset of $\mathbb{P}^n$ of this form are called projective varieties. An algebraic curve in the complex plane $\mathbb{P}^2(\mathbb{C})$ is defined as the zero locus of the homogeneous polynomial in the homogeneous coordinates denoted by x, y and z.

An *elliptic curve* is a smooth algebraic curve in $\mathbb{P}^2(\mathbb{C})$ of genus one with one marked point. For a smooth curves of degree d in the projective plane $\mathbb{P}^2$, the genus is expressed in terms of the associated polynomial degree as:

$$g = \frac{1}{2}(d-1)(d-2). \tag{14.5}$$

In general, for projective 2-dimensional plane over a field, it is possible to consider all points of the form $[x : y : 1]$, or $[x : 1 : z]$ or $[1 : y : z]$ and all the points with $z = 0$ lies on the line at infinity, defined by $[a : b : 0]$. For the elliptic curve we consider all the points as equivalence class of $[x : y : 1]$ and the marked point, that define an elliptic curve, as the point at infinity. The point at infinity for an elliptic curve is defined by $[0 : 1 : 0]$, but to understand this it is good to define the elliptic curve in the so-called Weierstrass form:

$$y^2\, z = x^3 + a\, x\, z + b\, z^3. \tag{14.6}$$

The line at infinity in this case if obtained by setting $z = 0$, then we obtain from eq. (14.6) that the solution correspond to $x^3 = 0$. Then we can consider as marked point the point at infinity at $[0 : 1 : 0]$.
The projective plane we are considering is defined for elliptic curves over $\mathbb{C}$, then as one complex dimension. It is well known the isomorphism:

$$\mathbb{C}^n \simeq \mathbb{R}^{2n}, \tag{14.7}$$

then we may consider real surfaces as two-dimensional real surfaces. This real surface is referred to as Riemann surface. We can explicitely see the isomorphism applied to an elliptic curve of the form:

$$y^2 = x^3 - 5x + 3, \tag{14.8}$$

represented in Fig. 2.14.6 for simplicity for real values of x and y. This elliptic curve is a complex one-dimensional smooth algebraic curve defined in $\mathbb{P}^n(\mathbb{C})$.

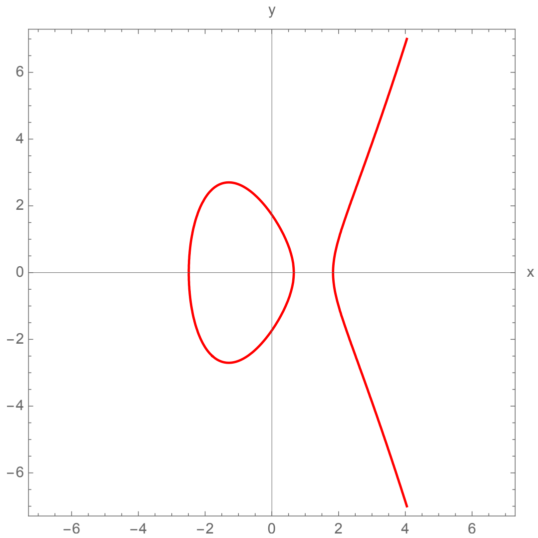

Figure 2.14.6. Elliptic curve $y^2 = x^3 - 5x + 3$ for real values of x and y.

The elliptic curve is defined with a marked point. Adding the point at infinity, we topologically obtain two circles for the curve represented in Fig. 2.14.6 and two more circles for the imaginary components in the general case. The real Riemann surface obtained is the genus one torus, represented in Fig. 2.14.7, where the red and yellow circles have been added to better understand the relationship with the elliptic curve for imaginary values of x and y.

If $f(z)$ is a holomorphic function which satisfies $f(z+c) = f(z)$ for $c \in \mathbb{C}$, we call f periodic with respect to c and c is defined as the period of f.

A function $f(z)$, $z \in \mathbb{C}$, is called instead doubly periodic if $\exists\, \varpi_0, \varpi_1 \in \mathbb{C}$, whose ratio is not purealy real, such that:

$$\begin{aligned} f(z+\varpi_0) &= f(z), \\ f(z+\varpi_1) &= f(z), \end{aligned} \tag{14.9}$$

$\forall z$. ϖ_0 and ϖ_1 are called the periods of f.

We can fix a complex number $\tau = \varpi_0/\varpi_1 \in \mathbb{C}$, such that $\mathfrak{Im}(\tau) > 0$, in order to define a lattice:

$$\Lambda_\tau = \{m + n\tau \;:\; m, n \in \mathbb{Z}\} \subset \mathbb{C}. \tag{14.10}$$

A function $f(z)$, $z \in \mathbb{C}$, is called doubly periodic with respect to Λ_τ if it is a meromorphic function $f : \mathbb{C} \to \mathbb{C}$ satisfying the condition:

$$f(z+c) = f(z) \quad \forall\, c \in \Lambda_\tau. \tag{14.11}$$

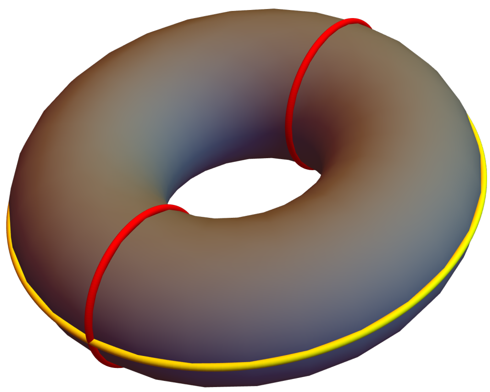

Figure 2.14.7. Real Riemann surface of genus one.

The only possibilities are:

$$\begin{aligned} f(z+1) &= f(z), \\ f(z+\tau) &= f(z), \end{aligned} \tag{14.12}$$

since any other points can be written by liner combination of 1 and τ that span the lattice Λ_τ. Then f has two independent periods, i.e. 1 and τ. We stress that this is exactly the same of considering the lattice spanned by the periods ϖ_0 and ϖ_1:

$$\Lambda_\varpi = \{m\varpi_0 + n\varpi_1 \, : \, m, n \in \mathbb{Z}\} \subset \mathbb{C}, \tag{14.13}$$

in which case the two periods are ϖ_0 and ϖ_1.
A doubly-periodic meromorphic function is called elliptic function. Elliptic functions can be viewed as meromorphic functions on $\mathbb{C} \setminus \Lambda_\tau$.
One of the most famous example of elliptic function is given by the Weierstrass $\wp$-function. Given a periodic lattice Λ_ϖ and $z \in \mathbb{C}$, it is defined by:

$$\wp(z) = \frac{1}{z^2} + \sum_{\varpi \in \Lambda_\varpi \{0\}} \left(\frac{1}{(z-\varpi)^2} - \frac{1}{\varpi^2} \right), \tag{14.14}$$

where the term $-\frac{1}{\varpi^2}$ is necessary for the convergence of the series. $\wp(z)$ is a meromorphic function with double poles at the lattice points, but with null residue.

Weierstrass $\wp$-function satisfies the differential equation:

$$\wp'(z)^2 = 4\,\wp(z)^3 - g_2\,\wp(z) - g_3, \tag{14.15}$$

where g_2 and g_3 are called lattice invariants and are defined by :

$$\begin{aligned} g_2 &= 60 \sum_{\varpi \in \Lambda_\varpi \setminus \{0\}} \varpi^{-4}, \\ g_3 &= 140 \sum_{\varpi \in \Lambda_\varpi \setminus \{0\}} \varpi^{-6}. \end{aligned} \tag{14.16}$$

In order to introduce the elliptic integrals, we follow the Abel procedure to compute the inverse function of the Weierstrass $\wp$-function.

Given the differential equations satisfied by $\wp(z)$ in eq. (14.15), since the derivative of the inverse function is:

$$(\wp^{-}1(\varpi))^{'} = \frac{1}{\wp'(\wp^{-1}(\varpi))}, \tag{14.17}$$

it follows that the inverse function is given by:

$$\wp^{-1}(\varpi) = \wp^{-1}(\varpi_x) + \int_{\varpi_x}^{\varpi} \frac{d\varpi}{\sqrt{4\varpi^3 - g_2\varpi - g_3}}. \tag{14.18}$$

It is possible to let $\varpi_x \to \infty$ to set $\wp^{-1}(\varpi_x)\Big|_{\varpi_x\to\infty} \to 0$. In this way we obtain that the inverse of the Weierstrass elliptic function is an elliptic integral:

$$\wp^{-}1(\varpi) = \int_{\infty}^{\varpi} \frac{d\varpi}{\sqrt{4\varpi^3 - g_2\varpi - g_3}}. \tag{14.19}$$

The generic classification in terms of elliptic integrals of the first, second or third kind depends on the so-called Abel differentials. Given a Riemann surface $\mathcal{M}$ with atlas $\{(U_\alpha, \varphi_\alpha)\}$, a complex differential one-form w is defined on each local chart $(U_\alpha, \varphi_\alpha)$ with local representation:

$$w = f_\alpha(z_\alpha)\, dz_\alpha, \tag{14.20}$$

where the poles of w are those of $f_\alpha(z_\alpha)$.

If $f_\alpha(z_\alpha)$ is a holomorphic function, then w is called an Abel differential of the first kind. Moreover, if $f_\alpha(z_\alpha)$ is a meromorphic function, it called Abel differential of the second kind if all its residues vanishes or Abel differential of the third kind if it has non vanishing residues.

An elliptic curve has one Abel differential of the first kind and it's possible to define the periods of the elliptic curve through its integration. We already discussed the representation of the elliptic curve as a genus one Riemann surface defined by $\mathbb{C} \setminus \Lambda_\tau$, i.e. a torus. From Fig. 2.14.8 we observe that there are two cycles γ_1 and γ_2, due to the isomorphism with the smooth complex algebraic curve. The periods are defined as the integral of the Abel differential of the first kind over the two independent cycles:

$$\begin{aligned} \varpi_0 &= \oint_{\gamma_1} w, \\ \varpi_1 &= \oint_{\gamma_2} w. \end{aligned} \tag{14.21}$$

In particular, given an elliptic curve as a cubic: $y^2 = (x - x_1)(x - x_2)(x - x_3)$ the holomorphic differential is given by $w = \frac{dx}{y}$. An elliptic curve may have other meromorphic differential, that we indicate here with w', and the integrals over the cycles define the quasi-periods:

$$\begin{aligned} \eta_1 &= \oint_{\gamma_1} w^{'}, \\ \eta_2 &= \oint_{\gamma_2} w^{'}. \end{aligned} \tag{14.22}$$

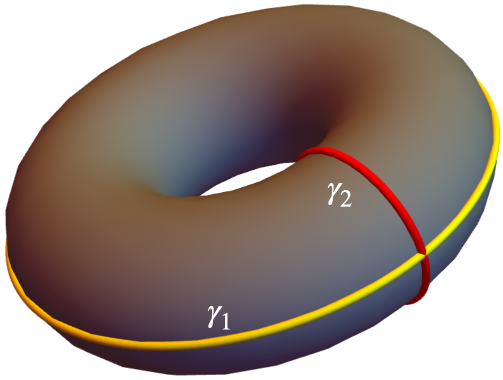

Figure 2.14.8. The two independent cycles of the torus, γ_1 and γ_2.

In case of the cubic, the meromorphic differential is $w' = \frac{x\,dx}{y}$.
Periods and semi-periods of an elliptic curve satisfies the well-know Legendre relation:

$$\varpi_0\,\eta_2 - \varpi_1\,\eta_1 = 2\pi i. \tag{14.23}$$

Throught the Weierstrass $\wp$-function we found correspondences between the lattice Λ_τ, the complex torus $\mathbb{C} \setminus \Lambda_\tau$ and the complex elliptic curve $y^2 = 4x^3 - g_2\,x - g_3$ defined in $\mathbb{P}^2(\mathbb{C})$. The only invariant associated to an elliptic curve in all the different representation is the j-invariant:

$$j(\mathbb{C} \setminus \Lambda_\tau) = j(\Lambda_\tau) = 1728\frac{g_2^3}{g_2^3 - 27g_3^2}. \tag{14.24}$$

It's important to mention that is possible to define a fundamental parallelogram for Λ_τ:

$$D = \{a + t_1 + t_2\,\tau\,:\,0 \leq t_1,\,t_2 < 1\} \quad a \in \mathbb{C}. \tag{14.25}$$

Any points outside this fundamental parallelogram can be shifted inside it due to the double periodicity of the elliptic functions. Then, any point inside the fundamental parallelogram correspond to a point of the elliptic curve.

This fix equivalence relations on the set of all lattices, and any equivalence class contains a lattice of the form:

$$\Lambda_\tau = \mathbb{Z} \oplus \mathbb{Z}\tau \qquad \tau \in \mathbb{H} = \{z \in \mathbb{C}\,:\,\mathfrak{Im}(z) > 0\}, \tag{14.26}$$

since $\tau = \frac{\varpi_1}{\varpi_0}$ and we can always swap the two periods or consider the basis with signs changed.

Very relevant for computation, here just briefly mentioned, is the action on $\mathbb{H}$ of the group:

$$\Gamma \subset SL(2,\mathbb{Z}) = \left\{ \begin{pmatrix} a & b \\ c & d \end{pmatrix} \in SL(2,\mathbb{Z})\,:\,a,b,c,d \in \mathbb{Z},\ det\begin{pmatrix} a & b \\ c & d \end{pmatrix} = 1 \right\} \tag{14.27}$$

via Möbius transformation:

$$\tau \mapsto \frac{a\,\tau + b}{c\,\tau + d} \qquad a,b,c,d \in \Gamma,\ \tau \in \mathbb{H}. \tag{14.28}$$

2.15 Elliptic multiple polylogarithms

In this section we briefly review the generalisation of MPLs on the elliptic curve defining the so-called *elliptic multiple polylogarithms* (eMPLs) [114, 115, 116, 117, 118, 119, 110, 79].

We defined an elliptic curve as the zero locus of a polynomial equation. Here, we consider an elliptic curved defined by a fourth-degree polynomial:

$$y^2 = P_4(x) = (x - a_1)(x - a_2)(x - a_3)(x - a_4), \tag{15.1}$$

where $\{a_i\}_{i=1,\cdots,4}$ are the roots of the polynomial. This case is particularly relevant in scattering amplitude computations and we are going to see through the maximal cut a case of an elliptic curve defined over $P_4(x)$.

Without loss of generality, we can assume $a_1 < a_2 < a_3 < a_4$ with all the $a_i \in \mathbb{R}$. The periods can be written as in eq. (14.21) integrating over the Abel differential of the first kind:

$$\begin{aligned} \varpi_0 &= 2\, c_4 \int_{a_2}^{a_3} \frac{dx}{y}, \\ \varpi_1 &= 2\, c_4 \int_{a_1}^{a_2} \frac{dx}{y}, \end{aligned} \tag{15.2}$$

where $c_4 = \frac{\sqrt{(a_1 - a_3)(a_2 - a_4)}}{2}$.

In eq.(14.22) we defined the quasi-periods associated, in the cubic polynomial case, to the Abel differential of the second kinf, i.e. a meromorphic differential $\frac{x\,dx}{y}$. However, in the fourth-degree polynomial case this lead to an Abel differential of the third kind, then it is usual to define a new differential of the second kind:

$$\tilde{\Phi}_4(x, \underline{a}) = \frac{1}{c_4\, y} \left(x^2 - \frac{s_1(\underline{a})}{2}\, x + \frac{s_2(\underline{a})}{6} \right), \tag{15.3}$$

where $s_n(\underline{a})$ is defined as:

$$s_n(a_1, \cdots, a_k) = \sum_{1 \leq j_1 < \cdots < j_n \leq k} a_{j_1} \cdots a_{j_n}, \tag{15.4}$$

thus in eq. (15.3):

$$\begin{aligned} s_1(a_1, a_2, a_3, a_4) &= a_1 + a_2 + a_3 + a_4, \\ s_2(a_1, a_2, a_3, a_4) &= a_1\, a_2 + a_1\, a_3 + a_1 + a_4 + a_2\, a_3 + a_2\, a_4 + a_3\, a_4. \end{aligned} \tag{15.5}$$

In this way it is possible to define the semi-periods integrating over this new Abel differential of the second kind.

The eMPLs associated to an elliptic curve defined by a fourth-degree polynomial can be defined as iterated integrals by:

$$E_4 \left(\begin{matrix} n_1 \ldots n_k \\ c_1 \ldots c_k \end{matrix} ; x, \underline{a} \right) = \int_0^x dt\, \psi_{n_1}(c_1, t, \underline{a})\, E_4 \left(\begin{matrix} n_2 \ldots n_k \\ c_2 \ldots c_k \end{matrix} ; t, \underline{a} \right) \qquad n_i \in \mathbb{Z},\, c_i \in \mathbb{C} \cup \{\infty\}, \tag{15.6}$$

where the recursion starts with $E_e(;\, x) = 1$ and ψ_n are the integration kernels.

The class of eMPLs contains as particular case the MPLs defined in eq. (11.9):

$$E_4 \left(\begin{matrix} 1 \ldots 1 \\ c_1 \ldots c_k \end{matrix} ; x, \underline{a} \right) = G(c_1, \cdots, c_k; x). \tag{15.7}$$

Furthermore, we could express any integrals of the form:

$$\int \frac{dx}{y} G(\underline{a}(x, y)), \tag{15.8}$$

in terms of eMPLs, just using the following four integration kernels:

$$\begin{aligned}
\psi_0(0, x) &= \frac{c_4}{y}, \\
\psi_{-1}(c, x) &= \frac{y_c}{y(x - c)}, \\
\psi_{-1}(\infty, x) &= \frac{x}{y}, \\
\psi_{+1}(c, x) &= \frac{1}{(x - c)},
\end{aligned} \tag{15.9}$$

where $y_c = y\Big|_{x=c}$.

Due to the isomorphism between the elliptic curve and the torus $\mathbb{C} \setminus \Lambda_\tau$, it is possible also to provide a definition of eMPLs on the torus [79, 117, 115].

2.16 ϵ-factorised differential equations beyond MPLs

We discussed the canonical logarithmic form for the system of DEs for MIs whose analytic structure involves MPLs. In more complicated cases, especially when masses are involved, the mathematical structure is much more complex and it is not possible to reach an ϵ-factorised DEs system with only $d\log$-forms. Beyond the space of logarithmic differential forms the situation becomes very complicated, but in literature there are plenty of examples where Feynman integrals are defined over higher genus surfaces or higher dimensional algebraic surfaces. In this section it is illustrated a procedure to put in ϵ-factorised form Feynman integrals related to arbitrary geometries [120, 121].
This procedure is based on the following five steps:

- **Choice of the initial basis**

  It has been conjectured that always exist a basis satisfying DEs in ϵ-factorised form. The choice of an initial basis is a crucial element, as it can simplify the subsequent steps leading to the final form. Moreover, depending on how we rotate the system, through eq. (9.9), the final form may turn out to be more or less complex. To understand how to choose a good basis, we can resort to the most understood case, i.e the polylogarithmic one. In this case, good candidates for canonical basis are identified by selecting integrand in $d\log$-form with unit leading singularities and in absence of double poles that may lead to UV or IR divergences in $d = d_0$ ($\epsilon = 0$). Generally, if the integrand is in $d\log$-form at $\epsilon = 0$, adding ϵ-terms will maintain the same form, as only logarithms with different powers will potentially be added. The goal is to go beyond the polylogarithmic case to define an initial basis where the integrands are defined in dimensional regularization. It is possible to work sector-by-sector in order to use the information from the previous case and separate the complicated sectors with coupled integrals. Based on the experiences we always avoid integrals with power-like UV or IR singularities in $d = d_0$. For sector with only one MIs, inspired by the MPLs, we select integrals with unit leading singularities, at least on the maximal cut. For sectors with more MIs, we are interested in determine the geometry associated throught the study of the homogeneous DEs. The case that requires the most attention is when there are coupled integrals. In this case, we first try to understand if these are a subsystem of the integrals in the sector, and in that case, we work on the others first. This ensures that we are left with a minimally coupled sector. Then, we work on the first integral and we try to express it as $d\log$-form and one remain integral, choose to be an Abel differential of the first kind (holomorphic), since we always expect an integral of this kind not only in the elliptic case but for any geometry considered. The other MIs of the sector are chosen as linear combinations of derivatives of the first integral with respect to the internal masses (related to the concept of pure functions). Lastly, we want to avoid, in the chosen basis, integrals whose DEs have coefficients with poles in ϵ or with a dependence on ϵ in polynomials in the denominator.

- **Calculation of the Wronskian and rotation by the inverse of its semi-simple part**

  For every coupled system we compute the Wronskian matrix W at $\epsilon = 0$. It was observed in [110, 122] that pure and UT Feynman integrals could be selected by a rotation of the MIs basis by the semi-simple part of the Wronskian matrix. Then, we split W into a unipotent part W_u and and semi-simple part W_{ss}:

$$W = W_{ss} \cdot W_u, \tag{16.1}$$

  where semi-simple means that $\exists\, P$ such that $P^{-1} W_{ss} P$ is diagonal, and unipotent means that $(W_u - \mathbb{I})$ is nilpotent, where $\mathbb{I}$ is the identity matrix. It is possible to split W such that W_{ss} has lower triangular form and W_u has upper triangular form. Then, we perform a rotation of the MIs basis with the inverse of W_{ss}.

- **Adjust ϵ-factors**

  This step consist in rescale some factors in ϵ and swap some MIs such that the non ϵ-factorised terms appear below the diagonal of the differential equation matrix.

- **Integrate out total derivatives**

  We want to remove the remaining terms in the homogeneous part. This can be achieved by shifting the MIs which generate non ϵ-factorised terms by terms proportional to the other MIs in the same sector. This frequently correspond to integrate out total derivatives of functions already present in the inverse of W_{ss}. In practice, this corresponds to multiply the MIs basis by a matrix whose entries are derivatives of terms proportional to the $\epsilon = 0$ part in the DEs matrix after the rotation by W_{ss}^{-1} and the ϵ-rescaling. In cases where this is not enough, it is necessary to introduce new functions as iterated integrals of products of rational or algebraic functions and the transcendental functions already present in W_{ss}.

- **Clean up the inhomogeneous DEs**

  Once all the homogeneous blocks have been put into the ϵ-factorised form, it is sufficient to shift some MIs in a given sector by MIs in the lower sectors.

2.16.1 ϵ-factorised form for the elliptic triangle

As example of this procedure, consider the family of two-loop non-planar triangle with a massive loop, shown in Fig. 2.16.9. This elliptic sector will be present in the works discussed later on concerning the production of two photons, both in the quark annihilation channel and in gluon fusion.

The kinematic for this process is described by two on-shell leg, i.e. $p_3^2 = p_4^2 = 0$ and by one kinematic variable $p_{12} = (p_1 + p_2)^2$.

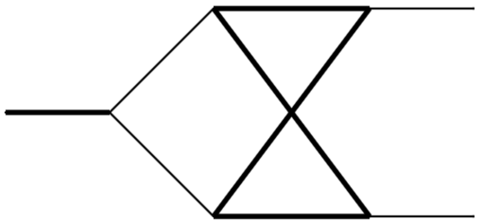

Figure 2.16.9. Non-planar triangle with massive loop. The thick lines in the loop represent the massive propagator, while the external thick line represents the off-shell momentum p_{12}.

The scalar integral family which describe the process is:

$$I(a_1, ..., a_7) = \int \mathcal{D}k_1\, \mathcal{D}k_2 \frac{1}{\prod_{j=1}^{7} D_j^{a_j}}, \tag{16.2}$$

where $a_1, ..., a_6 > 0$, $a_7 < 0$, and the integration measure is fixed to be:

$$\mathcal{D}k = \frac{\mathrm{d}^D\, k}{i\pi^{2-\epsilon}\Gamma(1+\epsilon)} \left(\frac{\mu^2}{m_t^2}\right)^{-\epsilon} \tag{16.3}$$

The denominators and scalar products are defined by:

$$\begin{aligned}
&D_1 = k_1^2, \quad D_2 = k_2^2 - m^2, \quad D_3 = (k_1 - k_2)^2 - m^2, \quad D_4 = (k_1 - p_{12})^2, \\
&D_5 = (k_1 - k_2 + p_3)^2 - m^2, \quad D_6 = (k_2 - p_{12} - p_3)^2 - m^2, \\
&D_7 = (k_1 - k_2 - p_{12})^2,
\end{aligned} \tag{16.4}$$

This family have a total number of 11 MIs, but we are interested in the top-sector which contains the following 2 MIs:

$$\begin{aligned}
&I(1,1,1,1,1,1,0), \\
&I(1,2,1,1,1,1,0).
\end{aligned} \tag{16.5}$$

In order to obtain an ϵ-factorised form for these coupled MIs, following the condition discussed in section 2.16, we choose as initial basis:

$$\begin{aligned}
&\mathcal{J}_1 = s\,\epsilon^4 I(1,1,1,0,0,1,1,1,0), \\
&\mathcal{J}_2 = \partial_{m^2}\mathcal{J}_1 = 4s\,\epsilon^4 I(1,2,1,0,0,1,1,1,0)
\end{aligned} \tag{16.6}$$

These MIs satisfy a coupled two-dimensional system:

$$\partial_{m_t^2}\begin{pmatrix}\mathcal{J}_1\\ \mathcal{J}_2\end{pmatrix} = \begin{pmatrix} 0 & 1 \\ -\frac{4(1+2\epsilon)(1+4\epsilon)}{m^2(s+16m^2)} & -\frac{s+32m^2+\epsilon(2s+48m^2)}{m^2(s+16m^2)}\end{pmatrix}\begin{pmatrix}\mathcal{J}_1\\ \mathcal{J}_2\end{pmatrix} + \begin{pmatrix}0\\ \Omega\end{pmatrix}, \tag{16.7}$$

where Ω states for the inhomogeneous part coming from the subsectors.
We need to solve differential equations for coupled system of MIs. The first step is to solve the associated homogeneous equation for $\epsilon = 0$:

$$\partial_{m^2}\left(\begin{array}{c}\mathcal{J}_1\\ \mathcal{J}_2\end{array}\right)=\mathbb{H}_0(s,m^2)\left(\begin{array}{c}\mathcal{J}_1\\ \mathcal{J}_2\end{array}\right) \tag{16.8}$$

where $\mathbb{H}_0$ is the $\mathcal{O}(\epsilon^0)$ of the ϵ-expansion of the differential equations matrix:

$$\mathbb{H}_0(s,m^2)=\left(\begin{array}{cc}0 & 1\\ -\frac{4}{m_t^2(s+16m_t^2)} & -\frac{s+32m_t^2}{m_t^2(s+16m_t^2)}\end{array}\right). \tag{16.9}$$

The solution of the homogeneous system is given by the Wronskian matrix, i.e. the maximal cut matrix:

$$W=\left(\begin{array}{cc}\varpi_0 & \varpi_1\\ \partial_{m_t^2}\varpi_0 & \partial_{m_t^2}\varpi_1\end{array}\right) \tag{16.10}$$

where ϖ_0 and ϖ_1 are the two period of the elliptic curves:

$$\varpi_0(s,m_t^2)\sim\frac{1}{\sqrt{s\left(s+8m_t^2+\sqrt{s(s+16m_t^2)}\right)}}\mathrm{K}\left(\lambda\right), \tag{16.11}$$

$$\varpi_1(s,m_t^2)\sim\frac{1}{\sqrt{s\left(s+8m_t^2+\sqrt{s(s+16m_t^2)}\right)}}\mathrm{K}\left(1-\lambda\right), \tag{16.12}$$

where:

$$\lambda=\frac{\left(\sqrt{s}-\sqrt{s+16m_t^2}\right)^2}{\left(\sqrt{s}+\sqrt{s+16m_t^2}\right)^2}. \tag{16.13}$$

Once constructed the Wronskian, we need to split it into unipotent and semi-simple part:

$$W=W_{ss}\,W_u. \tag{16.14}$$

The unipotent matrix is:

$$W_u=\begin{pmatrix}1 & \frac{\varpi_1}{\varpi_0}\\ 0 & 1\end{pmatrix} \tag{16.15}$$

such that its differential equation with respect to the modular parameter $\tau=\frac{\varpi_1}{\varpi_0}$ reads:

$$\partial_\tau W_u=\begin{pmatrix}0 & 1\\ 0 & 0\end{pmatrix}W_u. \tag{16.16}$$

The semi-simple part is obtained b y exploiting the Legendre relation:

$$\varpi_0(\partial_{m_t^2}\varpi_1)-\varpi_1(\partial_{m_t^2}\varpi_0)=\left[sm_t^2(s+16m_t^2)\right]^{-1}, \tag{16.17}$$

and its explicit form is:

$$W_{ss}=\left(\begin{array}{cc}\varpi_0 & 0\\ \partial_{m_t^2}\varpi_0 & \frac{1}{sm_t^2(s+16m_t^2)\varpi_0}\end{array}\right) \tag{16.18}$$

Now, it's possible to change basis to a `unipotent` basis:

$$\begin{pmatrix} K_1 \\ K_2 \end{pmatrix} = W_{ss}^{-1} \begin{pmatrix} \mathcal{J}_1 \\ \mathcal{J}_2 \end{pmatrix}, \tag{16.19}$$

and consider the differential equations of this new basis:

$$\begin{aligned} \partial_{m_t^2} \begin{pmatrix} K_1 \\ K_2 \end{pmatrix} = &\begin{pmatrix} 0 & \frac{1}{m_t^2 s(s+16m_t^2)\varpi_0^2} \\ -\epsilon\left(24s\varpi_0^2 + 2s(s+24m_t^2)\varpi_0(\partial_{m_t^2}\varpi_0)\right) - 32\epsilon^2 s\varpi_0^2 & -\frac{2\epsilon(s+24m_t^2)}{m_t^2(s+16m_t^2)} \end{pmatrix} \begin{pmatrix} K_1 \\ K_2 \end{pmatrix} \\ &+ \begin{pmatrix} 0 \\ \tilde{\Omega} \end{pmatrix}. \end{aligned} \tag{16.20}$$

We see that the entry $-\epsilon\left(24s\varpi_0^2 + 2s(s+24m_t^2)\varpi_0(\partial_{m_t^2}\varpi_0)\right) - 32\epsilon^2 s\varpi_0^2$ of the homogeneous matrix in eq. (16.20), has a part proportional to ϵ and one proportional to ϵ^2. In order to obtain the final ϵ-factorised form, we can rescale the second integral:

$$\begin{pmatrix} \tilde{K}_1 \\ \tilde{K}_2 \end{pmatrix} = \begin{pmatrix} 1 & 0 \\ 0 & \frac{1}{\epsilon} \end{pmatrix} \begin{pmatrix} K_1 \\ K_2 \end{pmatrix}. \tag{16.21}$$

From eq. (16.20) we obtain the DEs matrix for the new basis:

$$\begin{aligned} \partial_{m_t^2} \begin{pmatrix} \tilde{K}_1 \\ \tilde{K}_2 \end{pmatrix} = &\begin{pmatrix} 0 & \frac{\epsilon}{m_t^2 s(s+16m_t^2)\varpi_0^2} \\ -\left(24s\varpi_0^2 + 2s(s+24m_t^2)\varpi_0(\partial_{m_t^2}\varpi_0)\right) - 32\epsilon s\varpi_0^2 & -\frac{2\epsilon(s+24m_t^2)}{m_t^2(s+16m_t^2)} \end{pmatrix} \begin{pmatrix} K_1 \\ K_2 \end{pmatrix} \\ &+ \begin{pmatrix} 0 \\ \tilde{\tilde{\Omega}} \end{pmatrix}, \end{aligned} \tag{16.22}$$

where now we reached an ϵ-factorised form except for the term $-\left(24s\varpi_0^2 + 2s(s+24m_t^2)\varpi_0(\partial_{m_t^2}\varpi_0)\right)$ that does not depend on ϵ anymore. Furthermore:

$$-\left(24s\varpi_0^2 + 2s(s+24m_t^2)\varpi_0(\partial_{m_t^2}\varpi_0)\right) = \partial_{m_t^2}\left(-s(s+24m_t^2)\varpi_0^2\right). \tag{16.23}$$

Then, as last step we integrate out the total derivative:

$$\begin{pmatrix} f_1 \\ f_2 \end{pmatrix} = \begin{pmatrix} 1 & 0 \\ s(s+24m_t^2)\varpi_0^2 & 1 \end{pmatrix} \begin{pmatrix} \tilde{K}_1 \\ \tilde{K}_2 \end{pmatrix}, \tag{16.24}$$

and we finally obtain the final ϵ-factorised form:

$$\partial_{m_t^2} \begin{pmatrix} f_1 \\ f_2 \end{pmatrix} = \epsilon \begin{pmatrix} -\frac{(s+24m_t^2)}{m_t^2(s+16m_t^2)} & \frac{1}{m_t^2 s(s+16m_t^2)\varpi_0^2} \\ \frac{s(s+8m_t^2)^2\varpi_0^2}{m_t^2(s+16m_t^2)} & -\frac{(s+24m_t^2)}{m_t^2(s+16m_t^2)} \end{pmatrix} \begin{pmatrix} J_1 \\ J_2 \end{pmatrix} + \begin{pmatrix} 0 \\ \tilde{\tilde{\tilde{\Omega}}} \end{pmatrix}. \tag{16.25}$$

2.17 Cuts of Feynman integrals

We previously discussed the connection between Feynman integrals and the geometry associated with them. Systematically, especially in more complex cases, we aim to find a method that determines the algebraic variety on which the integrals are defined through the polynomial equation that can be obtained for a specific topology within which the Feynman integrals are defined. The polynomial equations we are interested in have constraints that derive from the kinematics imposed by on-shell conditions. A powerful tool for understanding the relationship between Feynman integrals and geometry is the maximal cut, based on the concept of the generalised cut of a Feynman integral. Cutting a Feynman integral means to constrain one (or more) virtual particles in the loops to be on-shell by replacing its propagator with a δ-function. The physical meaning of such operation derive from the unitarity of the scattering matrix related to the optical theorem. Unitarity is a fancy way of saying probabilities add up to 1. Conservation of probability in a quantum theory, implies that, in the Schrodinger picture, the norm of a state is the same at any time t:

$$\langle \Psi; t \mid \Psi; t \rangle = \langle \Psi; 0 \mid \Psi; 0 \rangle. \tag{17.1}$$

Since

$$\mid \Psi; t \rangle = e^{-iHt} \mid \Psi; 0 \rangle, \tag{17.2}$$

unitarity means that the Hamiltonian should be Hermitian, $H^\dagger = H$. Then, since the S-matrix is $S = e^{-iHt}$, unitarity implies:

$$S^\dagger S = 1, \tag{17.3}$$

then the S-matrix is a unitary matrix.

One of the most important implications of unitarity is a relation between scattering amplitudes and cross section, i.e. the optical theorem.
The non trivial part of the S-matrix is related to the non-hermitian *transition matrix* $\mathcal{T}$. Unitarity implies:

$$\left(1 - i\mathcal{T}^\dagger\right)(1 + i\mathcal{T}) = S^\dagger S = 1, \tag{17.4}$$

then we obtain a relation between the imaginary part of the transition matrix and its square modulus:

$$-i\left(\mathcal{T} - \mathcal{T}^\dagger\right) = \mathcal{T}\mathcal{T}^\dagger. \tag{17.5}$$

To understand the meaning of eq. (17.5), we can relate it to physical observables in the context of scattering amplitudes as transitions probabilities between a final state $|f\rangle$ and an initial state $|i\rangle$, both with an arbitrary number of particles:

$$\mathcal{A}_{i\to f}(\underline{x}) = i\langle f|\mathcal{T}|i\rangle, \tag{17.6}$$

where $\underline{x}$ is the set of scales.
In this way the left-hand side of eq. (17.5) reads:

$$-i\left(\langle f|\mathcal{T}|i\rangle - \langle f|\mathcal{T}^\dagger|i\rangle\right) = \mathcal{A}_{i\to f}(\underline{x}) - \mathcal{A}^\star_{i\to f}(\underline{x}). \tag{17.7}$$

To complete the other side, we use the feature that the Hilbert space is complete, then we have the following completeness relation:

$$\sum_y \int dy\, |y\rangle\langle y| = 1, \tag{17.8}$$

where the sum is over a generic multi-particle state $|y\rangle$.
Plugging right-hand side of eq. (17.5) into final and initial states:

$$\langle f|\mathcal{T}\mathcal{T}^\dagger|i\rangle = \sum_y \int dy\, \langle f|\mathcal{T}|y\rangle\langle y|\mathcal{T}^\dagger|i\rangle = \sum_y \int dy\, \mathcal{A}_{i\to y}(\underline{x})\, \mathcal{A}^\star_{y\to f}(\underline{x}). \tag{17.9}$$

Combining eq. (17.7) and (17.9) we obtain:

$$\mathcal{A}_{i\to f}(\underline{x}) \;-\; \mathcal{A}^\star_{i\to f}(\underline{x}) = \sum_y \int dy\, \mathcal{A}_{i\to y}(\underline{x})\, \mathcal{A}^\star_{y\to f}(\underline{x}). \tag{17.10}$$

eq. (17.10) relates the imaginary part of the amplitude to the different transition probabilities from an initial state to an arbitrary intermediate state and the eventual decay to the final state. The imaginary part of the amplitude is linked to its discontinuities around the branch cuts determined by the thresholds. The various ways in which an initial state can evolve towards a final state through arbitrary intermediate states are represented by the cuts. Cutting a Feynman diagram corresponds to separating the contributions of the intermediate states in a scattering process. The intermediate states represent particles that can contribute to the physical process, and therefore, to make sense, they must be on-shell. This further connects the meaning with the cutting of a Feynman diagram, as the virtual particles (off-shell) become real (on-shell) after a cut and thus contribute to the physical process. Moreover, this generalised optical theorem must hold order-by-order in perturbation theory. But while its left-hand side has the matrix elements, the right-hand side has matrix elements squared, and this means that at order λ^2 in some coupling the left-hand side must be a loop to match a tree-level calculation on the right-hand side. Thus, the imaginary parts of loop amplitudes are determined by tree-level amplitudes.
It's helpful now think to real and imaginary part of the Feynman propagator. In particular, for the imaginary part we have:

$$\begin{aligned}\mathfrak{Im}\left(\frac{1}{p^2-m^2+i\epsilon}\right) &= \frac{1}{2i}\left(\frac{1}{p^2-m^2+i\epsilon} - \frac{1}{p^2-m^2-i\epsilon}\right)\\ &= \frac{-\epsilon}{(p^2-m^2)^2+\epsilon^2}.\end{aligned} \tag{17.11}$$

This vanishes at $\epsilon \to 0$, except near $p^2 = m^2$ as expected. If we integrate in p^2:

$$\int_0^\infty dp^2 \frac{-\epsilon}{(p^2-m^2)^2+\epsilon^2} = -\pi, \tag{17.12}$$

implying that:

$$\mathfrak{Im}\left(\frac{1}{p^2-m^2+i\epsilon}\right) = -\pi\delta(p^2-m^2). \tag{17.13}$$

This is very useful, because it says that the propagator is real except for when the particles goes on-shell. Then, more generally, imaginary parts of loop amplitudes come from intermediate particles goes on-shell.
In general we can define the Cutosky rule [123] as:

$$\frac{1}{p^2 - m^2 + i\epsilon} \to -2i\pi\delta(p^2 - m^2). \tag{17.14}$$

The Cutosky rule was introduced in order to study the discontinuities over branch cuts for Feynman diagrams. The discontinuity of an amplitude across its branch cuts is strictly connected to the imaginary part of the amplitude through:

$$\text{Disc}(i\mathcal{M}) = -2\,\mathfrak{Im}(\mathcal{M}). \tag{17.15}$$

This can be easily seen with the discontinuity operator defined as:

$$\text{Disc}\left(\psi(x)\right) = \lim_{\epsilon\to 0}\left(\psi(x - i\epsilon)\ -\ \psi(x + i\epsilon)\right). \tag{17.16}$$

It's easy to see that:

$$\text{Disc}\left(\frac{1}{x}\right) = 2\pi i\delta(x), \tag{17.17}$$

according to eq.(17.15).
The Cutosky rules offers great advantages. First of all, we can discuss the one-loop amplitude case as an example. We know that we can decompose a generic one-loop amplitude in terms of box, triangle, bubble and tadpoble integrals:

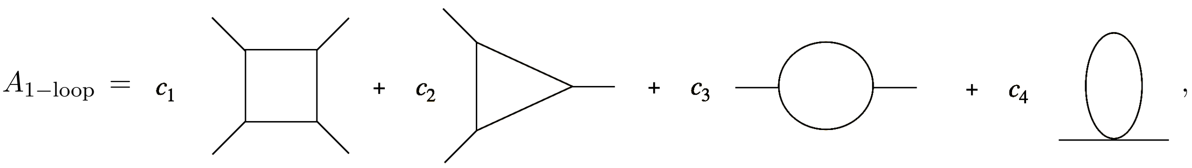

(17.18)

where c_1, c_2, c_3 and c_4 are rational functions of the kinematic invariants.
Using the Cutosky rule we can easily compute $2\mathfrak{Im}(A_{1-\text{loop}})$ as the interference between the two tree-level amplitude obtained cutting the one-loop as shown in Fig. 2.17.10, where the red line represents the cut and the tadpole contribution is zero.

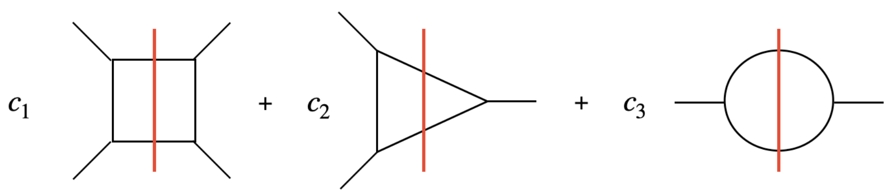

Figure 2.17.10. Result in terms of cutted diagrams.

In general, cutting Feynman diagrams into connected pieces, allows us to determine the discontinuity of an amplitude across its branch cuts.
This result suggest that cutting more propagators can provide further information about the structure of scattering amplitudes. We can extend the Cutkosky rule to the Feynman integral in eq. (5.13), were we set of all the $a_j = 1$. We define the multiple-cut $D_{k_1} = \ldots = D_{k_s} = 0$ as the integral:

$$Cut_{k_1,\ldots,k_s}\left(I(a_1,\cdots,a_{N_{sp}})\right) = \int\prod_{i=1}^{l}\mathcal{D}k_i\frac{1}{\prod_{j\neq k_1,\cdots,k_s}D_j}\,\delta(D_{k_1})\cdots\delta(D_{k_s}). \tag{17.19}$$

To be more precise, we can give a definition of generalised unitary cuts, which naturally assumes the loop momenta as complex variables, which consist in deforming the integration contour to a circle enclosing the singularity $D_i = 0$:

$$\int \mathcal{D}k \frac{1}{D_i(k)} \to \oint_{D_i=0} \mathcal{D}k \frac{1}{D_i}. \tag{17.20}$$

2.18 Baikov representation

The Feynman integrals associated to a scalar integral family are usually represented as in eq. (5.13). However, this is not a convenient form to try to evaluate them analytically or to find important properties of the integrals. There are several representations used for the analytical computation of integrals, among which the prominent parameterizations are those of Feynman, Mellin-Barnes, Lee-Pomeransky [124], and Schwinger.
Here, we want to introduce the Baikov representation [125] for a Feynman integral for any number of loops and external momenta.. The integration variables are the propagators that define the integral, and thus the scalar products between the independent external momenta and the loop momenta. This representation is not the most suitable for analytically computing Feynman integrals for various reasons, including the large number of integrations, which corresponds to the number of scalar products and, most importantly, due to the complicated integration boundaries determined by the physical constraints on the variables used in this parametrization. Despite this, the Baikov representation is widely used due to its close connection with the cuts of a Feynman diagram. Since the propagators are the integration variables z_i , making a cut corresponds simply to setting the propagator to zero. Consequently, when we will introduce the maximal cut as a powerful tool to solve the DEs homogeneous system and to find the underlying geometry associated to the integrals, the natural representation for Feynman integrals will be the Baikov parametric representation.
To define the Baikov representation, we work in dimensional regularization with dimension $d = d_0 - 2\epsilon$, where $d_0 \in \mathbb{N}$. We consider a generic integral with l-loop, n external momenta $p_1, ..., p_n$ and loop momenta $k_1, ..., k_l$. We normalize our integral with the integration measure defined in eq. (5.3).
With these premises, the general form of our Feynman integral is:

$$I(a_1, \cdots, a_{N_{sp}}) = \int \prod_{i=1}^{l} \mathcal{D}k_i \frac{1}{\prod_{j=1}^{N_{sp}} D_j^{a_j}} \quad a_j \in \mathbb{Z}, \tag{18.1}$$

where the propagators can be massive and in general can be written as in eq. (5.4). The momentum flowing through the propagators is a linear combination of loop momenta and external momenta as described in eq. (5.5).
In eq. (18.1) in the product $\prod_{j=1}^{N_{sp}} D_j^{a_j}$ some indices are positive and others negative, based on the number of scalar products:

$$N_{sp} = \frac{1}{2} l(l + 1) + l(n - 1). \tag{18.2}$$

The first step to obtain the Baikov representation for the integral in eq. (18.1) is to group in a unique set all the independent $(n - 1)$ external momenta and l loop momenta:

$$\{q_1, ..., q_{l+n-1}\} = \{p_1, ..., p_{n-1}, k_1, ..., k_l\}. \tag{18.3}$$

At this point is possible to define the Gram matrix for the set of momenta $q_1, ..., q_{l+n-1}$ as the Hermitian matrix of inner products, whose entries are given by the inner product $G_{ij} = \langle q_i, q_j \rangle$, where $i, j = 1, ..., l+n-1$.
Specifically, with our set of momenta, the Gram determinants reads:

$$G(q_1, ..., q_{l+n-1}) = \begin{pmatrix} q_1 \cdot q_1 & \cdots & q_1 \cdot q_{l+n-1} \\ \vdots & \ddots & \vdots \\ q_{l+n-1} \cdot q_1 & \cdots & q_{l+n-1} \cdot q_{l+n-1} \end{pmatrix} . \tag{18.4}$$

It is relevant to notice that $G(q_1, ..., q_{l+n-1})$ can be decomposed into four different blocks:

$$G(q_1, ..., q_{l+n-1}) = \left(\begin{array}{ccc|ccc} q_1 \cdot q_1 & \cdots & q_1 \cdot q_{n-1} & \star & \cdots & \star \\ \vdots & \ddots & \vdots & \vdots & \ddots & \vdots \\ q_{n-1} \cdot q_1 & \cdots & q_{n-1} \cdot q_{n-1} & \star & \cdots & \star \\ \hline \star & \cdots & \star & \star & \cdots & \star \\ \vdots & \ddots & \vdots & \vdots & \ddots & \vdots \\ \star & \cdots & \star & \star & \cdots & \star \end{array}\right) , \tag{18.5}$$

where the first $(n-1) \times (n-1)$ block depends only on the independent external momenta and it is exactly the Gram determinant of these momenta $G(q_1, ..., q_{n-1})$.
The remaining three blocks involves the loop momenta $q_n, ..., q_{l+n-1}$:

$$G(q_1, ..., q_{l+n-1}) = \left(\begin{array}{ccc|ccc} \star & \cdots & \star & q_1 \cdot q_n & \cdots & q_1 \cdot q_{l+n-1} \\ \vdots & \ddots & \vdots & \vdots & \ddots & \vdots \\ \star & \cdots & \star & q_{n-1} \cdot q_n & \cdots & q_{n-1} \cdot q_{l+n-1} \\ \hline q_n \cdot q_1 & \cdots & q_n \cdot q_{n-1} & q_n \cdot q_n & \cdots & q_n \cdot q_{l+n-1} \\ \vdots & \ddots & \vdots & \vdots & \ddots & \vdots \\ q_{l+n-1} \cdot q_1 & \cdots & q_{l+n-1} \cdot q_{n-1} & q_{l+n-1} \cdot q_n & \cdots & q_{l+n-1} \cdot q_{l+n-1} \end{array}\right) , \tag{18.6}$$

and from the upper right block, that is a sub-matrix $(n-1) \times l$, we have a total of $(n-1)l$ independent entries (in orange) corresponding to the product $q_i \cdot q_j$ with $i = 1, ..., n-1$ and $j = n, ..., n+l-1$. Furthermore, from the lower right block of dimension $l \times l$, there are $\frac{l(l+1)}{2}$ independent entries corresponding to the products $q_i \cdot q_j$ with $i = n, ..., l+n-1$ and $j = n, ..., l+n-1$. The number of independent entries of $G(q_1, ..., q_{l+n-1})$ with the dependencies of loop momenta, is given exactly by the number of scalar products. Therefore, each of the inverse propagator in eq. (18.1) can be written as a linear combination of the independent entries of the Gram matrix.
Finally, we can define the integration variable in the Baikov representation as the inverse propagators $z_i = D_i$ with $i = 1, ..., m$. We are able to change the integration variables from $\{k_i^\mu\}$ to $\{q_i \cdot q_j\}$ and then to the Baikov variables $\{z_i\}$, since we can write:

$$z_k = \sum_{i=1}^{l} \sum_{j=i}^{l+n-1} A_k^{ij} \, q_i \cdot q_j \, + f_k, \tag{18.7}$$

with $k = 1, ..., m$. A_k^{ij} are integer constants and f_k are functions that depends only on the external momenta and masses. We denote A_k^{ij} as the elements of the inverse of the matrix $\mathbb{A}$ and with s_{ij} the product $q_i \cdot q_j$, in analogy with the Mandelstam invariants.
Then, the Jacobian associated to the change of variable $\{k_i^\mu\} \to \{s_{ij}\}$ is given by the determinants of the Gram matrices discussed:

$$\begin{aligned} \mathcal{B} &= \det\left(G(q_1, ..., q_{l+n-1})\right), \\ U &= \det\left(G(q_1, ..., q_{n-1})\right), \end{aligned} \tag{18.8}$$

and the last change of variables to $\{z_k\}$ is given by:

$$\prod_{i=1}^{l} \prod_{j=i}^{l+n-1} ds_{ij} = \mid det\left(\mathbb{A}^{-1}\right) \mid \prod_{k=1}^{m} dz_k. \tag{18.9}$$

The Baikov representation of the integral in eq. (18.1) takes the form:

$$I_{a_1,\ldots,a_m}^{d(l,n)}(p) = C_{n-1}^{l}(d) U^{\frac{n-d+1}{2}} \int \frac{\prod_{i=1}^{m} dz_i}{\prod_{j=1}^{m} z_j^{a_j}} \mathcal{B}(z)^{\frac{d-l-n-1}{2}} \mathcal{N}(k,p), \tag{18.10}$$

where the overall factor $C_{n-1}^{l}(d)$ is the product of hypersphere areas, the Jacobian of the transformation and the Gram determinant:

$$C_{n-1}^{l}(d) = \frac{\pi^{\frac{-l(l-1)}{4} - \frac{l(n-1)}{2}}}{\prod_{k=1}^{l} \Gamma\left(\frac{d-l-n+1+k}{2}\right)} det\mathbb{A}. \tag{18.11}$$

Loop-by-Loop Baikov representation

Often, in multi-loop calculations, the so-called loop-by-loop approach is used. In the Baikov representation, the denominators are taken as variables, and a change of variable is performed for each variable independently of the number of loops. In the loop-by-loop approach [126, 127], however, a change of variable is carried out individually for each loop. We denote by n_l the number of independent external momenta to the l-th loop, then the number of integration variables is:

$$\tilde{n} = l + \sum_{i=1}^{l} n_i. \tag{18.12}$$

Similarly to what was done in the general case, in this approach we can define the Gram determinants that define the Baikov polynomial for the set $\{q_1 ..., q_{n_l+l}\} = \{k_l, q_1, \cdots, q_{n_l}\}$. In this case eq. (18.8) becomes:

$$\begin{aligned} \mathcal{B} &= \det\left(G(q_1, \cdots, q_{n_l+l})\right), \\ U &= \det\left(G(q_1, \cdots, q_{n_l})\right). \end{aligned} \tag{18.13}$$

The loop-by-loop Baikov representation of the integral in eq. (18.1) takes the form:

$$I(a_1, \cdots, a_m) = C_{n_l}^{l}(d) \int \frac{d^{\tilde{n}} z}{\prod_{j=1}^{m} z_j^{a_j}} \left(\prod_{i=1}^{l} U^{\frac{n_i-d+1}{2}} \mathcal{B}(z)^{\frac{d-n_i-2}{2}} \right), \tag{18.14}$$

where $C_{n_l}^{l}(d)$ is the equivalent of eq. (18.11) with n_l independent external momenta with respect to the l-th loop.

2.19 Maximal cut

We discussed in 2.17 how the cuts can be used to study the discontinuities of Feynman integrals. From a physical point of view, cutting a propagator in a Feynman diagram means to force the particle propagating through it to be on-shell. If the propagator we are going to cut is raised to power one, the computation become trivial since we just need to substitute the propagator with a δ-function which forces the momentum of the propagator on-shell. The maximal cut is defined as the simultaneous cut of all the propagators of a corresponding Feynman diagram. For a detailed review see Ref. [128, 129, 126, 130, 127, 131].
Defining an l-loop Feynman integral in a general form as in eq. (5.13), in the case of the simultaneous imposition of the on-shell condition to all denominators we have the maximal cut:

$$MC\left(I(1,\cdots,1)\right) = \int \prod_{i=1}^{l} \mathcal{D}k_i \, \frac{1}{\prod_{s=m+1}^{N_{sp}} D_s} \prod_{j=1}^{m} \delta(D_j). \tag{19.1}$$

The maximal cut is a powerful tool, especially when applied in the context of differential equations. To illustrate the connection explicitly, consider an integral family that can be reduces to N independent MIs $\{f_j\}_{j=1,\ldots,N}$. This set of MIs satisfy a first-order system of linear differential equations with respect to a single kinematic invariant, for simplicity, denoted by x:

$$\partial_x f_i(x,\epsilon) = H_{ij}(x,\epsilon) f_j(x,\epsilon) \, + \, \Omega_{ij}(x,\epsilon) g_j(x,\epsilon), \tag{19.2}$$

in which we separated the homogeneous part from $\Omega_{ij}(x,\epsilon)$ which is the differential equations matrix for the subtopologies $g_j(x,\epsilon)$. We have, in the general scenario, a system of N coupled differential equations. If we now apply the maximal cut, i.e. the simultaneous cut to all propagators, to eq. (19.2):

$$\begin{aligned} \partial_x \mathrm{MC}\left(f_i(x,\epsilon)\right) &= \mathrm{MC}\left(H_{ij}(x,\epsilon) f_j(x,\epsilon)\right) \, + \, \mathrm{MC}\left(\Omega_{ij}(x,\epsilon) g_j(x,\epsilon)\right) \\ &= H_{ij}(x,\epsilon)\, \mathrm{MC}\left(f_j(x,\epsilon)\right) \end{aligned} \tag{19.3}$$

since:

$$\mathrm{MC}\left(\Omega_{ij}(x,\epsilon) g_j(x,\epsilon)\right) = 0. \tag{19.4}$$

This follow directly to the definition of a subtopology, which correspond to an integral with fewer propagators than the top-sector. Consequently, applying the maximal cut, the constraints imposed by the δ-functions produces as result a zero. Then, by construction, the maximal cut correspond to the homogeneous solution of the differential equations satisfied by the MIs without cuts.
In a generic l-loop process we have often to deal with more than one scale, especially when we want to compute massive corrections, and the differential equations method increases its difficulty and laboriousness. The maximal cut provides the homogeneous solution for the system of coupled differential equations with respect to all the kinematic invariants.
In order to solve the differential equations for the vector of MIs, we can proceed with different steps:

- **step 1**: Solve the homogeneous system of DEs for $\epsilon = 0$. We know that the homogeneous matrix $\mathbb{H}(x,\epsilon)$, whose entries are the $H_{ij}(x,\epsilon)$ in eq. (19.2), can be written, after an appropriate rescaling of the basis integrals to guaranteed the finiteness condition on $\mathbb{H}(x,\epsilon)$, in its expanded form in the dimensional regulator:

$$\mathbb{H}(x,\epsilon) = \mathbb{H}_0(x) + \sum_{k\geq 1} \mathbb{H}_k(z)\epsilon^k. \tag{19.5}$$

Then, the homogeneous system for $\epsilon = 0$ reads:

$$\partial_x f_i(x,0) = H_{ij,0}(x,0) f_j(x,0). \tag{19.6}$$

We can identify the j-th solution of the homogeneous system associated to the MI $f_i(x,0)$ with:

$$W_i^{(j)}(x,0) = \mathrm{MC}_{\Gamma_j}\left(f_i(x,0)\right), \tag{19.7}$$

with $j = 1,...,n$. Thus, the solution space is spanned by the maximal cuts:

$$W_i(x,0) = \left(\mathrm{MC}_{\Gamma_1}\left(f_i(x,0)\right), \cdots \mathrm{MC}_{\Gamma_n}\left(f_i(x,0)\right)\right). \tag{19.8}$$

- **step 2:**

  The new matrix $\mathbb{W}$ can be used to change basis and define a new set of MIs:

$$\underline{f}(x,\epsilon) = \mathbb{W}(x,0)\,\underline{J}(x,\epsilon), \tag{19.9}$$

  which satisfy a system of DEs:

$$\partial_x \underline{J}(x,\epsilon) = \tilde{\mathbb{H}}(x,\epsilon)\underline{J}(x,\epsilon) \;+\; \tilde{\Omega}(x,\epsilon)\underline{\tilde{J}}(x,\epsilon), \tag{19.10}$$

  where $\underline{\tilde{J}}(x,\epsilon)$ represents the subtopologies MIs and :

$$\begin{aligned} \tilde{\mathbb{H}}(x,\epsilon) &= \mathbb{W}(x,0)^{-1}\left(\mathbb{H}(x,\epsilon) - \mathbb{H}_0(x)\right)\mathbb{W}(x,0), \\ \tilde{\Omega}(x,\epsilon) &= \mathbb{W}(x,0)^{-1}\Omega(x,\epsilon). \end{aligned} \tag{19.11}$$

- **step 3:**

  Finally, we can integrate eq. (19.10) to obtain the solution order-by-order in ϵ.

  The easiest example is for $\epsilon = 0$:

$$\underline{J}(x,0) = \underline{J}_0 + \int_0^x d\lambda\,\tilde{\Omega}(\lambda,\epsilon) = \underline{J}_0 + \int_0^x d\lambda\,\mathbb{W}(\lambda,0)^{-1}\Omega(\lambda,\epsilon). \tag{19.12}$$

This show the importance of being able to solve the homogeneous system of DEs in order to obtain a full solution order-by-order in ϵ. Since the solution space of the homogeneous system is spanned by the maximal cut, It constitutes an essential element in the computation of Feynman integrals though the differential equations method.

2.19.1 Maximal cut of one-loop bubble diagram

As a first example, we consider the one-loop bubble integral with different masses:

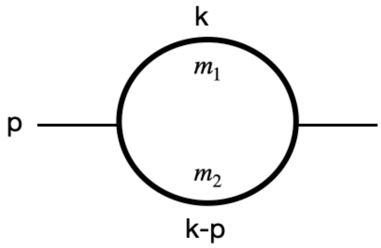

$$= \int \mathcal{D}k \frac{1}{(k^2 - m_1^2)((k+p)^2 - m_2^2)} \tag{19.13}$$

MC (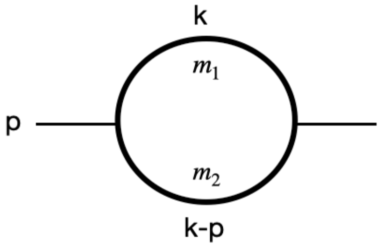

) = 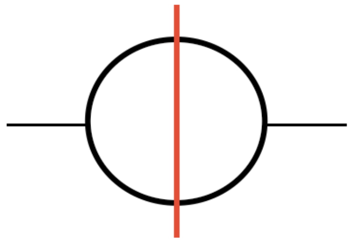 (19.14)

$$= \int \mathcal{D}k \, \delta(k^2 - m_1^2) \, \delta((k^2 - p^2) - m_2^2)$$

The maximal cut can be easily computed in the rest fram of the external particle, evaluating it for $p^\mu = (\sqrt{s}, 0, 0, 0)$:

$$\begin{aligned} &\int \mathcal{D}k \, \delta(k^2 - m_1^2) \, \delta((k-p)^2 - m_2^2) = \int \frac{d^d k}{i\pi^{d/2}} \delta(k^2 - m_1^2) \, \delta(k^2 - 2k \cdot p + p^2 - m_2^2) \\ &= \int \frac{d^d k}{i\pi^{d/2}} \delta(k^2 - m_1^2) \delta(m_1^2 - 2k_0\sqrt{s} + s - m_2^2), \end{aligned} \tag{19.15}$$

and using the property of the Dirac δ-function $\delta(a\,x) = \frac{1}{|a|}\delta(x)$:

$$\begin{aligned} &\int \frac{d^d k}{i\pi^{d/2}} \delta(k^2 - m_1^2) \frac{1}{|-2\sqrt{s}\,|} \delta\left(k_0 - \frac{s - m_2^2 + m_1^2}{2\sqrt{s}}\right) \\ &= \int \frac{dk_0 \, d^{d-1}\underline{k}}{i\pi^{d/2}} \frac{1}{2\sqrt{s}} \delta(k_0^2 - \underline{k}^2 - m_1^2) \, \delta\left(k_0 - \frac{s - m_2^2 + m_1^2}{2\sqrt{s}}\right) \\ &= \int \frac{d^{d-1}\underline{k}}{i\pi^{d/2}} \frac{1}{2\sqrt{s}} \delta\left(\frac{(s - m_2^2 + m_1^2)^2}{4s} - \underline{k}^2 - m_1^2\right) \\ &= \int \frac{d\Omega_{d-2}}{i\pi^{d/2}} \int d\underline{k} \, \underline{k}^{d-2} \frac{1}{2\sqrt{s}} \, \delta\left(\underline{k}^2 + m_1^2 - \frac{(s - m_2^2 + m_1^2)^2}{4s}\right). \end{aligned} \tag{19.16}$$

We can put the irrelevant factor coming from the integration over the solid angle in a factor $C(d)$:

$$
\begin{aligned}
&C(d)\int d\underline{k}\,\underline{k}^{d-2}\frac{1}{2\sqrt{s}}\delta\left(\underline{k}^2+m_1^2-\frac{(s-m_2^2+m_1^2)^2}{4s}\right)\\
&=C(d)\int d(\underline{k}^2)\,(\underline{k}^2)^{(d-3)/2}\frac{1}{2}\frac{1}{2\sqrt{s}}\,\delta\left(\underline{k}^2+\frac{4sm_1^2-(s-m_2^2+m_1^2)^2}{4s}\right)\\
&=S(d)\,(s)^{1-d/2}\left((s-m_2^2+m_1^2)^2-4sm_1^2\right)^{\frac{d-3}{2}},
\end{aligned}
\tag{19.17}
$$

where $S(d)$ is an irrelevant overall constant.

It's important to notice that if we compute the differential equations for the integral in eq. (19.13) we obtain the same result from the homogeneous part. In particular the homogeneous DEs with respect to s reads:

$$
\begin{aligned}
&\partial_s\int\mathcal{D}k\frac{1}{(k^2-m_1^2)((k+p)^2-m_2^2)}=\frac{1}{2}\left(\frac{(2-d)}{s}+\frac{(3-d)}{(m_1-m_2)^2-s}+\frac{(3-d)}{(m_1+m_2)^2-s}\right)\\
&\times\int\mathcal{D}k\frac{1}{(k^2-m_1^2)((k+p)^2-m_2^2)}
\end{aligned}
\tag{19.18}
$$

If we integrate directly we obtain the same structure of eq. (19.17).

In this case with two different masses, the bubble Feynman integral depends on three scales s, m_1^2, m_2^2. If we compute the differential equation with respect to only one scale, it is possible that the dependence on the other scales is not properly computed. In particular, in our case, if we had considered the differential equation with respect to a mass, say m_1, we would not have obtained the factor $s^{1-d/2}$.

This is one of the reasons why the maximal cut is such an important tool. It corresponds to the solution of homogeneous differential equations with respect to all scales.

The bubble integral is one of the easiest to compute, so it's not a great effort to perform the computation as in eq. (19.15,19.16). We introduced the Baikov representation in 2.18 because it is the most natural to perform the maximal cut. It offer the great advantages to have as integration variables the propagators and this is extremely useful to compute cuts.

If we look at the bubble Feynman integral, the computation is easier in the Baikov representation. The variables are:

$$
\begin{aligned}
z_1&=D_1=k^2-m_1^2,\\
z_2&=D_2=(k-p)^2-m_2^2.
\end{aligned}
\tag{19.19}
$$

In Baikov representation:

$$
\int\mathcal{D}k\frac{1}{(k^2-m_1^2)((k+p)^2-m_2^2)}\sim(-s)^{1-d/2}\int\frac{dz_1\,dz_2}{z_1\,z_2}\mathcal{B}(z_1,z_2)^{\frac{d-3}{2}},
\tag{19.20}
$$

where we didn't consider the overall constant and the Baikov polynomial is:

$$
\mathcal{B}(z_1,z_2)=\left((m_1-m_2+s+z_1-z_2)^2-4s(m_1^2+z_1)\right).
\tag{19.21}
$$

The maximal cut is easily obtained replacing $\frac{1}{z_i}$ with the $\delta(z_i)$:

MC

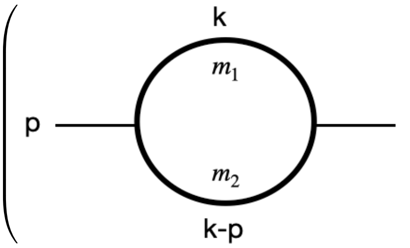

$$= (-s)^{1-\frac{d}{2}} \left(m_1^4 - 2m_1^2(s+m_2^2) + (m_2^2-s)^2\right)^{\frac{d-3}{2}}, \tag{19.22}$$

in complete agreement with what we have seen through the direct calculation of the homogeneous differential equations and through the computation of the maximal cut in momentum space [128].
It's important to notice that in the $d = 2$-dimensional case, the equal-mass bubble maximal cut reads:

MC

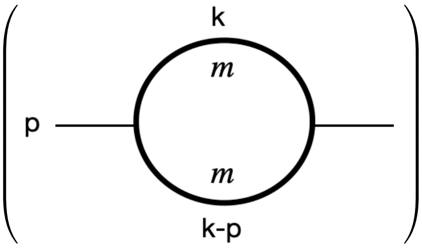

$$\Big|_{d=2} = \left(s(s-4m^2)\right)^{-\frac{1}{2}}. \tag{19.23}$$

This example, given its simplicity, is very important to better understand the mathematical structure behind a Feynman diagram. We will see, in fact, that in the most complicated cases, we can still obtain a solution to the homogeneous differential equation through the maximal cut, but the situation will be very complicated given the difficulty in performing the last integration. In the simple cases, in which it is possible to express the result analytically in terms of MPLs (at most), through maximal cut we will obtain rational functions or square roots of rational functions. In the cases in which the analytical structure is beyond the simple MPLs, it will be possible to perform a change of variables that will allow us to express the homogeneous solution in terms of the periods of the elliptic curve or, in general, of the algebraic variety considered.

2.19.2 Maximal cut of the sunrise integral

In section 2.13 we have shown the geometric connection between the one-forms that define the Feynman integrals and the Riemann surfaces associated with different genus. The maximal cut allows us to obtain this relationship without having to express the integral as an iterated integral in terms of one-forms, but simply by studying the diagram associated with the topology. In the simplest case, we obtained the Riemann sphere that describes the MPLs. Now, we want to study a case where a much more complex structure naturally emerges, namely a genus 1 surface.
We consider the two-loop sunrise diagram with equal-masses [129]:

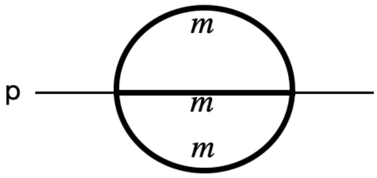

$$= \int \mathcal{D}k_1\, \mathcal{D}k_2 \frac{1}{(k_1^2 - m^2)\,(k_2^2 - m^2)\,\left((k_2 - k_1 + p)^2 - m^2\right)}. \tag{19.24}$$

It is possible to compute the maximal cut adopting the loop-by-loop approach, so first we can compute a one-loop bubble and then plug the result in the second integration:

$$\begin{aligned} &\int \mathcal{D}k_1\, \mathcal{D}k_2 \frac{1}{(k_1^2 - m^2)\,(k_2^2 - m^2)\,\left((k_2 - k_1 + p)^2 - m^2\right)} = \int \mathcal{D}k_1\, \delta(k_1^2 - m^2) \\ &\times \int \mathcal{D}k_2\, \delta(k_2^2 - m^2)\, \delta\left((k_2 - k_1 - p)^2 - m^2\right) \end{aligned} \tag{19.25}$$

Solving the last integral with the result obtained in eq. (19.22) we obtain the maximal cut in Baikov representation:

MC

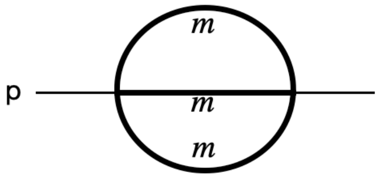

$$= (s)^{\frac{2-d}{2}} \int dz_1\, dz_2\, \delta(z_1) \frac{\mathcal{B}(z_1, z_2)^{\frac{d-3}{2}}}{\sqrt{z_2(z_2 - 4m^2)}}, \tag{19.26}$$

where we introduced the Baikov variables are $z_1 = k_1^2 - m^2$ and $z_2 = (k_1 - p^2)$ and the Baikov polynomial is the Gram determinant:

$$\mathcal{B}(z_1, z_2) = 4s(z_1 + m^2) - (s + z_2 - z_1 + m^2)^2. \tag{19.27}$$

Defining $x = \frac{p^2}{m^2}$ and $a = \frac{z_2}{m^2}$, we can easily perform the last integration:

MC

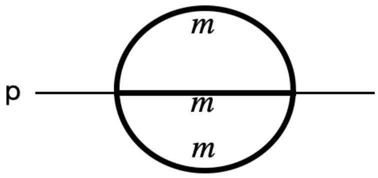

$$= \oint_\Gamma \frac{da}{\sqrt{\pm a(a-4)(a - (\sqrt{x} - 1)^2)(a - (\sqrt{x} + 1)^2)}}. \tag{19.28}$$

We notice the first big different respect to the bubble case, i.e. the presence of irreducible scalar products. Since we are dealing with a two-loop integral with one external momentum, we have a total of five scalar products, but only three denominators as we can see from eq. (19.24). Due to the presence of more scalar products, we remain with a final integration over a non-specified integration contour Γ. We can integrate over any Γ that do no cross any of the branch points of the integrand in order to obtain the solution of the homogeneous differential equation. We have four branch points:

$$a_1 = 0, \quad a_2 = 4, \quad a_3 = (\sqrt{x}-1)^2, \quad a_4 = (\sqrt{x}+1)^2, \tag{19.29}$$

and the last integration of eq. (19.28) is on the square root of a fourth degree polynomial:

$$P_4(a,x) = a(a-4)(a-(\sqrt{x}-1)^2)(a-(\sqrt{x}+1)^2). \tag{19.30}$$

As we have seen in section 2.14, this fourth degree polynomial correspond to an elliptic curve. We can now show explicitly that the solutions corresponds to the period of the elliptic curves obtaining a dependencies from the complete elliptic integrals, in this case, of the first kind.
We could have different ordering of the branch points, depending on the value of x. Assuming $x > 9$:

$$a_1 < a_2 < a_3 < a_4. \tag{19.31}$$

We are interested in integrating over a contour that do not cross the branch points. Depending on the sign of the fourth-degree polynomial under the square root, we could have only four possible contours satisfying this condition.
If we perform the integration for $\sqrt{P_4(a,x)}$, the branch cuts for the polynomial are for $a \in (0,4)$ and $a \in ((\sqrt{x}-1)^2, (\sqrt{x}+1)^2)$ and we can define three different integration contour $\Gamma_1, \Gamma_2, \Gamma_3$ as depicted in Fig. 2.19.11.

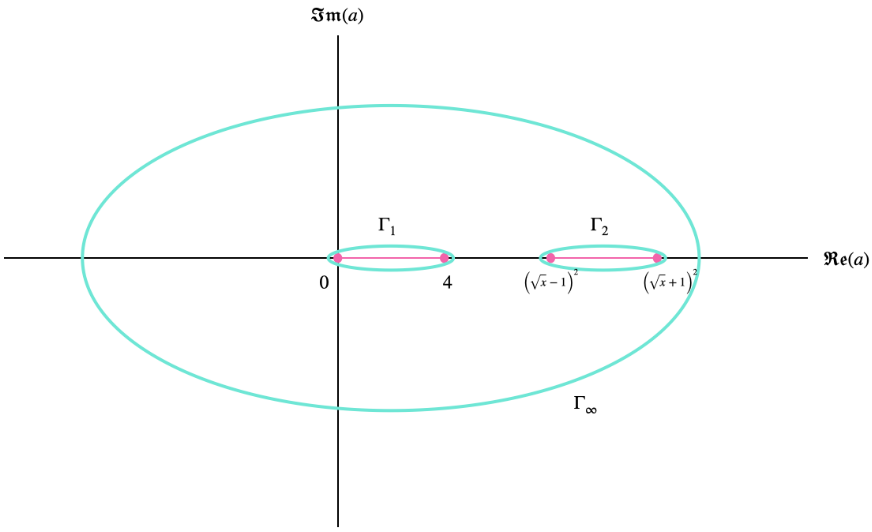

Figure 2.19.11. Three integration contour obtained for positive sign of the polynomial under the square roots.

The contour Γ_∞ encircles both branch cuts enclosed by the different contours Γ_1 and Γ_2. Γ_∞ is homotopic to $\Gamma_1 + \Gamma_2$ since we can continuously deform it into these smaller contours without crossing any non-analytic regions. Then, if we shrink the Γ_∞ contour around the branch points we can rewrite the integral around it as a sum of integrals around the smaller contours:

$$\oint_{\Gamma_\infty} \frac{da}{\sqrt{+P_4(a,x)}} = \oint_{\Gamma_1} \frac{da}{\sqrt{+P_4(a,x)}} + \oint_{\Gamma_2} \frac{da}{\sqrt{+P_4(a,x)}}. \tag{19.32}$$

However, the integral over the contour Γ_∞ is zero:

$$\oint_{\Gamma_\infty} \frac{da}{\sqrt{+P_4(a,x)}} \sim \frac{1}{a^2}\bigg|_{a\to\infty} = 0, \tag{19.33}$$

then the sum in eq. (19.32) is zero and we just need to compute on integral that we choose to be around Γ_1:

$$\oint_{\Gamma_1} \frac{da}{\sqrt{+P_4(a,x)}} = 2\,i\int_{a_1}^{a_2} \frac{da}{\sqrt{-P_4(a,x)}}, \tag{19.34}$$

where the minus sign inside the square root assure to deal with real integrals.
Changing the integration variable to:

$$y^2 = \frac{(a_4-a_2)(a-a_1)}{(a_2-a_1)(a_4-a)}, \tag{19.35}$$

the first period is:

$$\varpi_0 = \oint_{\Gamma_1} \frac{da}{\sqrt{+P_4(a,x)}} = \frac{2}{\sqrt{(a_3-a_1)(a_4-a_2)}} K(\lambda), \tag{19.36}$$

where $K(\lambda)$ is the complete elliptic integrals of the first kind defined by:

$$K(\lambda) = \int_0^1 dt \frac{1}{\sqrt{(1-t^2)(1-\lambda t^2)}}. \tag{19.37}$$

On the other hand, if we have $\sqrt{-P_4(a,x)}$, the branch cuts for the polynomial are for $a \in (-\infty, 0)$, $a \in (4, (\sqrt{x}-1)^2)$ and $a \in ((\sqrt{x}+1)^2, +\infty)$ and we can define only one possible integration contour for these three branch cuts, as depicted in Fig. 2.19.12.

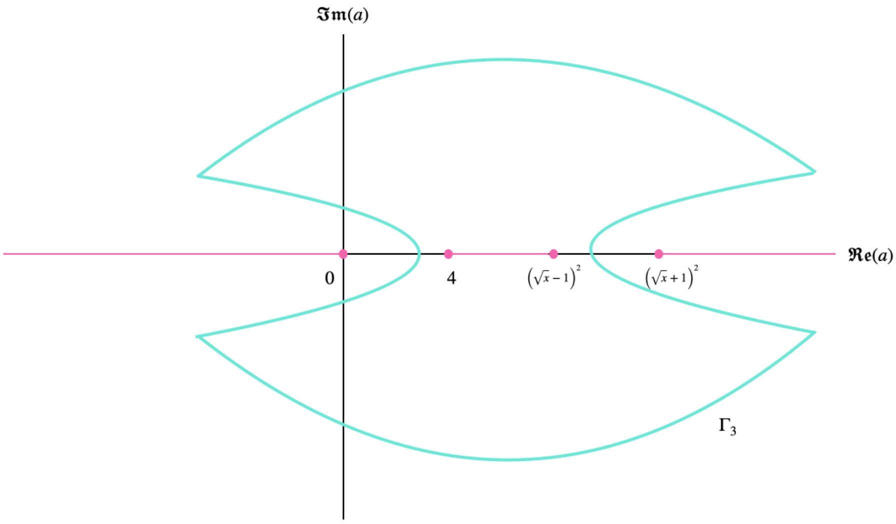

Figure 2.19.12. Integration contour obtained for negative sign of the polynomial under the square roots.

In this case we have:

$$\oint_{\Gamma_3} \frac{da}{\sqrt{-P_4(a,x)}} = 2\,i\int_{a_2}^{a_3} \frac{da}{\sqrt{P_4(a,x)}} = 2\,i\int_{-\infty}^{a_1} \frac{da}{\sqrt{+P_4(a,x)}} + 2\,i\int_{a_4}^{+\infty} \frac{da}{\sqrt{+P_4(a,x)}}. \tag{19.38}$$

Changing the variable to:

$$y^2 = \frac{(a_1 - a_3)(a - a_2)}{(a_3 - a_2)(a_1 - a)}, \tag{19.39}$$

the second period is given by:

$$\varpi_1 = \oint_{\Gamma_3} \frac{da}{\sqrt{-P_4(a,x)}} = \frac{2}{\sqrt{(a_3 - a_1)(a_4 - a_2)}} K(1 - \lambda). \tag{19.40}$$

Finally we can conclude with some important observations. Unlike the bubble case, here we obtained two solutions from the maximal cut, which corresponds to the solutions of the second order differential equations, due to the presence of a coupled sector, obtained for the sunrise integral. These solutions involves elliptic integrals and then its natural to understand that the geometry associated to the integral is more complicated than the previous one. In particular, after the maximal cut, we obtained the square root of a fourth-degree polynomial and this root can't be rationalized. This implies that the new square root intrinsically defines a new geometry. All the technical details used are discussed in Ref. [129]. In the bubble case, as in the case in which the analytic structure of the integral involves (at most) MPLs, the complex surface where the functions are defined is the punctured Riemann sphere, i.e. $\mathbb{C}^{\infty}/\{x_1, ..., x_n\}$, where $\{x_1, ..., x_n\}$ is the set of poles. However, the geometry associated to the Riemann surface associated to the curve $y = \sqrt{\pm P_4(a,x)}$ is a complex torus, as discussed in section 2.14. Furthermore, it's very relevant to notice that the two solutions ϖ_0 and ϖ_1 corresponds to the two periods of the elliptic curves, and it's always possible to obtain a solution as a linear combination of the two periods.

2.20 Generalised power series expansion

Given a set of MIs $\underline{\mathcal{J}} = \{\mathcal{J}_n\}_{n=1,\cdots,N}$ we discussed in details how they satisfy a system of first order linear differential equations with respect to the kinematic invariants. Once the system of DEs has been obtained, we need to evaluate the MIs either analytically or numerically. In the case where the system can be expressed in the ϵ-factorised form, a solution can be found in terms of Chen iterated integrals, and if the system can be cast in canonical logarithmic form, the analytic solution can be obtained in terms of MPLs. However, we have seen that there are more complex mathematical structures, and it is not always possible to express the system in canonical form. In practice, it is possible to work on the system of differential equations in order to find a rotation that allows the system to be expressed in canonical form, with the exception of certain coupled sectors. We will see in the original part of the thesis that the presence of the sector of elliptic MIs makes an analytical evaluation quite complicated, and thus, we will use a different semi-analytical method that allows us to obtain a numerical solution at every point in phase space, regardless of the function space on which the integrals are defined. This method is based on the *generalised power series expansion* technique [132] implemented in the Mathematica packages DiffExp [133] and SeaSyde[134]. The series expansion method was already used in literature for the computation of scattering amplitudes [135, 136, 137, 138, 139, 140, 141, 142, 143, 144, 141, 145, 146, 147, 148]

Suppose that we know the values of the MIs in a boundary point $\underline{x_0}$ and we want to evaluate them in another point $\underline{x}$. We can parametrise the curve connecting these points, as shown in Fig. 2.20.13, with a parameter λ:

$$\gamma(\lambda)\ :\lambda \in [\lambda_0,\, \lambda^\star] \quad \lambda \mapsto \{x_1(\lambda), ..., x_n(\lambda)\}, \quad \text{with} \quad \begin{cases} \gamma(\lambda_0) = \underline{x}_0 \\ \gamma(\lambda^\star) = \underline{x} \end{cases}, \tag{20.1}$$

where $\{x_i\}_{i=1,\cdots,n}$ is the set of scales.

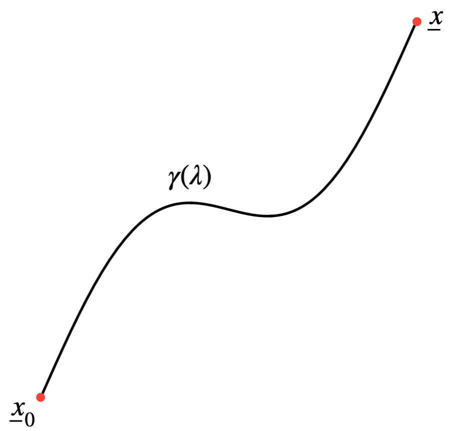

Figure 2.20.13. Parametrised contour connecting the boundary point $\underline{x}_0$ to another point $\underline{x}$.

In this way we pass from a multi-scale problem to a single-scale problem rewriting the system of DEs with respect to the new parameter λ:

$$\partial_\lambda \underline{\mathcal{J}}(\lambda,\epsilon) = \mathbb{B}(\lambda,\epsilon)\,\underline{\mathcal{J}}(\lambda,\epsilon), \tag{20.2}$$

where the matrix $\mathbb{B}$ is obtained from the previous one, which contains the dependencies from the set of scales $\underline{x}$, as:

$$\mathbb{B}(\lambda,\epsilon) = \sum_{i=1}^{n} \mathbb{A}(\underline{x},\epsilon)\Big|_{x_i \to \lambda} \partial_\lambda\, x_i(\lambda) \tag{20.3}$$

The method is based on finding series solutions around regular or singular points, order-by-order in ϵ. We can always consider the ϵ-expansion as a Taylor series for the MIs, as in eq. (10.7).
At each order in ϵ:

$$\underline{\mathcal{J}}^k\left(\gamma(\lambda^\star)\right) = \int_{\lambda_0}^{\lambda^\star} \mathbb{B}(\lambda,\epsilon)\,\underline{\mathcal{J}}^{k-1}(\lambda)\,d\lambda \,+\, \underline{\mathcal{J}}^k\left(\gamma(\lambda_0)\right). \tag{20.4}$$

Expanding in series $\mathbb{A}(\lambda,\epsilon)$ around a point Λ, leads to integrals of the type in eq. (20.4):

$$\int (\lambda\,-\,\Lambda)^\omega\, \log(\lambda\,-\,\Lambda)^m, \quad \omega \in \mathbb{Q},\, m \in \mathbb{N}. \tag{20.5}$$

In general, through series expansion we can obtain two different solution for the MIs, depending on the point Λ around which we perform the expansion:

- Λ **is a regular point**:

$$\underline{\mathcal{J}}(\lambda,\epsilon) = \sum_{k=0}^{\infty} \epsilon^k \sum_{i=0}^{\infty} \underline{c}^{(k,i)}\ (\lambda\,-\,\Lambda)^i\,, \tag{20.6}$$

  Then, in the vicinity of a regular point we have a standard Taylor series representation.

- **Λ is a singular point**:

$$\underline{\mathcal{J}}(\lambda,\epsilon)=\sum_{k=0}^{\infty}\epsilon^{k}\sum_{i=0}^{\infty}\sum_{l=0}^{N_k}\underline{c}^{k,i,l}\;(\lambda\,-\,\Lambda)^{\frac{i}{2}}\log(\lambda\,-\,\Lambda)^{l},\tag{20.7}$$

where $\underline{c}^{k,i,l}$ are vectors of dimensions equalt to the number of MIs and N_k is the maximal power of the logarithms at order ϵ^k.

It's important to stress that the series solutions founded are valid in a region centered around the regular or singular point with a specific radius of convergence. If our boundary point is $\underline{x}_0$ and we want to evaluate the MIs in a different point $\underline{x}$, where the points are connected through the parametrized contour $\gamma(\lambda)$, an expansion around the full contour is needed. In general, there will be different singular points and we need to perform multiple series expansions around these points in order to obtain a solution at any point in the phase-space. In Fig. 2.20.14 we illustrate a basic example in order to explain the matching of the solutions. Suppose that we have an initial point Λ_1 as boundary point and we want to obtain an evaluation in a point Λ_2. Then we introduce a new (regular) point Λ_3 such that the expansions centered in Λ_1 and in Λ_2 are matched in Λ_3. We can adopt this concatenation of solutions to fill all the contour and obtain iteratively the solution at any point.

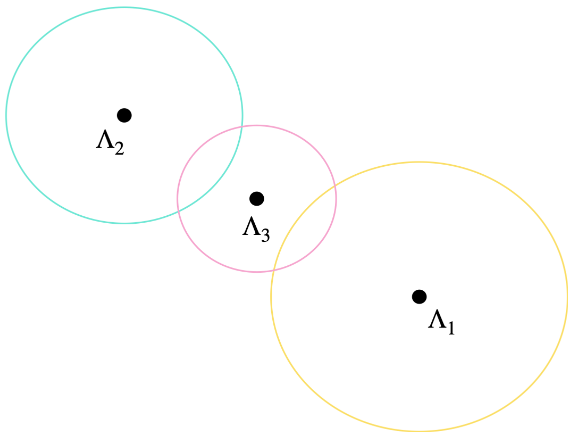

Figure 2.20.14. Example of matching between expanded solutions around different points.

A subtle point that needs to be analyzed, as it often occurs in practice, is when the expansion happens around a point that is a threshold singularity. Generally, in the expansion of the DEs matrix, logarithms and square roots are present, so we need to use analytic continuation in order to move above or below the threshold.
For the logarithmic case, suppose to have a $\lambda \in \mathbb{R}$ and we want to study $\log(\lambda)$. When $\lambda > 0$ there is no ambiguity and we just have the usual $\log(\lambda)$, but for $\lambda < 0$ the function become multi-valued. In order to uniquely define the logarithm, we add to the argument an infinitesimal imaginary part. If we approach λ from above (in the complex plane, from the upper half-plane):

$$\log(\lambda\,+\,i\,\xi)=\log(\lambda),\qquad \xi\to 0^{+}.\tag{20.8}$$

If we add a negative imaginary part, we approach λ from below (from lower half-plane):

$$\log(\lambda - i\,\xi) = \log(\lambda) - 2\pi i \Theta(-\lambda), \qquad \xi \to 0^-, \tag{20.9}$$

where Θ is the Heaviside step function defined in eq. (5.14). For $\lambda > 0$ we have the usual $log(\lambda)$ as in the previous case, while if $\lambda < 0$ there is a correction of $2\pi i$ that reflects the phase discontinuity when crossing the negative branch of the logarithmic function.
For the case of the square root, we proceed similarly. We consider $\lambda \in \mathbb{R}$ and add an infinitesimal imaginary part. If we add a positive infinitesimal imaginary part:

$$\sqrt{\lambda + i\,\xi} = \sqrt{\lambda}, \tag{20.10}$$

for a negative imaginary part:

$$\sqrt{\lambda - i\,\xi} = \sqrt{\lambda}\,\left(\Theta(\lambda) - \Theta(-\lambda)\right). \tag{20.11}$$

In this second case for $\lambda > 0$ we are still in the upper half-plane and there is no correction due to the presence of the Heaviside step function. Hovewer, if $\lambda < 0$, $(\Theta(\lambda) - \Theta(-\lambda)) \to -1$, then:

$$\sqrt{\lambda} \to -\sqrt{\lambda}. \tag{20.12}$$

We want to emphasise that this method can be applied in any case, both in the simplest scenario where only MPLs are present and in more complex cases where the function space is broader. In particular, the method of DEs provides a very powerful tool for analytical computations; however, it is not always possible to obtain a solution by calculating the iterated integrals explicitely. Specifically, if we are interested in obtaining numerical values for phenomenological analysis, the generalised power series expansion method can be used to numerically evaluate the MIs with arbitrary precision at any point of the phase space. This strategy, while powerful, also has limitations, as in more complicated cases, the computational time required by programs using this method can be significant. Additionally, it should be noted that often the problem lies in the computation of the amplitude, and writing a system of DEs not in ϵ-factorised form don't allows us to express the MIs in terms of iterated integrals. This may obscure potential simplifications at the amplitude level. This is because some integrals may not contribute actively, and the expected pole cancellation is not immediately visible, which must be explicitly derived by subsequently simplifying the amplitude and renormalizing.

2.20.1 Generalise power series - ϵ-factorised form and coupled sectors

We discuss how to obtain the solutions in eq. (20.6) and eq. (20.7), by the expansion of the DEs matrix around, respectively, regular and singular point and integrating order-by-order in ϵ. We analyze two different cases, the first where the DEs are in canonical logarithmic form and the second where we analyze a coupled sector for which a canonical form cannot be obtained.

DEs in ϵ-factorised form

Given the system of DEs in canonical form:

$$\partial_\lambda \underline{\mathcal{J}}(\lambda, \epsilon) = \epsilon\, \tilde{\mathbb{B}}(\lambda)\, \underline{\mathcal{J}}(\lambda, \epsilon), \tag{20.13}$$

where the curve is parametrised as in eq. (20.1) and the value of the MIs is known in a boundary point $\underline{\lambda}_0$.

The formal solution in this case can be written directly in terms of Chen iterated integrals:

$$\underline{\mathcal{J}}(\lambda,\epsilon) = \underline{\mathcal{J}}(\gamma(0)) + \sum_{k=1}^{\infty} \epsilon^k \sum_{j=1}^{k} \int_{\lambda_0}^{\lambda} \gamma^\star(\tilde{\mathbb{B}}(\lambda_1)) \cdots \int_{\lambda_0}^{\lambda_{j-1}} \gamma^\star(\tilde{\mathbb{B}}(\lambda_j))\ \underline{\mathcal{J}}^{(k-j)}(\gamma(0)). \tag{20.14}$$

We are interested in the solution around a regular or singular point Λ. We already discussed that this solution can be obtained by the expansion in series of the DEs matrix around Λ:

$$\tilde{\mathbb{B}}(\lambda) = \sum_{i=0}^{\infty} \tilde{\mathbb{B}}^{(i)}\,(\lambda\,-\,\Lambda)^{\omega_i}, \qquad \omega_i \in \mathbb{Q}. \tag{20.15}$$

eq. (20.14) becomes:

$$\begin{aligned}\underline{\mathcal{J}}(\lambda,\epsilon) =& \underline{\mathcal{J}}(\gamma(0))\,+\,\sum_{k=1}^{\infty} \epsilon^k \sum_{j=1}^{k} \sum_{i_1,\cdots,i_j=0}^{\infty} \tilde{\mathbb{B}}^{(i_1)}\,\ldots\,\tilde{\mathbb{B}}^{(i_j)} \\ &\times \int_{\lambda_0}^{\lambda} d\lambda_1\,(\lambda_1\,-\,\Lambda)^{\omega_{i_1}}\,\cdots\,\int_{\lambda_0}^{\lambda_{j-1}} d\lambda_j\,(\lambda_j\,-\,\Lambda)^{\omega_{i_j}}\ \underline{\mathcal{J}}(\gamma(0)).\end{aligned} \tag{20.16}$$

The solution is given by k-fold integrals of the form discussed in eq. (20.5). Then we obtained the desired series solution around a point Λ for $\underline{\mathcal{J}}(\lambda,\epsilon)$.

DEs for coupled sectors

Often, the system of DEs cannot be cast in canonical logarithmic form and an ϵ-factorised form is not easy to reach. We proceed by separating coupled sectors from those that instead are described by the previous case. Suppose that we have a system of DEs with $\{\mathcal{J}_j\}_{j=1,\cdots,r}$ coupled MIs in a sector. For any coupled block, at order ϵ, the system has the form:

$$\partial_\lambda \underline{\mathcal{J}}^{(k)}(\lambda)\;=\;\mathbb{B}^{(0)}(\lambda)\,\underline{\mathcal{J}}^{(k)}(\lambda)\,+\,\sum_{j=0}^{k-1} \mathbb{B}^{(k-j)}(\lambda)\,\underline{\mathcal{J}}^{(j)}(\lambda), \tag{20.17}$$

where, up to appropriate rescaling in ϵ, the DEs matrix is considered with the following expansion:

$$\mathbb{B}(\lambda,\epsilon)\;=\;\sum_{k=0}^{\infty} \epsilon^k\,\mathbb{B}^{(k)}(\lambda). \tag{20.18}$$

We represent the homogeneous DEs matrix by $\mathbb{H}$, whose entries are $H_{ij}\;=\;\left(\mathbb{B}^{(0)}(\lambda)\right)_{ij}$, such that eq. (20.17) can be written as:

$$\partial_\lambda \underline{\mathcal{J}}^{(k)} = \mathbb{H}\,\underline{\mathcal{J}}^{(k)}\;+\;\text{Subtopologies}. \tag{20.19}$$

We focus on the homogeneous DEs:

$$\partial_\lambda \underline{\mathcal{J}}^{(k)} = \mathbb{H}\,\underline{\mathcal{J}}^{(k)}, \tag{20.20}$$

and through the homogeneous solutions we could find the full solutions of the DEs in eq. (20.17).
Iteratively deriving eq. (20.20) with respect to λ, we obtain a r-th order DE for each MIs in the coupled sector. For the j-th MI, the DE reads:

$$\frac{\partial^r \mathcal{J}_j^{(k)}(\lambda)}{\partial \lambda^r} + a_1(\lambda)\frac{\partial^{r-1} \mathcal{J}_j^{(k)}(\lambda)}{\partial \lambda^{r-1}} + \cdots a_r(\lambda)\, \mathcal{J}_j^{(k)}(\lambda) = 0. \tag{20.21}$$

It is possible to find r independent homogeneous solutions for $\mathcal{J}_j^{(k)}$ that we represents with $\{h_i(\lambda)\}_{i=1,\cdots,r}$.
In order to obtain the homogeneous solution we rely on the Frobenius method. This method allows us to find series solutions in the vicinity of a regular or singular point Λ:

$$h_i(\lambda) = \sum_{i\in\{0,\cdots,r\}} \sum_{j=0}^{\infty} \sum_{l=0}^{N_k} c_i^{i,j,l} (\lambda - \Lambda)^{n_i+j} \log(\lambda - \Lambda)^l, \tag{20.22}$$

where n_i is the root of the indicial equation obtained from the Frobenius method and N_k is the maximal power of the logarithms.
The full solution can be obtained for each MIs from the Wronskian matrix W which contains the homogeneous solution $h_i(\lambda)$ and its derivatives.

Chapter 3

Universality of transverse-momentum cross sections and hard factors

In perturbative QCD, calculations beyond leading order (LO) encounter infrared (IR) divergences in intermediate stages. These divergences pose a challenge for phenomenological analyses at the LHC, which rely on Monte Carlo numerical codes. To address this, specialized techniques known as *subtraction methods*, are employed to handle and cancel these IR divergences within the Monte Carlo framework. This thesis utilizes the transverse momentum (q_T) subtraction method [149, 150] for this purpose.

As outlined in the Introduction (see chapter 1), the original work presented in this thesis is twofold: (i) the calculation of state-of-the-art multi-loop scattering amplitudes, and (ii) their subsequent application to produce high-precision predictions for LHC phenomenology. These two aspects are intrinsically related. This chapter provides a concise introduction to the q_T-subtraction method, detailing its essential components and elucidating how the newly calculated multi-loop scattering amplitudes are incorporated into the numerical computations.

Furthermore, at the fully differential level, *fixed-order* cross sections exhibit additional singularities in specific kinematic limits, such as the low transverse momentum region ($q_T \to 0$). These singularities manifest as logarithmic terms that enhance the cross section in the small-q_T limit. To ensure the physical validity of the calculation, these large logarithmic contributions must be *resummed to all orders* in the strong coupling. In this chapter we describe the details of the transverse momentum resummation formalism, which is crucial for obtaining reliable predictions for transverse momentum distributions, even in the low q_T region.

3.1 The transverse momentum subtraction method

Consider the inclusive hard scattering process involving two hadrons, h_1 and h_2, which collide to produce a final state F and additional hadronic activity denoted by X

$$h_1(p_1) + h_2(p_2) \to F(M, q_T) + X, \tag{1.1}$$

Here, F represents the specific final state under consideration (i.e., to be measured), while X includes any additional jets or particles produced in the process (extra partonic radiation) that are not directly observed. This extra radiation must be fully accounted for (integrated) in the calculation. The corresponding hadronic momenta are p_1 and p_2, such that the center of mass energy of the colliding hadrons is $s = (p_1 + p_2)^2$.

The final state F consists of one or more colorless particles with momenta q_i, and its total invariant mass M is defined as:

$$M^2 = \left(\sum_i q_i\right)^2 . \tag{1.2}$$

At LO the total transverse momentum $q_T = \sum_i q_{T_i}$ of the final state F vanishes due to momentum conservation (in the special case of two particles in the final state, they are produced back to back). At higher orders in perturbation theory, the emission of extra partonic radiation induces a recoil against the final state F, resulting in non-zero transverse momentum.

At next-to-leading order (NLO), the calculation incorporates two distinct types of contributions, classified according to the nature of the additional radiation:

- **Real Contributions:**

  At this perturbative order, these terms involve the single emission (see Fig. 3.1.2) of an additional particle during the process (generally partons in QCD or photons in QED). This emission modifies the final state phase-space and produces large logarithmic terms in the small-q_T limit that need to be canceled against dedicated counter-terms (CT). Such CT are provided by the transverse momentum subtraction method [149, 150].

- **Virtual Contributions:**

  Virtual corrections involve one-loop diagrams (see Fig. 3.1.2), where the virtual particle (for example a gluon or a photon) does not appear in the final state but contributes only to form a closed loop. In the virtual contributions, we can have not only IR singularities, but also UV singularities, consequently to the loop computation. The relevant information to be included in the Monte Carlo is the finite part of such contributions. Therefore, the transverse momentum subtraction method has to provide a dedicated methodology in order to subtract the IR poles (after UV regularization) and isolate the relevant finite part [150].

At the next-to-next-to-leading order (NNLO) there are three types of contributions:

- **Double-Real (RR) contributions:** These corrections arise from the emission of two additional partons (quarks or gluons or photons in QED) during the scattering process. This emission modifies the final state phase-space, and the momenta of both additional partons must be integrated over. As in the NLO case, real emissions can lead to IR singularities originating from soft and collinear divergences.

- **Real-Virtual (RV) contributions:** These are one-loop corrections that involve both real and virtual radiation. Specifically, one of the two emitted partons is a real emission, while the other is a virtual particle forming a closed loop. These contributions can exhibit both UV divergences (which are renormalized) and IR divergences (soft/collinear).

- **Double-Virtual (DV) contributions:** These contributions, typically the most computationally demanding, involve two-loop diagrams with no real emissions. These two-loop diagrams can contain both UV and IR divergences. As in the NLO case, the finite part has to be isolated from the IR poles and therefore the transverse momentum subtraction method has to provide a dedicated methodology in order to subtract the IR poles (after UV regularization) and isolate the relevant finite part [150] also at this perturbative order.

Under the light of the previous discussed points, we can write the general structure of the differential NNLO cross section in the following sketchy form:

$$d\sigma^F = d\sigma^F_{LO} + d\sigma^F_{NLO} + d\sigma^{F;RR}_{NNLO} + d\sigma^{F;RV}_{NNLO} + d\sigma^{F;DV}_{NNLO}\,, \tag{1.3}$$

where

$$d\sigma^F_{NLO} = d\sigma^{F;R}_{NLO} + d\sigma^{F;V}_{NLO}\,. \tag{1.4}$$

Numerically, the cancellation of IR divergences within the Monte Carlo framework presents a significant challenge, particularly for the RR and RV contributions. This necessitates the use of an additional NLO subtraction method, as the effective perturbative order of the RR and RV terms is one order lower than NNLO. We employ the Catani-Seymour dipole subtraction method [47] to handle and cancel these IR singularities locally at intermediate stages of the calculation. The combination of the RR and RV contributions within the Monte Carlo, achieved through this local subtraction method, produces a physical cross section for the final state F associated with one effective jet.

$$d\sigma^F_{NNLO} = d\sigma^{F+jets}_{NLO} \qquad q_T \neq 0. \tag{1.5}$$

This physical NLO cross section exhibits only one type of remaining IR singularity, associated with the small-q_T limit of F. These remaining singularities are treated and canceled by the NNLO counterterms of the transverse momentum subtraction method [149, 150],

$$d\sigma^{CT} = d\sigma^F_{LO} \otimes \Sigma^F \left(\frac{q_T}{M}\right) d^2_{q_T}, \tag{1.6}$$

where $\otimes$ represent the convolution over the momentum fractions and summation over the flavor indices of the partons, and $\Sigma^F\,(q_T/M)$ embodies all the logarithmic terms which become large in the small-q_T limit,

$$\lim_{q_T\to 0} \Sigma^F \left(\frac{q_T}{M}\right) = \sum_{n=1}^{\infty} \left(\frac{\alpha_s}{\pi}\right)^n \sum_{k=1}^{2n} \Sigma^{F\,(n,k)} \frac{M^2}{q_T^2}\, log^{k-1}\left(\frac{M^2}{q_T^2}\right). \tag{1.7}$$

Where the series coefficients $\Sigma^{F\,(n,k)}$ does not depend on q_T and can be obtained from the of the universal (i.e., independent of the final state F) resummation formalism for large logarithmic corrections to the cross section at low transverse momentum.

Adding back the contribution at $q_T = 0$, the sketchy form of the exclusive NNLO cross section can be written:

$$d\sigma^F_{NNLO} = \mathcal{H}^F_{NNLO} \otimes d\sigma^F_{LO} + \left[d\sigma^{F+jets}_{NLO} - d\sigma^{CT}_{NNLO}\right], \tag{1.8}$$

where $\mathcal{H}^F_{NNLO}$ is the so-called *hard virtual function* and contains the finite part of the two-loop virtual scattering amplitude $d\sigma^{F;DV}_{NNLO}$. As discussed before, in eq. (1.8), the term inside the bracket is IR safe and then integrable in q_T. At NNLO, $d\sigma^{CT}_{NNLO}$ acts on the sum on the RR and RV contributions for the $F + jets$ final state. At the NLO, the exclusive cross section can be simply written:

$$d\sigma^F_{NLO} = \mathcal{H}^F_{NLO} \otimes d\sigma^F_{LO} + \left[d\sigma^{F+jets}_{LO} - d\sigma^{CT}_{NLO}\right], \tag{1.9}$$

where trivially $d\sigma^{F+jets}_{LO} = d\sigma^{F;R}_{NLO}$ (see eq. (1.4)). The finite part of the one-loop virtual scattering amplitude $d\sigma^{F;V}_{NLO}$ is embodied in the hard-virtual function at the corresponding perturbative order ($\mathcal{H}^F_{NLO}$).
In the next section, the explicit form of the resummation coefficients Σ^F will be given, after the proper discussion of the transverse momentum resummation programme.

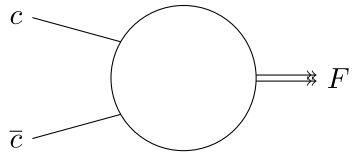

Figure 3.1.1. LO cross section initiated by the sub-process $c\,\bar{c} \to F$, with $c = q, g$, for F colourless.

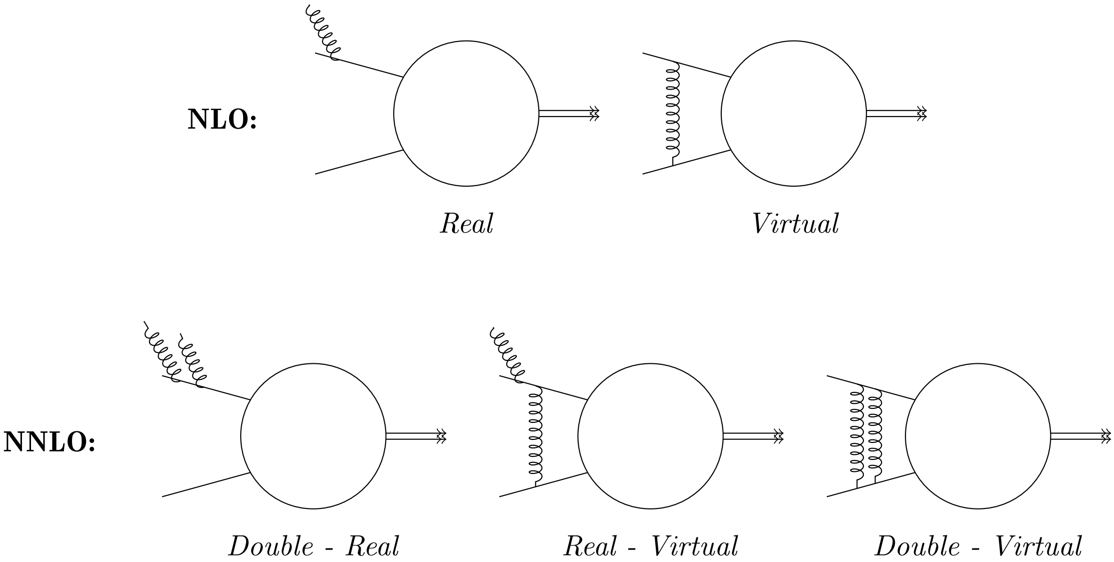

Figure 3.1.2. Different contributions at NLO and NNLO for the following sub-processes $c\,\bar{c} \to F$, with $c = q, g$.

3.2 Transverse momentum resummation

The b-space resummation[1] approach was fully formalized by Collins, Soper and Sterman [151, 152] in terms of perturbative coefficients. Consider the hard scattering reaction defined in eq. (1.1). According to the QCD factorisation theorem (see Ref. [16] and references therein), the corresponding transverse momentum differential cross section is cross section $d\hat{\sigma}_F/dq_T^2$ can be written as

$$\frac{d\sigma_F}{dq_T^2}(q_T, M, s) = \sum_{a,b} \int_0^1 dx_1 \int_0^1 dx_2\, f_{a/h_1}(x_1, \mu_F^2)\, f_{b/h_2}(x_2, \mu_F^2)\, \frac{d\hat{\sigma}_{F\,ab}}{dq_T^2}(q_T, M, \hat{s}; \alpha_s, \mu_R^2, \mu_F^2), \tag{2.1}$$

where $f_{a/h}(x, \mu_F^2)$ ($a = q_f, \bar{q}_f, g$) are the parton densities of the colliding hadrons at the factorisation scale μ_F, $d\hat{\sigma}_{F\,ab}/dq_T^2$ are the partonic cross sections, $\hat{s} = x_1 x_2 s$ is the partonic centre-of-mass energy, and μ_R is the renormalisation scale. Throughout the paper we use parton densities as defined in the $\overline{\text{MS}}$ factorisation scheme, and $\alpha_S(q^2)$ is the QCD running coupling in the $\overline{\text{MS}}$ renormalisation scheme.

The partonic cross section can be computed in perturbative QCD as a power series expansion in the strong coupling constant α_S. We begin by considering the production of the final state system F with no accompanying radiation, i.e., at zero transverse momentum ($q_T = 0$). In this lowest-order approximation, the cross section is proportional to $\delta(q_T^2)$: $d\hat{\sigma}^{(0)}_{F\,c\bar{c}}/dq_T^2 \propto \delta(q_T^2)$.

Since F is colourless, the lowest-order partonic sub-process, $c + c \to F$, occurs through

[1] The impact parameter b is the conjugate variable of the transverse momentum q_T.

either quark-antiquark annihilation ($c = q$), as in the production of γ^*, W, and Z bosons, or gluon-gluon fusion ($c = g$), as in the case of SM Higgs boson production.

However, as noted in sect. 1, higher-order corrections introduce logarithmic terms of the form $\log^m(M^2/q_T^2)$, which become large in the small-q_T region ($q_T \ll M$). To address this, we decompose the partonic cross section into two components:

$$\frac{d\hat{\sigma}_{F\,ab}}{dq_T^2} = \frac{d\hat{\sigma}_{F\,ab}^{(\text{res.})}}{dq_T^2} + \frac{d\hat{\sigma}_{F\,ab}^{(\text{fin.})}}{dq_T^2} \,. \tag{2.2}$$

The first term, $d\hat{\sigma}_{F\,ab}^{(\text{res.})}$, contains all logarithmically-enhanced contributions at small-q_T and is evaluated by resummation to all orders in α_S. The second term, $d\hat{\sigma}_{F\,ab}^{(\text{fin.})}$, is free of such enhancements and can be computed through fixed-order truncation of the perturbative series. We define this 'finite' component such that its integral vanishes order-by-order in perturbation theory in the small-q_T limit:

$$\lim_{Q_T \to 0} \int_0^{Q_T^2} dq_T^2 \left[\frac{d\hat{\sigma}_{F\,ab}^{(\text{fin.})}}{dq_T^2}\right]_{\text{f.o.}} = 0 \,. \tag{2.3}$$

This implies that any contributions proportional to $\delta(q_T^2)$ are included in the 'resummed' component, $d\hat{\sigma}_{F\,ab}^{(\text{res.})}$. While a complete evaluation of $d\hat{\sigma}_{F\,ab}^{(\text{res.})}$, is not possible, we can systematically organize the logarithmic contributions and truncate the series at a given logarithmic accuracy (LL, NLL, etc.), as discussed in sect. 3.2.1.

In practice, the q_T distribution is calculated by combining the resummed and finite components, each truncated at a specific accuracy:

$$\frac{d\hat{\sigma}_{F\,ab}}{dq_T^2} \longrightarrow \left[\frac{d\hat{\sigma}_{F\,ab}^{(\text{res.})}}{dq_T^2}\right]_{\text{l.a.}} + \left[\frac{d\hat{\sigma}_{F\,ab}^{(\text{fin.})}}{dq_T^2}\right]_{\text{f.o.}} \,. \tag{2.4}$$

This ensures uniform formal accuracy across the entire q_T range. To achieve a consistent matching between the resummed and fixed-order predictions, we subtract the perturbative truncation of the resummed component from the fixed-order cross section:

$$\left[\frac{d\hat{\sigma}_{F\,ab}^{(\text{fin.})}}{dq_T^2}\right]_{\text{f.o.}} = \left[\frac{d\hat{\sigma}_{F\,ab}}{dq_T^2}\right]_{\text{f.o.}} - \left[\frac{d\hat{\sigma}_{F\,ab}^{(\text{res.})}}{dq_T^2}\right]_{\text{f.o.}} \,. \tag{2.5}$$

This matching procedure, guarantees that the combined result retains the full information of the fixed-order calculation while incorporating the resummation of logarithmically-enhanced contributions.

To further improve the accuracy at large q_T, we impose a constraint on the total cross section, requiring that the integral of the resummed component matches the fixed-order result:

$$\int_0^\infty dq_T^2 \left[\frac{d\hat{\sigma}_{F\,ab}^{(\text{res.})}}{dq_T^2}\right]_{\text{l.a.}} = \int_0^\infty dq_T^2 \left[\frac{d\hat{\sigma}_{F\,ab}^{(\text{res.})}}{dq_T^2}\right]_{\text{f.o.}} \,. \tag{2.6}$$

This effectively acts as a unitarity constraint, ensuring that the resummation does not artificially enhance the total cross section.

Finally, we emphasise that this resummation formalism is implemented at the level of the partonic cross section, with parton densities evaluated at the factorisation scale μ_F. This approach explicitly accounts for the dominant effects in the region $q_T \ll M$ through all-order resummation, allowing us to set the central values of the renormalisation and factorisation scales to the remaining hard scale of the process, M.

3.2.1 The resummed component

The resummation of logarithmically-enhanced contributions at small-q_T is carried out in impact-parameter space to account for transverse-momentum conservation. The resummed component of the cross section is obtained through an inverse Fourier (Bessel) transformation:

$$\frac{d\hat{\sigma}^{(\text{res.})}_{F,ab}}{dq_T^2} = \frac{M^2}{\hat{s}} \int \frac{d^2\mathbf{b}}{4\pi}\, e^{i\mathbf{b}\cdot q_T}\, \mathcal{W}^F_{ab} = \frac{M^2}{\hat{s}} \int_0^\infty db\, \frac{b}{2}\, J_0(bq_T)\, \mathcal{W}^F_{ab}\,, \tag{2.7}$$

where $J_0(x)$ is the 0th-order Bessel function and $\mathcal{W}^F_{ab}$ embodies the all-order dependence on the large logarithms. The resummation structure is organized in exponential form:

$$\mathcal{W}^F_N(b, M; \alpha_S(\mu_R^2), \mu_R^2, \mu_F^2) = \mathcal{H}^F_N \times \exp \mathcal{G}_N\,, \tag{2.8}$$

where $\mathcal{H}^F_N$ contains constant contributions (independent of q_T) and $\exp \mathcal{G}_N$ resums to all order, the enhanced logarithmic terms. The exponent $\mathcal{G}_N$ can be systematically expanded (and organised) as:

$$\mathcal{G}_N(\alpha_S, L; M^2/\mu_R^2, M^2/Q^2) = L\, g^{(1)}(\alpha_S L) + g_N^{(2)}(\alpha_S L; M^2/\mu_R^2, M^2/Q^2) + \ldots\,, \tag{2.9}$$

where $L \equiv \ln(Q^2 b^2/b_0^2)$ and the functions $g_N^{(n)}$ resum logarithms at different logarithmic accuracies: leading logarithmic (LL), next-to-leading logarithmic (NLL), etc. The resummation scale Q appears due to the effective truncation in eq. (2.9) at a given logarithmic order.

The function $\mathcal{H}^F_N$ can be customarily expanded in powers of α_S:

$$\mathcal{H}^F_N(M, \alpha_S; M^2/\mu_R^2, M^2/\mu_F^2, M^2/Q^2) = \sigma_F^{(0)}(\alpha_S, M)\Big[1 + \frac{\alpha_S}{\pi}, \mathcal{H}^{F,(1)}_N + \ldots\Big]\,, \tag{2.10}$$

where $\sigma_F^{(0)}$ is the lowest-order (LO) cross section. The factorisation scale dependence and process dependence (dependence on the final state F) are embodied in the hard virtual factor, highlighting that the form factor $\exp \mathcal{G}_N$ is process independent. The dependence on the renormalisation scale μ_R enters in $\exp \mathcal{G}_N$ through the evolution of the coupling α_S. The truncation of the resummed component at a given logarithmic accuracy is well defined (see eq. (2.6)), and the combination with the fixed-order expansion is briefly discussed in the previous section (for more details see Ref. [153]).

A procedure to reduce the impact of unjustified enhanced logarithms at large q_T is introduced *via* the replacement $L \to \widetilde{L} = \ln(Q^2 b^2/b_0^2 + 1)$. This ensures that the integral of the resummed component reproduces the fixed-order total cross section [153]. This is known as *the unitarity constraint* and could be *slightly violated* (order 1% difference) in the presence of fiducial cuts.

The resummation programme aims to express the logarithmic functions $g_N^{(n)}$ in terms of perturbatively computable coefficients. This is achieved through the integral representation:

$$\mathcal{G}_N(\alpha_S(\mu_R^2), L; M^2/\mu_R^2, M^2/Q^2) = -\int_{b_0^2/b^2}^{Q^2} \frac{dq^2}{q^2}\left[A(\alpha_S(q^2))\, \ln \frac{M^2}{q^2} + \widetilde{B}_N(\alpha_S(q^2))\right]\,, \tag{2.11}$$

where $A(\alpha_S)$ and $\widetilde{B}_N(\alpha_S)$ are perturbative functions with coefficients related to perturbative quark and gluon form factors and parton anomalous dimensions:

$$\begin{aligned} A(\alpha_s) &= \sum_{n=1}^{\infty} \left(\frac{\alpha_s}{\pi}\right)^n A^{(n)}, \\ \tilde{B}_N(\alpha_s) &= \sum_{n=1}^{\infty} \left(\frac{\alpha_s}{\pi}\right)^n \tilde{B}_N^{(n)}. \end{aligned} \tag{2.12}$$

The resummation coefficient $A(\alpha_s)$ has no z-structure and therefore, it does not depend on N. But the $\tilde{B}_N(\alpha_s)$ has two sources of z-dependence (or N-dependence after Mellin transformation):

$$\tilde{B}_N(\alpha_s) \,=\, B(\alpha_s) \,+\, 2\beta(\alpha_s)\,\frac{d\log C_N(\alpha_s)}{d\log\alpha_s} \,+\, 2\gamma_N(\alpha_s)\,, \tag{2.13}$$

which are the collinear coefficient functions $C_N(\alpha_s)$ and the splitting functions $\gamma_N(\alpha_s)$. The resummation coefficient $B(\alpha_s)$ is free of z-dependence and its perturbative expansion is defined in eq. (3.5).

The explicit expressions for the LL, NLL, and NNLL functions $g_N^{(1)}$, $g_N^{(2)}$ and $g_N^{(3)}$ are provided in Ref. [153]). The extension at N^{4}LO was firstly published in [154] (coefficient functions $g_N^{(4)}$ and $g_N^{(5)}$). For the sake of completeness we write the first three coefficient functions, that expanded to fixed order give the NNLO counter term:

$$g^{(1)}(\alpha_S L) = \frac{A^{(1)}}{\beta_0}\frac{\lambda+\ln(1-\lambda)}{\lambda} \quad , \tag{2.14}$$

$$\begin{aligned} g_N^{(2)}\left(\alpha_S L; \frac{M^2}{\mu_R^2}, \frac{M^2}{Q^2}\right) &= \frac{\overline{B}_N^{(1)}}{\beta_0}\ln(1-\lambda) - \frac{A^{(2)}}{\beta_0^2}\left(\frac{\lambda}{1-\lambda}+\ln(1-\lambda)\right) \\ &+ \frac{A^{(1)}}{\beta_0}\left(\frac{\lambda}{1-\lambda}+\ln(1-\lambda)\right)\ln\frac{Q^2}{\mu_R^2} \\ &+ \frac{A^{(1)}\beta_1}{\beta_0^3}\left(\frac{1}{2}\ln^2(1-\lambda)+\frac{\ln(1-\lambda)}{1-\lambda}+\frac{\lambda}{1-\lambda}\right) \quad , \end{aligned} \tag{2.15}$$

$$\begin{aligned} g_N^{(3)}\left(\alpha_S L; \frac{M^2}{\mu_R^2}, \frac{M^2}{Q^2}\right) &= -\frac{A^{(3)}}{2\beta_0^2}\frac{\lambda^2}{(1-\lambda)^2} - \frac{\overline{B}_N^{(2)}}{\beta_0}\frac{\lambda}{1-\lambda} + \frac{A^{(2)}\beta_1}{\beta_0^3}\left(\frac{\lambda(3\lambda-2)}{2(1-\lambda)^2}\right. \\ &\left. -\frac{(1-2\lambda)\ln(1-\lambda)}{(1-\lambda)^2}\right) \\ &+ \frac{\overline{B}_N^{(1)}\beta_1}{\beta_0^2}\left(\frac{\lambda}{1-\lambda}+\frac{\ln(1-\lambda)}{1-\lambda}\right) - \frac{A^{(1)}}{2}\frac{\lambda^2}{(1-\lambda)^2}\ln^2\frac{Q^2}{\mu_R^2} \\ &+ \ln\frac{Q^2}{\mu_R^2}\left(\overline{B}_N^{(1)}\frac{\lambda}{1-\lambda} + \frac{A^{(2)}}{\beta_0}\frac{\lambda^2}{(1-\lambda)^2} + A^{(1)}\frac{\beta_1}{\beta_0^2}\left(\frac{\lambda}{1-\lambda}\right.\right. \\ &\left.\left. + \frac{1-2\lambda}{(1-\lambda)^2}\ln(1-\lambda)\right)\right) \\ &+ A^{(1)}\left(\frac{\beta_1^2}{2\beta_0^4}\frac{1-2\lambda}{(1-\lambda)^2}\ln^2(1-\lambda) + \ln(1-\lambda)\left[\frac{\beta_0\beta_2-\beta_1^2}{\beta_0^4}\right.\right. \\ &\left.\left. + \frac{\beta_1^2}{\beta_0^4(1-\lambda)}\right] + \frac{\lambda}{2\beta_0^4(1-\lambda)^2}(\beta_0\beta_2(2-3\lambda)+\beta_1^2\lambda)\right) \quad , \end{aligned} \tag{2.16}$$

where:

$$\lambda = \frac{1}{\pi}\,\beta_0\,\alpha_S(\mu_R^2)\,L \quad , \tag{2.17}$$

$$\overline{B}_N^{(n)} = \widetilde{B}_N^{(n)} + A^{(n)}\ln\frac{M^2}{Q^2} \quad , \tag{2.18}$$

and β_n are the coefficients of the QCD β function. The explicit expression of the first five coefficients of the β function, can be found in the following references: β_0, β_1 and β_2 in Refs. [155, 156], β_3 in Ref. [157] and β_4 in [158].

3.3 The fixed order expansion

We consider the transverse-momentum differential cross section for the hard-scattering process in eq. (2.1) and we impose the factorisation in eq. (2.7) for the partonic cross section. Following the resummation methodology described by Collins, Soper and Sterman in their foundational works [151, 152] it is possible to arrive to the following equation for the hadronic transverse momentum cross section in the b-space:

$$\frac{d\sigma_F}{dq_T^2}(q_T,\, M,\, s) \;=\; \frac{M^2}{s}\int_0^\infty db\,\frac{b}{2}\,J_0(b\,q_T)\,W^F(b,\,M,\,s)+\cdots\,, \tag{3.1}$$

where terms represented by "$\cdots$" are not divergent nor even finite in the limit $b\to\infty$ ($q_T\to 0$). Unlike the previous partonic case defined in eq. (2.7), W^F now depends on the PDFs and therefore, in the collinear coefficient functions C_N. This is one of the main differences between the partonic $\mathcal{W}^F_{ab}$ and the hadronic $W^F_N(b,M)$ tensors.

We proceed by performing Mellin transformation[2] of the corresponding $W^F_N(b,M)$ hadronic tensor. This strategy, which is justified for the resummed component (since our resummation methodology is based in b-space) can be avoided in the implementation of the fixed order calculation, integrating directly in z-space (or q_T-space). Besides the freedom to choose the space in order to perform the calculation regarding the fixed order cross section, presenting results using Mellin transform is evidently easier: convolutions in z-space are simply products after Mellin transformation. The Mellin N-moments of the hadronic tensor $W^F(b,M)$ are:

$$\begin{aligned} W^F_N(b,M) \;&=\; \sum_c \sigma^{(0)}_{c\bar c,\,F}(\alpha_S(M^2),M)\;H^F_c(\alpha_S(M^2))\;S_c(M,b) \\ &\times\; \sum_{a,b} C_{ca,\,N}(\alpha_S(b_0^2/b^2))\;C_{\bar c b,\,N}(\alpha_S(b_0^2/b^2))\;f_{a/h_1,\,N}(b_0^2/b^2)\;f_{b/h_2,\,N}(b_0^2/b^2)\;\;, \end{aligned} \tag{3.2}$$

where $f_{a/h,\,N}(\mu^2)$ are the N-moments of the parton distribution function $f_{a/h}(z,\mu^2)$, and $\sigma^{(0)}_{c\bar c,\,F}$ is the lowest-order cross section for the partonic sub-process $c+\bar c\to F$. The function $S_c(M,b)$ is the Sudakov form factor of the quark ($c=q,\bar q$) or of the gluon ($c=g$), and it can be written in the following form:

$$S_c(M,b)=\exp\left\{-\int_{b_0^2/b^2}^{M^2}\frac{dq^2}{q^2}\left[A_c(\alpha_S(q^2))\;\ln\frac{M^2}{q^2}+B_c(\alpha_S(q^2))\right]\right\}\;\;. \tag{3.3}$$

The functions A, B, C and H^F in eqs. (3.2) and (3.3) can be expanded in perturbative series in α_S:

$$A_c(\alpha_S) \;=\; \sum_{n=1}^\infty\left(\frac{\alpha_S}{\pi}\right)^n A_c^{(n)}\;\;, \tag{3.4}$$

$$B_c(\alpha_S) \;=\; \sum_{n=1}^\infty\left(\frac{\alpha_S}{\pi}\right)^n B_c^{(n)}\;\;, \tag{3.5}$$

$$C_{ab}(\alpha_S,z) \;=\; \delta_{ab}\,\delta(1-z)+\sum_{n=1}^\infty\left(\frac{\alpha_S}{\pi}\right)^n C_{ab}^{(n)}(z)\;\;, \tag{3.6}$$

$$H_c^F(\alpha_S) \;=\; 1+\sum_{n=1}^\infty\left(\frac{\alpha_S}{\pi}\right)^n H_c^{F\,(n)}\;\;. \tag{3.7}$$

[2] Throughout the paper, the N-moments h_N of any function $h(z)$ of the variable z are defined as $h_N=\int_0^1 dz\, z^{N-1}\,h(z)$.

The resummation coefficients A_c and B_c and the collinear coefficient functions C_{ab} are process independent, while H_c^F depends on the specific hard-scattering process, since it embodies the finite part of the multi-loop scattering amplitudes. Comparing the partonic and the hadronic cross sections in eqs. (2.7) and (3.2), we see that the resummed factors $\mathcal{W}_{ab}^F$ and $W^F(b,M)$ are related by

$$W_N^F(b,M) = \sum_{a,b} \mathcal{W}_{ab,\,N}^F(b,M;\alpha_S(\mu_R^2),\mu_R^2,\mu_F^2)\; f_{a/h_1,\,N}(\mu_F^2)\; f_{b/h_2,\,N}(\mu_F^2) \quad . \tag{3.8}$$

In order to express $\mathcal{W}_{ab}^F$ in terms of the perturbative coefficients in eqs. (3.4), (3.5), (3.6) and (3.7), we need to use the definition of W_N^F and evolve the PDFs evaluated at the resummation scale (b_0^2/b^2) to the proper factorisation scale μ_F. This can be done with the QCD evolution operator $U_{ab\,N}(\mu^2,\mu_0^2)$:

$$f_{a/h\,N}(\mu^2) \;=\; \sum_b U_{ab\,N}(\mu^2,\mu_0^2)\; f_{b/h\;,M}(\mu_0^2)\,. \tag{3.9}$$

The operator $U_{ab\,N}(\mu^2,\mu_0^2)$ satisfy the customary evolution equation:

$$\frac{dU_{ab\,N}(\mu^2,\mu_0^2)}{d\log\mu^2} \;=\; \sum_c \gamma_{ac\,N}(\alpha_s(\mu^2))\, U_{cb\,N}(\mu^2,\mu_0^2)\,, \tag{3.10}$$

where we introduced the N-moments of the anomalous dimensions, defined as the Mellin transformation of the Altarelli-Parisi splitting functions:

$$\gamma_{ab\,N}(\alpha_s) \;=\; \int_0^1 dz\, z^{N-1}\, P_{ab}(\alpha_s,z)\,. \tag{3.11}$$

The solution to this eq. (3.11) is given by the corresponding integral and it can be written as

$$U_N\left(\frac{b_0^2}{b^2},\,\mu_F^2\right) \;=\; \exp\left(-\int_{\frac{b_0^2}{b^2}}^{\mu_F^2} \frac{dq^2}{q^2}\,\gamma_N(\alpha_s(q^2))\right)\,. \tag{3.12}$$

Therefore, taking into account the precedent results it is possible to write the resummed partonic cross section in eq. (2.7) to the perturbative coefficients in eqs. (3.4)–(3.7) and the anomalous dimensions coefficients in eq. (3.11):

$$\begin{aligned}\mathcal{W}_{ab,\,N}^F(b,M;\alpha_S(\mu_R^2),\mu_R^2,\mu_F^2) \;=\; & \sum_c \sigma_{c\bar{c},\,F}^{(0)}(\alpha_S(M^2),M)\; H_c^F(\alpha_S(M^2))\; S_c(M,b)\\ & \times \sum_{a_1,\,b_1} C_{ca_1,\,N}(\alpha_S(b_0^2/b^2))\; C_{\bar{c}b_1,\,N}(\alpha_S(b_0^2/b^2))\\ & \times\; U_{a_1a,\,N}(b_0^2/b^2,\mu_F^2)\; U_{b_1b,\,N}(b_0^2/b^2,\mu_F^2) \quad .\end{aligned} \tag{3.13}$$

Expanding at fixed order precedent eq. (3.13) we will obtain two kind of contributions: (i) terms which are logarithmically enhanced (which are organised in the coefficient functions $\widetilde{\Sigma}_{c\bar{c}\leftarrow ab}^{F\,(n)}$ under their perturbative order n and logarithmic power $1\leq m\leq$ 2n) ; (ii) finite terms, or equivalently, terms which are proportional to $\delta(q_T^2)$ are organised in the $\mathcal{H}_{c\bar{c}\leftarrow ab}^{F\,(n)}$ coefficient functions depending on their perturbative order n. The fixed order expansion of eq. (3.13) reads:

$$\begin{aligned}\mathcal{W}_{ab}^F(b,M,\hat{s};\alpha_S,\mu_R^2,\mu_F^2,Q^2) \;=\; & \sum_c \sigma_{c\bar{c},\,F}^{(0)}(\alpha_S,M)\Big\{\delta_{ca}\;\delta_{\bar{c}b}\;\delta(1-z)\\ & +\;\sum_{n=1}^{\infty}\left(\frac{\alpha_S}{\pi}\right)^n\left[\widetilde{\Sigma}_{c\bar{c}\leftarrow ab}^{F\,(n)}\left(z,\widetilde{L};\frac{M^2}{\mu_R^2},\frac{M^2}{\mu_F^2},\frac{M^2}{Q^2}\right)\right.\end{aligned}$$

$$+ \mathcal{H}^{F\,(n)}_{c\bar{c}\leftarrow ab}\left(z; \frac{M^2}{\mu_R^2}, \frac{M^2}{\mu_F^2}, \frac{M^2}{Q^2}\right)\Bigg]\Bigg\} , \tag{3.14}$$

where $z = M^2/\hat{s}$, $\alpha_S = \alpha_S(\mu_R^2)$, $\sigma^{(0)}_{c\bar{c},\,F}(\alpha_S, M) = \alpha_S^{p_{cF}}\, \sigma^{(\mathrm{LO})}_{c\bar{c},\,F}(M)$ and, in general, the power p_{cF} depends on the lowest-order partonic sub-process $c + \bar{c} \to F$[3].

The explicit form of the $\widetilde{\Sigma}^{F\,(n)}_{c\bar{c}\leftarrow ab}$ and $\mathcal{H}^{F\,(n)}_{c\bar{c}\leftarrow ab}$ coefficients where presented for first time in Ref. [153] and extended to N^{3}LO and N^{4}LO in Refs. [159] and [154] respectively. Here, for the sake of completeness we present the corresponding coefficient functions up to NNLO (which is enough for the purposes of the present thesis). The explicit inclusion of the resummation coefficients will be of value in order to discuss which are the terms that are modified in the presence of massive multi-loop corrections, which is the original work of this thesis. The perturbative expansion of eq. (2.8) or, more precisely, of eq. (3.13) gives:

$$\widetilde{\Sigma}^{F\,(1)}_{c\bar{c}\leftarrow ab}(z, \widetilde{L}) = \Sigma^{F\,(1;2)}_{c\bar{c}\leftarrow ab}(z)\; \widetilde{L}^2 + \Sigma^{F\,(1;1)}_{c\bar{c}\leftarrow ab}(z)\; \widetilde{L} \;, \tag{3.15}$$

$$\widetilde{\Sigma}^{F\,(2)}_{c\bar{c}\leftarrow ab}(z, \widetilde{L}) = \Sigma^{F\,(2;4)}_{c\bar{c}\leftarrow ab}(z)\; \widetilde{L}^4 + \Sigma^{F\,(2;3)}_{c\bar{c}\leftarrow ab}(z)\; \widetilde{L}^3 + \Sigma^{F\,(2;2)}_{c\bar{c}\leftarrow ab}(z)\; \widetilde{L}^2 + \Sigma^{F\,(2;1)}_{c\bar{c}\leftarrow ab}(z)\; \widetilde{L} \;, \tag{3.16}$$

where the dependence on the scale ratios $M^2/\mu_R^2, M^2/\mu_F^2$ and M^2/Q^2 is understood. The b-independent coefficients $\Sigma^{F\,(1;k)}(z), \mathcal{H}^{F\,(1)}(z), \Sigma^{F\,(2;k)}(z)$ and $\mathcal{H}^{F\,(2)}(z)$ are more easily presented by considering their N-moments with respect to the variable z. We have:

$$\Sigma^{F\,(1;2)}_{c\bar{c}\leftarrow ab,\,N} = -\frac{1}{2} A_c^{(1)}\; \delta_{ca}\delta_{\bar{c}b} \;, \tag{3.17}$$

$$\Sigma^{F\,(1;1)}_{c\bar{c}\leftarrow ab,\,N}(M^2/Q^2) = -\left[\delta_{ca}\delta_{\bar{c}b}\, \left(B_c^{(1)} + A_c^{(1)}\, \ell_Q\right) + \delta_{ca}\gamma^{(1)}_{\bar{c}b,\,N} + \delta_{\bar{c}b}\gamma^{(1)}_{ca,\,N}\right] \;, \tag{3.18}$$

$$\begin{aligned}
\mathcal{H}^{F\,(1)}_{c\bar{c}\leftarrow ab,\,N}\left(\frac{M^2}{\mu_R^2}, \frac{M^2}{\mu_F^2}, \frac{M^2}{Q^2}\right) \;&=\; \delta_{ca}\delta_{\bar{c}b}\left[H_c^{F\,(1)} - \left(B_c^{(1)} + \frac{1}{2}A_c^{(1)}\ell_Q\right)\ell_Q - p_{cF}\beta_0\ell_R\right] \\
&+\; \delta_{ca}C^{(1)}_{\bar{c}b,\,N} + \delta_{\bar{c}b}C^{(1)}_{ca,\,N} \\
&+\; \left(\delta_{ca}\gamma^{(1)}_{\bar{c}b,\,N} + \delta_{\bar{c}b}\gamma^{(1)}_{ca,\,N}\right)(\ell_F - \ell_Q) \;,
\end{aligned} \tag{3.19}$$

$$\Sigma^{F\,(2;4)}_{c\bar{c}\leftarrow ab,\,N} = \frac{1}{8}\left(A_c^{(1)}\right)^2\; \delta_{ca}\delta_{\bar{c}b} \;, \tag{3.20}$$

$$\Sigma^{F\,(2;3)}_{c\bar{c}\leftarrow ab,\,N}(M^2/Q^2) = -\,A_c^{(1)}\left[\frac{1}{3}\,\beta_0\;\delta_{ca}\delta_{\bar{c}b} + \frac{1}{2}\,\Sigma^{F\,(1;1)}_{c\bar{c}\leftarrow ab,\,N}(M^2/Q^2)\right] \;, \tag{3.21}$$

$$\begin{aligned}
\Sigma^{F\,(2;2)}_{c\bar{c}\leftarrow ab,\,N}\left(\frac{M^2}{\mu_R^2}, \frac{M^2}{\mu_F^2}, \frac{M^2}{Q^2}\right) \;&=\; -\,\frac{1}{2}\,A_c^{(1)}\Big[\mathcal{H}^{F\,(1)}_{c\bar{c}\leftarrow ab,\,N}\Big(\frac{M^2}{\mu_R^2}, \frac{M^2}{\mu_F^2}, \frac{M^2}{Q^2}\Big) \\
&-\; \beta_0\;\delta_{ca}\delta_{\bar{c}b}\,(\ell_R - \ell_Q)\Big] \\
&-\; \frac{1}{2}\sum_{a_1,b_1}\Sigma^{F\,(1;1)}_{c\bar{c}\leftarrow a_1b_1,\,N}(M^2/Q^2)\left[\delta_{a_1a}\gamma^{(1)}_{b_1b,\,N} + \delta_{b_1b}\gamma^{(1)}_{a_1a,\,N}\right] \\
&-\; \frac{1}{2}\Big[A_c^{(2)}\;\delta_{ca}\delta_{\bar{c}b} \\
&+\; \left(B_c^{(1)} + A_c^{(1)}\,\ell_Q - \beta_0\right)\;\Sigma^{F\,(1;1)}_{c\bar{c}\leftarrow ab,\,N}(M^2/Q^2)\Big] \;,
\end{aligned} \tag{3.22}$$

$$\Sigma^{F\,(2;1)}_{c\bar{c}\leftarrow ab,\,N}\left(\frac{M^2}{\mu_R^2}, \frac{M^2}{\mu_F^2}, \frac{M^2}{Q^2}\right) = \Sigma^{F\,(1;1)}_{c\bar{c}\leftarrow ab,\,N}(M^2/Q^2)\,\beta_0\,(\ell_Q - \ell_R) \tag{3.23}$$

[3]For instance, for diphoton production $p_{cF} = 0$, but for Higgs boson production is $p_{cF} = 2$.

$$
\begin{aligned}
&- \sum_{a_1,b_1} \mathcal{H}^{F\,(1)}_{c\bar{c}\leftarrow a_1 b_1,\,N}\left(\frac{M^2}{\mu_R^2},\frac{M^2}{\mu_F^2},\frac{M^2}{Q^2}\right)\Big[\delta_{a_1 a}\delta_{b_1 b}\left(B_c^{(1)}+A_c^{(1)}\,\ell_Q\right)\\
&+ \delta_{a_1 a}\gamma^{(1)}_{b_1 b,\,N}+\delta_{b_1 b}\gamma^{(1)}_{a_1 a,\,N}\Big]\\
&- \left[\delta_{ca}\delta_{\bar{c}b}\left(B_c^{(2)}+A_c^{(2)}\,\ell_Q\right)-\beta_0\left(\delta_{ca}C^{(1)}_{\bar{c}b,\,N}+\delta_{\bar{c}b}C^{(1)}_{ca,\,N}\right)+\delta_{ca}\gamma^{(2)}_{\bar{c}b,\,N}+\delta_{\bar{c}b}\gamma^{(2)}_{ca,\,N}\right]\,,
\end{aligned}
$$

$$
\begin{aligned}
&\mathcal{H}^{F\,(2)}_{c\bar{c}\leftarrow ab,\,N}\left(\frac{M^2}{\mu_R^2},\frac{M^2}{\mu_F^2},\frac{M^2}{Q^2}\right)=\delta_{ca}\delta_{\bar{c}b}\,H_c^{F\,(2)}+\delta_{ca}\,C^{(2)}_{\bar{c}b,\,N}+\delta_{\bar{c}b}\,C^{(2)}_{ca,\,N}+C^{(1)}_{ca,\,N}\,C^{(1)}_{\bar{c}b,\,N}\\
&+ H_c^{F\,(1)}\left(\delta_{ca}\,C^{(1)}_{\bar{c}b,\,N}+\delta_{\bar{c}b}\,C^{(1)}_{ca,\,N}\right)+\frac{1}{6}\,A_c^{(1)}\,\beta_0\,\ell_Q^3\,\delta_{ca}\delta_{\bar{c}b}+\frac{1}{2}\Big[A_c^{(2)}\,\delta_{ca}\delta_{\bar{c}b}\\
&+ \beta_0\,\Sigma^{F\,(1;1)}_{c\bar{c}\leftarrow ab,\,N}(M^2/Q^2)\Big]\ell_Q^2\\
&- \left[\delta_{ca}\delta_{\bar{c}b}\left(B_c^{(2)}+A_c^{(2)}\,\ell_Q\right)-\beta_0\left(\delta_{ca}C^{(1)}_{\bar{c}b,\,N}+\delta_{\bar{c}b}C^{(1)}_{ca,\,N}\right)+\delta_{ca}\gamma^{(2)}_{\bar{c}b,\,N}+\delta_{\bar{c}b}\gamma^{(2)}_{ca,\,N}\right]\ell_Q\\
&+ \frac{1}{2}\,\beta_0\,\left(\delta_{ca}\gamma^{(1)}_{\bar{c}b,\,N}+\delta_{\bar{c}b}\gamma^{(1)}_{ca,\,N}\right)\ell_F^2+\left(\delta_{ca}\gamma^{(2)}_{\bar{c}b,\,N}+\delta_{\bar{c}b}\gamma^{(2)}_{ca,\,N}\right)\ell_F\\
&- \mathcal{H}^{F\,(1)}_{c\bar{c}\leftarrow ab,\,N}\left(\frac{M^2}{\mu_R^2},\frac{M^2}{\mu_F^2},\frac{M^2}{Q^2}\right)\beta_0\ell_R\\
&+ \frac{1}{2}\sum_{a_1,b_1}\left[\mathcal{H}^{F\,(1)}_{c\bar{c}\leftarrow a_1 b_1,\,N}\left(\frac{M^2}{\mu_R^2},\frac{M^2}{\mu_F^2},\frac{M^2}{Q^2}\right)+\delta_{ca_1}\delta_{\bar{c}b_1}\,H_c^{F\,(1)}+\delta_{ca_1}\,C^{(1)}_{\bar{c}b_1,\,N}+\delta_{\bar{c}b_1}\,C^{(1)}_{ca_1,\,N}\right]\\
&\times \Big[\left(\delta_{a_1 a}\gamma^{(1)}_{b_1 b,\,N}+\delta_{b_1 b}\gamma^{(1)}_{a_1 a,\,N}\right)(\ell_F-\ell_Q)-\delta_{a_1 a}\delta_{b_1 b}\Big(\left(B_c^{(1)}+\frac{1}{2}\,A_c^{(1)}\,\ell_Q\right)\ell_Q\\
&+ p_{cF}\,\beta_0\,\ell_R\Big)\Big]-\delta_{ca}\delta_{\bar{c}b}\,p_{cF}\left(\frac{1}{2}\,\beta_0^2\,\ell_R^2+\beta_1\,\ell_R\right)\quad. \qquad (3.24)
\end{aligned}
$$

A couple of comments are in order. Up to this point, this chapter was dedicated to the "Universality of the transverse momentum cross sections", transverse momentum resummation and their corresponding fixed order expansion. All the concepts presented up to this point were already developed and published in the literature. However, we will summarize the present section making the effective connection with the original work in this thesis.

One of the main results in this thesis is the calculation of massive two-loop scattering amplitudes (see chapter 4). But also, massive double-real corrections for diphoton production were computed and implemented in Chapter 6. Since the final state F of the described observables are always colourless (Higgs or two photons), the massive corrections entering through loops or present at effective leading order in double real corrections the transverse momentum resummation and subtraction methods are not substantially modified. In first place the massive real corrections are finite after integration over the whole phase-space. Therefore, the corresponding inclusion of these corrections is straightforward. The only modification is to take into account massive real corrections in the description of the phase space in the Monte Carlo. In second place, the multi-loop scattering amplitudes comprehend two sub-cases: (i) Real-virtual corrections and (ii) two-loop virtual scattering amplitudes. Case (i) embodies only finite contributions, therefore they can be included in the Monte Carlo on the top of what already implemented for the completely massless case[4]. The precedent considerations imply that the equations that govern the cancellation of the infrared divergencies (the counterterm) inside de Monte Carlo (eqs. (3.17) to (3.23)) do not suffer any modification and can be left as they are in previous implementations of

[4]Since the massive correction is entering in the loop, it is not necessary to modify the phase space.

the massless cases. Same conclusions can be made for the resummation functions $g_N^{(i)}$ in eqs. (2.14) and (2.15). However, case (ii) effectively modifies one of the transverse momentum subtraction/resummation elements. Since in this particular case we are treating with two-loop massive corrections, the hard virtual factor $H_c^{F\,(2)}$ present in eq. (3.24) is modified. Thus the unique modification to the transverse momentum subtraction/resummation method is appearing in a finite contribution (proportional to $\delta(q_T^2)$). The hard virtual factor $H_c^{F\,(2)}$ embodies the finite contributions from the two-loop virtual scattering amplitudes. Therefore we have to provide a methodology in order to cancel the IR poles present in such contributions but suitable for the transverse momentum subtraction formalism. More clearly, we have to remove the IR poles from the two-loop scattering amplitudes taking care of the *universal constant of soft origin* at each perturbative order [150]. This is the subject of the next section.

3.4 Hard-virtual coefficients and their universal structure

This section analyzes the process-dependent hard-virtual coefficient H^F a necessary component in the transverse momentum subtraction/resummation method. We will establish a process-independent relation between H^F and the multi-loop virtual amplitude of the partonic process $c\bar{c} \to F$. We will closely follow the notation in Ref. [150] and we will evaluate all the steps at the light of the inclusion of the massive corrections.

3.4.1 Preliminary considerations and notation

In first place we define the notation for the all-loop virtual amplitude $\mathcal{M}_{c\bar{c}\to F}$ and introduce an auxiliary hard-virtual amplitude $\widetilde{\mathcal{M}}_{c\bar{c}\to F}$. This auxiliary amplitude is directly derived from $\mathcal{M}_{c\bar{c}\to F}$ by defining a specific procedure (only relevant for the q_T subtraction/resummation method) in order to remove all the IR poles. The master formula which defines the hard virtual coefficient H^F is based on $\widetilde{\mathcal{M}}_{c\bar{c}\to F}$ and plays a crucial role in expressing the hard-virtual coefficient H^F up to NNLO [150]. This relation was further extended up-to N^{3}LO [159] and subsequently at N^{4}LO in Ref. [154]. Whereas int the N^{3}LO all the elements are present in literature, for the N^{4}LO the corresponding *universal constant of soft origin* is still messing.

We consider the partonic *elastic*-production process

$$c(\hat{p}_1) + \bar{c}(\hat{p}_2) \to F(\{q_i\})\,, \tag{4.1}$$

where $c\bar{c} = gg$ or $c\bar{c} = q\bar{q}$ and $F(\{q_i\})$ represents the triggered final-state system. It is the inclusive hard scattering process of eq. (1.1) but without extra partonic radiation. The loop scattering amplitude of this process contains UV and IR singularities, which are regularized using CDR in $d = 4 - 2\epsilon$ space-time dimensions.

We work with the renormalized on-shell scattering amplitude, obtained by expressing the bare coupling α_S^u in terms of the running coupling $\alpha_S(\mu_R^2)$ in the $\overline{\text{MS}}$ scheme. The renormalized all-loop amplitude is denoted by $\mathcal{M}_{c\bar{c}\to F}$ and has the following perturbative (loop) expansion:

$$\begin{aligned}\mathcal{M}_{c\bar{c}\to F}(\hat{p}_1, \hat{p}_2; \{q_i\}) \;&=\; \left(\alpha_S(\mu_R^2)\,\mu_R^{2\epsilon}\right)^k \Bigg[\mathcal{M}^{(0)}_{c\bar{c}\to F}(\hat{p}_1, \hat{p}_2; \{q_i\}) \\ &+\; \left(\frac{\alpha_S(\mu_R^2)}{2\pi}\right) \mathcal{M}^{(1)}_{c\bar{c}\to F}(\hat{p}_1, \hat{p}_2; \{q_i\}; \mu_R)\end{aligned}$$

$$
\begin{aligned}
&+ \left(\frac{\alpha_S(\mu_R^2)}{2\pi}\right)^2 \mathcal{M}^{(2)}_{c\bar{c}\to F}(\hat{p}_1,\hat{p}_2;\{q_i\};\mu_R) \\
&+ \sum_{n=3}^{\infty} \left(\frac{\alpha_S(\mu_R^2)}{2\pi}\right)^n \mathcal{M}^{(n)}_{c\bar{c}\to F}(\hat{p}_1,\hat{p}_2;\{q_i\};\mu_R)\Bigg], \qquad (4.2)
\end{aligned}
$$

where the value k of the overall power of α_S depends on the specific process (for instance, $k = 0$ in the case of the vector boson production process $q\bar{q} \to V$, and $k = 1$ in the case of the Higgs boson production process $gg \to H$ through a heavy-quark loop).

3.4.2 Hard-virtual amplitude and subtraction operators

The hard-virtual amplitude $\widetilde{\mathcal{M}}_{c\bar{c}\to F}$ is defined as:

$$
\begin{aligned}
\widetilde{\mathcal{M}}_{c\bar{c}\to F}(\hat{p}_1,\hat{p}_2;\{q_i\}) = &\left(\alpha_S(\mu_R^2)\,\mu_R^{2\epsilon}\right)^k \Bigg[\widetilde{\mathcal{M}}^{(0)}_{c\bar{c}\to F}(\hat{p}_1,\hat{p}_2;\{q_i\}) \\
&+ \left(\frac{\alpha_S(\mu_R^2)}{2\pi}\right) \widetilde{\mathcal{M}}^{(1)}_{c\bar{c}\to F}(\hat{p}_1,\hat{p}_2;\{q_i\};\mu_R) \\
&+ \left(\frac{\alpha_S(\mu_R^2)}{2\pi}\right)^2 \widetilde{\mathcal{M}}^{(2)}_{c\bar{c}\to F}(\hat{p}_1,\hat{p}_2;\{q_i\};\mu_R) \\
&+ \sum_{n=3}^{\infty} \left(\frac{\alpha_S(\mu_R^2)}{2\pi}\right)^n \widetilde{\mathcal{M}}^{(n)}_{c\bar{c}\to F}(\hat{p}_1,\hat{p}_2;\{q_i\};\mu_R)\Bigg]. \qquad (4.3)
\end{aligned}
$$

and is related to $\mathcal{M}_{c\bar{c}\to F}$ through subtraction operators $\tilde{I}_c^{(1)}$ and $\tilde{I}_c^{(2)}$ at NLO and NNLO, respectively. These operators remove IR divergences and are defined as: $\tilde{I}_a^{(1)}$ is:

$$
\tilde{I}_a^{(1)}(\epsilon, M^2/\mu_R^2) = \tilde{I}_a^{(1)\,\mathrm{soft}}(\epsilon, M^2/\mu_R^2) + \tilde{I}_a^{(1)\,\mathrm{coll}}(\epsilon, M^2/\mu_R^2)\,, \qquad (4.4)
$$

with

$$
\tilde{I}_a^{(1)\,\mathrm{soft}}(\epsilon, M^2/\mu_R^2) = -\frac{e^{\epsilon\gamma_E}}{\Gamma(1-\epsilon)} \left(\frac{1}{\epsilon^2} + i\pi\,\frac{1}{\epsilon} + \delta^{q_T}\right) C_a \left(\frac{M^2}{\mu_R^2}\right)^{-\epsilon}\,, \qquad (4.5)
$$

$$
\tilde{I}_a^{(1)\,\mathrm{coll}}(\epsilon, M^2/\mu_R^2) = -\frac{1}{\epsilon}\,\gamma_a \left(\frac{M^2}{\mu_R^2}\right)^{-\epsilon}\,, \qquad (4.6)
$$

and

$$
\gamma_q = \gamma_{\bar{q}} = \frac{3}{2}\,C_F\,, \qquad \gamma_g = \frac{11}{6}\,C_A - \frac{1}{3}\,N_f\,. \qquad (4.7)
$$

The coefficient δ^{q_T} affects only the IR finite part of the subtraction operator. The known results on the NLO hard-collinear coefficients $H_c^{F\,(1)}$ [160] are recovered by fixing:

$$
\delta^{q_T} = 0\,. \qquad (4.8)
$$

Notice that the choice on the δ^{q_T} coefficient can be used to change the resummation scheme: CSS [152], SCET [161], q_T resummation in direct space [162], etc.

The second-order (two-loop) subtraction operator $\tilde{I}_c^{(2)}$ is:

$$
\tilde{I}_a^{(2)}(\epsilon, M^2/\mu_R^2) = -\frac{1}{2}\left[\tilde{I}_a^{(1)}(\epsilon, M^2/\mu_R^2)\right]^2 + \Bigg\{\frac{2\pi\beta_0}{\epsilon}\Bigg[\tilde{I}_a^{(1)}(2\epsilon, M^2/\mu_R^2)
$$

$$- \tilde{I}_a^{(1)}(\epsilon, M^2/\mu_R^2)\Big] + K\, \tilde{I}_a^{(1)\,\mathrm{soft}}(2\epsilon, M^2/\mu_R^2) + \widetilde{H}_a^{(2)}(\epsilon, M^2/\mu_R^2)\Big\} \ , \quad (4.9)$$

with

$$\widetilde{H}_a^{(2)}(\epsilon, M^2/\mu_R^2) = \widetilde{H}_a^{(2)\,\mathrm{coll}}(\epsilon, M^2/\mu_R^2) + \widetilde{H}_a^{(2)\,\mathrm{soft}}(\epsilon, M^2/\mu_R^2) \quad (4.10)$$

$$= \frac{1}{4\epsilon}\left(\frac{M^2}{\mu_R^2}\right)^{-2\epsilon}\left(\frac{1}{4}\,\gamma_{a\,(1)} + C_a\, d_{(1)} + \epsilon\, C_a\, \delta_{(1)}^{q_T}\right) \ , \quad (4.11)$$

where $\widetilde{H}_a^{(2)\,\mathrm{coll}}$ is the contribution that is proportional to $\gamma_{a\,(1)}$ and $\widetilde{H}_a^{(2)\,\mathrm{soft}}$ is the remaining contribution (which is proportional to C_a) in eq. (4.11). The QCD coefficients K in eq. (4.9) and $d_{(1)}$ in eq. (4.11) (they control the IR divergences of $\tilde{I}_a^{(2)}$) are [163]:

$$K = \left(\frac{67}{18} - \frac{\pi^2}{6}\right) C_A - \frac{5}{9} N_f \ , \quad (4.12)$$

$$d_{(1)} = \left(\frac{28}{27} - \frac{1}{3}\zeta_2\right) N_f + \left(-\frac{202}{27} + \frac{11}{6}\zeta_2 + 7\zeta_3\right) C_A \,, \quad (4.13)$$

and the coefficients $\gamma_{a\,(1)}$ $(a = q, g)$ are written in the following form:

$$\gamma_{q\,(1)} = \gamma_{\bar{q}\,(1)} = (-3+24\zeta_2-48\zeta_3)\, C_F^2 + \left(-\frac{17}{3} - \frac{88}{3}\zeta_2 + 24\zeta_3\right) C_F C_A + \left(\frac{2}{3} + \frac{16}{3}\zeta_2\right) C_F N_f \ , \quad (4.14)$$

$$\gamma_{g\,(1)} = \left(-\frac{64}{3} - 24\zeta_3\right) C_A^2 + \frac{16}{3} C_A N_f + 4\, C_F N_f \ , \quad (4.15)$$

where ζ_n is the Riemann zeta-function ($\zeta_2 = \pi^2/6, \zeta_3 = 1.202\ldots, \zeta_4 = \pi^4/90$).

The coefficient $\delta_{(1)}^{q_T}$ in Eq. (4.11) affects only the IR finite part of the two-loop subtraction operator:

$$\delta_{(1)}^{q_T} = \frac{20}{3}\zeta_3 \pi \beta_0 + \left(-\frac{1214}{81} + \frac{67}{18}\zeta_2\right) C_A + \left(\frac{164}{81} - \frac{5}{9}\zeta_2\right) N_f \,. \quad (4.16)$$

The $\delta_{(1)}^{q_T}$ coefficient can be understood as the next order correction of δ^{q_T}, which can be used also to change among different resummation schemes.

Having introduced the subtracted amplitude $\widetilde{\mathcal{M}}_{c\bar{c}\to F}$, we can relate it to the process-dependent resummation coefficients H_c^F of eqs. (3.7) and (3.2). In the case of processes initiated by $q\bar{q}$ annihilation[5], the *all-order* coefficient H_q^F can be written as:

$$\alpha_S^{2k}(M^2)\, H_q^F(x_1p_1, x_2p_2; \alpha_S(M^2)) = \frac{|\widetilde{\mathcal{M}}_{q\bar{q}\to F}(x_1p_1, x_2p_2; \{q_i\})|^2}{|\mathcal{M}^{(0)}_{q\bar{q}\to F}(x_1p_1, x_2p_2; \{q_i\})|^2} \ , \quad (4.17)$$

where k is the value of the overall power of α_S in the expansion of $\mathcal{M}_{c\bar{c}\to F}$ (see eqs. (4.2) and (4.3)).

In eq. (4.17), the notation $|\widetilde{\mathcal{M}}_{q\bar{q}\to F}|^2$ and $|\mathcal{M}^{(0)}_{gg\to F}|^2$ denotes the squared amplitudes *summed* over the colours of the colliding partons and over the (*physical*) spin polarization states of the colliding partons and of the particles in the final-state system F.

To be precise, we also note that H_c^F is computed in $d = 4$ space-time dimensions and, therefore, the right-hand side of eq. (4.17) has to be evaluated in the limit $\epsilon \to 0$ (this limit

[5]For the sub-processes initiated by gluon fusion we recommend the reader to consult Ref. [150]. The universal relation between the hard virtual factor and the multi-loop scattering amplitude is not relevant at NNLO for the purposes of this thesis.

is well-defined and straightforward, since $\mathcal{M}^{(0)}_{c\bar{c}\to F}$ and the order-by-order expansion of the hard-virtual amplitude $\widetilde{\mathcal{M}}_{c\bar{c}\to F}$ are IR finite).

The expressions (4.17) and the explicit results in eqs. (4.4) and (4.9) permit the straightforward computation of the process-dependent resummation coefficients H_c^F for an arbitrary process of the class in Eq. (1.1). The explicit computation of H_c^F up to the desired perturbative order is elementary, provided the scattering amplitude $\mathcal{M}_{c\bar{c}\to F}$ of the corresponding partonic sub-process is available (known) up to the same perturbative order.

In particular, in Appendix A of Ref. [150] the NNLO hard-virtual coefficient $H_q^{\gamma\gamma(2)}$ for the process of massless diphoton production [164] is presented. For massless diphoton production the current state of the art is the three-loop virtual scattering amplitude [75], therefore $H_q^{\gamma\gamma(3)}$ can be computed with the corresponding subtraction operators obtained in [159].

In the case of two-loop virtual massive corrections, the subtraction operators are not modified, since the final state F is still colourless and therefore no QCD radiation can be attached. In summary, eq. (4.17) still holds for two-loop hard virtual factors in the presence of loop massive corrections.

Chapter 4

Two-loop form factors for diphoton production in quark annihilation channel with heavy quark mass dependence

The production of two isolated prompt photons (diphotons) remains one of the most important processes at the Large Hadron Collider (LHC). It is a probe of the Standard Model (SM) of particle physics [165, 166, 167, 168] and was one of the two most important channels in the search and study of the Higgs boson [9, 10, 169, 170, 171, 172, 173, 174, 175, 176].

Several new physics searches [177, 178, 179, 180, 181, 182] are still being carried out using the diphoton channel, due to the clean signature of the photons in the LHC electromagnetic calorimeters.

Because of its phenomenological relevance, precise theoretical results are needed to compare with the LHC data. The state of the art for diphoton production is the next-to-next-to-leading order (NNLO) accuracy (taking into account five light quark flavours) [164, 183, 184, 185] in perturbative QCD. Although all the necessary elements of the (massless) next-to-next-to-leading order ($\mathrm{N^3LO}$) are already known [186, 187, 188, 189, 190, 191, 192, 39], they have not yet been considered together to obtain phenomenological results with full $\mathrm{N^3LO}$ accuracy. First-order electroweak/QED corrections are also known [193, 194].

The NLO calculations include the fragmentation contributions with the same precision [195] and the transverse momentum resummation with the corresponding precision, the next-to-leading order logarithmic (NLL) precision [196]. At that time, the so-called box (one-loop $gg \to \gamma\gamma$) contribution was already known [197]. Due to the large gluon luminosity at the LHC, the size of the box contribution is of the order of the Born sub-process ($q\bar{q} \to \gamma\gamma$) and for this reason, although formally of order $\mathcal{O}(\alpha_S^2)$, it has been included in the NLO phenomenological calculations [198, 199].

The state of the art regarding transverse momentum (q_T) resummation for diphoton production is the next-to-next-to-leading logarithmic precision (NNLL) [200] and at $\mathrm{N^3LL}$ [201] in association with fixed-order results at NNLO.

The possibility of measuring the top quark mass from the diphoton background has been pointed out in the literature [202, 203], if massive scattering amplitudes in diphoton production are taken into account (via loop corrections). These threshold effects of top quark pair production are manifested in the diphoton-invariant mass spectrum around two times the value of the top quark mass.

Non-trivial QCD massive corrections (including the dependence on the top quark mass) appear for the first time at NNLO. In Ref. [183], the one-loop $gg \to \gamma\gamma$ scattering amplitude was considered taking into account the top quark mass dependence (together with partial N^{3}LO contributions).

Regarding the inclusion of corrections beyond the NNLO ($\mathcal{O}(\alpha_S^3)$), the simplest approach for the gluon fusion channel is to consider the NLO effective QCD corrections to the box contribution (which captures some of the largest contributions). These NLO corrections form a gauge invariant subset [198] of the whole N^{3}LO gluon fusion channel. In the massless case, the NLO corrections to the box contribution have been calculated in Ref. [198] using the massless two-loop scattering amplitudes of Ref. [186]. In the context of the massive contributions, two recent papers have shown the impact of these massive corrections on the gluon fusion channel [204, 205], which turned out to be substantial.

Even in the light of previous efforts to calculate the scattering amplitudes that capture the main contributions to diphoton production, the full massive QCD NNLO corrections for this process were still missing (mainly due to the previously unknown two-loop scattering amplitudes [2]).

4.1 Amplitude structure

In this section, we consider the computation of the two-loop form factors in the quark annihilation channel with a heavy quark running in the loop. At the partonic level the process is:

$$q(p_1) + \overline{q}(p_2) \to \gamma(p_3) + \gamma(p_4), \tag{1.1}$$

where all the external particles are on-shell, i.e. $p_i^2 = 0$ and there is a heavy quark with mass m_t running in the loop. The kinematics for this $2 \to 2$ process is described by the Mandelstam invariants:

$$s = (p_1 + p_2)^2, \quad t = (p_1 - p_3)^2, \quad u = (p_2 - p_3)^2, \quad \text{with} \quad s + t + u = 0\,. \tag{1.2}$$

The bare scattering amplitude can be written as

$$\mathcal{A}_{q\bar{q}\gamma\gamma} = (4\pi\alpha_{em})\, \delta_{ij}\, \epsilon^{*\mu}_{\lambda_3}(p_3)\, \epsilon^{*\nu}_{\lambda_4}(p_4)\, \overline{v}_{s_2}(p_2)\, A_{\mu\nu}(s,t,u,m_t^2)\, u_{s_1}(p_1)\,, \tag{1.3}$$

where δ_{ij} is the Kronecker delta function with indices i and j representing the color of the incoming quark and anti-quark, $\overline{v}_{s_2}(p_2)$ and $u_{s_1}(p_1)$ are the quark spinors, $\epsilon^{*\mu}_{\lambda_3}(p_3)$ and $\epsilon^{*\nu}_{\lambda_4}(p_4)$ are the external photons polarization vectors, α_{em} is the fine-structure constant, determined by the electric charge $e = \sqrt{4\pi\alpha_{em}}$.

At any order in perturbative QCD, as explained in section 2.3, the amplitude can be decomposed in terms of a set of Lorentz invariant tensors T_i and scalar form factors $\mathcal{F}_i$ as:

$$\mathcal{A}_{q\bar{q}\gamma\gamma} = \sum_i \mathcal{F}_i T_i\,. \tag{1.4}$$

The tensors T_i are built from the external momenta $\{p_i^\mu\}$, the polarizations vectors $\{\epsilon_i^\mu\}$ and the metric tensor $g^{\mu\nu}$.

To simplify the number of independent Lorentz invariant tensors, we start working in d-dimensions and we impose the physical conditions $p_i \cdot \epsilon_{\lambda_i} = 0$ with $i = 3, 4$, in order to remove the tensors proportional to p_3^μ, p_4^ν. By making a specific choice on the reference vectors for the external photons:

$$\begin{aligned} \epsilon_{\lambda_3}(p_3) \cdot p_2 &= 0\,, \\ \epsilon_{\lambda_4}(p_4) \cdot p_1 &= 0\,, \end{aligned} \tag{1.5}$$

which implies for the polarization sums in d-dimension

$$\begin{aligned}
\sum_{pol} \epsilon^{\mu}_{\lambda_3} \epsilon^{*\nu}_{\lambda_3} &= -g^{\mu\nu} + \frac{p_2^\mu p_3^\nu + p_3^\mu p_2^\nu}{p_2 \cdot p_3}, \\
\sum_{pol} \epsilon^{\mu}_{\lambda_4} \epsilon^{*\nu}_{\lambda_4} &= -g^{\mu\nu} + \frac{p_1^\mu (p_1^\nu + p_2^\nu - p_3^\nu) + (p_1^\mu + p_2^\mu - p_3^\mu) p_1^\nu}{p_1 \cdot (p_2 - p_3)},
\end{aligned} \tag{1.6}$$

where $p_4 = p_1 + p_2 - p_3$ and $p_i^2 = 0$.

With these choices, we are left with 5 Lorentz invariant tensors

$$\begin{aligned}
T_1 &= \overline{v}_{s_2}(p_2) \not{\epsilon}^*_{\lambda_3}(p_3) u_{s_1}(p_1) \epsilon^*_{\lambda_4}(p_4) \cdot p_2, \\
T_2 &= \overline{v}_{s_2}(p_2) \not{\epsilon}^*_{\lambda_4}(p_4) u_{s_1}(p_1) \epsilon^*_{\lambda_3}(p_3) \cdot p_1, \\
T_3 &= \overline{v}_{s_2}(p_2) \not{p}_3 u_{s_1}(p_1) \epsilon^*_{\lambda_3}(p_3) \cdot p_1 \epsilon^*_{\lambda_4}(p_4) \cdot p_2, \\
T_4 &= \overline{v}_{s_2}(p_2) \not{p}_3 u_{s_1}(p_1) \epsilon^*_{\lambda_3}(p_3) \cdot \epsilon^*_{\lambda_4}(p_4), \\
T_5 &= \overline{v}_{s_2}(p_2) \not{\epsilon}^*_{\lambda_3}(p_3) \not{p}_3 \not{\epsilon}^*_{\lambda_4}(p_4) u_{s_1}(p_1).
\end{aligned} \tag{1.7}$$

In common dimensional regularisation (CDR), i.e. keeping the external states in d dimensions, these 5 tensors are independent. In the $d \to 4$ limit, not all tensors are independent. Preliminarily, if we count the helicities, we expect $2^3 = 8$ helicities, reduced to 4 by parity. Therefore, we expect to be able to describe our amplitude in terms of 4 independent tensor structures. This can be shown by studying the rank of the matrix

$$M_{ij} = \sum_{pol} T_i^\dagger T_j. \tag{1.8}$$

For $d = 4$ the matrix M_{ij} is not of full rank and in particular $\mathrm{rank}(M_{ij}) = 4$. The coefficients of the projectors are $c_{ij} = (M_{ij})^{-1}$ with:

$$M^{-1} = \begin{pmatrix}
-\frac{u}{2(d-3)s^2(s+u)} & 0 & -\frac{u}{2(d-3)s^2(s+u)^2} & 0 & 0 \\
0 & -\frac{u}{2(d-3)s^2(s+u)} & \frac{u}{2(d-3)s^2(s+u)^2} & 0 & 0 \\
-\frac{u}{2(d-3)s^2(s+u)^2} & \frac{u}{2(d-3)s^2(s+u)^2} & -\frac{du^2+4s^2+4su}{2(d-3)s^2u(s+u)^3} & \frac{2s+u}{2(d-3)su(s+u)^2} & 0 \\
0 & 0 & \frac{2s+u}{2(d-3)su(s+u)^2} & -\frac{1}{2(d-3)u(s+u)} & 0 \\
0 & 0 & 0 & 0 & -\frac{1}{2(d^2-7d+12)u(s+u)}
\end{pmatrix}. \tag{1.9}$$

It immediately follows that the fifth tensor decouples from the others, as shown in Ref. [206].

In the tHV scheme it is possible to separate the four-dimensional tensor structures from the unphysical -2ϵ-dimensional ones by a simple orthogonalisation procedure. We introduce a new tensor basis $\{\overline{T}_i\}$ as

$$\begin{aligned}
\overline{T}_i &= T_i, \quad i = 1, ..., 4, \\
\overline{T}_5 &= T_5 - \frac{u}{s} T_1 + \frac{u}{s} T_2 - \frac{2}{s} T_3 + T_4.
\end{aligned} \tag{1.10}$$

The tensor $\overline{T}_5$ is constructed so that it vanishes in $d = 4$ external states and can be safely omitted from the calculation of helicity amplitudes in the tHV scheme.

We denote by $\mathcal{A}_{\lambda_{q\bar{q}},\lambda_3,\lambda_4}$ the scattering amplitude between helicity states represented by a set of four helicity configurations $\{\lambda_{q\bar{q}}, \lambda_3, \lambda_4\}$. It's possible to compute only four helicities for a well-defined configuration of the quark helicity, and obtain the others by a charge-conjugation transformation:

$$\mathcal{A}_{\lambda^2_{q\bar{q}},\lambda_3,\lambda_4} = \mathcal{A}_{\lambda^1_{q\bar{q}},-\lambda_3,-\lambda_4}(\langle ij \rangle \leftrightarrow [ji]), \tag{1.11}$$

where $-\lambda_i$ represents the opposite helicity of λ_i.

For a given helicity configuration we write:

$$A_{\lambda^1_{q\bar{q}},-\lambda_3,-\lambda_4}(s,t,u,m_t^2)) = \mathcal{S}_{\lambda^1_{q\bar{q}},-\lambda_3,-\lambda_4} f_{\lambda^1_{q\bar{q}},-\lambda_3,-\lambda_4}(s,t,u,m_t^2), \tag{1.12}$$

where the spinor part is given by:

$$\begin{aligned} \mathcal{S}_{\lambda^1_{q\bar{q}},+,+} &= \frac{2\langle 34\rangle^2}{\langle 31\rangle[23]}, & \mathcal{S}_{\lambda^1_{q\bar{q}},+,-} &= \frac{2\langle 23\rangle[41]}{\langle 24\rangle[32]}, \\ \mathcal{S}_{\lambda^1_{q\bar{q}},-,+} &= \frac{2\langle 24\rangle[13]}{\langle 23\rangle[24]}, & \mathcal{S}_{\lambda^1_{q\bar{q}},-,-} &= \frac{2[34]^2}{\langle 13\rangle[23]}, \end{aligned} \tag{1.13}$$

and the free-spinor helicity amplitudes are defined by:

$$\begin{aligned} f_{\lambda^1_{q\bar{q}},+,+} &= \frac{t}{2}\overline{F}_1 + \frac{t^2}{4}\overline{F}_3 - \frac{t}{2}\overline{F}_4, \\ f_{\lambda^1_{q\bar{q}},+,-} &= \frac{st}{2u}\overline{F}_2 - \frac{st}{2u}\overline{F}_1 - \frac{st^2}{4u}\overline{F}_3 - \frac{t^2}{2u}\overline{F}_4, \\ f_{\lambda^1_{q\bar{q}},-,+} &= \frac{st}{4}\overline{F}_3 + \frac{t}{2}\overline{F}_4, \\ f_{\lambda^1_{q\bar{q}},-,-} &= \frac{t}{2}\overline{F}_2 - \frac{t^2}{4}\overline{F}_3 + \frac{t}{2}\overline{F}_4. \end{aligned} \tag{1.14}$$

Then, for the computation of the helicity amplitudes we just need to compute the four independent scalar form factors. Given the Lorentz invariant tensors in eq. (1.7) the form factors are computed through eq. (3.2) with the following set of projectors:

$$\begin{aligned} \mathcal{P}_1 &= \frac{u}{2\,(d-3)\,s^2\,(s+u)^2}\left[T_3^\dagger + (s+u)\,T_1^\dagger\right], \\ \mathcal{P}_2 &= \frac{u}{2\,(d-3)\,s^2\,(s+u)^2}\left[(s+u)T_2^\dagger - T_3^\dagger\right], \\ \mathcal{P}_3 &= \frac{1}{2\,(d-3)\,s^2\,u\,(s+u)^3}\Big[(s\,u^2+u^3)T_1^\dagger - (s\,u^2+u^3)T_2^\dagger + (4s^2+4s\,u+d\,u^2)T_3^\dagger \\ &\quad -(2s^3+3s^2\,u+s\,u^2)T_4^\dagger\Big], \\ \mathcal{P}_4 &= \frac{1}{2\,(d-3)\,s\,u\,(s+u)^2}\left[-(2s+u)T_3^\dagger + (s^2+s\,u)T_4^\dagger\right], \end{aligned} \tag{1.15}$$

applied to the amplitude written in terms of the two-loop massive Feynman diagrams. The form factors $\overline{F}_k$ admit the following perturbative expansion in the strong coupling constant α_s:

$$\overline{F}_k = \overline{F}_k^{(0)} + \left(\frac{\alpha_s}{\pi}\right)\overline{F}_k^{(1)} + \left(\frac{\alpha_s}{\pi}\right)^2\overline{F}_k^{(2)} + \cdots, \tag{1.16}$$

We are interested in the computation of the massive corrections that start to appear $\mathcal{O}(\alpha_s^2)$. Therefore, they affect only the term $\overline{F}_k^{(2)}$, that will be the main focus of this chapter.

4.2 Scalar integral families and MIs computation

In this section we discuss the details of the calculation of the MIs. In particular, we define the scalar integral families that describe all the MIs that appear in the helicity amplitudes (modulo permutation of the external legs). Consequently, we provide the set of MIs obtained from the reduction of the full set of scalar integrals.

For the two-loop massive corrections to $q\bar{q} \to \gamma\gamma$, we have two planar integral topologies PLA and PLB, and a non-planar topology NPL, each topology with nine scalar products.

The scalar integral families describing the relevant MIs for this process are defined as:

$$\mathcal{I}_{topo}(a_1, ..., a_9) = \int \frac{\mathcal{D}k_1 \mathcal{D}k_2}{D_1^{a_1} D_2^{a_2} D_3^{a_3} D_4^{a_4} D_5^{a_5} D_6^{a_6} D_7^{a_7} D_8^{a_8} D_9^{a_9}}, \tag{2.1}$$

where $topo \in \{\text{PLA}, \text{PLB}, \text{NPL}\}$ labels the families and $D_1, ..., D_9$ are the scalar productions, according to eq. (5.13). The indices $a_1, ..., a_7$ are non-negative, while the indices a_8 and a_9 are non-positive, since we have two ISPs.

The integration measure in CDR with $d = 4 - 2\epsilon$ is:

$$\mathcal{D}k = \frac{d^d k}{i\pi^{2-\epsilon}\Gamma(1+\epsilon)} \left(\frac{\mu^2}{m_t^2}\right)^{-\epsilon}, \tag{2.2}$$

where μ is the dimensional regularization scale.

The families, which we have mentioned, are defined through the following sets of scalar products:

PLA

$$\begin{aligned}
&D_1 = k_1^2, \quad D_2 = (k_1 - p_1)^2, \quad D_3 = (k_1 + p_2)^2, \quad D_4 = k_2^2 - m_t^2, \\
&D_5 = (k_1 + k_2 - p_1)^2 - m_t^2, \quad D_6 = (k_1 + k_2 + p_2)^2 - m_t^2, \\
&D_7 = (k_1 + k_2 - p_1 + p_3)^2 - m_t^2, \quad D_8 = (k_1 + p_3)^2, \quad D_9 = (k_1 + k_2)^2,
\end{aligned} \tag{2.3}$$

PLB

$$\begin{aligned}
&D_1 = k_1^2, \quad D_2 = (k_1 - p_1)^2, \quad D_3 = (k_1 + p_2)^2, \quad D_4 = k_2^2 - m_t^2, \\
&D_5 = (k_2 - k_1)^2 - m_t^2, \quad D_6 = (k_1 - p_1 + p_3)^2, \quad D_7 = (k_2 + p_1)^2, \\
&D_8 = (k_2 + p_2)^2, \quad D_8 = (k_2 + p_3)^2,
\end{aligned} \tag{2.4}$$

NPL

$$\begin{aligned}
&D_1 = k_1^2, \quad D_2 = (k_1 - p_1)^2, \quad D_3 = (k_1 + p_2)^2, \quad D_4 = k_2^2 - m_t^2, \\
&D_5 = (k_1 + k_2 - p_1)^2 - m_t^2, \quad D_6 = (k_2 - p_1 - p_2 + p_3)^2 - m_t^2, \\
&D_7 = (k_1 + k_2 - p_1 + p_3)^2 - m_t^2, \quad D_8 = (k_1 + p_3)^2, \quad D_9 = (k_1 + k_2)^2.
\end{aligned} \tag{2.5}$$

The representative two-loop diagrams with a massive loop corresponding to a top quark are shown in Fig. 4.2.1.

The Feynman diagrams were generated using QGRAF [207], and only 14 of them actually contribute to the helicity amplitudes. On the other hand, if we consider all the diagrams generated, some of them are associated with an additional planar topology, which we call **PLC**, with the corresponding diagrams shown in Fig. 4.2.2. This planar topology is defined by the following nine scalar products:

PLC

$$\begin{aligned}
&D_1 = k_1^2, \quad D_2 = (k_1 + p_3)^2, \quad D_3 = (k_1 + p_2)^2, \quad D_4 = k_2^2 - m_t^2, \\
&D_5 = (k_1 + k_2 - p_1 + p_3)^2 - m_t^2, \quad D_6 = (k_1 + k_2 + p_2)^2 - m_t^2, \\
&D_7 = (k_1 - p_1 + p_3)^2, \quad D_8 = (k_2 - p_1)^2, \quad D_9 = (k_1 + k_2)^2.
\end{aligned} \tag{2.6}$$

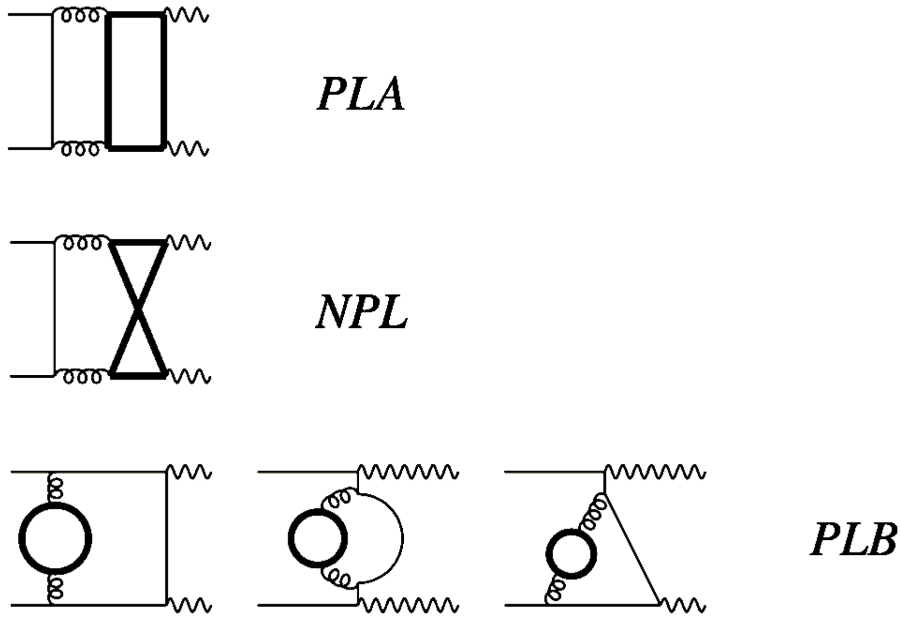

Figure 4.2.1. Representative set of two-loop diagrams with internal heavy quark loops.

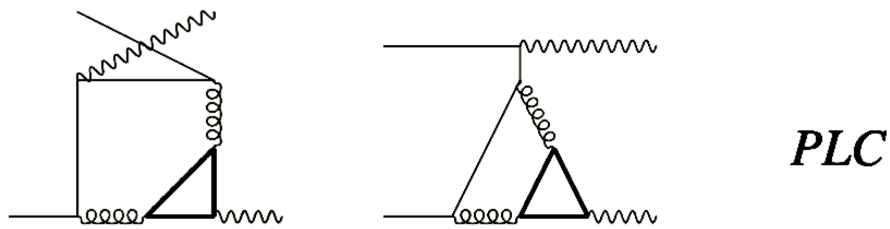

Figure 4.2.2. Representative set of diagrams associated with the PLC topology, which do not contribute to the helicity amplitudes.

However, these diagrams, which belong to the **PLC** family, do not contribute to the helicity amplitudes as a consequence of Furry's theorem. In particular, the contribution of these diagrams is zero when we consider the sum of a diagram in which the top quark circulates in one direction in the massive triangle with the same diagram in which the top quark circulates in the opposite direction.

Then we can describe the form factors only with the three topologies defined in eqs. (2.3-2.5), with the corresponding crossing due to the exchange of photons:

$$\mathrm{PLA}_{\sigma_{34}} = \mathrm{PLA}\Big|_{p_3\to p_4, p_4\to p_3}, \quad \mathrm{PLB}_{\sigma_{34}} = \mathrm{PLB}\Big|_{p_3\to p_4, p_4\to p_3}, \quad \mathrm{NPL}_{\sigma_{34}} = \mathrm{NPL}\Big|_{p_3\to p_4, p_4\to p_3}. \tag{2.7}$$

4.2.1 MIs

The MIs that appear in the form factors are shown in the appendix B. In Fig. 4.2.3 we show the 42 MIs for the PLA, PLB and NPL topologies as defined in the Appendix. The corresponding MIs obtained by permutations of the external legs are not shown. The MIs

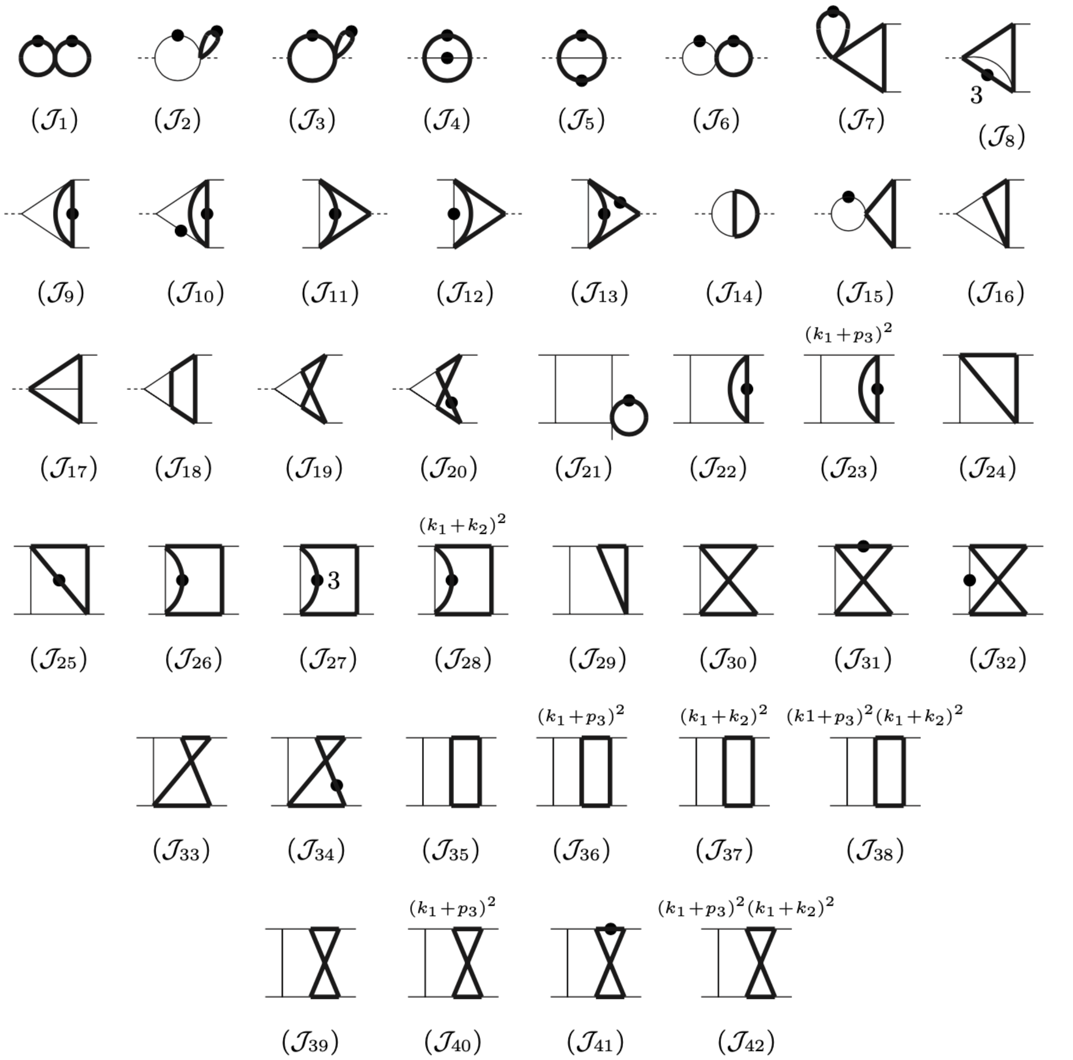

Figure 4.2.3. Master integral basis for PLA, PLB and NPL topologies. The figure does not show the MIs defined by a permutation of the external moments.

for the PLA and PLB families have already been studied [208]. As an original result, we presented a new set of MIs coming from the NPL, shown in Fig. 4.2.4

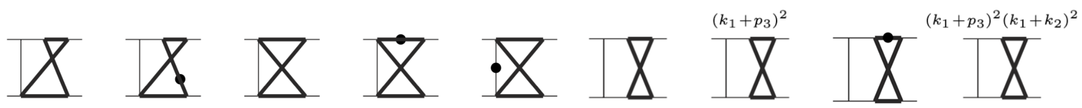

Figure 4.2.4. New set of MIs coming from the NPL integral family

4.3 renormalisation

In this section we will discuss what kind of singularities appear in the bare form factors and which renormalisation scheme is used to obtain the finite remainder.

In the perturbative expansion in eq. (1.16), as explained earlier, we are interested in the term $\overline{F}_k^{(2)}$. The bare form factors are expressed as a linear combination of the 72 MIs, $\{\mathcal{J}_i\}$, defined in eq. (B.1) and eq. (B.2).

We find the following expression for the form factors $\overline{F}_k^{(2)}$:

$$\overline{F}_k^{(2)} = (4\pi\alpha_{em})\,\delta_{ij}\,C_F\left[Q_q^2\,\overline{F}_{k;0}^{(2)} + Q_t^2\,\overline{F}_{k;2}^{(2)}\right], \tag{3.1}$$

where $C_F = \frac{N_c^2-1}{2\,N_c}$ is the Casimir of the fundamental representation of $SU(N_c)$, Q_q is the electric charge of the light quark and Q_t is the electric charge of the top quark running in the loop. The two contributions $\overline{F}_{k;0}^{(2)}$ and $\overline{F}_{k;2}$ are related to different powers of the top electric charge Q_t. The contribution $\overline{F}_{k;0}^{(2)}$ is associated with diagrams (c), (d) and (e) in Fig. 4.2.1, where the top quark does not couple to the external photons, while the second contribution $\overline{F}_{k;2}$ comes from diagrams (a) and (b), where the top quark does couple to the photons.

We perform our calculations in dimensional regularisation. As a consequence, potential UV and IR singularities can appear as poles in the dimensional regulator $\epsilon = \frac{4-d}{2}$. However, since the massive corrections to the $q\bar{q}$ channel start at the two-loop order, $\overline{F}_k^{(2)}$ has no IR singularities. This is due to the fact that the IR singularities are present even after renormalisation and are actually cancelled between virtual and real corrections, but in this channel the real part has no IR singularities, then our form factors are IR safe and all possible ϵ poles are of UV origin.

We have split our form factors into two different terms proportional to the electric charge of the top quark. $\overline{F}_{k;2}^{(2)}$ is free of UV divergences, since there are no other terms in the amplitude at $\mathcal{O}(\alpha_{em}^2\alpha_s^2)$ in the $q\bar{q}$ channel proportional to Q_t^2 with UV singularities. Then all UV poles come only from the $\overline{F}_{k;0}^{(2)}$ contribution.

UV renormalisation

We renormalised the bare form factors in a mixed renormalisation scheme. Specifically:

- `External quark fields`: renormalised on-shell
- `Strong couling constant`: renormalised in a mixed scheme
  - The light-quark contribution is treated in $\overline{MS}$
  - The heavy-quark contribution is renormalized at zero momentum
- `Top quark mass`: no renormalisation is needed at $\mathcal{O}(\alpha_{em}^2\alpha_s^2)$
- `External photon field` no renormalisation is needed at $\mathcal{O}(\alpha_{em}^2\alpha_s^2)$.

In this scheme, we can rewrite our renormalised form factors as:

$$\overline{F}_k^R = Z_q\overline{F}_k\left(\alpha_s^B \to Z_{\alpha_s}\alpha_s\right), \tag{3.2}$$

where the subscript "R" stands for "renormalised" and "B" for "bare".

The renormalisation factors Z_q and Z_{α_s} admit a perturbative expansion in the strong coupling constant:

$$
\begin{aligned}
Z_q &= 1 + \left(\frac{\alpha_s}{\pi}\right) \delta Z_q^{(1)} + \left(\frac{\alpha_s}{\pi}\right)^2 \delta Z_q^{(2)} + \mathcal{O}(\alpha_s^4), \\
Z_{\alpha_s} &= 1 + \left(\frac{\alpha_s}{\pi}\right) \delta Z_\alpha^{(1)} + \mathcal{O}(\alpha_s^2),
\end{aligned} \tag{3.3}
$$

where, in our renormalisation scheme, for the external quark fields we have:

$$
\delta Z_q^{(1)} = 0, \tag{3.4}
$$

since is the contribution from a massless bubble integrals which is zero in dimensional regularisation, and

$$
\delta Z_q^{(2)} = \pi^{-2\epsilon}\Gamma^2(1+\epsilon) \left(\frac{\mu^2}{m_t^2}\right)^{2\epsilon} C_F \, N_h \, T_F \left(\frac{1}{16\epsilon} - \frac{5}{96}\right). \tag{3.5}
$$

For the strong coupling constant we have the sum of two different contributions:

$$
\delta Z_{\alpha_s}^{(1)} = \delta Z_{\alpha, N_l, \overline{MS}}^{(1)} + \delta Z_{\alpha, N_h, OS}^{(1)}, \tag{3.6}
$$

where:

$$
\begin{aligned}
\delta Z_{\alpha, N_l, \overline{MS}}^{(1)} &= -\pi^{-\epsilon} e^{-\epsilon \gamma_E} \frac{1}{2\epsilon} \left(\frac{11}{6} C_A - \frac{1}{3} N_l\right), \\
\delta Z_{\alpha, N_h, OS} &= \pi^{-\epsilon}\Gamma(1+\epsilon) \left(\frac{\mu^2}{m_t^2}\right)^{\epsilon} \frac{N_h}{6\epsilon}.
\end{aligned} \tag{3.7}
$$

Here μ is the renormalisation scale, N_l is the number of light flavours, N_h is the number of heavy quarks, C_A is the casimir of the adjoint representation of $SU(N_c)$ and T_F is the invariant needed to fix the trace of the Gell-Mann matrices in the fundamental representation of $SU(N_c)$.

From eq. (3.2), the renormalised form factors are determined by the following formula:

$$
\overline{F}_k^{(2)\,R} = \overline{F}_k^{(2)} + \delta Z_q^{(2)} \, \overline{F}_k^{(0)} + \delta Z_{\alpha_s, N_h, OS} \overline{F}_k^{(1)}. \tag{3.8}
$$

4.3.1 Hard-virtual function

Our two-loop amplitude was the last missing ingredient for a fully massive NNLO QCD diphoton production calculation at hadron colliders. Our helicity amplitudes are finite after UV renormalisation, according to eq. (3.8). When the massive corrections are considered together with the corresponding massless two-loop scattering amplitudes [209, 206], the subtraction operators (defined in section 3.4) are sufficient to remove the IR poles of the complete two-loop virtual correction.

At NNLO, the total or differential cross section for this process can be calculated using the q_T subtraction method introduced in Chapter 3. From eq. (1.8) with the final state corresponding to the diphoton $F = \gamma\gamma$, the master formula reads:

$$
d\sigma_{\mathrm{NNLO}}^{\gamma\gamma} = \mathcal{H}_{\mathrm{NNLO}}^{\gamma\gamma} \otimes d\sigma_{\mathrm{LO}}^{\gamma\gamma} + \left[d\sigma_{\mathrm{NLO}}^{\gamma\gamma+\mathrm{jets}} - d\sigma_{\mathrm{NNLO}}^{CT} \right]. \tag{3.9}
$$

In Chapter 3, all the elements of the precedent eq. (3.9) are explained in detail. Here we focus on the hard-virtual coefficient function $\mathcal{H}_{\mathrm{NNLO}}^{\gamma\gamma}$, which contains the relevant information of the two-loop virtual scattering amplitude. This information enters through the hard virtual factor at NNLO $H_q^{\gamma\gamma\,(2)}$ defined in eqs. (3.24) and (3.7). In our specific case of diphoton production we can write:

$$H_q^{\gamma\gamma} = 1 + \left(\frac{\alpha_s}{\pi}\right) H_q^{\gamma\gamma(1)} + \left(\frac{\alpha_s}{\pi}\right)^2 H_q^{\gamma\gamma(2)} + \cdots . \tag{3.10}$$

At NLO the hard virtual coefficient $H_q^{\gamma\gamma(1)}$ contains only massless corrections. At NNLO $H_q^{\gamma\gamma(2)}$ has two well-defined (and additive) contributions: the massless and the massive corrections. As discussed earlier, our complete two-loop massive form factors proceed by simple addition to that of the massless case. Applying the subtraction operators defined in section 3.4, we obtain the finite remainder $\mathcal{A}_{q\bar{q},\gamma\gamma}^{(fin)}$ of the amplitude (which is written in 3.4 as $\widetilde{\mathcal{M}}_{c\bar{c}\to F}$). And so with the master formula of eq. (4.17) we can write:

$$H_q^{\gamma\gamma(2)} = \frac{|\mathcal{A}_{q\bar{q},\gamma\gamma}^{(\mathrm{fin})}|^2}{|\mathcal{A}_{q\bar{q},\gamma\gamma}^{(0)}|^2}, \tag{3.11}$$

where $\mathcal{A}_{q\bar{q},\gamma\gamma}^{(0)}$ is the Born-level amplitude for this process:

$$|\mathcal{A}_{q\bar{q},\gamma\gamma}^{(0)}|^2 = 128\,\pi^2\,\alpha_{em}^2\,Q_q^4\,N_c\left(\frac{t}{u} + \frac{u}{t}\right), \tag{3.12}$$

where α_{em} is the QED coupling, Q_q is the electric charge of the incoming quarks and N_c is the number of colours. The sum over initial and final polarisations and initial colours is already done.

4.4 DEs & canonical basis

In this section we discuss how to solve the MIs by the differential equations method. We analyse the different families of scalar integrals separately and derive the system of DEs in terms of a new set of dimensionless kinematic invariants:

$$\{\underline{x}\} = \{y, z\}, \quad \text{where} \quad y = \frac{s}{m_t^2} \quad \text{and} \quad z = \frac{t}{m_t^2}. \tag{4.1}$$

We will discuss the different topologies separately. The system for the two planar families, PLA and PLB, is in canonical logarithmic form, while for the non-planar family, NPL, we have canonical differential equations only for those sectors whose analytic solution could be given in terms of MPLs.

4.4.1 Planar family PLA

The family of scalar integrals PLA is described by a set of 32 MIs $\underline{\mathcal{I}}_{PLA}(\underline{x}, \epsilon)$. The system of first-order differential equations for these integrals has been derived in canonical logarithmic form:

$$d\,\underline{\mathcal{I}}_{\mathrm{PLA}}(\underline{x}, \epsilon) = \epsilon\, d\mathbb{A}(\underline{x})\,\underline{\mathcal{I}}_{\mathrm{PLA}}(\underline{x}, \epsilon), \tag{4.2}$$

where $d = \sum_i dx_i \frac{\partial}{\partial x_i}$ is the total differential with respect to the kinematic invariants and $\mathbb{A}(\underline{x})$ is the matrix of dlog one-forms written as linear combination of logarithms:

$$\mathbb{A}(\underline{x}) = \sum c_i \log(w_i(\underline{x})). \tag{4.3}$$

The c_i represent matrices of rational numbers, while $\{w_i(\underline{x})\}$ is the set of one-forms (letters), i.e. algebraic functions in the kinematic invariants, composing the alphabet $\mathbf{W}_{\text{PLA}}$.

Specifically, the alphabet for this DE system consists of the following 21 letters:

$$
\begin{aligned}
&w_1(y,z) = r_1, \quad w_2(y,z) = r_2, \quad w_3(y,z) = r_3, \quad w_4(y,z) = r_4,\\
&w_5(y,z) = \frac{r_4 - r_5}{r_4 + r_5}, \quad w_6(y,z) = y, \quad w_7(y,z) = \frac{r_1 - y}{r_1 + y},\\
&w_8(y,z) = r_4 - y\, r_2, \quad w_9(y,z) = \frac{r_3 + y}{r_3 - y}, \quad w_{10}(y,z) = \frac{z\, r_1 - r_1 - r_5}{z\, r_1 - r_1 + r_5},\\
&w_{11}(y,z) = -\frac{y - y\, z + r_5}{y(z-1)}, \quad w_{12}(y,z) = \frac{z\, r_1 - r_4}{z\, r_1 + r_4},\\
&w_{13}(y,z) = \frac{z\, r_1 - r_5}{z\, r_1 + r_5}, \quad w_{14}(y,z) = 1 - z, \quad w_{15}(y,z) = z,\\
&w_{16}(y,z) = y + z, \quad w_{17}(y,z) = \frac{r_2 - z}{r_2 + z}, \quad w_{18}(y,z) = -\frac{y + 2z - y\, z + r_5}{y - 2z - y\, z + r_5},\\
&w_{19}(y,z) = \frac{r_4 + z\, r_4 - z\, r_5}{r_4 + z\, r_4 + z\, r_5}, \quad w_{20}(y,z) = \frac{r_2 - r_3 - y - z}{r_2 + r_3 + y + z},\\
&w_{21}(y,z) = \frac{4y\, r_2 + 4z\, r_2 + z\, r_2^2 + z\, r_4 - y\, z\, r_2 - z^2\, r_2 - 4r_4}{-4y\, r_2 - 4z\, r_2 + z\, r_2^2 - z\, r_4 + y\, z\, r_2 + z^2\, r_2 + 4r_4},
\end{aligned}
\tag{4.4}
$$

with the dependencies on the following set of five square roots in the kinematic invariants:

$$
\begin{aligned}
&r_1 = \sqrt{(y-4)y}, \quad r_2 = \sqrt{(z-4)z}, \quad r_3 = \sqrt{y(y+4)},\\
&r_4 = \sqrt{yz(y(z-4) - 4z)}, \quad r_5 = \sqrt{y\,(y(z-1)^2 - 4z^2)}.
\end{aligned}
\tag{4.5}
$$

Canonical basis and boundary conditions

Given the set of 32 MIs for the PLA family defined in the Appendix B, the system of DEs has been rotated to the canonical form and the corresponding canonical MIs, $f_1^{PLA}, \ldots, f_{32}^{PLA}$, are presented in the Appendix. C.

The boundary conditions $\underline{f}_0^{PLA}(\epsilon)$ for all MIs are fixed at the point $\{\underline{x}\} = 0$, where $\{\underline{x}\} = \{y, z\}$. In this point all MIs vanish except for the tadpole f_1^{PLA}, which is known analytically, and for f_2^{PLA}, which is also known analytically since it is a product of two one-loop integrals. The boundary condition vector is:

$$
\begin{aligned}
&\underline{f}_0^{PLA}(\epsilon) = \{f_{0,1}^{PLA}, f_{0,2}^{PLA}, 0,0,0,0,0,0,0,0,0,0,0,\\
&0,0,0,0,0,0,0,0,0,0,0,0,0,0,0,0,0,0\},
\end{aligned}
\tag{4.6}
$$

where:

$$
\begin{aligned}
f_{0,1}^{PLA} &= 1,\\
f_{0,2}^{PLA} &= \left(-\frac{1}{y}\right)^{\epsilon} \epsilon\, \frac{\Gamma(1-\epsilon)\Gamma(-\epsilon)}{\Gamma(1-2\epsilon)}.
\end{aligned}
\tag{4.7}
$$

4.4.2 Planar family PLB

Regarding the second planar family, PLB, we observe that we do not need to set up a system of differential equations for it. In fact, each master integral of this family, except $\mathcal{J}_{21}$, is equal to one of the MIs of the other two families (modulo permutations). For $\mathcal{J}_{21}$, shown in Fig. 4.2.3, by analytic integration of its differential equation, we obtain the following analytic expression:

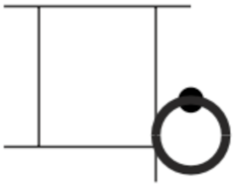

$$
\begin{aligned}
= \frac{1}{y\,z}\Bigg[& \frac{4}{\epsilon^3} - \frac{2(\log(-y)+\log(-z))}{\epsilon^2} - \frac{5\pi^2 - 6\log(-y)\log(-z)}{3\epsilon} \\
& + 2\mathrm{Li}_3\left(-\frac{z}{y}\right) - 2\log(-z)\mathrm{Li}_2\left(-\frac{z}{y}\right) + 2\log(-y)\mathrm{Li}_2\left(-\frac{z}{y}\right) \\
& - \log(-y)\log^2(-z) + \log(y)\log^2(-z) - \log^2(-z)\log(y+z) \\
& - \log^2(-y)\log(y+z) - 2\log(-y)\log(y)\log(-z) \\
& + 2\log(-y)\log(-z)\log(y+z) - \pi^2\log(y+z) \\
& + \log^2(-y)\log(y) + \frac{\pi^2}{3}\log(-y) + \pi^2\log(y) \\
& \quad + \frac{1}{3}\log^3(-z) + \frac{4}{3}\pi^2\log(-z) - 10\zeta(3)\Bigg] \; + \; \mathcal{O}(\epsilon).
\end{aligned}
$$

4.4.3 Non-planar family NPL

The NPL integral family is the most complicated of the topologies describing amplitude, since it involves a more complicated geometry than the genus 0 case described by the other two topologies. The scalar integral family NPL is described by a set of 36 MIs $\underline{\mathcal{I}}_{\mathrm{NPL}}(\underline{x},\epsilon)$. The system of differential equations can be divided into two different subsets:

- **Canonical Logarithmic**: the subset of MIs whose differential equations are in canonical logarithmic form,
- **Elliptic sectors**: this subset contains MIs whose analytic solution involves elliptic functions and is not written in ϵ-factorised form,

so that the system reads:

$$
d\,\underline{\mathcal{I}}_{\mathrm{NPL}}(\underline{x},\epsilon) = \epsilon\, d\mathbb{A}(\underline{x})\,\underline{\mathcal{I}}_{\mathrm{NPL}}(\underline{x},\epsilon) \; + \; d\tilde{\mathbb{A}}(\underline{x},\epsilon)\,\underline{\mathcal{I}}_{\mathrm{NPL}}(\underline{x},\epsilon). \tag{4.8}
$$

Canonical logarithmic subset

The system of differential equations for this subset has been written in canonical logarithmic form. The alphabet $\mathbf{W}_{\mathrm{NPL}}$ for this subset is described by the following 30 letters:

$$\begin{aligned}
&w_1(y,z) = q_1, \quad w_2(y,z) = q_3, \quad w_3(y,z) = q_4, \quad w_4(y,z) = q_5, \\
&w_5(y,z) = q_6, \quad w_6(y,z) = -\frac{q_4 - 2\,i\,q_8}{q_4 + 2\,i\,q_8}, \quad w_7(y,z) = \frac{q_5 - 2\,q_8}{q_5 + 2\,q_8}, \\
&w_8(y,z) = -\frac{q_9 - 2}{q_9 + 2}, \quad w_9(y,z) = q_9, \quad w_{10}(y,z) = -\frac{q_5 - i\,y\,q_7}{q_5 + i\,q_7}, \\
&w_{11}(y,z) = y, \quad w_{12}(y,z) = \frac{q_1 + y}{q_1 - y}, \quad w_{13}(y,z) = q_4 - y\,q_2, \\
&w_{14}(y,z) = \frac{q_3 + y}{q_3 - y}, \quad w_{15}(y,z) = \frac{z\,q_1 - q_4}{z\,q_1 + q_4}, \quad w_{16}(y,z) = -\frac{q_6 - z\,q_7}{q_6 + z\,q_7}, \\
&w_{17}(y,z) = z, \quad w_{18}(y,z) = y + z, \quad w_{19}(y,z) = 4 + y + z, \\
&w_{20}(y,z) = \frac{q_2 + z}{q_2 - z}, \quad w_{21}(y,z) = \frac{z\,q_1 + y\,q_1 + i\,q_5}{z\,q_1 + y\,q_1 - i\,q_5}, \quad w_{22}(y,z) = \frac{z\,q_2 + y\,q_2 + q_6}{z\,q_2 + y\,q_2 - q_6}, \\
&w_{23}(y,z) = -\frac{q_5 + i\,y^2 + i\,y\,z}{q_5 - i\,y^2 - i\,y\,z}, \quad w_{24}(y,z) = \frac{y\,q_3 + z\,q_3 - y\,q_7}{y\,q_3 + z\,q_3 + y\,q_7}, \\
&w_{25}(y,z) = -\frac{q_6 - y\,z - z^2}{q_6 + y\,z + z^2}, \quad w_{26}(y,z) = -\frac{q_6 + y\,z + z^2}{q_6 - y\,z - z^2}, \\
&w_{27}(y,z) = \frac{q_7 + y + z}{q_7 - y - z}, \quad w_{28}(y,z) = \frac{q_2 + q_3 + y + z}{q_2 - q_3 - y - z}, \\
&w_{29}(y,z) = \frac{2\,z\,q_8\,q_9 + 4\,z\,q_8 + 4\,y\,q_8 + i\,y\,q_6\,q_9 - y\,z\,q_8 - z^2\,q_8}{2\,z\,q_8\,q_9 - 4\,z\,q_8 - 4\,y\,q_8 - i\,y\,q_6\,q_9 + y\,z\,q_8 + z^2\,q_8}, \\
&w_{30}(y,z) = \frac{z^2 + q_4 - y\,q_2 - z\,q_2}{z^2 - q_4 + y\,q_2 + z\,q_2},
\end{aligned} \tag{4.9}$$

with the dependencies on the following set of nine square roots in the kinematic invariants:

$$\begin{aligned}
&q_1 = \sqrt{y(y-4)}, \quad q_2 = \sqrt{z(z-4)}, \quad q_3 = \sqrt{y(y+4)}, \\
&q_4 = \sqrt{yz(y(z-4) - 4z)}, \quad q_5 = \sqrt{y(y+z)(-4z + y(y+z))}, \\
&q_6 = \sqrt{z(y+z)\,(y(z-4) + z^2)}, \quad q_7 = \sqrt{(y+z)(y+z+4)}, \\
&q_8 = \sqrt{-yz(y+z)}, \quad q_9 = \sqrt{4-z}.
\end{aligned} \tag{4.10}$$

Elliptic sectors

This subset contains two sectors, in Fig. (4.4.5) , and it is associated to the MIs whose analytic structure involves elliptic functions. The first sector is a non-planar triangle with a massive top-quark loop. This sector has 2 MIs, which admit a representation in terms of elliptic multiple polylogarithms (eMPLs). We choose the same normalization as in Ref. [210]:

$$f_{31}^{NPL} = \epsilon^4\,y^2\,\mathcal{J}_{19}(y), \qquad f_{32}^{NPL} = \frac{\epsilon^4\,y^2\,(y+16)}{4\epsilon + 2}\mathcal{J}_{20}(y). \tag{4.11}$$

The second sector is the top-sector of the NPL topology, i.e. the double-box integral in Fig. 4.4.5 (b), which contains 4 MIs: f_{33}^{NPL}, f_{34}^{NPL}, f_{35}^{NPL} and f_{36}^{NPL}. We choose, as basis for this top-sector, the following scalar integrals:

$$\begin{aligned}
f_{33}^{NPL} &= -\epsilon^4\,y^3\,\mathcal{J}_{39}(y,z), \qquad f_{34}^{NPL} = \epsilon^4\,y^2\,\mathcal{J}_{40}(y,z), \\
f_{35}^{NPL} &= \epsilon^4\,y^4\,\mathcal{J}_{41}(y,z), \qquad f_{36}^{NPL} = -\epsilon^4\,y\,\mathcal{J}_{42}(y,z).
\end{aligned} \tag{4.12}$$

Figure 4.4.5. Diagrams representing the two elliptic sectors in the non planar topology NPL. Thin lines represent massless particles, while thick lines massive particles.

The non-polylogarithmic structure of this sector is a two-fold. The differential equation for the MIs f_{33}^{NPL}, f_{34}^{NPL}, f_{35}^{NPL} and f_{36}^{NPL} contain the triangle MIs f_{31}^{NPL} and f_{32}^{NPL} in the non-homogeneous part of the system. As a consequence the analytic solution of the differential equations requires the integration over kernels that contains eMPLs. Moreover, also the homogeneous part of the differential equation itself contains elliptic functions. We verified this studying the maximal cut of the double-box integral.

Given the set of MIs for the NPL family defined in Appendix B, the system of DEs has been rotated to the canonical form, except for the MIs whose analytic structures involve elliptic functions. With the choices made in eq. (4.11) and eq. (4.12) we define the canonical basis $f_1^{NPL}, ..., f_{36}^{NPL}$ in Appendix C.

The boundary conditions $\underline{f}_0^{NPL}(\epsilon)$ for all MIs of the NPL topology are fixed at the point $\{\underline{x}\} = 0$, where $\{\underline{x}\} = \{y, z\}$. In this point all MIs vanish except for the tadpole f_1^{NPL}, which is known analytically, and for f_2^{NPL}, which is also known analytically since it is a product of two one-loop integrals:

$$\begin{aligned}&\underline{f}_0^{NPL}(\epsilon) = \{f_{0,1}^{NPL}, f_{0,2}^{NPL}, 0,0,0,0,0,0,0,0,0,0,0,\\&0,0,0,0,0,0,0,0,0,0,0,0,0,0,0,0,0,0,0,0,0,0,0\},\end{aligned} \tag{4.13}$$

where:

$$\begin{aligned}f_{0,1}^{NPL} &= 1,\\ f_{0,2}^{NPL} &= \left(-\frac{1}{y}\right)^{\epsilon} \epsilon \,\frac{\Gamma(1-\epsilon)\Gamma(-\epsilon)}{\Gamma(1-2\epsilon)}.\end{aligned} \tag{4.14}$$

4.4.4 Maximal Cut

The computation of the maximal cut is performed in Baikov representation using a loop-by-loop approach. We start by defining the first loop as:

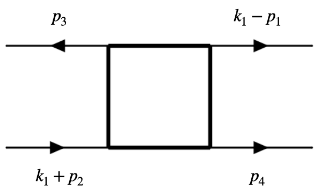

$$= \int \mathcal{D}k \frac{1}{D_1\, D_2\, D_3\, D_4}, \tag{4.15}$$

where the denominators are chosen to be:

$$\begin{aligned}&D_1 = k_2^2 - m_t^2, \quad D_2 = (k_2 + q_3)^2 - m_t^2,\\&D_3 = (k_2 - p_4)^2 - m_t^2, \quad D_4 = (k_2 + q_3 + p_3)^2 - m_t^2,\end{aligned} \tag{4.16}$$

where we defined $q_3 = (k_1 - p_1)$ and $q_4 = (k_1 + p_2)$ with $p_3^2 = p_4^2 = 0$ and $q_3^2 \neq q_4^2 \neq 0$. With this specific configuration the Mandelstam invariants are:

$$\begin{aligned} s' &= (q_4 - p_3)^2 = (q_3 + p_4)^2, \\ t' &= (-p_3 - q_3)^2 = (p_4 - q_4)^2, \\ u' &= (-p_3 - p_4)^2 = (q_3 - q_4)^2. \end{aligned} \tag{4.17}$$

In Baikov parametrization, eq. (4.15) is rewritten as:

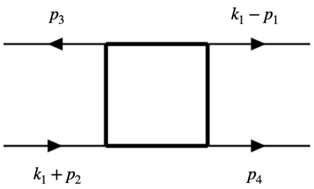

$$= \frac{\pi^{-3/2}}{\Gamma(\frac{1}{2}(d-3))} G(q_3, p_4, p_3)^{\frac{4-d}{2}} \int dz_1\, dz_2\, dz_3\, dz_4\, G(z_i)^{\frac{d-5}{2}} \frac{1}{z_1\, z_2\, z_3\, z_4}, \tag{4.18}$$

where $z_i = D_i$ and

$$\begin{aligned} G(q_3, p_4, p_3) &= det \begin{pmatrix} q_3 \cdot q_3 & q_3 \cdot p_4 & q_3 \cdot p_3 \\ p_4 \cdot q_3 & p_4 \cdot p_4 & p_4 \cdot p_3 \\ p_3 \cdot q_3 & p_3 \cdot p_4 & p_3 \cdot p_3 \end{pmatrix} \\ &= -\frac{1}{4}(q_3^2 + q_4^2 - s' - t')(q_3^2\, q_4^2 - s'\, t'). \end{aligned} \tag{4.19}$$

$G(z_i)$ is obtained by rewriting the Gram determinant $G(k_2, q_3, p_4, p_3)$ in terms of the variables z_i :

$$G(k_2, q_3, p_4, p_3) = det \begin{pmatrix} k_2 \cdot k_2 & k_2 \cdot q_3 & k_2 \cdot p_4 & k_2 \cdot p_3 \\ q_3 \cdot k_2 & q_3 \cdot q_3 & q_3 \cdot p_4 & q_3 \cdot p_3 \\ p_4 \cdot k_2 & p_4 \cdot q_3 & p_4 \cdot p_4 & p_4 \cdot p_3 \\ p_3 \cdot k_2 & p_3 \cdot q_3 & p_3 \cdot p_4 & p_3 \cdot p_3 \end{pmatrix} \tag{4.20}$$

with the following substitutions:

$$\begin{aligned} &k_2 \cdot k_2 = z_1 + m_t^2, \quad k_2 \cdot q_3 = \frac{z_2 - z_1 - q_3^2}{2}, \quad k_2 \cdot p_4 = \frac{z_1 - z_3}{2}, \\ &p_3 \cdot q_3 = \frac{t' - q_3^2}{2}, \quad k_2 \cdot p_3 = \frac{z_4 - z_2 + q_3^2 - t'}{2}, \quad q_3 \cdot p_4 = \frac{s' - q_3^2}{3}, \\ &p_3 \cdot p_4 = \frac{u'}{2}. \end{aligned} \tag{4.21}$$

At this point, for the first loop, the maximal cut is obtained by the replacing $\frac{1}{z_i} \to \delta(z_i)$:

MC (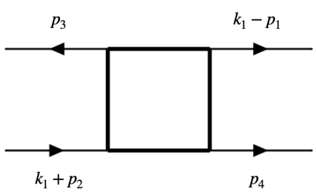)

$$\begin{aligned} &= \frac{\pi^{-3/2}}{\Gamma(\frac{1}{2}(d-3))} G(q_3, p_4, p_3)^{\frac{4-d}{2}} \int dz_1\, dz_2\, dz_3\, dz_4\, G(z_i)^{\frac{d-5}{2}} \\ &\quad \times \delta(z_1)\, \delta(z_2)\, \delta(z_3)\, \delta(z_4) \\ &= \frac{\pi^{-3/2}}{\Gamma(\frac{1}{2}(d-3))} (-\frac{1}{4}(q_3^2 + q_4^2 - s' - t')(q_3^2\, q_4^2 - s'\, t'))^{\frac{4-d}{2}} \\ &\quad \times (\frac{1}{16}(q_3^2\, q_4^2 - s'\, t')(q_3^2\, q_4^2 - s'\, t' + 4m_t^2(s' + t' - q_3^2 - q_4^2)))^{\frac{d-5}{2}}. \end{aligned} \tag{4.22}$$

Now we can proceed with the second loop integration, defining the remaining Baikov parameters as:

$$z_5 = k_1^2, \quad z_6 = (k_1 - p_1)^2, \quad z_7 = (k_1 + p_2)^2, \quad z_8 = (k_1 + p_3)^2, \tag{4.23}$$

where z_8 is the ISP, so the remaining integration will be over this variable. Explicitly:

$MC\Bigg($ 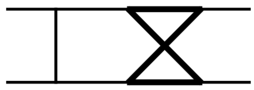 $\Bigg)$

$$= \frac{\pi^{3/2}}{\Gamma(\frac{1}{2}(d-3))} G(p_1, p_2, p_3)^{\frac{4-d}{2}} \int dz_5 dz_6 dz_7 dz_8 \times$$

$MC\Bigg($ 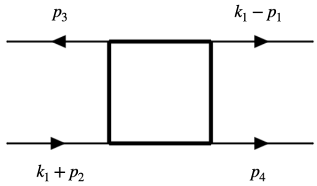 $\Bigg)$

$$\delta(z_5)\delta(z_6)\delta(z_7)\delta(z_8) \times$$

$$G(k_1, p_1, p_2, p_3)\Big|_{z_5, z_6, z_7, z_8}, \tag{4.24}$$

where the Gram determinant $G(k_1, p_1, p_2, p_3)\Big|_{z_5,z_6,z_7,z_8}$ is computed using the Mandelstam invariants defined in eq. (1.2) and the following substitutions:

$$\begin{aligned}
&k_1 \cdot k_1 = z_1, \quad k_1 \cdot p_1 = \frac{z_5 - z_6}{2}, \quad k_1 \cdot p_2 = \frac{z_7 - z_5}{2}, \\
&k_1 \cdot p_3 = \frac{z_8 - z_5}{2}, \quad p_1 \cdot p_2 = \frac{s}{2}, \quad p_1 \cdot p_3 = -\frac{t}{2}, \\
&p_2 \cdot p_3 = \frac{s+t}{2},
\end{aligned} \tag{4.25}$$

with $p_1^2 = p_2^2 = p_3^2 = 0$. For the second loop:

$$\begin{aligned}
G(q_3, p_4, p_3) &= det \begin{pmatrix} p_1 \cdot p_1 & p_1 \cdot p_2 & p_1 \cdot p_3 \\ p_2 \cdot p_1 & p_2 \cdot p_2 & p_2 \cdot p_3 \\ p_3 \cdot p_1 & p_3 \cdot p_2 & p_3 \cdot p_3 \end{pmatrix} \\
&= -\frac{1}{4} s\, t(s+t),
\end{aligned} \tag{4.26}$$

and

$$\begin{aligned}
G(k_1, p_1, p_2, p_3) &= det \begin{pmatrix} k_2 \cdot k_2 & k_2 \cdot p_1 & k_2 \cdot p_2 & k_2 \cdot p_3 \\ p_1 \cdot k_2 & p_1 \cdot p_1 & p_1 \cdot p_2 & p_1 \cdot p_3 \\ p_2 \cdot k_2 & p_2 \cdot p_1 & p_2 \cdot p_2 & p_2 \cdot p_3 \\ p_3 \cdot k_2 & p_3 \cdot p_1 & p_3 \cdot p_2 & p_3 \cdot p_3 \end{pmatrix} \\
&= \frac{1}{32}(s^{3/2} t \sqrt{16 m_t^2 + s}(3t - 2z_7 + 6z_8) + 6 s^{5/2} \sqrt{16 m_t^2 + s}(t + z_8) \\
&\quad + 3 s^{7/2} \sqrt{16 m_t^2 + s} - 2\sqrt{s} t^2 z_7 \sqrt{16 m_t^2 + s} + 8 m_t^2 s(s+t)(9s+t) \\
&\quad + 5s^4 + 2s^3(5t + z_8) + s^2(5t^2 + 2t(z_7 + z_8) + 2z_8^2) \\
&\quad + 2s\, t\, z_7(t + 2z_8) + 2t^2 z_7^2).
\end{aligned} \tag{4.27}$$

For the integration in eq.(4.24) we need before to express the previous Mandelstam invariants defined in eq. (4.17) in terms of the ones defined in (1.2):

$$\begin{aligned}
s' &= (k_1 + p_2 - p_3)^2 = z_7 + z_5 - z_8 + u, \\
t' &= (-p_3 - q_3)^2 = z_8 - z_5 + z_6 + t.
\end{aligned} \tag{4.28}$$

Finally, in $d \to 4$ space-time dimensions, we obtain the result for the maximal cut of the non-planar double-box integral:

MC (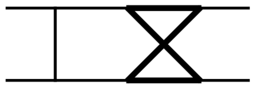)

$$\propto \int \frac{dz_8}{s\, z_8 \sqrt{(z_8+t)(s+t+z_8)((z_8+t)(s+t+z_8)-4sm_t^2)}}, \tag{4.29}$$

where we ignore the overall constant coming from the Baikov representation. Performing a Möbius transformation $z_8 \to z_8 - t$, ignoring the overall constant, we arrive at:

MC (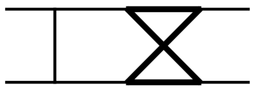)

$$\propto \frac{1}{s} \int \frac{dz_8}{(z_8 \,-\, t)\,\sqrt{z_8(z_8+s)(z_8(z_8+s)-4\,s\,m_t^2)}}. \tag{4.30}$$

As we can see from eq. (4.3), the result of the maximal cut for the double box non-planar integral is a one-fold integral, related to the elliptic curve:

$$y_c^2 = z_8(z_8+s)(z_8(z_8+s)-4\,s\,m_t^2), \tag{4.31}$$

with following set of branching points:

$$\begin{aligned} a_1 &= 0, \\ a_2 &= -s, \\ a_3 &= \frac{1}{2}(-\sqrt{s}\sqrt{16\,m_t^2+s}-s), \\ a_4 &= \frac{1}{2}(\sqrt{s}\sqrt{16\,m_t^2+s}-s). \end{aligned} \tag{4.32}$$

The elliptic curve y_c is exactly the same obtained for the non-planar massive triangle. This can be shown from the maximal cut of the latter:

MC (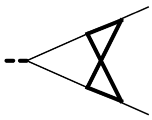)

$$\propto \frac{1}{s} \int \frac{dz_8}{\sqrt{z_8(z_8+s)(z_8(z_8+s)-4\,s\,m_t^2)}}. \tag{4.33}$$

More rigorously, it is possible to write the elliptic curve, represented in Fig. 4.4.6, in the so-called Weierstrass form:

$$z_8^3+(-\frac{16}{3}m_t^4\,s^2-\frac{16}{3}m_t^2\,s^3-\frac{1}{3}s^4)\,z_8+\frac{128}{27}m_t^6\,s^3-\frac{80}{9}m_t^4\,s^4-\frac{16}{9}m_t^2\,s^5-\frac{2}{27}s^6+y_c^2=0, \tag{4.34}$$

and computing the *j-invariant*:

$$j = \frac{(16\,m_t^4+16m_t^2\,s+s^2)^3}{s\,m_t^8\,(16\,m_t^2+s)} \tag{4.35}$$

to explicitly show the isomorphism between the two elliptic curves.

4.5 Semi-Analytic solution with Generalised power series

We discussed in detail the differential equations for the different scalar integral families. In particular, we were able to put the differential equations for the PLA family into canonical logarithmic form, and we split the differential equation system for the NPL family into a canonical logarithmic form and a part consisting of elliptic sectors. We have

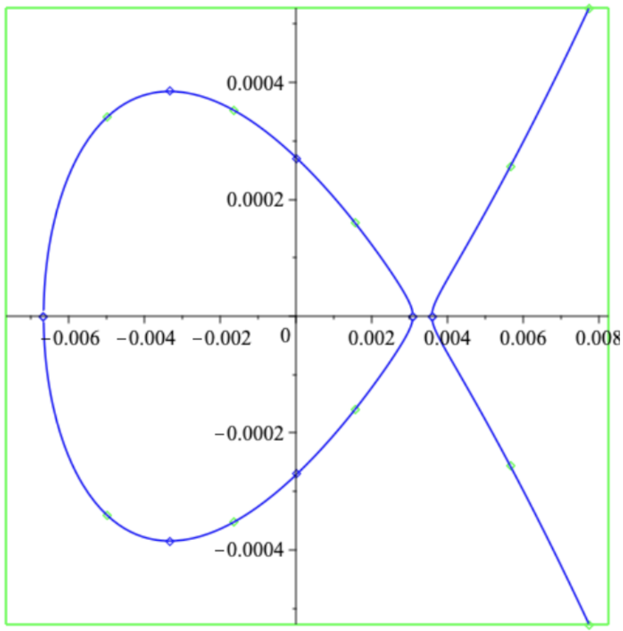

Figure 4.4.6. Elliptic curve in Weierstrass form for $m_t^2 = 1$ and $s = \frac{1}{400}$.

several problems, first of all, also for the PLA, we have a set of five non-simultaneously rationalisable square roots. The situation is even more complicated for the NPL family, since we have nine different non-simultaneously rationalisable square roots and we have to deal with eMPLs. Consequently, in order to obtain a fully analytic representation of the solution, we need to use symbol-level techniques and also to write the solution explicitly in terms of eMPLs. We are interested in evaluating the amplitude in order to perform phenomenology. We then decided to use a generalised power series expansion method to evaluate the MIs.

This method allow us to build a grid of points directly in the physical phase-space region for our process

$$y > 0, \quad z = -\frac{y}{2}(1 - \cos(\theta)), \quad -y < z < 0, \tag{5.1}$$

where θ is the scattering angle in the partonic center of mass frame, with value in the interval $\theta \in (0, \pi)$. The grid was generated in `DiffExp` on a single-core CPU with the following procedure. We consider a total number of 13752 points in the following range for the scattering angle θ and the energy of the center of mass $\sqrt{y}$

$$-0.99 < \cos\theta < 0.99, \quad 8\,\text{GeV} < \sqrt{y} < 2.2\,\text{TeV}\,. \tag{5.2}$$

In the coordinate system (y, z) the points $p_{i,j}$ of the grid are equally spaced as

$$p_{i,j} := \begin{cases} y_i = y_0 + (y_f - y_0)\frac{i}{572} \\ z_j = -\frac{y_i}{2}(1 - \cos\theta_j), \quad \cos\theta_j = \cos\theta_0 + (\cos\theta_f - \cos\theta_0)\frac{j}{23} \end{cases} \tag{5.3}$$

where $y_0 = 64\ \text{GeV}^2$, $y_f = 4.4\ \text{TeV}^2$, $\cos\theta_0 = -0.99$, $\cos\theta_f = 0.99$ and the indices i, j take the values $i \in [0, 572]$, $j \in [0, 23]$. We construct the grid by performing sequential numerical evaluations of the MIs as depicted schematically in Fig. 4.5.7.

Starting from the boundary conditions of the system of differential equations, we perform a first evaluation at the physical point $p_{0,0}$. From this point, with a fixed value

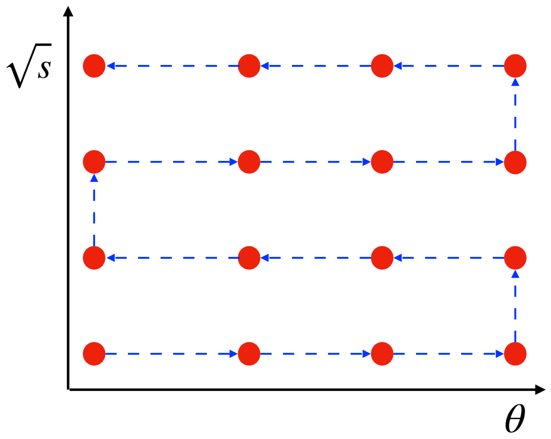

Figure 4.5.7. Schematic representation of the procedure exploited to optimise the grid construction within `DiffExp`. Red dots represents the points in which the MIs are evaluated and the blue dashed lines connect the sequential evaluations.

of y, we move along the θ axis, from $\cos\theta = -0.99$ to $\cos\theta = 0.99$, up to the point $p_{0,23}$. Then we increase the value of y and move in the other direction along the θ axis to the point $p_{1,0}$, and so on. In order to optimise the grid generation, for each evaluation we use as boundary conditions the value of the MIs obtained at the previous point. This procedure effectively increases the efficiency of the evaluation for the MIs. On a single-core laptop, we were able to evaluate the MIs at all points of the lattice with an accuracy of 16 digits in a time of $\mathcal{O}(2.5\,h)$ for the PLA family and $\mathcal{O}(10.5\,h)$ for the NPL family.
We performed some numerical checks for the MIs using different and independent numerical evaluations through the Mathematica package `AMFlow` [211], which implements the auxiliary mass flow method. We proceeded with two different checks.

- We evaluate the MIs in a phase space point with `AMFlow`. Then we use the main function of `DiffExp`, **TransportTo[...]**, to transport the boundary conditions defined in eq. (4.6,4.13) to arbitrary (real-valued) points in the phase space of the kinematic invariants and internal masses and pass the output of this function to the function **ToPiecewise[...]**, which combines the results of all line segments into a single function. The check between the two packages has been made for the value $\cos\theta = 0.3$, and it's shown in Fig. 4.5.8 for the four non-planar double box MIs.

- We evaluate the MIs at another point in phase space, specifically the centre of mass energy and the scattering angle were chosen to be $\sqrt{s} = 52.1615\,\text{GeV}$ and $\cos\theta = -0.99$. The result is shown in the Table 4.5.1. In the table we have shown the first 60 digits for the ϵ^0 order of the four non-planar double-box MIs of the NPL topology. The check between the two independent numerical solutions showed an agreement up to 200 digits.

After the numerical evaluation of the MIs, throught the eq. (3.10) we were able to construct a grid for the NNLO hard function $\mathcal{H}^{\gamma\gamma}_{NNLO}$ in the phase-space physical region between 8 GeV and 2.2 TeV, as shown in Fig. 4.5.9.
As we said, we obtained the grid for 13752 different points in the desired region. In order to perform the phenomenology, the grid was interpolated using cubic spline interpolation. We decided to use this particular interpolation instead of the polynomial interpolation [212] $p(x) = \sum_{k=0}^{n_p} a_k x^k$. With the polynomial interpolation, given a set of $n+1$ data, we

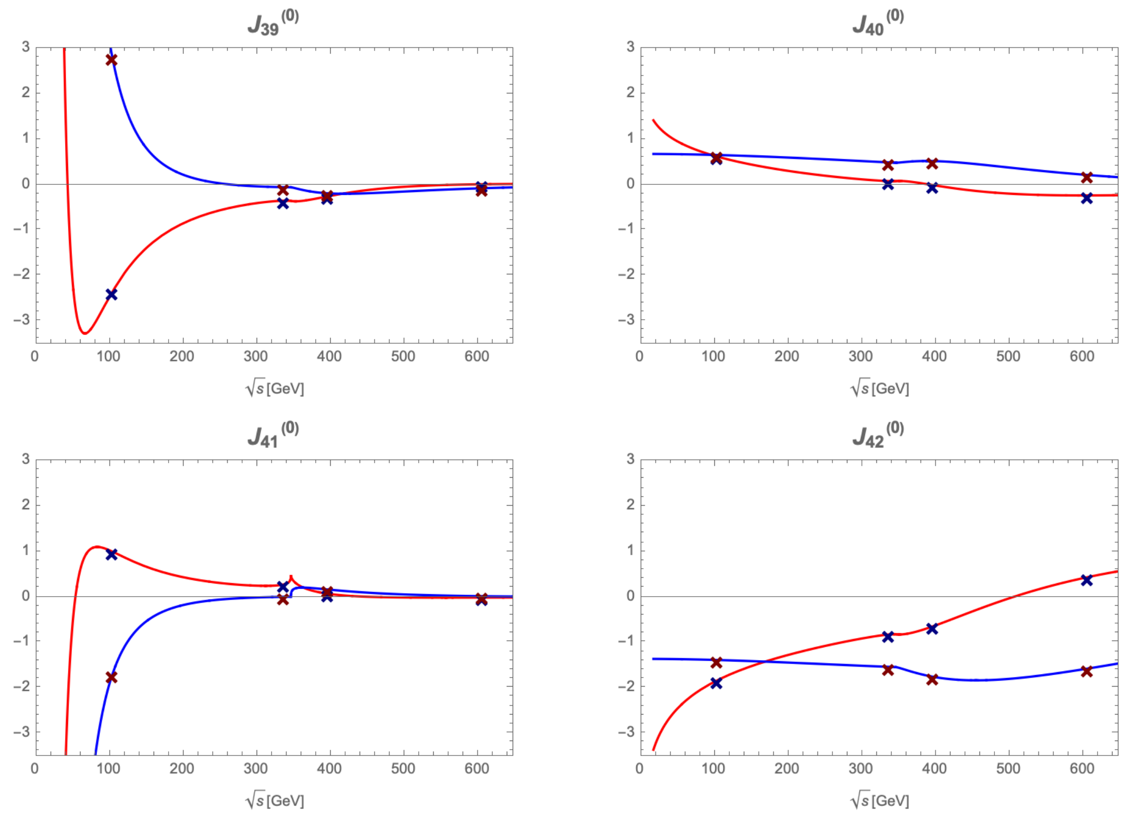

Figure 4.5.8. Numerical checks for the non-planar double box MIs $\mathcal{J}_{39}, \mathcal{J}_{40}, \mathcal{J}_{41}$ and $\mathcal{J}_{42}$. The plots show the order $\mathcal{O}(\epsilon^0)$ of the masters. The red and blue lines represent the numerical values of the real and imaginary parts of the MIs obtained with `DiffExp`. The crossed dots represent the numerical values obtained with `AMFlow`. The evaluations are performed for different values of $\sqrt{s}$ at a fixed angle θ (in this case $\cos\theta = 0.3$).

can fit a polynomial of n^{th} degree, while with spline interpolations for $n+1$ points, we form n splines $f : [x_1, ..., x_{n+1}] \to \mathbb{R}$ consisting of n polynomials of degree 3:

$$f(x) = \begin{cases} a_1 x^3 + b_1 x^2 + c_1 x + d_1 & \text{if } x \in [x_1, x_2] \\ a_2 x^3 + b_2 x^2 + c_2 x + d_2 & \text{if } x \in (x_2, x_3] \\ \dots & \\ a_n x^3 + b_n x^2 + c_n x + d_n & \text{if } x \in (x_n, x_{n+1}] \end{cases} \tag{5.4}$$

There are several advantages of using spline interpolation [213, 214, 215]. It provides a smooth interpolant and we can avoid some problems as the Runge's phenomenon [216], i.e. a problem of oscillation at the edges of an interval that occurs when using polynomial interpolation with polynomials of high degree over a set of equispaced interpolation points. In order to check the result of the interpolated grid, made with a program we wrote in `Fortran` [217], we decided to prepare a second small grid in `DiffExp`, as shown in Fig. 4.5.10. Then we made a numerical check between the value obtained from the second grid and the value obtained interpolating. To confirm the validity of the cubic spline interpolation for our grid, we computed the percentage error as:

$$\frac{\mathcal{H}^{\gamma\gamma}_{NNLO-grid}(p_{i,j}) - \mathcal{H}^{\gamma\gamma}_{NNLO-spline}(p_{i,j})}{\mathcal{H}^{\gamma\gamma}_{NNLO-grid}(p_{i,j})} \sim \mathcal{O}(0.3\%). \tag{5.5}$$

$\mathcal{J}_{42}^{(0)}$	`Diffexp`	Re	+0.73229133983930426889370536546880071419196880255135349324906
		Im	+0.01063600986474977455448357856767079241193558304513195335839
	`AMFlow`	Re	+0.73229133983930426889370536546880071419196880255135349324906
		Im	+0.01063600986474977455448357856767079241193558304513195335839

Table 4.5.1. Numerical comparison between `DiffExp` and `AMFlow` for the order ϵ^0 of the non-planar MI $\mathcal{J}_{42}$. The centre of mass energy and the photon scattering angle are respectively $\sqrt{s} = 52.1615\,\text{GeV}$ and $\cos\theta = -0.99$. The two independent numerical solutions are equal up to 200 digits, of which only 60 are shown.

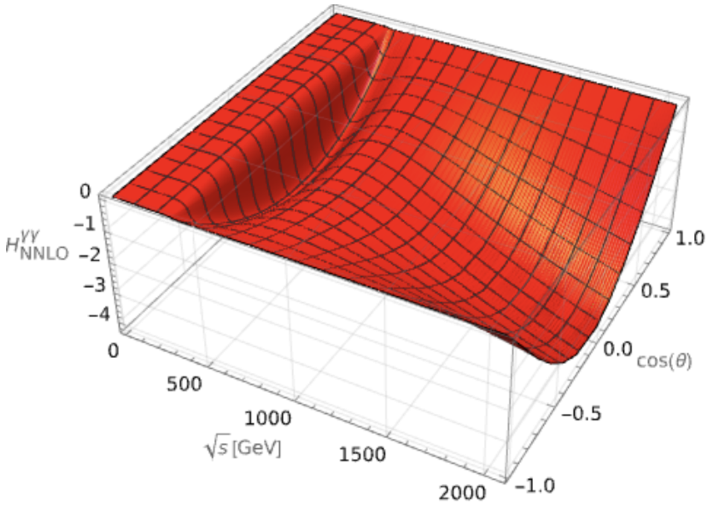

Figure 4.5.9. NNLO hard function grid in the physical phase-space region between 8 GeV and 2.2 TeV.

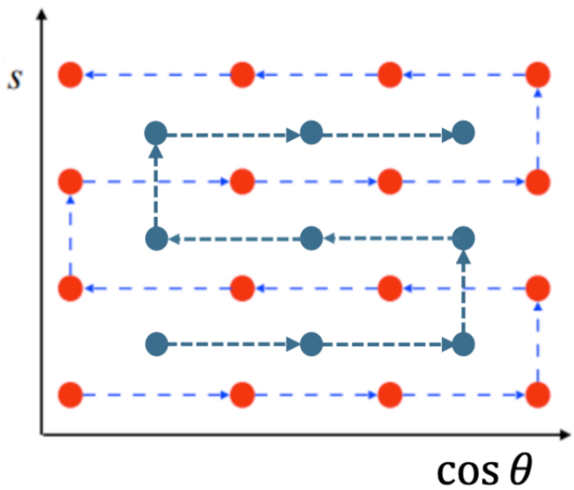

Figure 4.5.10. Schematic representation of the procedure exploited to build the two grids with DiffExp. The dots represents the points in which the MIs are evaluated and the dashed lined connect two sequential evaluations.

Chapter 5

Analytic evaluation of the helicity amplitudes for diphoton production in gluon fusion with heavy quark mass dependence

In this chapter we aim to compute the two-loop helicity amplitudes for the production of two photons in gluon fusion with a heavy quark loop. This process is phenomenologically important, and a numerical evaluation of the amplitude has been known for some years [204]. However, in this chapter we want to take a different approach to studying the process, as we want to evaluate the MIs in terms of iterated integrals. The process is complex for several reasons, including the presence of elliptic integrals. In fact, the elliptic sector is the same as that discussed previously in the case of the production of two photons in the quark-annihilation channel. For the evaluation of the integrals we use the method of differential equations, and with the approach discussed in section 2.16 we obtain a ϵ-factorised form for the whole system of MIs. Through the boundary conditions and the system of DEs, it is possible to obtain an expression for the helicity amplitudes in terms of iterated integrals, and we will see that this form is greatly simplified.

5.1 Analytic scattering amplitude for $gg \to \gamma\gamma$

In this chapter, we consider the two-loop helicity amplitudes for diphoton production in gluon fusion with a heavy quark loop. For the construction of Lorentz tensor structures, we follow the construction of Ref. [75]. The tensor structure in fact depends on the polarization vectors and the external momenta, independently of the number of loops. In our case, the amplitude written in terms of Feynman diagrams changes. At the partonic level:

$$g(p_1) + g(p_2) \to \gamma(-p_3) + \gamma(-p_4), \tag{1.1}$$

the minus sign are there because we choose all the particles incoming such that $p_1 + p_2 + p_3 + p_4 = 0$. The kinematics for this process is described by the Mandelstam invariants:

$$s = (p_1 + p_2)^2, \quad t = (p_1 + p_3)^2, \quad u = (p_2 + p_3)^2, \quad \text{with} \quad s + t + u = 0, \tag{1.2}$$

where all the external particles are on-shell, i.e. $p_i^2 = 0$. We indicate with m_t the mass of the heavy-quark running in the loop. The physical region is represented by:

$$s > 0, \quad t < 0, \quad u < 0. \tag{1.3}$$

The bare scattering amplitude can be written as:

$$\mathcal{A}_{gg\gamma\gamma} = (4\pi\alpha_{em})\delta_{ij} A_{\mu\nu\rho\sigma} \epsilon^{\mu}_{\lambda_1} \epsilon^{\nu}_{\lambda_2} \epsilon^{\rho}_{\lambda_3} \epsilon^{\sigma}_{\lambda_4}, \tag{1.4}$$

where δ_{ij} is the Kronecker delta function with i and j the color indices of the incoming gluons, $\epsilon^{\mu}_{\lambda_1}$ and $\epsilon^{\nu}_{\lambda_2}$ are the external gluon polarization vectors and $\epsilon^{\rho}_{\lambda_3}$ and $\epsilon^{\sigma}_{\lambda_4}$ are the external photon polarization vectors. α_{em} is the fine-structure constant, determined by the electric charge $e = \sqrt{4\pi\alpha_{em}}$. At any order in perturbative QCD, the amplitude can be decomposed in terms of a set of Lorentz invariant tensors T_i and scalar form factors F_i as:

$$\mathcal{A}_{gg\gamma\gamma} = \sum_i \mathcal{F}_i T_i \,. \tag{1.5}$$

The tensors are built from the external momenta $\{p_i^{\mu}\}$, the polarization vectors $\{\epsilon^{\mu}_{\lambda_i}\}$ and the metric tensor $g^{\mu\nu}$. Counting the possible combinations we have a total number of 138 tensor structures. Imposing the physical conditions $p_i \cdot \epsilon_{\lambda_i} = 0$, we can remove all the tensors proportional to $p_1^{\mu}, p_2^{\nu}, p_3^{\rho}, p_4^{\sigma}$ and in this way all vanish except 57 tensor structures. By making as specific choice for the reference vectors $q_i = p_{i+1}$ for all the external gauge bosons such that:

$$\epsilon_{\lambda_i} \cdot p_{i+1} = 0, \quad \text{where} \quad i = 1, ..., 4 \quad \text{and} \quad p_5 \equiv p_1, \tag{1.6}$$

which implies for the polarization sums:

$$\sum_{pol} \epsilon^{\mu}_{\lambda_i} \epsilon^{\nu}_{\lambda_i} = -g^{\mu\nu} + \frac{p_i^{\mu} p_{i+1}^{\nu} + p_i^{\nu} p_{i+1}^{\mu}}{p_i \cdot p_{i+1}}. \tag{1.7}$$

With these choices, we are left with 10 independent Lorentz invariant tensors:

$$\begin{aligned}
T_1 &= p_3 \cdot \epsilon_{\lambda_1}(p_1)\, p_1 \cdot \epsilon_{\lambda_2}(p_2)\, p_1 \cdot \epsilon_{\lambda_3}(p_3)\, p_2 \cdot \epsilon_{\lambda_4}(p_4), \\
T_2 &= p_3 \cdot \epsilon_{\lambda_1}(p_1)\, p_1 \cdot \epsilon_{\lambda_2}(p_2)\, \epsilon_{\lambda_3}(p_3) \cdot \epsilon_{\lambda_4}(p_4), \\
T_3 &= p_3 \cdot \epsilon_{\lambda_1}(p_1)\, p_1 \cdot \epsilon_{\lambda_3}(p_3)\, \epsilon_{\lambda_2}(p_2) \cdot \epsilon_{\lambda_4}(p_4), \\
T_4 &= p_3 \cdot \epsilon_{\lambda_1}(p_1)\, p_2 \cdot \epsilon_{\lambda_4}(p_4)\, \epsilon_{\lambda_2}(p_2) \cdot \epsilon_{\lambda_3}(p_3), \\
T_5 &= p_1 \cdot \epsilon_{\lambda_2}(p_2)\, p_1 \cdot \epsilon_{\lambda_3}(p_3)\, \epsilon_{\lambda_1}(p_1) \cdot \epsilon_{\lambda_4}(p_4), \\
T_6 &= p_1 \cdot \epsilon_{\lambda_2}(p_2)\, p_2 \cdot \epsilon_{\lambda_4}(p_4)\, \epsilon_{\lambda_1}(p_1) \cdot \epsilon_{\lambda_3}(p_3), \\
T_7 &= p_1 \cdot \epsilon_{\lambda_3}(p_3)\, p_2 \cdot \epsilon_{\lambda_4}(p_4)\, \epsilon_{\lambda_1}(p_1) \cdot \epsilon_{\lambda_2}(p_2), \\
T_8 &= \epsilon_{\lambda_1}(p_1) \cdot \epsilon_{\lambda_2}(p_2)\, \epsilon_{\lambda_3}(p_3) \cdot \epsilon_{\lambda_4}(p_4), \\
T_9 &= \epsilon_{\lambda_1}(p_1) \cdot \epsilon_{\lambda_4}(p_4)\, \epsilon_{\lambda_2}(p_2) \cdot \epsilon_{\lambda_3}(p_3), \\
T_{10} &= \epsilon_{\lambda_1}(p_1) \cdot \epsilon_{\lambda_3}(p_3)\, \epsilon_{\lambda_2}(p_2) \cdot \epsilon_{\lambda_4}(p_4).
\end{aligned} \tag{1.8}$$

In CDR, these 10 tensor structures are independent. In four-dimensional external states, not all the tensors are independent. We expect to be able to describe the amplitude in terms of 8 independent tensor structures since there are $2^4 = 16$ helicities, but for four external legs these helicities are reduced to 8 by parity. Formally this can be shown studying the rank of the matrix:

$$M_{ij} = \sum_{pol} T_i^{\dagger} T_j \,. \tag{1.9}$$

Specifically, in $d = 4$, the matrix M_{ij} is not full rank and in particular $rank(M_{ij}) = 8$. As explained in section 2.3, in the tHV scheme we separate the four-dimensional tensor structure from the non-physical $-2\,\epsilon$ tensors. We introduce the new tensor basis $\{\overline{T}_i\}$:

$$\begin{aligned}
\overline{T}_i &= T_i, \quad i = 1, ..., 7, \\
\overline{T}_8 &= T_8 + T_9 + T_{10},
\end{aligned} \tag{1.10}$$

such that we can define a new matrix:

$$M_{ij}^{(8\times 8)} = \sum_{pol} \overline{T}_i^{\dagger} \overline{T}_j, \tag{1.11}$$

invertible in $d = 4$ dimensions also if the polarizations sum is still performed in d-dimensions. This allows us to build 8 intermediate projectors:

$$P_i^{(8\times 8)} = \sum_{j=1}^{8} (M_{ij}^{(8\times 8)})^{-1} \overline{T}_j^{\dagger}, \tag{1.12}$$

in order to find the last two orthogonal tensors $\overline{T}_9$ and $\overline{T}_{10}$:

$$\begin{aligned} \overline{T}_9 &= T_9 - \sum_{i=1}^{8} (P_i^{(8\times 8)} T_9) \overline{T}_i, \\ \overline{T}_{10} &= T_{10} - \sum_{i=1}^{8} (P_i^{(8\times 8)} T_{10}) \overline{T}_i, \end{aligned} \tag{1.13}$$

just by removing their projections along the independent tensors, where the projectors satisfies the condition:

$$\sum_{pol} \mathcal{P}_i \overline{T}_j = \delta_{ij}\,. \tag{1.14}$$

The tensors in eq. (1.13), that vanish in $d = 4$ external states, reads:

$$\begin{aligned} \overline{T}_9 &= T_9 - \frac{1}{3}\left(-\frac{2}{su}\overline{T}_1 - \frac{1}{s}\overline{T}_6 - \frac{1}{t}\left(\overline{T}_2 + \overline{T}_3 + 2\overline{T}_4 - 2\overline{T}_5 - \overline{T}_6 - \overline{T}_7\right) + \frac{1}{u}\overline{T}_3 + \overline{T}_8\right), \\ \overline{T}_{10} &= T_{10} - \frac{1}{3}\left(\frac{4}{su}\overline{T}_1 + \frac{2}{s}\overline{T}_6 - \frac{1}{t}\left(\overline{T}_2 - 2\overline{T}_3 - \overline{T}_4 + \overline{T}_5 + 2\overline{T}_6 - \overline{T}_7\right) - \frac{2}{u}\overline{T}_3 + \overline{T}_8\right). \end{aligned} \tag{1.15}$$

It is possible to show that the tensors $\overline{T}_1, ..., \overline{T}_8$ form a complete physical basis, and fixing the helicities in all the possible way the two additional tensors evaluate to zero:

$$\begin{aligned} \overline{T}_{9,\lambda_1,\lambda_2,\lambda_3,\lambda_4} &= 0, \\ \overline{T}_{10,\lambda_1,\lambda_2,\lambda_3,\lambda_4} &= 0, \end{aligned} \tag{1.16}$$

then, we can safely drop them in the computation of the helicity amplitudes. For a given helicity configuration we write:

$$A_{\lambda_1,\lambda_2,\lambda_3,\lambda_4}(s,t,u,m_t^2) = \sum_{i=1}^{8} \overline{\mathcal{F}}_i(s,t,u,m_t^2) \overline{T}_{i,\lambda_1,\lambda_2,\lambda_3,\lambda_4}. \tag{1.17}$$

Helicity amplitudes factorize into an overall spinor phases: $\mathcal{S}_{\lambda_1,\lambda_2,\lambda_3,\lambda_4}$ and the little-group-scalar helicity amplitudes $f_{\lambda_1,\lambda_2,\lambda_3,\lambda_4}$ as:

$$A_{\lambda_1,\lambda_2,\lambda_3,\lambda_4}(s,t,u,m_t^2) = \mathcal{S}_{\lambda_1,\lambda_2,\lambda_3,\lambda_4} f_{\lambda_1,\lambda_2,\lambda_3,\lambda_4}(s,t,u,m_t^2), \tag{1.18}$$

where:

$$\begin{aligned} \mathcal{S}_{++++} &= \frac{[12][34]}{\langle 12\rangle\langle 34\rangle}, \quad \mathcal{S}_{+-++} = \frac{\langle 21\rangle\langle 24\rangle[14]}{\langle 34\rangle\langle 13\rangle\langle 14\rangle}, \\ \mathcal{S}_{++-+} &= \frac{\langle 32\rangle\langle 34\rangle[24]}{\langle 14\rangle\langle 21\rangle\langle 24\rangle}, \quad \mathcal{S}_{+++-} = \frac{\langle 42\rangle\langle 43\rangle[23]}{\langle 13\rangle\langle 21\rangle\langle 23\rangle}, \\ \mathcal{S}_{+--+} &= \frac{\langle 23\rangle[14]}{[23]\langle 14\rangle}, \quad \mathcal{S}_{-+++} = \frac{\langle 12\rangle\langle 14\rangle[24]}{\langle 34\rangle\langle 23\rangle\langle 24\rangle}, \\ \mathcal{S}_{--++} &= \frac{\langle 12\rangle[34]}{[12]\langle 34\rangle}, \quad \mathcal{S}_{-+-+} = \frac{\langle 13\rangle[24]}{[13]\langle 24\rangle}, \end{aligned} \tag{1.19}$$

and

$$
\begin{aligned}
f_{++++} &= \frac{t^2}{4}(\frac{2}{u}\overline{F}_6 - \frac{2}{s}\overline{F}_3 - \overline{F}_1) + (\frac{s}{u} + \frac{u}{s} + 4)\overline{F}_8 + \frac{t}{2}(\overline{F}_2 - \overline{F}_4 + \overline{F}_5 - \overline{F}_7), \\
f_{+-++} &= -\frac{t^2}{4}(\frac{2}{u}\overline{F}_6 - \overline{F}_1) + \frac{t}{u}\overline{F}_8 - \frac{t}{2}(\overline{F}_2 + \overline{F}_3 + \overline{F}_5), \\
f_{++-+} &= \frac{2t^2}{4s}\overline{F}_3 + \frac{t^2}{4}\overline{F}_1 + \frac{t}{s}\overline{F}_8 + \frac{t}{2}(\overline{F}_6 + \overline{F}_7 - \overline{F}_5), \\
f_{+++-} &= -\frac{2t^2}{4u}\overline{F}_6 - \frac{t^2}{4}\overline{F}_1 + \frac{t}{u}\overline{F}_8 + \frac{t}{2}(\overline{F}_4 + \overline{F}_7 - \overline{F}_3), \\
f_{+--+} &= -\frac{t^2}{4}\overline{F}_1 + \frac{t}{2}(\overline{F}_3 - \overline{F}_4 + \overline{F}_5 - \overline{F}_6) + 2\overline{F}_8, \\
f_{-+++} &= \frac{2t^2}{4s}\overline{F}_3 + \frac{t^2}{4}\overline{F}_1 + \frac{t}{s}\overline{F}_8 + \frac{t}{2}(\overline{F}_4 + \overline{F}_6 - \overline{F}_2), \\
f_{--++} &= -\frac{t^2}{4}\overline{F}_1 + \frac{t}{2}(\overline{F}_2 + \overline{F}_3 - \overline{F}_6 - \overline{F}_7) + 2\overline{F}_8, \\
f_{-+-+} &= \frac{t^2}{su}\overline{F}_8 - \frac{t^2}{2s}\overline{F}_3 + \frac{t^2}{2u}\overline{F}_6 - \frac{t^2}{4}\overline{F}_1.
\end{aligned}
\tag{1.20}
$$

The helicity amplitudes are written for 8 helicity states, while the remaining ones can be obtained by parity invariance:

$$
A_{\lambda_1,\lambda_2,\lambda_3,\lambda_4} = A_{-\lambda_1,-\lambda_2,-\lambda_3,-\lambda_4}(\langle ij\rangle \leftrightarrow [ji]). \tag{1.21}
$$

5.1.1 Scalar integral families and MIs computation

In this section we describe the scalar integral families which define the scalar Feynman integrals that appear in the helicity amplitudes. Consequently, we provide the set of MIs obtained from the reduction of the full set of integrals. For the two-loop massive corrections to $gg \to \gamma\gamma$, we three planar integral topologies, PLA, PLB and PLC, and two non-planar ones, NPA and NPB, each with nine scalar products. The scalar integral families which describe the relavant MIs for this process are defined as:

$$
\mathcal{I}_{topo}(a_1, ..., a_9) = \int \frac{\mathcal{D}k_1 \mathcal{D}k_2}{D_1^{a_1} D_2^{a_2} D_3^{a_3} D_4^{a_4} D_5^{a_5} D_6^{a_6} D_7^{a_7} D_8^{a_8} D_9^{a_9}}, \tag{1.22}
$$

where $topo \in \{\mathrm{PLA}, \mathrm{PLB}, \mathrm{PLC}, \mathrm{NPA}, \mathrm{NPB}\}$ labels the families and $D_1, ..., D_9$ are the scalar products, according to eq. (5.13). We have two ISPs, then the indices $a_1, ..., a_7$ are non-negative while the indices a_8 and a_9 are non-positive. The integration measure is:

$$
\mathcal{D}k = \frac{\mathrm{d}^D\, k}{i\pi^{2-\epsilon}\Gamma(1+\epsilon)} \left(\frac{\mu^2}{m_t^2}\right)^2, \tag{1.23}
$$

being μ the dimensional regularization scale. Within this framework, the topologies (modulo permutations of the external legs) are defined by the following set of scalar products:

PLA

$$
\begin{aligned}
&D_1 = k_1^2, \quad D_2 = k_2^2 - m_t^2, \quad D_3 = (k_1 - k_2)^2 - m_t^2, \quad D_4 = (k_1 - p_1)^2, \\
&D_5 = (k_2 - p_1)^2, \quad D_6 = (k_1 - p_1 - p_2)^2, \quad D_7 = (k_2 - p_1 - p_2)^2 - m_t^2, \\
&D_8 = (k_1 - p_1 - p_2 - p_3)^2, \quad D_9 = (k_2 - p_1 - p_2 - p_3)^2 - m_t^2,
\end{aligned}
\tag{1.24}
$$

PLB

$$\begin{aligned} &D_1 = k_1^2, \quad D_2 = k_2^2 - m_t^2, \quad D_3 = (k_1 - k_2)^2 - m_t^2, \quad D_4 = (k_1 - p_1)^2, \\ &D_5 = (k_2 - p_1)^2 - m_t^2, \quad D_6 = (k_1 - p_1 - p_2)^2, \quad D_7 = (k_2 - p_1 - p_2)^2 - m_t^2, \\ &D_8 = (k_1 - p_1 - p_2 - p_3)^2, \quad D_9 = (k_2 - p_1 - p_2 - p_3)^2 - m_t^2, \end{aligned} \tag{1.25}$$

PLC

$$\begin{aligned} &D_1 = k_1^2 - m_t^2, \quad D_2 = k_2^2 - m_t^2, \quad D_3 = (k_1 - k_2)^2, \quad D_4 = (k_1 - p_1)^2 - m_t^2, \\ &D_5 = (k_2 - p_1)^2 - m_t^2, \quad D_6 = (k_1 - p_1 - p_2)^2 - m_t^2, \quad D_7 = (k_2 - p_1 - p_2)^2 - m_t^2, \\ &D_8 = (k_1 - p_1 - p_2 - p_3)^2 - m_t^2, \quad D_9 = (k_2 - p_1 - p_2 - p_3)^2 - m_t^2, \end{aligned} \tag{1.26}$$

NPA

$$\begin{aligned} &D_1 = k_1^2, \quad D_2 = k_2^2 - m_t^2, \quad D_3 = (k_1 - k_2)^2 - m_t^2, \quad D_4 = (k_1 - p_1)^2, \\ &D_5 = (k_2 - p_1)^2, \quad D_6 = (k_1 - p_1 - p_2)^2, \quad D_7 = (k_1 - k_2 + p_3)^2 - m_t^2, \\ &D_8 = (k_2 - p_1 - p_2 - p_3)^2 - m_t^2, \quad D_9 = (k_1 - k_2 - p_1 - p_2)^2, \end{aligned} \tag{1.27}$$

NPB

$$\begin{aligned} &D_1 = k_1^2 - m_t^2, \quad D_2 = k_2^2, \quad D_3 = (k_1 - k_2)^2 - m_t^2, \quad D_4 = (k_1 - p_1)^2 - m_t^2, \\ &D_5 = (k_2 - p_1)^2, \quad D_6 = (k_1 - p_1 - p_2)^2 - m_t^2, \quad D_7 = (k_1 - k_2 + p_3)^2 - m_t^2, \\ &D_8 = (k_2 - p_1 - p_2 - p_3)^2, \quad D_9 = (k_1 - k_2 - p_1 - p_2)^2. \end{aligned} \tag{1.28}$$

The representative diagrams to these different topologies are shown in Fig. 5.1.1.

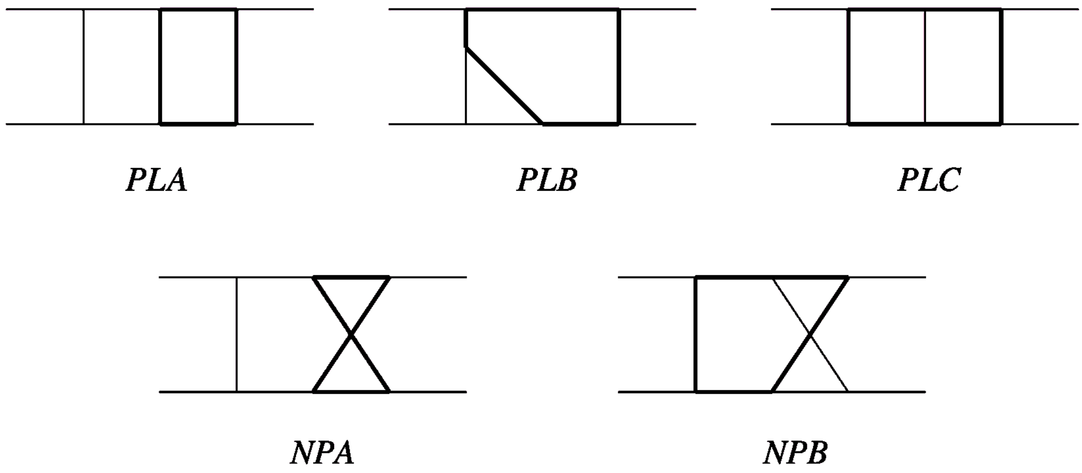

Figure 5.1.1. Representative set of two-loop diagrams with internal heavy-quark loops associated to the relevant scalar integral families.

Feynman diagrams were generated using QGRAF [207] and as a result, we obtained 166 diagrams. The Feynman integrals associated to them were grouped into the topologies described in eqs. (1.24-1.28), along with the respective crossings obtained by the following exchanges of external legs:

$$
\begin{aligned}
&\mathrm{PLA}_{\sigma_{12}} = \mathrm{PLA}\Big|_{p_1\to p_2,\, p_2\to p_1} && \mathrm{NPB}_{\sigma_{124}} = \mathrm{NPB}\Big|_{p_1\to p_2,\, p_2\to p_4,\, p_4\to p_1}\\
&\mathrm{PLB}_{\sigma_{12}} = \mathrm{PLB}\Big|_{p_1\to p_2,\, p_2\to p_1} && \mathrm{NPB}_{\sigma_{142}} = \mathrm{NPB}\Big|_{p_1\to p_4,\, p_4\to p_2,\, p_2\to p_1}\\
&\mathrm{PLB}_{\sigma_{123}} = \mathrm{PLB}\Big|_{p_1\to p_2,\, p_2\to p_3,\, p_3\to p_1} && \mathrm{NPB}_{\sigma_{1234}} = \mathrm{NPB}\Big|_{p_1\to p_2,\, p_2\to p_3,\, p_3\to p_4,\, p_4\to p_1}\\
&\mathrm{PLC}_{\sigma_{12}} = \mathrm{PLC}\Big|_{p_1\to p_2,\, p_2\to p_1} && \mathrm{NPB}_{\sigma_{1342}} = \mathrm{NPB}\Big|_{p_1\to p_3,\, p_3\to p_4,\, p_4\to p_2,\, p_2\to p_1}\\
&\mathrm{PLC}_{\sigma_{123}} = \mathrm{PLC}\Big|_{p_1\to p_2,\, p_2\to p_3,\, p_3\to p_1} && \mathrm{NPB}_{\sigma_{13}\sigma_{24}} = \mathrm{NPB}\Big|_{p_1\to p_3,\, p_3\to p_1,\, p_2\to p_4,\, p_4\to p_2}\\
&\mathrm{NPB}_{\sigma_{14}\sigma_{23}} = \mathrm{NPB}\Big|_{p_1\to p_4,\, p_4\to p_1,\, p_2\to p_3,\, p_3\to p_2}
\end{aligned}
\tag{1.29}
$$

Given the eight tensor structures described previously, we computed the two-loop form factors in terms of 32936 scalar integrals. After implementing relations between the integrals, due to symmetry, through the reductions performed with Reduze [92, 93] and Kira [88, 89], the set of integrals has been reduced to a total of 161 MIs, including the crossings, provided in Appendix E.

The MIs are described by the following topologies: PLA, PLB, PLC, NPA, NPB, $\mathrm{PLA}_{\sigma_{12}}$, $\mathrm{PLA}_{\sigma_{123}}$, $\mathrm{PLA}_{\sigma_{1234}}$, $\mathrm{PLA}_{\sigma_{124}}$, $\mathrm{PLA}_{\sigma_{1243}}$, $\mathrm{PLC}_{\sigma_{12}}$, $\mathrm{PLC}_{\sigma_{123}}$, $\mathrm{NPA}_{\sigma_{123}}$, $\mathrm{NPA}_{\sigma_{124}}$, $\mathrm{NPB}_{\sigma_{123}}$,

$\mathrm{NPB}_{\sigma_{124}}$, where we introduced the following new crossings:

$$
\begin{aligned}
&\mathrm{PLA}_{\sigma_{123}} = \mathrm{PLA}\Big|_{p_1\to p_2,\, p_2\to p_3,\, p_3\to p_1} && \mathrm{NPA}_{\sigma_{123}} = \mathrm{NPA}\Big|_{p_1\to p_2,\, p_2\to p_3,\, p_3\to p_1}\\
&\mathrm{PLA}_{\sigma_{1234}} = \mathrm{PLA}\Big|_{p_1\to p_2,\, p_2\to p_3,\, p_3\to p_4,\, p_4\to p_1} && \mathrm{NPA}_{\sigma_{124}} = \mathrm{NPA}\Big|_{p_1\to p_2,\, p_2\to p_4,\, p_4\to p_1}\\
&\mathrm{PLA}_{\sigma_{124}} = \mathrm{PLA}\Big|_{p_1\to p_2,\, p_2\to p_4,\, p_4\to p_1} && \mathrm{NPB}_{\sigma_{123}} = \mathrm{NPB}\Big|_{p_1\to p_2,\, p_2\to p_3,\, p_3\to p_1}\\
&\mathrm{PLA}_{\sigma_{1243}} = \mathrm{PLA}\Big|_{p_1\to p_2,\, p_2\to p_4,\, p_4\to p_3,\, p_3\to p_1}\,. &&
\end{aligned}
\tag{1.30}
$$

It's important to note that the PLB family does not contribute to the amplitude, since we were able to map each integral of this family into the others through their crossings.

5.2 DEs and evaluation in terms of iterated integrals

In this section we discuss how to evaluate the MIs using the DEs method. The system of DEs for all MIs has been put into ϵ-factorised form, using the procedure described in section 2.16. This is an original result in itself, since we previously evaluated the elliptic sector semi-analytically, and in the literature there is a solution on the maximal cut (so only for the homogeneous part) [218]. Once the ϵ-factorised form is obtained, we obtain a solution in terms of iterated integrals for the kernels appearing in the DEs.
The difficulty in bringing the system into a ϵ-factorised form arises from the presence of elliptic integrals. Here the elliptic sector is the same as that defined for diphoton production in the quark-annihilation channel, described in section 4.4.3. In the notation used in this chapter, the MIs of this elliptic sector are part of the NPA topology:

$$
\begin{aligned}
&I_{\mathrm{NPA}}(1,1,1,1,0,1,1,1,-1), \quad && I_{\mathrm{NPA}}(1,2,1,1,0,1,1,1,-1),\\
&I_{\mathrm{NPA}}(1,1,1,1,0,1,1,1,-2), \quad && I_{\mathrm{NPA}}(1,1,1,1,0,1,1,1,0)\,.
\end{aligned}
\tag{2.1}
$$

The maximal cut in Baikov representation for the top-sector gives:

$$
\mathrm{MC}\left(I_{\mathrm{NPA}}(1,1,1,1,0,1,1,1,a)\right) \propto \frac{1}{s}\int dz_9 \frac{z_9^{-a}}{(m_t^2 - t - z_9)\sqrt{P_4(z_9)}}, \tag{2.2}
$$

where $P_4(z_9)$ is the fourth-degree polynomial that define the elliptic curve:

$$
P_4(z_9) = (m_t^2 - z_9)(s + m_t^2 - z_9)(m_t^2(m_t^2 - 3s) - (2m_t^2 + s)z_9 + z_9^2). \tag{2.3}
$$

As explained in section 2.16, the first step in obtaining a ϵ-factorised form is to choose the basis of the MIs to rotate. The choice for the first two MIs is the same as for the elliptic triangle, i.e. we choose an Abel differential of the first kind and then its derivative with respect to m_t^2:

$$
\begin{aligned}
&\mathcal{J}_1 = s\,\epsilon^4 \left(\left(m_t^2 - t\right) I_{\mathrm{NPA}}(1,1,1,1,0,1,1,1,0) - I_{\mathrm{NPA}}(1,1,1,1,0,1,1,1,-1)\right),\\
&\mathcal{J}_2 = \partial_{m_t^2}\mathcal{J}_1.
\end{aligned}
\tag{2.4}
$$

The remaining integrals of the sector correspond to Abel differentials of the third kind, i.e. meromorphic functions with non-vanishing residues. If we calculate the residue at infinity:

$$
\mathrm{Res}_{z_9}\left(\mathrm{MC}\left(I_{\mathrm{NPA}}(1,1,1,1,0,1,1,1,-2)\right)\right) \propto \frac{1}{s}\oint_{z_9=\infty} dz_9 \frac{z_9^2}{(m_t^2 - t - z_9)\sqrt{P_4(z_9)}}, \tag{2.5}
$$

and the second residue at the finite point $m_t^2 - t$:

$$\mathrm{Res}_{z_9}\left(\mathrm{MC}\left(I_{\mathrm{NPA}}(1,1,1,1,0,1,1,1,0)\right)\right) \propto \frac{1}{s}\oint_{z_9=m_t^2-t} dz_9 \frac{1}{(m_t^2 - t - z_9)\sqrt{P_4(z_9)}}, \tag{2.6}$$

we can choose as third and fourth integrals in the basis:

$$\begin{aligned}\mathcal{J}_3 &= -s\,\epsilon^4\left(\left(m_t^2 - t\right) I_{\mathrm{NPA}}(1,1,1,1,0,1,1,1,-1) - I_{\mathrm{NPA}}(1,1,1,1,0,1,1,1,-2)\right),\\ \mathcal{J}_4 &= s\sqrt{t\,(s + t)\,(-4\,m_t^2\,s + s\,t + t^2)}\,\epsilon^4\, I_{\mathrm{NPA}}(1,1,1,1,0,1,1,1,0)\,.\end{aligned} \tag{2.7}$$

Performing the rotation as explained in section 2.16, we obtain the ϵ-factorised form for this elliptic sector by introducing new transcendental functions coming from the Wronskian matrix. The situation is slightly different from the elliptic-triangle case, since here we have the two periods of the elliptic curve:

$$\begin{aligned}\varpi_0(s,\,m_t^2) &= \frac{1}{\sqrt{s\sqrt{s\,(16m_t^2 + s)}}}\,\mathrm{K}\left(\frac{-8m_t^2 - s + \sqrt{s\,(16m_t^2 + s)}}{2\sqrt{s\,(16m_t^2 + s)}}\right),\\ \varpi_1(s,\,m_t^2) &= \frac{1}{\sqrt{s\sqrt{s\,(16m_t^2 + s)}}}\,\mathrm{K}\left(1 - \frac{-8m_t^2 - s + \sqrt{s\,(16m_t^2 + s)}}{2\sqrt{s\,(16m_t^2 + s)}}\right),\end{aligned} \tag{2.8}$$

but also a new transcendental function corresponding to the homogeneous solution of the DEs for the integrals with kernels that are Abel differentials of the third kind:

$$\begin{aligned}G(s,\,t,\,m_t^2) &= \frac{\sqrt{s\,(s+16m_t^2)}\sqrt{t\,(s + t)\,(-4\,m_t^2\,s + s\,t + t^2)}}{(t(s+t) - 4sm_t^2)\,s\sqrt{s\left(s + 8m_t^2 + \sqrt{s\,(s+16m_t^2)}\right)}}\\ &\times\left(K\left(\frac{\left(\sqrt{s} - \sqrt{s+16m_t^2}\right)^2}{\left(\sqrt{s} + \sqrt{s+16m_t^2}\right)^2}\right)\right.\\ &\left.- 2\,\Pi\left(\frac{8sm_t^2 - (s - \sqrt{s(s+16m_t^2)})t}{8m_t^2 s - (s + \sqrt{s(s+16m_t^2)})t},\,\frac{\left(\sqrt{s} - \sqrt{s+16m_t^2}\right)^2}{\left(\sqrt{s} + \sqrt{s+16m_t^2}\right)^2}\right)\right).\end{aligned} \tag{2.9}$$

$G(s,t,m_t^2)$ and $\varpi_0(s,m_t^2)$ are related by the following set of DEs:

$$\begin{aligned}\partial_s\, G(s,t,m_t^2) \;&= \frac{m_t^2\,(16m_t^2\,s - t(3s + 2t))\,r_9}{(s + t)(t(s + t) - 4m_t^2\,s)^2}\,\varpi_0(s,m_t^2)\\ &\quad - \frac{m_t^2(16m_t^2 + s)\,r_9}{2(s + t)(t(s + t) - 4m_t^2\,s)}\partial_{m_t^2}\,\varpi_0(s,m_t^2),\\ \partial_t\, G(s,t,m_t^2) \;&= -\frac{m_t^2\,s^2(16m_t^2 + s)\,r_9}{t(s + t)(t(s + t) - 4m_t^2)^2}\varpi_0(s,t,m_t^2)\\ &\quad + \frac{m_t^2\,s(s + 16m_t^2)\,r_9}{2s(s + t)(t\,(s + t) - 4m_t^2\,s)}\partial_{m_t^2}\,\varpi_0(s,m_t^2),\\ \partial_{m_t^2} G(s,t,m_t^2) \;&= \frac{s(s + 2t)\,r_9}{(t(s + t) - 4m_t^2\,s)^2}\varpi_0(s,m_t^2)\,.\end{aligned} \tag{2.10}$$

r_9 in eq. (2.10) is one of the square roots of the kinematic invariants and mass appearing in the full system of DEs. We define the set $r_1, \cdots, r_{16}$ by:

$$
\begin{aligned}
&r_1 = \sqrt{s(s-4m_t^2)}, \quad r_2 = \sqrt{t(t-4m_t^2)}, \quad r_3 = \sqrt{(s+t)(4m_t^2+s+t)},\\
&r_4 = \sqrt{s(s+4m_t^2)}, \quad r_5 = \sqrt{t+t(4m_t^2)}, \quad r_6 = \sqrt{(s+t)(s+t-4m_t^2)},\\
&r_7 = \sqrt{st(st-4m_t^2(s+t))}, \quad r_8 = \sqrt{s(s+t)(s(s+t)-4m_t^2 t)},\\
&r_9 = \sqrt{t(s+t)(t(s+t)-4m_t^2 s)}, \quad r_{10} = \sqrt{s(-4m_t^2(s+t)^2+s(m_t^2+s+t)^2)},\\
&r_{11} = \sqrt{s(-4m_t^2t^2+s(-m_t^2+t)^2)}, \quad r_{12} = \sqrt{(s+t)(4m_t^2t^2+(-m_t^2+t)^2(s+t))},\\
&r_{13} = \sqrt{t(-4m_t^2s^2+(-m_t^2+s)^2t)}, \quad r_{14} = \sqrt{(s+t)(4m_t^2s^2+(-m_t^2+s)^2(s+t))},\\
&r_{15} = \sqrt{t(-4m_t^2(s+t)^2+t(m_t^2+s+t)^2)}, \quad r_{16} = \sqrt{-(m_t^2st(s+t))}\,.
\end{aligned}
\tag{2.11}
$$

5.2.1 Alphabet for the system of DEs

Previously we saw how the system of DEs was transformed into a ϵ-factorised form using the procedure described in section 2.16. We have seen how this introduces a new transcendental function $G(s,t,m_t^2)$ in addition to the period $\varpi_o(s,m_t^2)$. By analysing the resulting system of DEs, we can divide the alphabet into four sets of letters, depending on the type of functions they contain. All the letters are defined in the appendix. F.

Rational letters:

We define $\mathbf{W}_R$ as the set of rational letters:

$$\mathbf{W}_R = \{R_i\}_{i=1,\cdots,11}, \tag{2.12}$$

which depends on the set of kinematic invariants defined in eq. (1.2) and on the square roots defined in eq. (2.11).

Algebraic letters:

$$\mathbf{W}_A = \{A_i\}_{i=1,\cdots,45}, \tag{2.13}$$

where each letter depends on the square roots and on algebraic functions of the kinematic invariants.

Modular letters:

Previously we discussed how the periods are introduced and how they relate to the underlying elliptic curve of Feynman integrals whose analytic structure involves eMPLs. In this case it is not possible to write the letters of the DEs only in terms of rational or algebraic functions. The modular letters encode the dependencies of the periods and these are related to modular transformations [219] of the form obtained in eq. (14.28). We define the modular letters M_i thorough the differential relations:

$$dM_i = M_i^s\, ds + M_i^t\, dt + M_i^{m_t^2}\, dm_t^2. \tag{2.14}$$

Elliptic letters:

The elliptic letters are characterised by the presence of the transcendental function $G(s, t, m_t^2)$. The latter can be written, as shown in eq. (2.9), in terms of elliptic integrals of the first and third kind. The presence of the elliptic integral of the third kind ruins the modular invariance due to the presence of an extra parameter in its definition. We provide the entries of the connection matrix corresponding to the derivative with respect to s, t and m_t^2. The notation for the elliptic kernels is:

$$\mathrm{d}E_i = E_i^s\,\mathrm{d}s + E_i^t\,\mathrm{d}t + E_i^{m_t^2}\,dm_t^2. \tag{2.15}$$

5.2.2 Boundary conditions

Boundary conditions are evaluated in $\{s, t\} = \{0, 0\}$:

$$\underline{f}_0(\epsilon) = \{f_{0,1},\, f_{0,2},\, \underline{0}_i\}\,, \tag{2.16}$$

where we represent all the null MIs, at the point where we evaluate the boundaries, with a generic zero vector $\underline{0}_i$ with $i = 3, \cdots, 161$. The non-zero components of the boundary vector in eq. (2.16) are:

$$\begin{aligned} f_{0,1} &= m_t^{-4\,\epsilon}, \\ f_{0,2} &= -\frac{\Gamma(1-\epsilon)^2}{m_t^{2\,\epsilon}\,(-s)^{\epsilon}\,\Gamma(1-2\,\epsilon)}. \end{aligned} \tag{2.17}$$

5.2.3 Iterated integrals

Given the DEs in ϵ-factorised form, a formal solution in terms of iterated integrals can be found as explained in eq. (10.3). In particular, we can compute iterated integrals up to weight four by expanding the solution in ϵ as in eq. (10.9). From the matrix of differential equations we have each one-form corresponding to one of the integration kernels described in section 5.2. Special attention must be paid to the boundary conditions, since they diverge in the limit $s \to 0$, as we can see from equation (2.17). Therefore, we have to write a symbolic vector of the boundary conditions and then adjust it at the point where we want to take them into account.
If we represent with $\mathrm{II}(x)$ the iterated integrals of weight 1, we can obtain the iterated integrals up to weight 4:

- **Weight 1:**

$$x \in \{A_\alpha \in \mathbf{W}_A,\, R_\beta \in \mathbf{W}_R, E_\gamma^s,\, E_\gamma^t,\, E_\gamma^m,\, M_\delta\} \qquad x \longrightarrow \mathrm{II}(x), \tag{2.18}$$

- **Weight 2:**

$$\mathrm{II}(x)\,\mathrm{II}(y) = \mathrm{II}(y, x), \tag{2.19}$$

- **Weight 3:**

$$\mathrm{II}(x)\,\mathrm{II}(y)\,\mathrm{II}(z) = II(z, y, z), \tag{2.20}$$

- **Weight 4:**

$$\mathrm{II}(x)\,\mathrm{II}(y)\,\mathrm{II}(z)\,\mathrm{II}(l) = \mathrm{II}(l, z, y, x), \tag{2.21}$$

where the integration order in $\mathrm{II}(a, b, c, d)$ starts from d and proceeds towards a. Just as in the case of MPLs, we have to regularise the iterated integrals, because among the integration kernels we have $d\log(\omega_i)$, and as we can see from the set of rational letters in Appendix F we could have s and t which may be zero.

5.2.4 UV renormalisation

Once the MIs are expressed in terms of iterated integrals, we can rewrite the amplitude in terms of the latter. In particular, the spinor-free helicity amplitudes $f_{\underline{\lambda}}$, for the different combinations of $\underline{\lambda} = (\lambda_1,\, \lambda_2,\, \lambda_3,\, \lambda_4)$ described in eq. (1.20), can be expanded in terms of the bare coupling constant α_s^B:

$$f_{\underline{\lambda}} = \sum_{l=1}^{2} \left(\frac{\alpha_s^B}{2\,\pi}\right)^l f_{\underline{\lambda}}^{(l)}. \tag{2.22}$$

As explained in section 4.3, we perform the UV renormalisation in a mixed renormalisation scheme. We adopt the renormalisation as described in Ref. [138], adapting the treatment to the process $gg \to \gamma\gamma$. The bare strong coupling α_s^B is renormalised so that the mass quark contribution is treated in $\overline{MS}$, the top quark contribution is renormalised at zero momentum. This implies:

$$\alpha_s^B\, \mu_0^{2\epsilon} \;=\; \alpha_s\, \mu_R^{2\epsilon}\, S_\epsilon^{-1} \left(1 \,-\, \left(\frac{\alpha_s}{2\,\pi}\right) \frac{1}{\epsilon}\, (\beta_0 \,+\, \delta_\omega) \,+\, \mathcal{O}(\alpha_s^2)\right), \tag{2.23}$$

where α_s is the renormalised strong coupling, $S_\epsilon = e^{\epsilon\,(log(4\,\pi)\,-\,\gamma_E)}$ is the phase space volume factor, $\beta_0 = \frac{11}{6} C_A - \frac{2}{3} T_R\, N_l$ is the general form of the first coefficient of the QCD β function, the $SU(3)$ Casimir C_A correspond to the number of colours N_c, T_R fixes the traces of the Gell-Mann matrices and N_l is the number of massless flavours. We define $\delta_\omega = -\frac{2}{3}\, T_R \left(\frac{m_t^2}{\mu_R^2}\right)^{-\epsilon}$ so that in eq. (2.23) the massless contribution contained in β_0 is instead separated from the heavy quark contribution placed in δ_ω.

The top quark mass is renormalised on the shell, replacing the bare mass with the physical mass:

$$m_t \to Z_m\, m_t, \qquad Z_m \;=\; 1 \,+\, \left(\frac{\alpha_s}{2\,\pi}\right) \delta Z_m^{(1)} \,+\, \mathcal{O}(\alpha_s^2)\,, \tag{2.24}$$

where:

$$\delta Z_m^{(1)} = C_F \left(\frac{m_t^2}{\mu_R^2}\right)^{-\epsilon} \left(-\frac{3}{2\epsilon} \,-\, 2 \,+\, \mathcal{O}(\epsilon)\right), \tag{2.25}$$

where C_F is the Casimir of the fundamental representation of $SU(3)$ and ϵ is the dimensional regulator introduced in DR. The mass renormalisation acts on the one-loop in the following way:

$$f_{\underline{\lambda}}^{(1)}(m_t \to Z_m\, m_t) = f_{\underline{\lambda}}^{(1)}(m_t) \,+\, \frac{\partial f_{\underline{\lambda}}^{(1)}}{\partial m_t}\, \delta Z_m \left(\frac{\alpha_s}{2\,\pi}\right) \,+\, \mathcal{O}(\alpha_s^2). \tag{2.26}$$

We do not need to renormalise the photons, since the correction is of higher order in α_{em}.

Once the strong coupling and the top quark mass are renormalised, we proceed by multiplying each spinor-free helicity amplification by the gluon field renormalisation (for each external gluon). For a single gluon, if we denote the bare gluon field by $A_\mu^{a\,B}$, then

$$A_\mu^{a\,B} = \sqrt{Z_g} A_\mu^a, \tag{2.27}$$

where:

$$Z_g = \left(1 + \left(\frac{\alpha_s}{2\pi}\right)\frac{\delta_\omega}{\epsilon} + \mathcal{O}(\alpha_s^2)\right). \tag{2.28}$$

In this renormalisation scheme we are able to remove the UV poles. However, there are still poles in ϵ of IR nature, indicating soft and/or collinear divergences.

5.2.5 IR subtraction

Catani [150] showed that for a generic two-loop amplitude in QCD there exists a factorisation formula similar to the one-loop case, where the infrared poles can be subtracted using the one-loop and tree-level amplitudes. In the one-loop case, the amplitude has both double and single poles with universal coefficients. For the $gg \to \gamma\gamma$ process, the leading order (LO) is the one-loop, because the production of two photons in gluon fusion requires a quark loop to mediate the interaction, so the two-loop case simply reduces to the one-loop case. Therefore we can subtract the $\frac{1}{\epsilon}$ and $\frac{1}{\epsilon^2}$ poles using the Catani operator $I^{(1)}$:

$$\begin{aligned} f_{\underline{\lambda}}^{(1)\,fin} &= f_{\underline{\lambda}}^{(1)}, \\ f_{\underline{\lambda}}^{(2)\,fin} &= f_{\underline{\lambda}}^{(2)} - I^{(1)}\, f_{\underline{\lambda}}^{(1)}, \end{aligned} \tag{2.29}$$

where the suffix $'fin'$ indicates the finite remainder without poles. The operator $I^{(1)}$ in eq. (2.29) is defined as:

$$I^{(1)} = -\frac{e^{\epsilon\gamma_E}}{\Gamma(1-\epsilon)}\left(\frac{C_A}{\epsilon^2} + \frac{\beta_0}{\epsilon}\right)\left(-\frac{s}{\mu_R}\right)^{-\epsilon}. \tag{2.30}$$

It is important to emphasise that, because of the universality of the pole coefficients, we know that in this case there cannot be $\frac{1}{\epsilon^3}$ and $\frac{1}{\epsilon^4}$ poles. However, when calculating such complex amplitudes, it often happens that there are no explicit cancellations of the poles and one has to proceed numerically. Despite the length of the two-loop helicity amplitudes obtained by expressing the MIs in terms of iterated integrals, there are explicit cancellations at the amplitude level and no unexpected poles of the operator $I^{(1)}$.

5.3 Helicity amplitudes in terms of iterated integrals

In the previous section of this chapter we discussed the structure of the two-loop helicity amplitudes for the massive two-loop corrections for $gg \to \gamma\gamma$. Once the expression for the canonical MIs has been obtained in terms of iterated integrals, we can express the amplitude in terms of the latter and proceed with renormalisation to obtain the finite remainder. Writing the amplitude in terms of iterated integrals has several advantages. First of all, as discussed earlier, there are no $\frac{1}{\epsilon^3}$ and $\frac{1}{\epsilon^4}$ poles or poles associated with elliptic integrals as we expect, but this may not remain simplified by a generic formula for the amplitude in terms of MIs.
Here we want to discuss the simplifications at the integrand and amplitude level that result from rewriting the finite remainder in terms of iterated integrals.
In the appendix E we provide the list of MIs for the process and in the appendix F the set of letters that go into the DEs for the canonical MIs. In particular, from the DEs of the 161 MIs we have 73 integration kernels and among them 17 are elliptic, i.e. related to the periods and the transcendental function defined in eq.(2.8) and eq. (2.9) respectively. Using integration kernels, we are able to express the finite remainder in terms of iterated integrals up to weight 4. Specifically, we have 5 of weight 1, 32 of weight 2, 291 of weight

3, and 1832 of weight 4, for a total of 2160 iterated integrals contributing to the helicity amplitudes. Of the 73 integration kernels, only 65 contribute to the finite remainder of the helicity amplitudes. We group them into the letter set $\mathbf{W}_{fin}$:

$$\begin{aligned}\mathbf{W}_{fin} = \{&A_1,\, A_2,\, A_3,\, A_4,\, A_5, A_6,\, A_7,\, A_8,\, A_9,\, A_{10},\, A_{11},\, A_{12},\, A_{13},\, A_{14},\, A_{15},\, A_{16},\\ &A_{17},\, A_{18},\, A_{19},\, A_{20},\, A_{21},\, A_{22},\, A_{23},\, A_{24},\, A_{25},\, A_{26},\, A_{27},\, A_{28},\, A_{29},\, A_{30},\, A_{31},\\ &A_{32},\, A_{33},\, A_{34},\, A_{35},\, A_{36},\, A_{37},\, A_{38},\, A_{39},\, A_{40},\, A_{41},\, A_{42},\, A_{43},\, A_{44},\, A_{45},\, E_1,\, E_2,\\ &E_3,\, E_5,\, E_7,\, E_8,\, E_9,\, E_{10},\, M_1,\, M_2,\, M_3, R_1,\, R_2,\, R_3,\, R_4,\, R_6,\, R_7,\, R_8,\, R_9,\, R_{10}\}.\end{aligned} \tag{3.1}$$

From eq. (3.1) we can see that not all elliptic functions contribute explicitly. In particular, we go from 17 integration kernels related to the period and the transcendental function $G(s,t,m_t^2)$, introduced to rotate the system into a ϵ-factorised form, to a total of 11 elliptic kernels appearing in the finite part of the amplitude. In $\mathbf{W}_{fin}$ we have indicated the elliptic and modular letters that appear as E_i and M_i, generally representing the letters obtained from the DEs with respect to the different scales of the process. In Table 5.3.1 we briefly summarise the simplifications obtained at the integrand and amplitude levels.

Canonical DEs	**Helicity amplitudes in terms of iterated integrals**
161 MIs	2160 iterated integrals up to weight 4
73 integration kernels	65 integration kernels
17 elliptic kernels	11 elliptic kernels

Table 5.3.1. Simplifications at the integrand and amplitude levels for the finite remainder of the helicity amplitudes, rewritten in terms of iterated integrals.

Chapter 6

Diphoton production at the LHC

In this chapter we present the application of our original results to perform precise calculations for LHC phenomenology. We will use our massive hard virtual coefficient $H_q^{\gamma\gamma(2)}$ defined in eqs. (4.17), (3.11) and explained in Chapter 4 and in sections 4.3.1 and 3.4. As we anticipated in Chapter 3, the hard-virtual factor is a necessary ingredient of the q_T subtraction/resummation formalism at the NNLO. Here we will show the impact of the novel massive corrections over the very well known massless predictions at the NNLO in perturbative QCD [164, 183, 184, 220]. These original results were published in Ref. [1].

Diphoton production at high-energy hadron colliders is a very relevant process both in the context of Standard Model (SM) studies and in the search for new physics signals. Experimentally, a photon pair is a very clean final state, and photon energies and momenta can be measured with high precision in modern electromagnetic calorimeters. Since photons do not interact strongly with other final state particles, prompt photons are ideal probes to test the properties of the SM and the corresponding theoretical predictions[1].

In high-energy collisions, final-state prompt photons with high transverse momentum can be produced by direct production from hard scattering sub-processes and by fragmentation sub-processes of QCD partons. The theoretical calculation of fragmentation sub-processes requires non-perturbative information in the form of parton fragmentation functions of the photon, which are typically associated with large uncertainties.

Photon isolation is a crucial requirement to obtain a meaningful and computable definition of prompt photons in perturbative QCD. In theoretical calculations, it is useful to distinguish between the direct (hard) component and the fragmentation component. The direct component is when the photon is produced directly from the hard scattering, while the fragmentation component is when the photon is produced from the fragmentation of a hard parton.

In this chapter we will study the phenomenology of diphoton production at the LHC. The theoretical framework for calculating the cross sections for diphoton production has already been discussed in Chapter 3. Here we will present the different isolation criteria used to define prompt photons, the phenomenological setup and a brief enumeration of the different novel (massive) contribution to the NNLO cross section (for more details in section 3.1). Finally, we will discuss the implications of our results for future studies of diphoton production at the LHC.

[1]For more details about the importance of diphoton production and a detailed list of the relevant theoretical works and experimental analyses, please read the introduction of Chapter 4.

6.1 Standard isolation criterion

In this section we define the standard cone isolation criterion used to identify prompt photons (i.e to reduce the fragmentation component) in high-energy collisions.

Before defining the criterion, we first introduce the variables commonly used to describe the kinematics of the particles involved. The rapidity of a particle is defined as:

$$y = \frac{1}{2} \log \left(\frac{E + p_b}{E - p_b} \right) , \tag{1.1}$$

where E is the total energy of the particle and p_b is the momentum component along the beam axis. Given two particles with velocities y_1 and y_2, the rapidity difference $\Delta y = y_1 - y_2$ is a Lorentz invariant along the beam axis.

The pseudo-rapidity η is closely related to the rapidity. If the momentum of the particle is much larger than its mass (or the particle is considered in the massless limit), then the rapidity is approximately equal to the pseudorapidity $y \approx \eta$. Pseudorapidity is defined by:

$$\eta = - \log \left(\tan \left(\frac{\theta}{2} \right) \right) , \tag{1.2}$$

where θ is the polar angle of the particle relative to the beam axis. The pseudorapidity is often used in particle physics to describe the angle of a particle relative to the beam axis.

Another variable used to describe the direction of a particle is the azimuthal angle ϕ. This variable describes the direction of a particle in the transverse plane (the plane perpendicular to the beam axis). To define the standard cone isolation criterion, we define

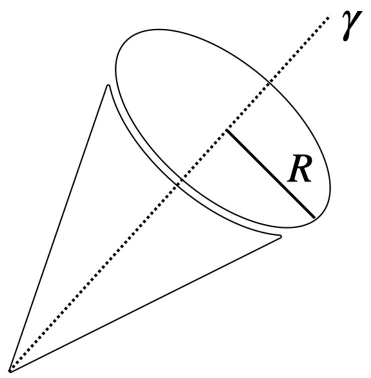

Figure 6.1.1. Cone centred on the direction of the photon.

a cone of radius R centred on the direction of the photon$\eta - phi$ plane, as shown in Figure 6.1.1.

We define an isolated photon by imposing a condition on the allowed hadronic transverse energy E_T^{had} inside the cone. Specifically, for:

$$(\eta - \eta_\gamma)^2 + (\phi - \phi_\gamma)^2 \leq R^2 , \tag{1.3}$$

we require that:

$$E_T^{had} \leq E_T^{max} , \tag{1.4}$$

where E_T^{max} is the maximum transverse energy determined by the experiment.

This criterion is called standard cone isolation. It imposes a hard cutoff on the hadronic transverse energy inside the cone, but does not prevent soft partons from being included inside the cone. This means that a soft gluon can still be inside the isolation cone, which can lead to IR divergences in the calculation of the cross section. Furthermore, the fixed threshold E_T^{max} does not distinguish between prompt photons and fragmentation radiation.

6.2 Frixione isolation criterion

To deal with both IR singularities and fragmentation, Frixione introduced a new method [221, 222]. We refer to this criterion as *Frixione cone isolation* or *smooth cone isolation.*

Given a final state with a photon (γ) and a jet (a quark or a gluon), we define the cone centred on the direction of the photon as in Fig. 6.2.2. Here, instead of setting a threshold

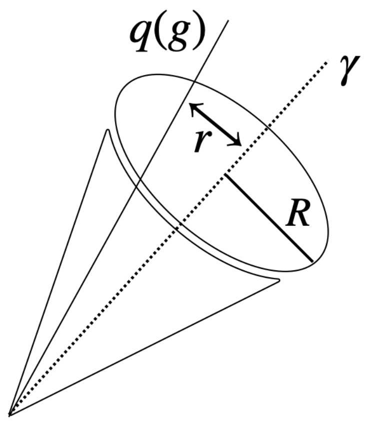

Figure 6.2.2. Cone centred around the photon's direction. R is the radius of the cone and r is the distance between the photon and the parton (a quark or a gluon) inside the cone.

for the transverse energy as in the previous case, we set a variable energy as a function of another radius r, which decreases as we get closer to γ. r is defined in terms of the pseudorapidity and the azimuthal angle of the jet and the photon as:

$$r = \sqrt{\left(\eta_{q(g)} - \eta_\gamma\right)^2 + \left(\phi_{q(g)} - \phi_\gamma\right)}. \tag{2.1}$$

$$E_T^{had}(r) \leq \epsilon \, p_{T_\gamma} \, \chi(r; R) \,, \tag{2.2}$$

in all cones with $r \leq R$. In equation (2.2) $E_T^{\max} = \epsilon \, p_{T_\gamma}$, where p_{T_γ} is the transverse momentum of the photon. The function $\chi(r; R)$ is a smooth function such that $\chi(r; R) \to 0$ for $r \to 0$ and in general $0 < \chi(r; R) < 1$. The function is usually defined as:

$$\chi(r; R) = \left(\frac{1 - \cos(r)}{1 - \cos(R)}\right)^n , \tag{2.3}$$

or by:

$$\chi(r; R) = \left(\frac{r}{R}\right)^{2n} . \tag{2.4}$$

which is more justified [184] for hadron colliders than eq. (2.3). For $n = 1$ they present the same behaviour with the radius r (see figure 6.2.3).

The parameters ϵ and n define the isolation. In Fig. 6.2.3 we can see the behaviour of $\chi(r; R)$ in eq. (2.3) for different values of n. The choice of n as a parameter is not arbitrary, but is constrained by the value of the cross section obtained with the standard isolation criterion, which imposes a physical limit on the cross section with the Frixione isolation criterion. The smooth cone isolation criterion is widely used among precise fixed order tools, since it removes the fragmentation contribution by dynamically adjusting the allowed energy as a function of the distance between the photon and the partons. It also excludes the possibility of having IR singularities due to soft gluon emission and quark-photon collinear divergences.

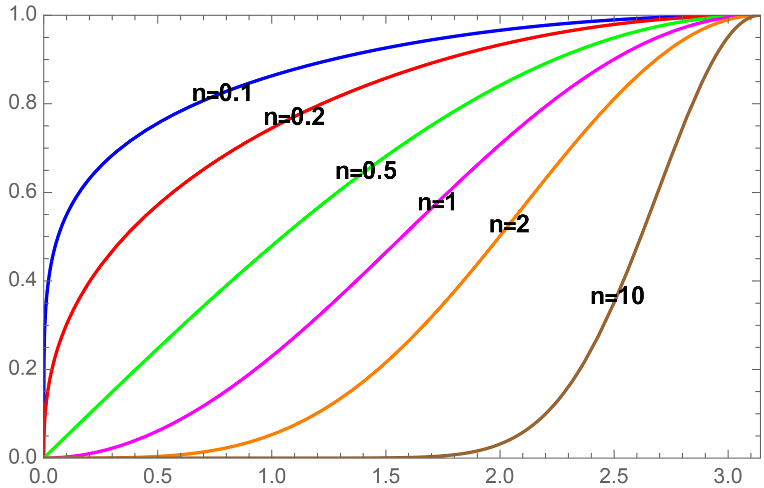

Figure 6.2.3. Plot of $\chi(r;R)$ for various values of n.

In general, the number of events in the Frixione isolation is lower than in the standard isolation and, in both cases, lower than in the inclusive case:

$$d\sigma_{Frixione}(E_T^{max}) \leq d\sigma_{standard}(E_T^{max}) \leq d\sigma_{inclusive}(E_T^{max})\,. \tag{2.5}$$

6.3 Phenomenological setup

In the following paragraphs we describe in detail the setup used in our phenomenological analyses of section 6.5.

We fix the top quark mass m_t to the value $m_t = 173\,\text{GeV}$. The QED coupling constant α_{em} is fixed at $1/\alpha_{em} = 137.035999139$. We use the central set of the `NNPDF3.1` PDFs [223] as implemented in the `LHAPDF` framework [224] and the associated strong coupling with $\alpha_s(m_Z) = 0.118$.

We consider isolated diphoton production in a pp collision at the centre-of-mass energy $\sqrt{s} = 13\,\text{TeV}$. We apply the kinematic cuts used in the ATLAS collaboration study [165]. The minimum transverse momentum allowed for the photons is $p_{T_\gamma}^{hard} \geq 40\,\text{GeV}$ for the harder photon and $p_{T_\gamma}^{soft} \geq 30\,\text{GeV}$ for the softer photon. The photon pseudorapidity is required to be $|\eta_\gamma| < 2.37$, excluding the interval $1.37 < |\eta_\gamma| < 1.52$ corresponding to the transition region between the barrel and the end caps of the electromagnetic calorimeter used experimentally to identify the photons. The minimum angular separation between the two photons is required to be $R_{\gamma\gamma}^{\min} = 0.4$.

We used the smooth cone isolation criterion described in section 6.2. In our case the specific values of the isolation parameters are $R = 0.4$, $\epsilon = 0.09$ and $n = 1$.

The central factorisation and renormalisation scales are chosen to be equal to the diphoton invariant mass $\mu \equiv \mu_R = \mu_F = M_{\gamma\gamma}$. The theoretical uncertainty is estimated from $(\mu_R, \mu_F) = (K_R, K_F)M_{\gamma\gamma}$ by varying $K_R, K_F \in \{1/2, 2\}$, omitting the combinations $(2, 1/2)$ and $(1/2, 2)$.

We adopt the q_T subtraction method to perform our full NNLO calculations (see section 3.1). We use as a technical parameter a cut on the transverse momentum of the diphoton pair $r_{cut} = 0.0005 < p_T^{\gamma\gamma}/M_{\gamma\gamma}$. The large diphoton invariant mass tail is not particularly sensitive to variations in r_{cut} around this chosen value, and therefore the invariant mass region around two times the top quark mass is not affected.

6.4 Massive contributions to the NNLO cross section

In this section we briefly enumerate the massive contributions to the NNLO diphoton cross section. This section completes and emphasises the discussion in section 3.1.

For the full NNLO QCD corrections to diphoton production we have contributions from the massless (five light quark flavours) [164, 183, 184, 220] and the massive scattering amplitudes [2, 1].

The massive corrections starts to appear at NNLO and we can classify the massive scattering amplitudes into four different types of contributions:

- Massive one-loop box scattering amplitude $gg \to \gamma\gamma$ [197, 183] (see Fig. 6.4.4).

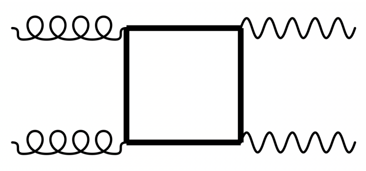

Figure 6.4.4. Representative diagram for the one-loop box contribution.

- Double-Virtual corrections to the Born sub-process $q\bar{q} \to \gamma\gamma$, (see Fig. 6.4.5).

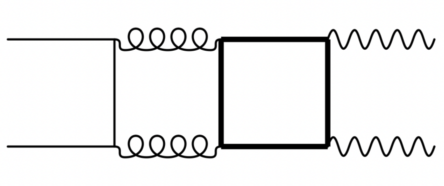

Figure 6.4.5. Representative diagram for the Double-Virtual contribution.

- Real-Virtual contributions to diphoton production, where the diphoton pair is produced in association with real radiation (quarks and gluons) (see Fig. 6.4.6). This scattering amplitude is interfered with the corresponding tree-level matrix element ($q\bar{q} \to \gamma\gamma g$ or $qg \to \gamma\gamma q$ depending on the partonic channel).

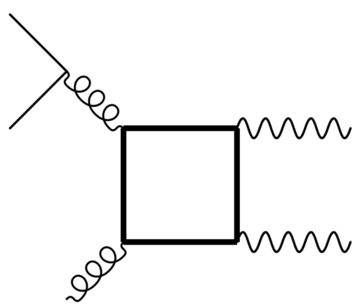

Figure 6.4.6. Representative diagram for the Real-Virtual contribution.

- Double-Real contributions related to diphoton production associated with the emission of two on-shell top quarks ($q\bar{q} \to \gamma\gamma t\bar{t}$ and $gg \to \gamma\gamma t\bar{t}$) (see Fig. 6.4.7). The massive one-loop box scattering amplitude $gg \to \gamma\gamma$ was already known, and the double-virtual

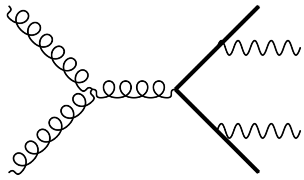

Figure 6.4.7. Representative diagram for the Double-Real contribution.

contribution is an original result discussed in detail in Chapter 4. The real-virtual and double-real contributions were numerically implemented in `OpenLoops` [70]. We calculated the latter contributions analytically in order to check them numerically with `OpenLoops`. All our massive contributions are encoded in a new version of the 2γ`NNLO` [164] code, which has been checked against the `MATRIX` [225] numerical code, which includes the massless NNLO QCD corrections to diphoton production.

6.5 Full NNLO results with top quark mass dependence

In this section we present our results for diphoton production at NNLO in perturbative QCD, taking into account the full top quark mass dependence. Our calculation has been encoded in a new version of the 2γ`NNLO` code, which is much faster than the previous one thanks to the fast integration routines of the numerical program `DYTurbo` [226, 227].

6.5.1 Two-loop contribution and comparison with the one-loop box

Here we comment on the contribution of the two-loop form factor to the NNLO invariant mass distribution. In Fig. 6.5.8 (top panel) we show the ratio between the fully massive two-loop form factors and the massless case. The ratio is performed explicitly using the hard function $H_q^{\gamma\gamma(2)}$, defined in (3.10), in the hard resummation scheme [150]. The central scale is shown with a black dashed line, and the bands are computed by implementing the 7-point scale variation described in 6.3.

We are interested in the invariant mass distribution of the differential cross section, and in particular we show the importance of our contribution around the top quark pair threshold (the energy level at which it becomes possible to produce a top quark pair) $M_{\gamma\gamma} = 2\,m_t$.

We immediately see that the ratio has the typical peak around the top quark threshold, as in any massive loop contribution. For $M_{\gamma\gamma}$ greater than $2\,m_t$ there is a second peak around $M_{\gamma\gamma} \sim 2.3 \times 2\,m_t$ and then the tail decreases due to the fact that the two-loop massive scattering amplitude becomes increasingly negative in the tail. This is consistent with the following observation: the result obtained by considering the massless two-loop form factors with six light quark flavours is smaller than the result with five light quark flavours in the whole invariant mass regime. Consequently, the asymptotic behaviour of the ratio between the massless results $H^{(2)}(n_f = 6lf)/H^{(2)}(n_f = 5lf)$ is decreasing, showing exactly the same behaviour as that obtained with the massive result.

In Fig. 6.5.8 (bottom panel) we show the well-known ratio between the fully massive one-loop box contribution and the corresponding one with five light quark flavours.

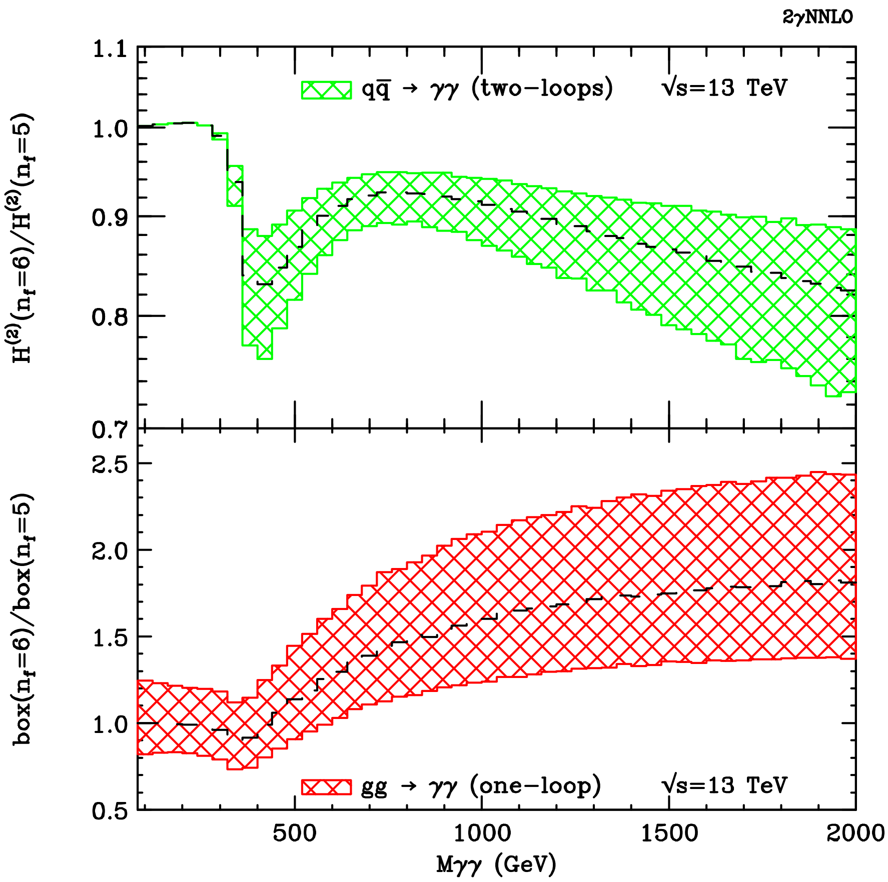

Figure 6.5.8. Ratios of different massive corrections to the massless case. In the top panel we show the ratio of our two-loop massive form factors for $q\bar{q} \to \gamma\gamma$ to the massless one. In the lower panel we show the ratio of the massive one-loop box $gg \to \gamma\gamma$ to the massless one.

We have the negative peak around the top quark pair threshold, but unlike in the two-loop case $q\bar{q}$, the tail does not decrease. Furthermore, asymptotically ($M_{\gamma\gamma} \gg m_t$) its ratio becomes

$$\frac{box(n_f=6)}{box(n_f=5)} \sim \frac{\left(\sum_{n_f=6} e_q^2\right)^2}{\left(\sum_{n_f=5} e_q^2\right)^2} = \frac{225}{121} \sim 1.85\ldots, \tag{5.1}$$

which means that the massive contribution behaves as if it were composed of 6 light quark flavours in the tail.

The two contributions described in this section are the most sizable among the massive ones up to NNLO accuracy. The size of both ratios around the negative peak, at the top quark pair threshold, is quantitatively similar and amounts to -15%.

The opposite behaviour of the two contributions along the tail of the distribution, for large values of $M_{\gamma\gamma}$, determines the position of the positive peak and the shape along the tail of the ratio between the fully massive and the 5 light quark flavours of the NNLO invariant mass distribution (see Fig. 6.5.12).

6.5.2 Massive Double-Real corrections

We now consider the massive Double-Real corrections to the partonic sub-process $pp \to \gamma\gamma t\bar{t}$. In the upper panel of Fig. 6.5.9 we show the invariant mass distribution obtained for this process and for the two different channels discussed in D.0.2. Unlike

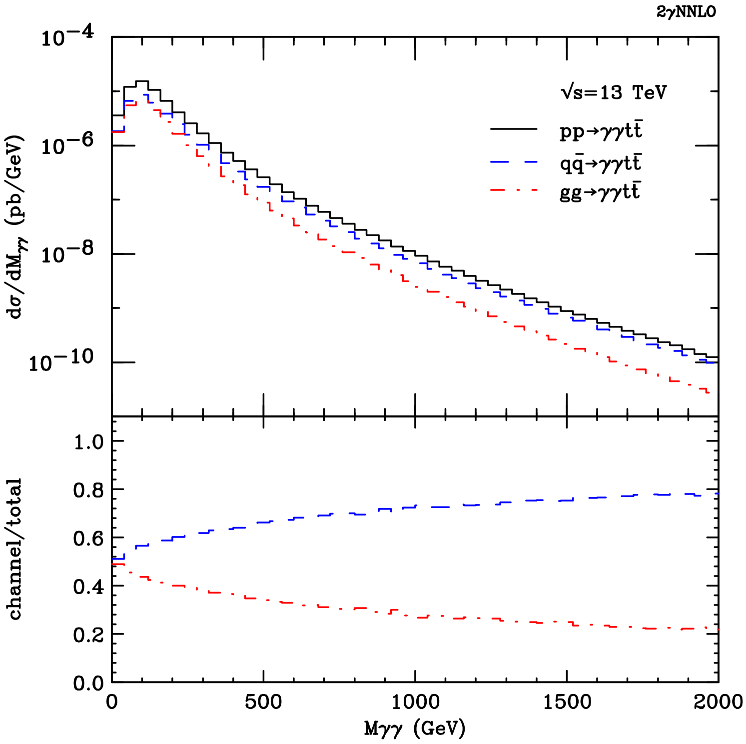

Figure 6.5.9. Invariant mass distribution of the double-real contribution to the NNLO fully massive result and comparison between the different channels with respect to the total double-real contributions.

the previous case, there is no top quark threshold in the invariant mass distribution and it has a continuously decreasing logarithmic tail, as in the massless case. The absence of the peak is due to absence of massive loop since we are dealing here with tree-level scattering amplitudes with the production of two on-shell top quarks. As in the massless case, the only peak in the invariant mass distribution, due to kinematic effects, is around $2\,p_{T_\gamma}^{hard} = 80\,\text{GeV}$.

In the bottom panel of Fig. 6.5.9 we show the relative size of the different channels, $q\bar{q}$ and gg, with respect to the total. The fast decreasing behaviour in the gluon PDFs at large momentum leads to a significant reduction in the gluon luminosity at high invariant mass and the quark-antiquark annihilation becomes the dominant channel for the diphoton production. This is because the quark PDFs do not decrease as rapidly as gluon PDFs at large momentum, and the leading-order $q\bar{q}$-channel is less suppressed compared to the gg-channel.

6.5.3 Massive Real-Virtual corrections

Now we consider the Real-Virtual contribution of the one-loop discussed in D.0.1. In particular, we show the contribution of the $pp \to \gamma\gamma j$ comparing the invariant mass distribution of the different channels with respect to the total correction. In

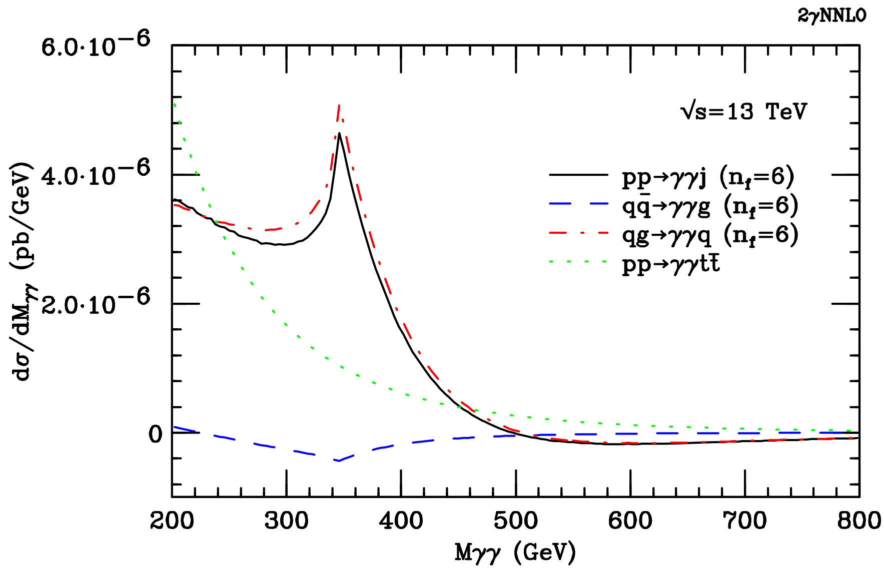

Figure 6.5.10. Invariant mass distribution of the one-loop diphoton production in association with the emission of one jet. We show the different partonic channels and a comparison with the size of the Double-Real corrections.

Fig. 6.5.10 we show the invariant mass distribution of the massive corrections to diphoton production in association with jets. In particular, we discuss the different behaviour of the one-loop scattering amplitude for the different channel $q\bar{q} \to \gamma\gamma g$ and $qg \to \gamma\gamma q$.

The $q\bar{q}$-channel (blue dashed line) exhibits the negative peak around the top quark pair threshold. The qg-channel (red dashed line) dominates the contribution around the top quark threshold and exhibits a completely different behaviour around the top quark threshold. At NNLO the one-loop scattering amplitude is interfered with the three-level matrix elements and, as discussed in D.0.1 only the massive top quark is circulating in the loop. The positive peak around the top quark threshold is also found in the box contribution when only the massive quark is running in the loop [204]. If we include also the five light quark flavours in the loop, there is a destructive interference between these two types of terms and, as a consequence, we have the typical negative peak. Here we don't have this destructive interference since there is no mixing of massive and massless quarks in the loop.

The black line corresponds to the contribution of the whole $pp \to \gamma\gamma j$ channel given by the two contributions discussed.

The green dotted line correspond to the $pp \to \gamma\gamma t\bar{t}$ sub-process. The size of the Real-Virtual and the Double-Real contributions are roughly of the same order, and they are subdominant with respect to the one-loop box and the two-loop form factors.

6.5.4 NNLO invariant mass distribution with full top quark mass dependence

Finally, we discuss our results for the diphoton production at NNLO in perturbative QCD, taking into account the full top quark mass dependence.

In the upper panel of Fig. 6.5.12 we present our result (including the scale variation dependence) for the invariant mass distribution of the photon pair at NNLO using the kinematical cuts described in section 6.3. In the bottom panel of Fig. 6.5.12 we

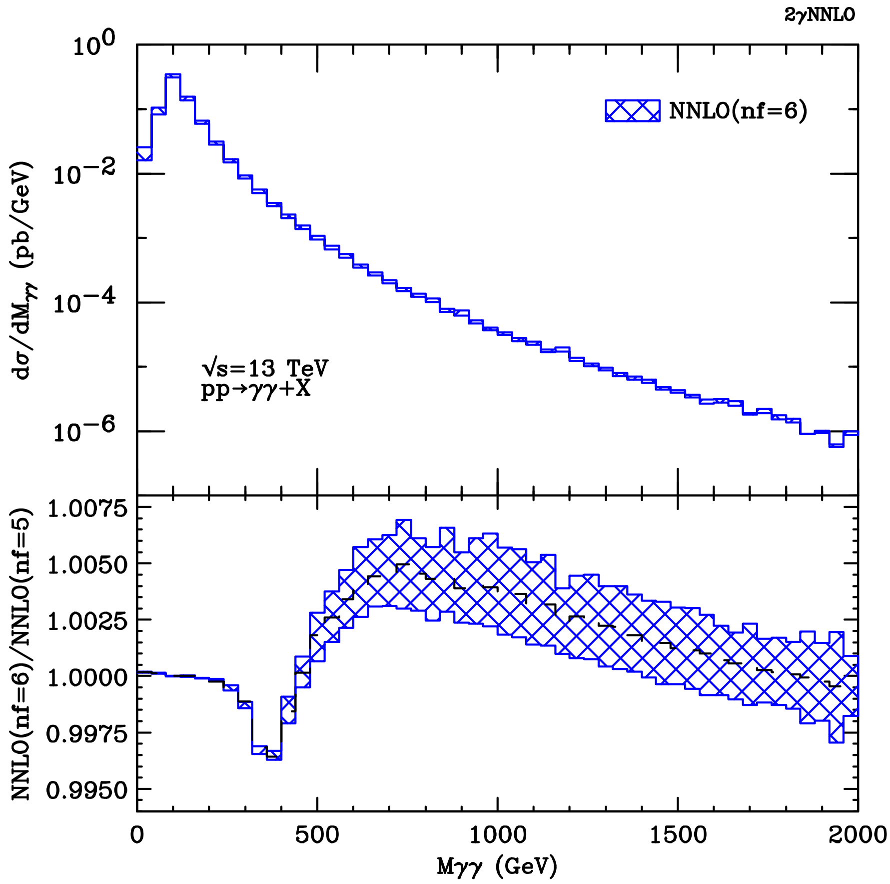

Figure 6.5.11. NNLO invariant mass distribution with full top quark mass dependence.

show the ratio between the fully massive NNLO result and the NNLO prediction for five light quark flavours. We can divide the analysis into three specific regions, i.e. invariant mass $M_{\gamma\gamma}$ less than, equal to and greater than the top quark pair threshold:

- In the low-mass region, $M_{\gamma\gamma} < 2\,m_t$, the total centre-of-mass energy in the real correction can be above $2\,m_t$, and thus the top-quark loop can be resolved, leaving the massive result still slightly larger than the massless one.
- Around $M_{\gamma\gamma} \sim 2\,m_t$ the invariant mass distribution shows the negative peak due to a superposition of the effects of the different contributions discussed in sections 6.5.1, 6.5.2 and in Appendix D.0.1.
- Beyond the negative spike, there is a maximum deviation at about $2.3 \times 2\,m_t$. We have already shown that the largest contributions are the one-loop scattering amplitude in the gg channel and the two-loop corrections in the $q\bar{q}$ channel. The position and shape of this positive peak is the result of a competition between the opposite behaviour of these two contributions after the top quark threshold.

  For large values of $M_{\gamma\gamma}$, the luminosity of the gluon decreases and the largest massive contribution along the tail becomes the $q\bar{q}$ channel. This explains why the tail decreases at large values of the invariant mass, even though the fully massive box contribution is almost twice the massless result in the tail. The negative corrections from the massive two-loop contribution in the $q\bar{q}$ channel are still present at large invariant masses, and the ratio turns out to be negative in this kinematic region for $M_{\gamma\gamma} \sim 2\,\mathrm{TeV}$.

6.5.5 Ratios of each massive contributions

Summarizing, we show the different size of each of the contributions discussed in section 6.4. In particular, we compare the size of each contribution with respect to the massless NNLO cross section in function of the invariant mass of the photon pair. We see explicitly that the dominant contributions come from the two-loop in the quark annihilation channel (black dot-dashed line) and from the one loop box in gluon fusion (red line).

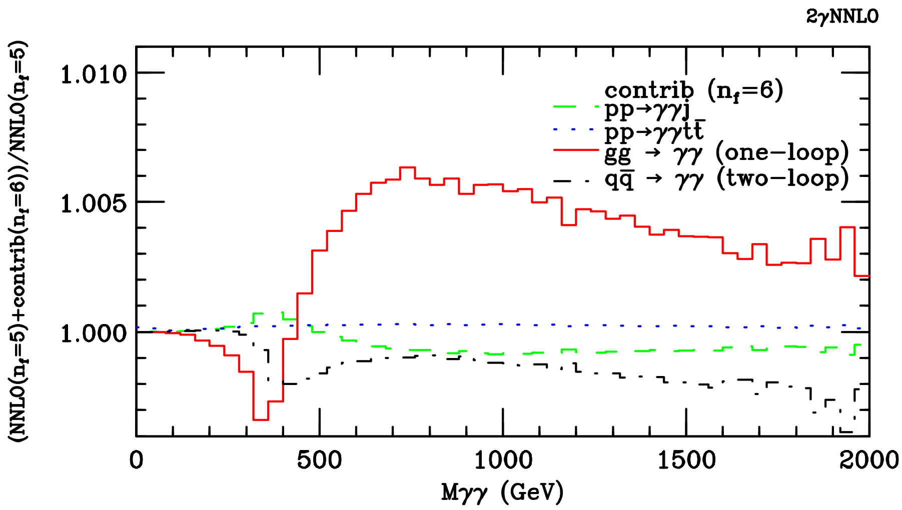

Figure 6.5.12. Ratios of each massive contributions with respect to the NNLO massless cross section as a function of the invariant mass.

Chapter 7

Conclusions and outlooks

In this thesis we have discussed the state-of-the-art techniques currently used to calculate higher order corrections to scattering amplitudes. The precision achieved experimentally requires a deep understanding of these techniques, and increasingly complex calculations are required to compare theoretical predictions with experimental results. Using the various methods presented, the original contribution of this thesis is to compute massive corrections for several processes relevant to LHC phenomenology.

In Chapter 1 we discussed some fundamental properties of QCD that allow us to perform a perturbative expansion in the coupling constant α_s, analysing the different components needed to calculate the cross section between hadrons.

In Chapter 2 we have shown how the scattering amplitudes are essential elements in the calculation of the cross section. After giving a general overview of the amplitude structure, we focused on the calculation of form factors and helicity amplitudes. In particular, we studied in detail the Feynman integrals that make up the amplitude. Using the method of differential equations, we analysed the solution of these integrals in both analytic and semi-analytic form for subsequent numerical evaluation in phase space. Using the method of differential equations, we studied the solution of the integrals in analytic form when it is possible to obtain the so-called canonical logarithmic form. The analytic structure of the amplitude in this case is described by functions known as multiple polylogarithms, defined on the punctured Riemann sphere. However, especially when considering massive corrections, the functional space characterising the amplitude becomes much wider. Through the study of the maximum cut, we explored the deep connection with active research areas in mathematics. Particular attention has been paid to the generalisation of multiple polylogarithms in the case of elliptic curves. When the function space includes these extensions, obtaining an analytic solution that can be evaluated in phase space for phenomenology becomes challenging. For this reason, we introduced the method of generalised power series, which allows us to bypass the function space of the process and achieve a fast evaluation at any point in phase space.

In Chapter 3 we discuss the q_T subtraction method as an essential tool for dealing with IR divergences. Subtraction methods are essential to perform phenomenology once the amplitude has been calculated. We consider the different contributions up to NNLO that are needed to calculate the differential cross section. In the low transverse momentum regime, the singularities appear as logarithms, which had to be taken up to all orders in the strong coupling in order to obtain reliable predictions from the cross section calculation.

The methods described in the first three chapters were used for the original work of the thesis presented in the following chapters.

In Chapter 4 we computed the two-loop form factors needed for the helicity amplitudes for diphoton production at NNLO in the heavy quark loop quark annihilation channel [2]. We have described in detail the calculation of the MIs by the method of differential equations. The MIs are written in the so-called canonical logarithmic form, except for those whose analytic structure involves elliptic functions. Through the maximal cut, we have shown the underlying elliptic curves which define the geometry associated to the non-planar integral family. In order to obtain numbers for a phenomenological analysis, we decided to use the generalised power series technique to construct a grid for the hard function between 8 GeV and 2 TeV in the phase space.

In Chapter 5 we computed the two-loop helicity amplitudes for the diphoton productions in gluon fusion with a heavy quark loop. We described the relevant scalar integral families and the MIs were evaluated by means of DEs. We discussed in detail, through the study of the maximum cut, the elliptic sector, which turns out to be the same as that studied in Chapter 1. Unlike the previous case, in which we evaluated the MIs semi-analytically using the generalised power series expansion, in this original work, which has not yet been published, the system of differential equations was put into ϵ-factorised form and then the MIs were expressed analytically in terms of iterated integrals. The iterated integrals were expressed in terms of four different types of integration kernels. The rewriting of the MIs in terms of iterated integrals leads to significant simplifications at both the amplitude and integral levels. As a preview, we study the numerical evaluation of the integrals by serially expanding the periods and transcendental functions introduced by the procedure used to rotate the system into the ϵ-factorised form.

In Chapter 6 we considered for the first time the full NNLO corrections in perturbative QCD, taking into account the full top quark mass dependence for photon pair production [1]. The last missing ingredient for the complete NNLO study was the DV contribution, which was obtained in chapter 4. The other massive contributions, RV and DR, were computed and checked with the one implemented in `OpenLoops`. All computed massive corrections have been implemented in a new version of 2γ`NNLO` using the integration routines of `DYTurbo`. We have shown several numerical distributions in the invariant mass of the photon pair to study the impact of the massive corrections, especially around the top quark threshold. We have discussed the dominant contributions of the total NNLO massive result, i.e. the one-loop $gg \to \gamma$ and the two-loop massive form factors computed as work in this thesis. We emphasize that the corrections are not only important around the top quark threshold, but also in the large invariant mass region, especially for physics beyond the SM (BSM) searches.

Chapter 8

Resumen de la tesis

8.1 Introducción

El Modelo Estándar de la física de partículas describe las fuerzas, con la excepción de la gravedad, dentro de un marco matemático coherente. Desde su formulación, las predicciones del modelo han sido notables y se han logrado con gran precisión. El SM sigue siendo, hasta la fecha, el mejor modelo desarrollado para describir partículas y sus interacciones. Sin embargo, quedan algunos aspectos sin explicar, como la inclusión de la fuerza gravitatoria, la existencia de la materia oscura y la energía oscura, la masa de los neutrinos, entre otros.

El uso de colisionadores de hadrones es la herramienta fundamental para desvelar los secretos de la física de partículas, y el Gran Colisionador de Hadrones (LHC) juega actualmente un papel crucial. El descubrimiento del bosón de Higgs, que tuvo lugar durante el primer período de funcionamiento del LHC, marcó un punto de inflexión en la física moderna y provocó un importante cambio de rumbo. La era de la precisión, en la que nos encontramos, se centra en la búsqueda de discrepancias entre las predicciones teóricas y los datos experimentales recopilados en los ciclos de funcionamiento del LHC. Las mejoras continuas y las sesiones de funcionamiento del colisionador han permitido alcanzar un umbral de error de alrededor $\sim \mathcal{O}(\,\%)$, lo que hace que las previsiones teóricas cada vez más precisas sean esenciales. Esta necesidad lleva a calcular las correcciones de orden superior a las amplitudes de interacción para procesos que se vuelven cada vez más complejos a medida que aumentan las escalas involucradas. En el Capítulo 1 se explica por qué es posible expandir la interacción de las fuerzas de forma perturbativa, especialmente en la cromodinámica cuántica (QCD), y por qué es fundamental para calcular el perfil de choque hadrónico. Para alcanzar la precisión de las últimas y actuales sesiones de funcionamiento del LHC, debemos tener en cuenta un número cada vez mayor de escalas en los procesos estudiados, en particular, los heavy quarks en el bucle de la teoría perturbativa de la QCD. Las correcciones masivas no solo afectan a las predicciones fenomenológicas, sino también a la estructura matemática de las amplitudes de interacción. También se discutirán algunos resultados importantes de áreas de investigación activa en matemáticas, como la geometría algebraica y la geometría compleja, en el contexto de integrales de Feynman. Para la aplicación fenomenológica, utilizaremos un método semi-analítico para evaluar integrales mediante una generalizada expansión en potencias, que nos permite evaluar nuestro amplo con precisión arbitraria en el espacio de fases.

Para alcanzar la precisión de los últimos y actuales ciclos de funcionamiento del

LHC, debemos tener en cuenta un número cada vez mayor de escalas en los procesos estudiados, en particular los quarks pesados en el anillo en la cromodinámica cuántica perturbativa. Las correcciones de masa no solo afectan a las predicciones fenomenológicas, sino también a la estructura matemática de las amplitudes de interacción. Hablaremos de algunos resultados importantes de áreas de investigación activa en matemáticas, como la geometría algebraica y la geometría compleja, en el contexto de integrales de Feynman. Para la aplicación fenomenológica, utilizaremos un método semi-analítico para evaluar integrales mediante una generalizada expansión en potencias, que nos permite evitar el espacio de funciones y evaluar nuestra amplitud.

8.2 Objetivos Alcanzados

Este trabajo de tesis se centra en la aplicación de técnicas avanzadas para calcular correcciones de orden superior a procesos relevantes para la física del LHC, en particular, aquellas que surgen de la presencia de partículas con masa en los bucles. En concreto, analizamos tres objetivos:

– El primer trabajo se centra en las correcciones de dos loops a la producción de fotones en el canal de aniquilación de quarks [2]. Las form factors necesarias para calcular los momentos de helicidad se calculan en términos de diagramas de Feynman de dos loops, en los que uno de los loops involucra a un quark pesado. El gran número inicial de integrales presentes en el amplo es reducido a un número mínimo de integrales, denominadas integrales master (MIs). La evaluación de los MIs se lleva a cabo utilizando el método de las ecuaciones diferenciales (DEs). Se estudia la geometría asociada a una topología no plana y se presenta la correspondiente curva elíptica. Debido a la presencia de la curva elíptica, la situación es muy compleja y el sistema se encuentra en la llamada forma canónica logarítmica, excepto para los MIs cuya estructura analítica involucra funciones elípticas. Para realizar una evaluación numérica eficiente, se han computado todos los integrales con precisión arbitraria en el espacio de fase en un tiempo increíblemente corto en un único núcleo de proceso.

– El segundo trabajo trata sobre las grandes correcciones en la producción de un fotón en la colisión de gluones. Esta situación es mucho más compleja que la anterior, debido al mayor número de formadores y integrales, y a la presencia de múltiples familias de integrales escalares. Los amplitudes de helicidad se expresaron en términos de 161 MIs, y en este caso también se utilizó el método DEs. También está presente un sector elíptico, el mismo que se estudió en el caso anterior. Se implementó una técnica para colocar el sistema de ecuaciones diferenciales en la forma factorizada en función del período de la curva elíptica y una nueva función transcendental necesaria para alcanzar esta forma específica. El hecho de obtener la forma factorizada en ϵ simplificó mucho tanto la cálculo de las amplitudes como el de los integrales involucrados.

– El tercer trabajo se refiere a correcciones completas NNLO en el marco de la teoría perturbativa. QCD, teniendo en cuenta la dependencia completa de la masa del top quark para el fotón [1]. El estudio de los total correcciones fue posible gracias a la cálculo de dos factores de forma en el canal de aniquilación de quarks, que resultó ser el elemento más difícil de calcular. Además, se calcularon y incorporaron a la biblioteca de código abierto `2`γ`NNLO` todos los contribuciones de masa, aprovechando la tecnología `DYTurbo`. Se compararon todos los resultados recalculados previamente con los implementados en `OpenLoops`. Esto permitió presentar diversas distribuciones numéricas en la masa invariante de los dos fotones y analizar diferentes tipos de contribuciones.

Estas obras se discuten en detalle en los capítulos 4, 5 y 6. En conjunto, representan una investigación de vanguardia en cálculos de precisión dentro de la QCD, combinando técnicas avanzadas para el cálculo de amplitudes con métodos matemáticos relacionados con curvas elípticas y integrales iteradas definidas sobre ellas. Es importante destacar que hemos llevado a cabo un cálculo completo de las amplitudes, desde la construcción de los factores de forma hasta su uso fenomenológico.

8.3 Metodología

En los capítulos 1, 2 y 3 se describen en detalle todos los métodos utilizados para calcular, analíticamente o numéricamente, los integrales de Feynman involucrados en los procesos discutidos anteriormente. A continuación, resumimos sus aspectos principales y destacamos sus características.

8.3.1 Amplitudes y correcciones de orden superior.

El parámetro físico que permite comparar la predicción teórica con los datos experimentales es el sección transversal hadrónica. Puede factorizarse mediante el teorema de factorización:

$$\sigma_{h_1\,h_2}(s) = \sum_{a,b} \int dx_1\, f_{a/h_1}(x_1,\, \mu_F) \int dx_2\, f_{b/h_2}(x_2,\, \mu_F)\, \widehat{\sigma}_{a\,b}(\widehat{s},\, \mu_R,\, \mu_F), \tag{3.1}$$

Se trata de la convolución de dos componentes diferentes: las funciones de distribución de partones (PDFs) $f_{i/h}(x,\mu_F)$ y el cross section partónico $\widehat{\sigma}_{a,b}$.

Para calcular el cross section hadrónico se requieren varios componentes de las interacciones. En nuestro trabajo nos centramos en la comprobación de las amplitudes de interacción, ya que son la herramienta esencial para calcular el sección cruzado partónico. Para obtener predicciones teóricas dentro del umbral experimental, expandimos el proceso en una serie perturbativa en powers del paréntesis de la fuerza fuerte, α_s:

$$\sigma = \sigma_{\mathrm{LO}} + \left(\frac{\alpha_s}{2\pi}\right) \sigma_{\mathrm{NLO}} + \left(\frac{\alpha_s}{2\pi}\right)^2 \sigma_{\mathrm{NNLO}} + \cdots\,, \tag{3.2}$$

LO representa el orden de magnitud principal, NLO el siguiente en importancia y NNLO el siguiente en importancia después del NLO. En este marco general, calculamos las correcciones de orden superior expandiendo el amplo de la función de onda en potencias de α_s:

$$\mathcal{A} = \sum_{l=0}^{\infty} \left(\frac{\alpha_s}{2\pi}\right)^l \mathcal{A}^{(l)}, \tag{3.3}$$

where $\mathcal{A}^{(l)}$ represents the l-loop amplitude that can be expressed in terms of Feynman diagrams.

Dentro del marco de regularización dimensional, a partir de esta representación pictórica en forma de diagramas, podemos resumir la estructura del amplitud en función de los tipos de partículas implicadas en las interacciones en tres estructuras principales:

$$\mathcal{A} = \mathcal{C} \times T \times I. \tag{3.4}$$

In eq. (3.4), C es un conjunto de factores de color, T codifica la dependencia de los tensores de Lorentz y I representa los integrales escalares asociados a la estructura de la curva del amplitud.

La estructura de colores puede separarse de las amplitudes ordenadas por color, que son invariantes de Gauge que trabajan con las constantes de estructura del álgebra de Lie $SU(N_c)$.

8.3.2 Estructuras de Lorentz tensoriales

La estructura tensorial del amplo podría analizarse en las amplitudes ordenadas por color. Los métodos desarrollados para tratar integrales de Feynman de varios loops y con varios leg se basan en integrales escalares. Por tanto, debemos factorizar la estructura tensorial de los integrales. Dado que la expresión de la amplitudes para un proceso genérico está escrita en términos de diagramas de Feynman, separamos la estructura tensorial de los llamados formadores escalares:

$$\mathcal{A}(p_1, \cdots, p_n) = \sum_{i=1}^{n} F_i(p_1, \cdots, p_n)\, T_i, \tag{3.5}$$

En este método, los tensores dependen de los momentos, vectores de polarización y compuestos bilineales de spinores mediante los matrices de Dirac γ. La técnica moderna que se utiliza para obtener el factor escalar es la del *método proyector*. Definimos el operador de proyección de modo que, al aplicarlo al amplo después de sumar sobre la polarización, se obtiene:

$$\sum_{pol} \mathcal{P}_j \mathcal{A}(p_1, \cdots, p_n) = F_j(p_1, \cdots, p_n). \tag{3.6}$$

El número de tensores se puede reducir a un conjunto mínimo de tensores independientes que trabajan en el esquema de 't Hooft-Veltman (tHV), donde los estados externos se consideran en cuatro dimensiones, mientras que los estados internos permanecen en tres dimensiones. Esto nos permite construir form factors a partir de un pequeño número de tensores independientes. Al fijar las helicidades, es posible calcular las llamadas amplitudes de helicidad directamente a partir de la ecuación 3.5. En particular, podemos utilizar la formalismo de spinor-helicidad, en el que utilizamos spinores y helicidades en lugar de momenta y vectores de polarización. Esto simplifica la expresión del amputado, ya que podemos separar los diferentes estados de helicidad y estos términos no interactúan entre sí.

8.3.3 Integrales de Feynman de múltiples bucles y múltiples patas

Una vez extraídas las estructuras de color y tensoriales, tenemos que tratar con integrales escalares de Feynman asociadas a los diagramas utilizados para escribir la amplitud general. En la regularización dimensional, podemos escribir una integral de Feynman genérica de l-bucles con n-patas externas como:

$$I(a_1, \cdots, a_m) = \int \prod_{i=1}^{l} \mathcal{D}k_i \frac{\mathcal{N}\left(\{k_i \cdot q_j\}\right)}{\prod_{s=1}^{m} D_s^{a_s}}., \tag{3.7}$$

expresada en términos de una medida de integración $\mathcal{D}k$, un polinomio $\mathcal{N}\left(k_i \cdot q_j\right)$ que depende de los productos escalares entre momentos internos de bucle y momentos internos o externos, y un conjunto de propagadores $D_s^{a_s}$ escritos en términos de combinaciones lineales de momentos de bucle, momentos externos y masas. A través del método de descomposición tensorial, el polinomio en el numerador puede expresarse en términos de productos escalares irreducibles (ISPs). Si representamos el número de productos escalares que ocurren en el proceso como N_{sp}, podemos escribir la integral de Feynman general de l bucles como:

$$I(a_1, \cdots, a_{N_{sp}}) = \int \prod_{i=1}^{l} \mathcal{D}k_i \frac{1}{\prod_{j=1}^{N_{sp}} D_j^{a_j}}, \quad a_j \in \mathbb{Z}. \tag{3.8}$$

Utilizamos la notación de familias de integrales escalares o topología para representar todas las integrales escalares con el mismo conjunto de denominadores, pero con diferentes índices a_j. De este modo, definimos las subtopologías como el conjunto de integrales asociados a una topología con algunos índices nulos.

8.3.4 Reducción integral

En el cálculo de un amputador de dispersión, especialmente cuando se consideran un gran número de bucles y extremos externos, aparecen inicialmente muchos integrales escalares. En casos más complejos, resulta inviable evaluar cada integral, ya sea numéricamente o analíticamente. Por tanto, es esencial reducir los integrales de función escalar pertenecientes a la misma topología a un mínimo número de integrales denominadas integrales master (MIs). Existe una base finita de MIs, pero no es única y no se ha comprendido aún cuál es la opción óptima. Aun así, una buena elección puede simplificar en gran medida las operaciones necesarias para calcular un amputado. La propiedad fundamental de la regularización dimensional es que el integral de un total derivado es cero. Esta propiedad da lugar a un conjunto de importantes relaciones utilizadas en varios paquetes de software para la reducción a MIs, conocidas como *identidades-de-integración-por-partes* (IBPs). Otro conjunto de relaciones utilizadas en el proceso de reducción se deriva de la propiedad de invarianza bajo transformaciones de Lorentz en la teoría de campos cuántica (QFT), lo que implica que el amplitud debe ser invariante bajo transformaciones de Lorentz.

La resolución de IBPs para encontrar el conjunto mínimo de MIs es un desafío y a menudo sigue siendo un cuello de botella en las cálculos de amplitudes de dispersión. Una de las técnicas ampliamente utilizadas para reducir los integrales a MIs es el algoritmo de Laporta, que ordena los integrales y selecciona aquellos con menor complejidad según ciertos criterios para simplificar el sistema de ecuaciones lineales proporcionado por los IBPs y obtener una solución mediante métodos sencillos de álgebra lineal. El algoritmo se ha implementado en varios programas y paquetes utilizados en la tesis, como `Kira`, `LiteRed`, `Reduze`, `FIRE`.

8.3.5 Método de ecuaciones diferenciales

Una vez hallado el fundamento de los MIs, es necesario un método para evaluar estas integrales. En la tesis se adopta el método de las ecuaciones diferenciales (DEs). Como los MIs son funciones de las escalas (invariantes cinemáticos y masas), al diferenciarlos con respecto a los invariantes cinemáticos es posible obtener un sistema de primeras orden de ecuaciones diferenciales lineales, que se pueden resolver teóricamente para hallar los MIs.

Si denotamos el conjunto de escalas como $\underline{x}$ y las MIs como $\underline{\mathcal{J}}(\underline{x},\epsilon)$ donde ϵ es el regulador dimensional, podemos escribir el sistema de DEs como:

$$d\underline{\mathcal{J}}(\underline{x},\epsilon) = \mathbb{A}(\underline{x},\epsilon)\,\underline{\mathcal{J}}(\underline{x},\epsilon), \tag{3.9}$$

donde d es el total diferencial y $\mathbb{A}(\underline{x},\epsilon)$ es la matriz de formas diferenciales. La elección de una buena base de MIs es fundamental para resolver el sistema de ecuaciones diferenciales, y es posible realizar una rotación que permite escribir el sistema en una nueva base.

Cambiando la base con coeficientes algebraicos, es posible encontrar una transformación que factorice las dependencias de ϵ de la matriz. Esto da una nueva matriz $\tilde{\mathbb{A}}(\underline{x})$ y se dice que el sistema de EDs está en forma factorizada en ϵ:

$$d\underline{f}(\underline{x},\epsilon) = \epsilon\,\tilde{\mathbb{A}}(\underline{x})\,\underline{f}(\underline{x},\epsilon), \tag{3.10}$$

donde $\underline{f}(\underline{x},\epsilon)$ son las nuevas MIs después de la rotación a la nueva base. En este caso, es posible obtener una solución en términos de integrales iteradas de Chen:

$$\underline{f}(\underline{x},\epsilon) = \mathbb{P}\,exp\left(\epsilon\int_{\underline{x}_0}^{\underline{x}} \tilde{\mathbb{A}}(\underline{x}^{'})\right)\underline{f}(\underline{x}_0,\epsilon), \tag{3.11}$$

en la cual $\mathbb{P}$ es el operador de ordenación de camino. Esta solución es particularmente útil porque se puede expandir orden por orden en el regulador dimensional.

La solución en términos de integrales iteradas es formal; sin embargo, se ha demostrado que existe una forma especial del sistema de ED en la cual ϵ se factoriza de la cinemática, y además la matriz contiene formas $d\log$:

$$\tilde{\mathbb{A}}(\underline{x}) = \sum_i \tilde{A}_i\,d\log\left(\alpha_i(\underline{x})\right), \tag{3.12}$$

donde $\tilde{A}i$ son matrices constantes con coeficientes en $\mathbb{Q}$ y $\alpha_i(\underline{x})$ son funciones algebraicas de las escalas llamadas *letras*. El conjunto αi de letras se llama *alfabeto*. A este caso lo llamamos *forma canónica logarítmica.*

8.3.6 Núcleos de integración y geometría

Existe una conexión profunda entre las formas diferenciales presentes en el sistema de ecuaciones diferenciales y el espacio de funciones que abarcan las soluciones de los integrales de Feynman. Incluso en los casos más simples, se introducen funciones que van mucho más allá de los logaritmos simples. En los cálculos necesarios para la física del LHC, especialmente cuando se incluyen correcciones masivas, surgen estructuras geométricas mucho más complejas. En particular, los integrales de Feynman pueden definirse en superficies de Riemann de diferentes géneros: En el caso canónico

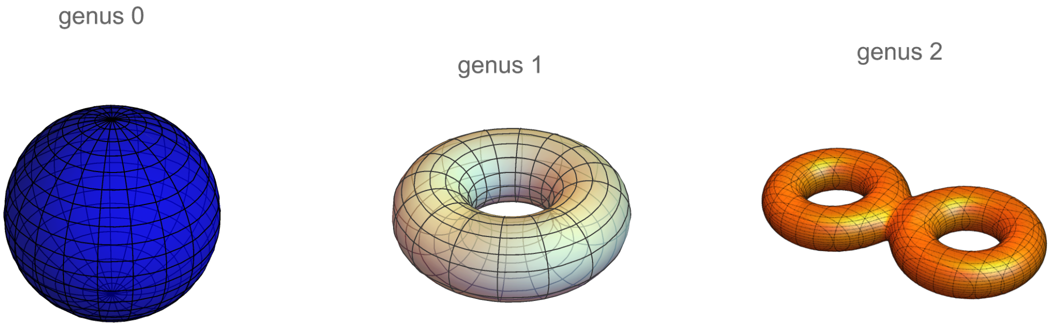

Figura 8.3.1. Ejemplos de superficies de Riemann con diferentes géneros.

logarítmico, los núcleos de integración, $\frac{dt}{t,-,a_i}$, son funciones meromorfas con polos simples en $t,=,a_i$. En este caso, las integrales iteradas sobre estos núcleos definen los *logaritmos polimórficos múltiples* (MPLs):

$$G(a_1, \cdots, a_n; z) = \int_0^z \frac{dt_1}{t_1 - a_1} \int_0^{t_1} \frac{dt_2}{t_2 - a_2} \cdots \int_0^{t_{n-1}} \frac{dt_n}{t_n - a_n}. \tag{3.13}$$

Estas funciones meromorfas están definidas sobre la esfera de Riemann perforada (género 0), mostrada en la Fig. 8.3.2. Por supuesto, los MPLs no son las únicas

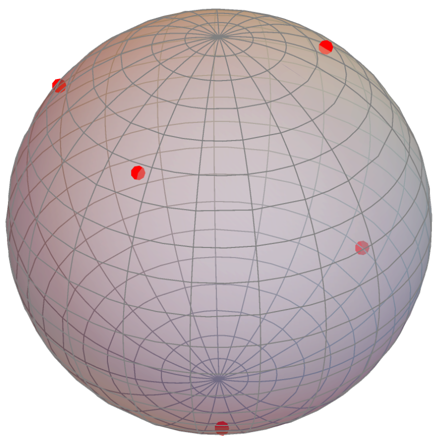

Figura 8.3.2. Esfera de Riemann perforada. Los puntos rojos son los polos de los núcleos de integración.

estructuras que aparecen en los cálculos de amplitud; de hecho, la situación es mucho más compleja. En nuestro trabajo mostraremos cómo una topología no plana de dos bucles está relacionada con una curva elíptica. Esto requiere una generalización de los MPLs al caso de curvas elípticas. Definimos una curva elíptica como el punto cero de una ecuación polinómica. A continuación, consideraremos curvas elípticas definidas por polinomios cuárticos:

$$y^2 = P_4(x) = (x - a_1)(x - a_2)(x - a_3)(x - a_4), \tag{3.14}$$

incluso si se podría usar un polinomio de tercer grado en su lugar. En este caso, proporcionamos una generalización a los llamados *logaritmos polimórficos múltiples elípticos* (eMPLs):

$$E_4\left(\begin{matrix} n_1 \dots n_k \\ c_1 \dots c_k \end{matrix}; x, \underline{a}\right) = \int_0^x dt\, \psi_{n_1}(c_1, t, \underline{a})\, E_4\left(\begin{matrix} n_2 \dots n_k \\ c_2 \dots c_k \end{matrix}; t, \underline{a}\right) \qquad n_i \in \mathbb{Z},\, c_i \in \mathbb{C} \cup \{\infty\}, \tag{3.15}$$

donde ψ_n son los núcleos de integración. Definimos los núcleos en términos de diferenciales de Abel de primer, segundo y tercer tipo. Una curva elíptica siempre tiene un diferencial holomorfo de primer tipo, que define el período de la curva. La curva elíptica puede representarse como una superficie de Riemann de género uno, es decir, un toro.

8.3.7 Forma factorizada en ϵ más allá de los MPLs

Ya hemos discutido la complejidad de las estructuras matemáticas involucradas en los procesos de dispersión de múltiples bucles y múltiples patas. En el caso de la forma canónica logarítmica, donde la solución analítica involucra MPLs, el sistema de ED se puede poner en una forma factorizada en ϵ, permitiendo obtener fácilmente la solución en términos de integrales iteradas. En el caso de curvas elípticas y estructuras aún más complejas, la situación se vuelve mucho más complicada. Recientemente, se ha desarrollado un método que permite, aunque de manera no algorítmica, obtener una forma factorizada en ϵ independiente de la geometría considerada. El procedimiento se basa en observaciones realizadas en varios casos y consta de cinco pasos clave. El primero es la elección de la base inicial; de hecho, hemos notado que la elección de la base no es única y que existe una rotación que permite un cambio de base. La elección de la base es crucial, ya que simplifica enormemente los cálculos. Se dan criterios para la elección de la base, especialmente en lo que respecta a la construcción en el caso de curvas elípticas. A continuación, se calcula el Wronskiano W, que corresponde a la solución homogénea de las ecuaciones diferenciales. Luego se realiza una rotación utilizando la matriz inversa de la parte semisimple del Wronskiano, ya que el Wronskiano se puede descomponer en una parte semisimple y una parte unipotente:

$$W = W_{ss} \cdot W_u. \tag{3.16}$$

Basado en observaciones en varios casos, la rotación que conduce a la forma deseada está dada por la parte semisimple. Luego, se reescalan los factores en ϵ, y posiblemente se intercambian los MIs dentro del mismo sector para obtener una forma triangular en ϵ. El cuarto paso consiste en integrar las derivadas totales de funciones ya presentes en la inversa de la matriz semisimple. Esto es equivalente a multiplicar la base de MI por una matriz cuyos elementos son derivadas de términos correspondientes a la parte $\epsilon = 0$ de la matriz de ED. Luego, el último paso es ajustar la parte inhomogénea

El procedimiento se aplica al triángulo elíptico, que utilizamos, junto con el caso de topología no plana más complejo, para alcanzar la forma factorizada en ϵ para el conjunto completo de MIs para las correcciones masivas de dos bucles a $gg \to \gamma\gamma$.

8.3.8 Corte máximo

Anteriormente discutimos la conexión entre los integrales de Feynman y la geometría. Para encontrar la variedad algebraica definida, introducimos el método del corte máximo. Específicamente, se basa en el concepto de corte generalizado de un integral de Feynman. Cortar un integral significa imponer que una (o más) partículas virtuales en los bucles estén en la capa de masa, reemplazando su propagador con una función δ. Introducimos la representación de Baikov, como la representación natural para realizar cortes, y discutimos el enfoque bucle por bucle utilizado para separar los diferentes bucles y simplificar el cálculo. Luego, definimos el *corte máximo* como el corte simultáneo de todos los propagadores de un diagrama de Feynman correspondiente. El corte máximo es una herramienta poderosa, especialmente cuando se aplica en el contexto de EDs. Por definición, corresponde a la solución homogénea de las EDs. Luego, a partir de la solución del corte máximo, podríamos obtener la solución completa de las EDs. Para mostrar la conexión con la geometría, aplicamos explícitamente el corte máximo al diagrama de burbuja de un bucle con dos masas y al diagrama sunrise con masas iguales.

8.3.9 Expansión en serie de potencias generalizada

Dado el conjunto de MIs, discutimos cómo satisfacen un sistema de EDs lineales de primer orden con respecto a los invariantes cinemáticos. Hablamos de la solución analítica en términos de integrales iteradas de Chen y de las diferentes estructuras matemáticas que surgen en los cálculos. La evaluación numérica de funciones expresadas en términos de integrales iteradas sigue siendo un cuello de botella en el cálculo. Si estamos interesados en un análisis fenomenológico, podríamos usar la técnica de la serie de potencias generalizada en su lugar. Este método evita completamente el espacio de funciones que aparecen en diferentes topologías y permite una evaluación en el espacio de fases con la precisión deseada. Si conocemos los valores de los MIs en un punto de frontera $\underline{x}_0$, podemos obtener el valor numérico en otro punto $\underline{x}$ parametrizando la curva que conecta estos dos puntos con un parámetro λ:

$$\gamma(\lambda) \, : \lambda \in [\lambda_0, \, \lambda^\star] \quad \lambda \mapsto \{x_1(\lambda), ..., x_n(\lambda)\}, \quad \text{with} \quad \begin{cases} \gamma(\lambda_0) = \underline{x}_0 \\ \gamma(\lambda^\star) = \underline{x} \end{cases}, \tag{3.17}$$

como se muestra en la Fig. 8.3.3. El método se basa en encontrar soluciones en

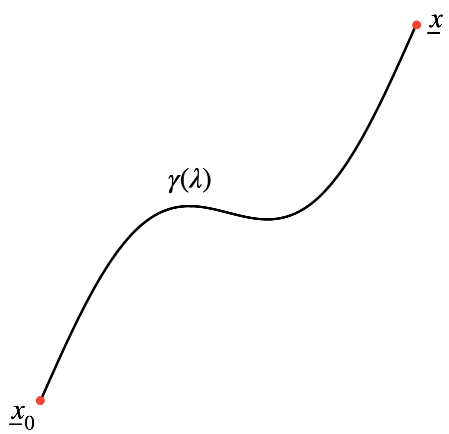

Figura 8.3.3. Curva paramétrica que conecta el punto de frontera con un nuevo punto.

serie alrededor de puntos regulares o singulares, orden por orden en ϵ. La solución encontrada de esta manera es válida en una región centrada alrededor del punto en consideración. Este método está implementado en los paquetes `DiffExp` y `SeaSyde`.

8.3.10 Método de sustracción en momento transverso y resumación

"Las correcciones de orden superior en la QCD perturbativa encuentran divergencias infrarrojas (IR) en las etapas intermedias del cálculo. Para eliminar estas divergencias y permitir una implementación en códigos numéricos de Monte Carlo para realizar análisis fenomenológicos, necesitamos un método de sustracción. En esta tesis utilizamos el método de sustracción q_T. Dentro de este formalismo, la sección eficaz diferencial a NNLO para el estado final genérico F se obtiene a partir de la fórmula maestra:

$$d\sigma^F_{NNLO} = \mathcal{H}^F_{NNLO} \otimes d\sigma^F_{LO} + \left[d\sigma^{F+jets}_{NLO} - d\sigma^{CT}_{NNLO}\right], \tag{3.18}$$

donde $\mathcal{H}^F_{NNLO}$ es la *función virtual dura* y contiene la parte finita de la amplitud de dispersión virtual de dos bucles, $d\sigma^{F,+,jets}_{NLO}$ es la sección eficaz diferencial correspondiente para el estado final $F,+,jets$ y $d\sigma^{CT}_{NNLO}$ es el contratérmino (CT) necesario para cancelar las singularidades en el límite de q_T pequeño.

Para asegurar la validez física del cálculo, introducimos el formalismo de resumación. La sección eficaz partónica puede descomponerse en una parte resumada y una parte finita. La parte resumada contiene todos los términos logarítmicamente divergentes en el límite de q_T pequeño y se evalúa mediante resumación a todos los órdenes en α_s.

8.4 Resultados y conclusiones

Los resultados en la tesis se describen en detalle en los Capítulos 4, 5 y 6. A continuación, los resumimos.

8.4.1 Factores de forma masivos a dos bucles para $q\bar{q} \to \gamma\gamma$

Con este objetivo, consideramos el cálculo de los factores de forma a dos bucles en el canal de aniquilación de quarks con un quark pesado en el bucle. Este era el último ingrediente faltante para el NNLO completo en la producción de dos fotones en QCD perturbativa. Para el proceso partónico:

$$q(p_1) + \overline{q}(p_2) \to \gamma(p_3) + \gamma(p_4), \tag{4.1}$$

adoptamos la descomposición tensorial para descomponer la amplitud en términos de factores de forma escalares y tensores invariantes de Lorentz:

$$\mathcal{A}_{q\bar{q}\gamma\gamma} = \sum_{i=1}^{4} \overline{\mathcal{F}}_i \overline{T}_i, \tag{4.2}$$

donde $\overline{T}i, =, \overline{v}(p_2)\Gamma_i^{\mu\nu} u(p_1)\epsilon 3, \mu\epsilon_{4,\nu}$. Los cuatro tensores de Lorentz independientes se calculan en el esquema tHV.

Los diagramas de Feynman relevantes (sin considerar el intercambio de fotones externos) se muestran en la Fig. 8.4.4. Los integrales correspondientes a (a) pueden

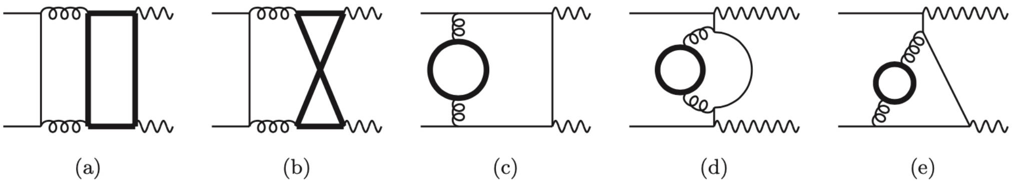

Figura 8.4.4. Conjunto representativo de diagramas de dos bucles con bucle de quarks pesados internos, que contribuyen a las correcciones de QCD a NNLO para la producción de dos fotones en el canal de aniquilación de quarks. Las líneas negras delgadas representan quarks ligeros, las líneas negras gruesas quarks pesados, las líneas rizadas gluones y las líneas onduladas fotones.

agruparse en una topología planar, PLA; los correspondientes a (b) en una topología no planar, NPL, y los correspondientes a (c), (d) y (e) juntos en una topología planar, PLB.

Todos los integrales se reducen a un conjunto de 72 MIs utilizando la reducción de IBPs. En el artículo presentamos un nuevo conjunto de MIs, correspondiente a la topología no planar, que se muestra en la Fig. 8.4.5.

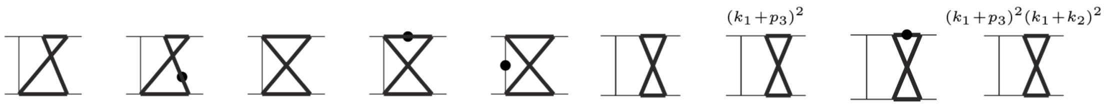

Figura 8.4.5. Nuevas MIs provenientes de la topología NPL.

Las MIs se evalúan mediante el método de EDs. Separaremos el estudio en las diferentes familias de integrales. Para la familia NPB, no necesitamos construir un sistema de EDs, ya que todas las MIs se pueden mapear en MIs de las otras dos topologías, excepto una, que ya se conocía analíticamente. Para la familia PLA, el sistema de EDs se coloca en la forma logarítmica canónica y proporcionamos el conjunto de letras del alfabeto y el conjunto de raíces cuadradas que complican el cálculo analítico. Para la topología NPL, tenemos dos subconjuntos diferentes. En particular, ponemos el sistema en forma logarítmica canónica, excepto para dos sectores elípticos. Realizamos un estudio de la curva elíptica asociada a estos sectores mediante el corte máximo:

MC (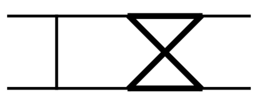)

$$\propto \frac{1}{s}\int \frac{dz_8}{(z_8\,-\,t)\sqrt{z_8(z_8+s)(z_8(z_8+s)-4\,s\,m_t^2)}}, \tag{4.3}$$

Obtenemos, como era de esperar, un polinomio de cuarto grado que corresponde a una curva elíptica.

En este caso también proporcionamos el conjunto de letras y raíces cuadradas provenientes del sistema de EDs. La situación es complicada, no solo en este caso, sino también en el caso planar para el cálculo analítico. Dado que necesitamos la evaluación numérica para fines fenomenológicos, adoptamos el método de expansión en serie de potencias generalizada. De este modo, construimos la cuadrícula para la función virtual dura desde 8 GeV hasta 2,2 TeV en el espacio de fases físico, como se muestra en la Fig. 8.4.6.

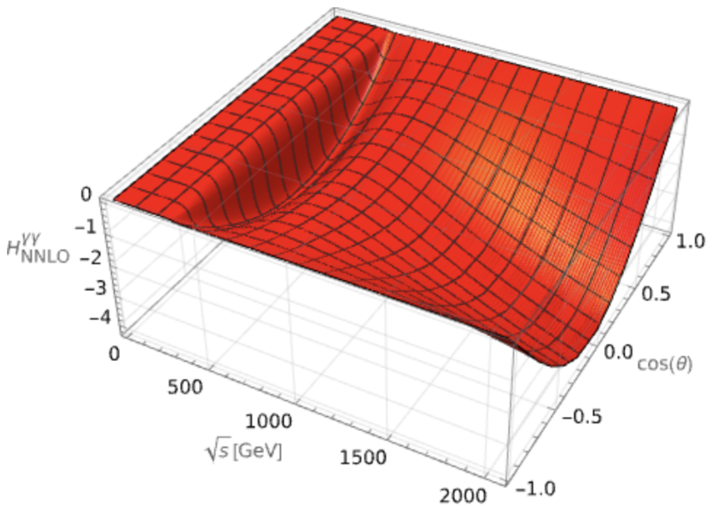

Figura 8.4.6. Cuadrícula de la función virtual dura desde 8 GeV hasta 2.2 TeV.

8.4.2 Evaluación analítica de las amplitudes de helicidad masivas a dos bucles para $gg \to \gamma\gamma$

Con este objetivo, consideramos el cálculo de las amplitudes de helicidad a dos bucles para la producción de un par de fotones en el canal de fusión de gluones con un quark pesado en el bucle.

Con respecto al proceso anterior, $q\bar{q} \to \gamma\gamma$, la situación es más complicada, ya que tenemos más topologías, más diagramas y, por lo tanto, un mayor número de MIs. En particular, obtuvimos las siguientes topologías (sin contar el intercambio de partículas externas) que se muestran en la Fig. 8.4.7.

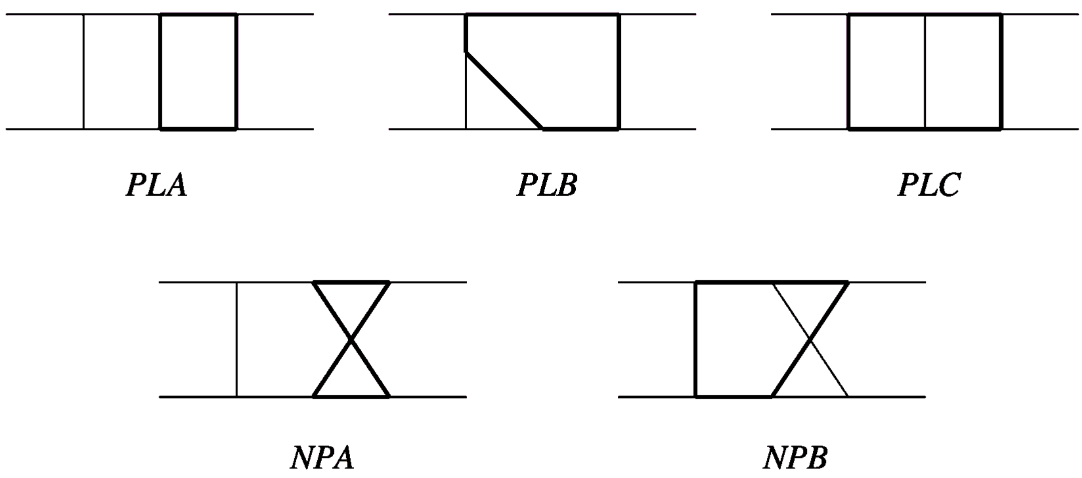

Figura 8.4.7. Diferentes topologías para los diagramas de dos bucles con bucle de quarks pesados internos.

Reducimos todos los integrales escalares, aprovechando las simetrías de las diferentes topologías, en términos de un conjunto mínimo de 161 MIs. Las MIs se evalúan mediante EDs. En particular, el sector elíptico encontrado es el mismo discutido en el canal de aniquilación de quarks. Adoptamos el procedimiento para poner el sistema en la forma factorizada en ϵ, a pesar de la presencia de MIs cuya estructura analítica involucra funciones elípticas. El procedimiento introduce períodos y funciones trascendentales en la matriz de EDs. Luego proporcionamos cuatro conjuntos diferentes de letras: algebraicas, racionales, elípticas y modulares, basadas en el tipo de funciones que aparecen como elementos de la matriz de formas diferenciales. Las MIs se expresan formalmente en términos de integrales iteradas sobre los diferentes núcleos de integración, lo que implica simplificaciones a nivel de amplitud e integrando. Resumimos estas simplificaciones en la Tabla 8.4.1.

EDs canónicas	**Amplitudes de helicidad en términos de integrales iteradas**
161 MIs	2160 integrales iteradas hasta peso 4
73 núcleos de integración	65 núcleos de integración
17 núcleos elípticos	11 núcleos elípticos

Cuadro 8.4.1. Simplificaciones obtenidas al escribir las amplitudes de helicidad en términos de integrales iteradas.

8.4.3 Dependencia completa de la masa del quark top en la producción de dos fotones a NNLO en QCD

Para este fin, incluimos la amplitud de dispersión calculada en [1] junto con los resultados previamente conocidos para presentar nuestros resultados sobre la producción completa de dos fotones a NNLO en QCD perturbativa, teniendo en cuenta la dependencia de la masa del quark top. Estudiamos la producción aislada de dos fotones en colisiones pp a una energía en el centro de masas de $\sqrt{13}$ TeV, utilizando los cortes fiduciales del estudio de la Colaboración ATLAS [165]. Consideramos todas las contribuciones masivas hasta NNLO y también calculamos las contribuciones Real-Virtual (RV) y Double-Real (RR) ya conocidas para incluirlas en una nueva versión del código 2γ`NNLO`. Presentamos varias distribuciones numéricas en la masa invariante del par de fotones. Entre los diferentes gráficos, los más importantes son el que corresponde a nuestros factores de forma de dos bucles en comparación con el cuadro de un bucle $gg \to \gamma\gamma$ en la Fig. 8.4.8, el resultado completo a NNLO en la Fig. 8.4.9 y la comparación de todos los resultados masivos en la Fig. 8.4.10.

En la Fig. 8.4.8 (panel superior) mostramos la proporción entre la distribución de masa invariante completamente masiva y sin masa de la función dura de dos bucles. Como era de esperar, la distribución muestra su pico característico alrededor del umbral de pares de quarks top ($2m_t$). La comparación es con el panel inferior, en el cual mostramos las contribuciones ya conocidas del cuadro de un bucle $gg \to \gamma\gamma$. Las dos contribuciones son relevantes para el estudio completo a NNLO de las contribuciones masivas, como podemos ver en la Fig. 8.4.10.

En la Fig. 8.4.9 mostramos la distribución completa de masa invariante a NNLO en el panel superior, y en el panel inferior la proporción entre la distribución de masa invariante completamente masiva y la sin masa.

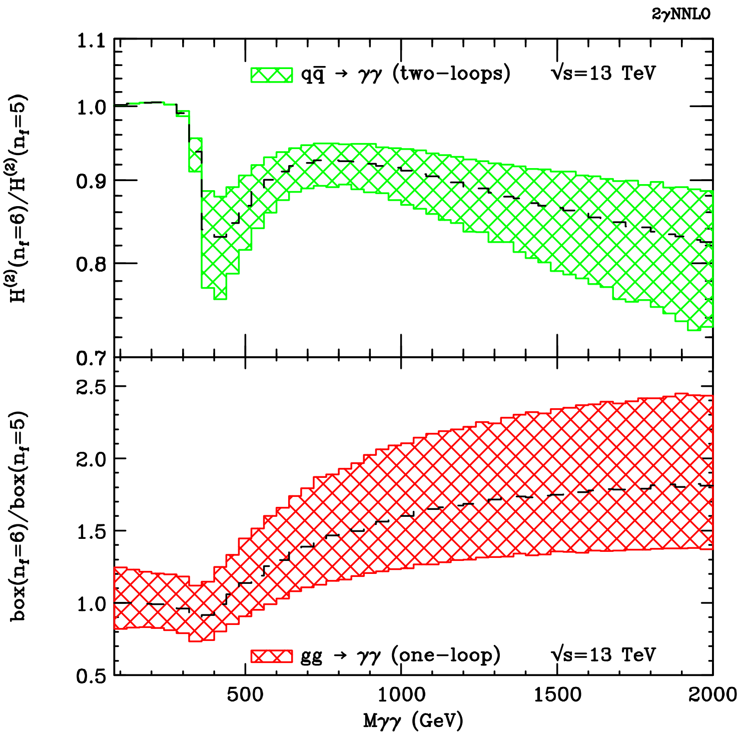

Figura 8.4.8. Proporción de correcciones masivas de dos bucles para $q\bar{q}$ respecto al caso sin masa (panel superior) y proporción del cuadro de un bucle $gg \to \gamma\gamma$ respecto al caso sin masa (panel inferior).

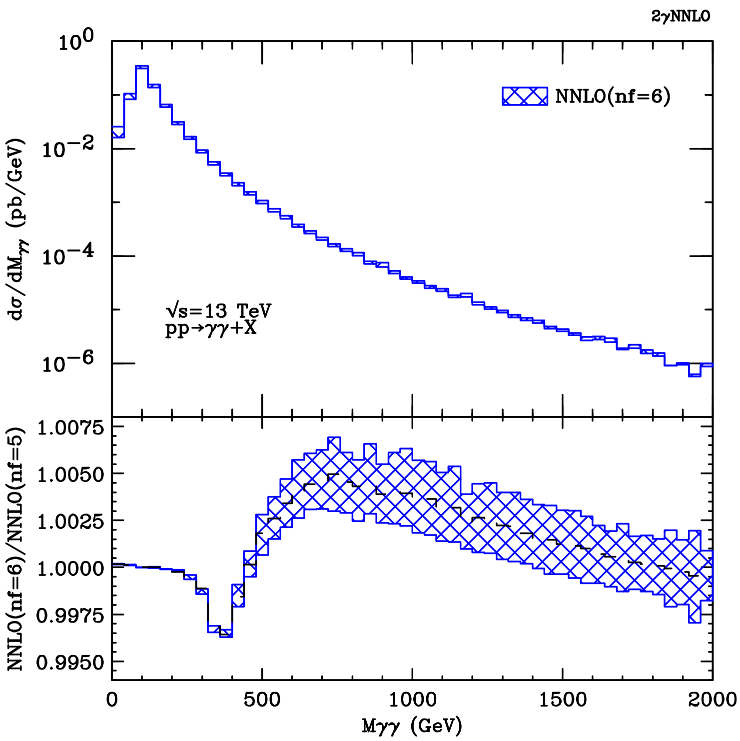

Figura 8.4.9. Distribución de masa invariante a NNLO con dependencia completa de la masa del quark top.

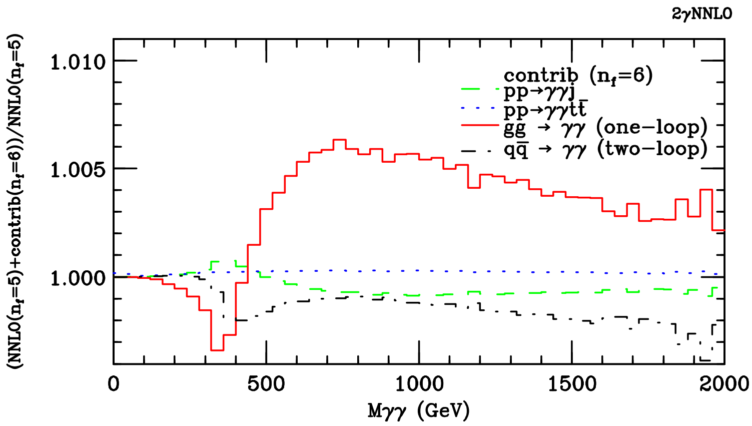

Figura 8.4.10. Proporciones de cada contribución masiva respecto a la sección eficaz sin masa a NNLO.

Appendix A

One-forms and wedge product

In this Appendix we provide a detailed mathematical description about one-forms and wedge product. For a detailed review see Ref. [228, 229, 230]. Given a $\mathbb{C}^k$ differentiable manifold M and a point $p \in M$, we denote by T_pM the tangent space at p, defined as the set of all tangent vectors at p. We can assign to every point on M a tangent space in order to obtain a new manifold, this is the so-called *tangent bundle*:

$$TM = \bigsqcup_{p\in M} T_pM. \tag{0.1}$$

In order to define the one-forms we need to introduce the *cotangent vector bundle* $T^\star M$. We denote by $T_p^\star M$ the dual vector space of the tangent space T_pM:

$$T_p^\star M = \mathrm{Hom}(T_pM, \mathbb{R}), \tag{0.2}$$

where $Hom(T_pM, \mathbb{R})$ is the space of all linear maps from T_pM to $\mathbb{R}$. Then, in a manner similar to eq. (0.1), we can define the cotangent vector bundle as:

$$T^\star M = \bigsqcup_{p\in M} T_p^\star M. \tag{0.3}$$

Elements of the cotangent bundle are called differential one-forms. More rigorously, a one-form on a manifold M is a smooth section of the cotangent bundle $T^\star M$, i.e. the one-form ω is a map:

$$\omega :\ M \to T^\star M, \tag{0.4}$$

such that $\forall v \in T_pM \longrightarrow w_p(v) \in \mathbb{R}$.

Locally we can define a one-form on a differentiable manifold M as:

$$\omega = \sum_i f_i(p)\, dp^i, \tag{0.5}$$

where $f_i(p)$ are smooth functions depending on $p \in M$ and dp^i are a set of differentials.

The product between one-forms is the *wedge product*, that is a bilinear and anti-symmetric operation that satisfy:

$$
\begin{aligned}
&(a\,\omega_1 \;+\; b\,\omega_2) \wedge w_3 = a\,(w_1 \wedge w_3) \;+\; b\,(\omega_2 \wedge w_3),\\
&\omega_1 \wedge \omega_2 = -\omega_2 \wedge \omega_1,
\end{aligned}
\tag{0.6}
$$

from which it follows that $\omega_1 \wedge \omega_1 = 0$.

In local coordinates, given $\omega_1 = \sum_i f_i(p)\,dp^i$ and $\omega_2 = \sum_j g_j(p)\,dp^j$:

$$
\omega_1 \wedge \omega_2 = \sum_i \sum_j \, f_i(p)\, g_j(p)\,(dp^i \wedge dp^j) \tag{0.7}
$$

We already said that $\mathbb{A}(\underline{x}, \epsilon)$ is a matrix which entries are the one-forms. It is possible to wedge matrix-valued forms to obtain a two-form matrix, where each entry is the wedge product of the corresponding forms.

As example, we consider two 2×2 matrix-valued one forms:

$$
\mathbb{A} = \begin{pmatrix} \alpha_1 & \alpha_2 \\ \alpha_3 & \alpha_4 \end{pmatrix}, \qquad \mathbb{B} = \begin{pmatrix} \beta_1 & \beta_2 \\ \beta_3 & \beta_4 \end{pmatrix}, \tag{0.8}
$$

where $\{\alpha_i\}_{i=1,\cdots,4}$ and $\{\beta_i\}_{i=1,\cdots,4}$ are one-forms.

The wedge product between two matrices can be defined as a resulting matrix $\mathbb{C}$. If we represents the elements of $\mathbb{A}$ by A_{ij} and the elements of $\mathbb{B}$ as B_{ij}, the elements of the resulting matrix are:

$$
C_{ij} = \sum_{s=1}^{2} A_{is} \wedge B_{sj}, \tag{0.9}
$$

such that:

$$
\mathbb{A} \wedge \mathbb{B} = \mathbb{C} = \begin{pmatrix} \alpha_1 \wedge \beta_1 \;+\; \alpha_2 \wedge \beta_3 & \alpha_1 \wedge \beta_2 \;+\; \alpha_2 \wedge \beta_4 \\ \alpha_3 \wedge \beta_1 \;+\; \alpha_4 \wedge \beta_3 & \alpha_3 \wedge \beta_2 \;+\; \alpha_4 \wedge \beta_4 \end{pmatrix}. \tag{0.10}
$$

Appendix B

MIs for $q\overline{q} \to \gamma\gamma$

B.1 MIs

$$
\begin{aligned}
&\mathcal{J}_1 = \mathcal{I}_{\mathrm{PLA}}(0,0,0,2,0,0,2,0,0), && \mathcal{J}_{22}(s,t) = \mathcal{I}_{\mathrm{PLA}}(1,1,1,2,0,0,1,0,0),\\
&\mathcal{J}_2(s) = \mathcal{I}_{\mathrm{PLA}}(0,1,2,0,0,0,2,0,0), && \mathcal{J}_{23}(s,t) = \mathcal{I}_{\mathrm{PLA}}(1,1,1,2,0,0,1,-1,0),\\
&\mathcal{J}_3(s) = \mathcal{I}_{\mathrm{PLA}}(0,0,0,2,1,2,0,0,0), && \mathcal{J}_{24}(s,t) = \mathcal{I}_{\mathrm{PLA}}(1,0,1,1,1,0,1,0,0),\\
&\mathcal{J}_4(s) = \mathcal{I}_{\mathrm{PLA}}(0,0,2,1,2,0,0,0,0), && \mathcal{J}_{25}(s,t) = \mathcal{I}_{\mathrm{PLA}}(1,0,1,2,1,0,1,0,0),\\
&\mathcal{J}_5(s) = \mathcal{I}_{\mathrm{PLA}}(0,0,1,2,2,0,0,0,0), && \mathcal{J}_{26}(s,t) = \mathcal{I}_{\mathrm{PLA}}(1,0,0,2,1,1,1,0,0),\\
&\mathcal{J}_6(s) = \mathcal{I}_{\mathrm{PLA}}(0,1,2,0,2,1,0,0,0), && \mathcal{J}_{27}(s,t) = \mathcal{I}_{\mathrm{PLA}}(1,0,0,3,1,1,1,0,0),\\
&\mathcal{J}_7(s) = \mathcal{I}_{\mathrm{PLA}}(0,0,0,2,1,1,1,0,0), && \mathcal{J}_{28}(s,t) = \mathcal{I}_{\mathrm{PLA}}(1,0,0,2,1,1,1,0,-1),\\
&\mathcal{J}_8(s) = \mathcal{I}_{\mathrm{PLA}}(0,0,1,3,1,0,1,0,0), && \mathcal{J}_{29}(s,t) = \mathcal{I}_{\mathrm{PLA}}(1,1,1,1,1,0,1,0,0),\\
&\mathcal{J}_9(s) = \mathcal{I}_{\mathrm{PLA}}(0,1,1,2,0,0,1,0,0), && \mathcal{J}_{30}(s,t) = \mathcal{I}_{\mathrm{NPL}}(1,0,0,1,1,1,1,0,0),\\
&\mathcal{J}_{10}(s) = \mathcal{I}_{\mathrm{PLA}}(0,1,2,1,0,0,2,0,0), && \mathcal{J}_{31}(s,t) = \mathcal{I}_{\mathrm{NPL}}(2,0,0,1,1,1,1,0,0),\\
&\mathcal{J}_{11}(s) = \mathcal{I}_{\mathrm{PLA}}(1,0,0,2,1,1,0,0,0), && \mathcal{J}_{32}(s,t) = \mathcal{I}_{\mathrm{NPL}}(1,0,0,1,2,1,1,0,0),\\
&\mathcal{J}_{12}(s) = \mathcal{I}_{\mathrm{PLA}}(2,0,0,1,1,1,0,0,0), && \mathcal{J}_{33}(s,t) = \mathcal{I}_{\mathrm{NPL}}(1,1,0,1,1,1,1,0,0),\\
&\mathcal{J}_{13}(s) = \mathcal{I}_{\mathrm{PLA}}(1,0,0,2,1,2,0,0,0), && \mathcal{J}_{34}(s,t) = \mathcal{I}_{\mathrm{NPL}}(1,1,0,2,1,1,1,0,0),\\
&\mathcal{J}_{14}(s) = \mathcal{I}_{\mathrm{PLA}}(0,1,1,1,1,1,0,0,0), && \mathcal{J}_{35}(s,t) = \mathcal{I}_{\mathrm{PLA}}(1,1,1,1,1,1,1,0,0),\\
&\mathcal{J}_{15}(s) = \mathcal{I}_{\mathrm{PLA}}(0,2,1,0,1,1,1,0,0), && \mathcal{J}_{36}(s,t) = \mathcal{I}_{\mathrm{PLA}}(1,1,1,1,1,1,1,-1,0),\\
&\mathcal{J}_{16}(s) = \mathcal{I}_{\mathrm{PLA}}(0,1,1,1,0,1,1,0,0), && \mathcal{J}_{37}(s,t) = \mathcal{I}_{\mathrm{PLA}}(1,1,1,1,1,1,1,0,-1),\\
&\mathcal{J}_{17}(s) = \mathcal{I}_{\mathrm{NPL}}(0,1,0,1,1,1,1,0,0), && \mathcal{J}_{38}(s,t) = \mathcal{I}_{\mathrm{PLA}}(1,1,1,1,1,1,1,-1,-1),\\
&\mathcal{J}_{18}(s) = \mathcal{I}_{\mathrm{PLA}}(0,1,1,1,1,1,1,0,0), && \mathcal{J}_{39}(s,t) = \mathcal{I}_{\mathrm{NPL}}(1,1,1,1,1,1,1,0,0),\\
&\mathcal{J}_{19}(s) = \mathcal{I}_{\mathrm{NPL}}(0,1,1,1,1,1,1,0,0), && \mathcal{J}_{40}(s,t) = \mathcal{I}_{\mathrm{NPL}}(1,1,1,1,1,1,1,-1,0),\\
&\mathcal{J}_{20}(s) = \mathcal{I}_{\mathrm{NPL}}(0,1,1,2,1,1,1,0,0), && \mathcal{J}_{41}(s,t) = \mathcal{I}_{\mathrm{NPL}}(1,1,1,1,2,1,1,0,0),\\
&\mathcal{J}_{21}(s,t) = \mathcal{I}_{\mathrm{PLB}}(1,1,1,2,0,1,0,0,0), && \mathcal{J}_{42}(s,t) = \mathcal{I}_{\mathrm{NPL}}(1,1,1,1,1,1,1,-1,-1).
\end{aligned}
$$

B.2 Crossings

To complete the whole set of MIs appearing in the form factors, we have to consider also the following masters, obtained from the previous list permuting the kinematic variables:

$$
\begin{aligned}
&\mathcal{J}_{43}(t) = \mathcal{J}_{2}(t), && \mathcal{J}_{58}(s,t) = \mathcal{J}_{28}(s,-s-t),\\
&\mathcal{J}_{44}(-s-t) = \mathcal{J}_{2}(-s-t), && \mathcal{J}_{59}(s,t) = \mathcal{J}_{29}(s,-s-t),\\
&\mathcal{J}_{45}(-s-t) = \mathcal{J}_{4}(-s-t), && \mathcal{J}_{60}(s,t) = \mathcal{J}_{30}(s,-s-t),\\
&\mathcal{J}_{46}(t) = \mathcal{J}_{4}(t), && \mathcal{J}_{61}(s,t) = \mathcal{J}_{31}(s,-s-t),\\
&\mathcal{J}_{47}(-s-t) = \mathcal{J}_{5}(-s-t), && \mathcal{J}_{62}(s,t) = \mathcal{J}_{32}(s,-s-t),\\
&\mathcal{J}_{48}(t) = \mathcal{J}_{5}(t), && \mathcal{J}_{63}(s,t) = \mathcal{J}_{33}(s,-s-t),\\
&\mathcal{J}_{49}(-s-t) = \mathcal{J}_{8}(-s-t), && \mathcal{J}_{64}(s,t) = \mathcal{J}_{34}(s,-s-t),\\
&\mathcal{J}_{50}(t) = \mathcal{J}_{8}(t), && \mathcal{J}_{65}(s,t) = \mathcal{J}_{35}(s,-s-t),\\
&\mathcal{J}_{51}(s,t) = \mathcal{J}_{21}(s,-s-t), && \mathcal{J}_{66}(s,t) = \mathcal{J}_{36}(s,-s-t),\\
&\mathcal{J}_{52}(s,t) = \mathcal{J}_{22}(s,-s-t), && \mathcal{J}_{67}(s,t) = \mathcal{J}_{37}(s,-s-t),\\
&\mathcal{J}_{53}(s,t) = \mathcal{J}_{23}(s,-s-t), && \mathcal{J}_{68}(s,t) = \mathcal{J}_{38}(s,-s-t),\\
&\mathcal{J}_{54}(s,t) = \mathcal{J}_{24}(s,-s-t), && \mathcal{J}_{69}(s,t) = \mathcal{J}_{39}(s,-s-t),\\
&\mathcal{J}_{55}(s,t) = \mathcal{J}_{25}(s,-s-t), && \mathcal{J}_{70}(s,t) = \mathcal{J}_{40}(s,-s-t),\\
&\mathcal{J}_{56}(s,t) = \mathcal{J}_{26}(s,-s-t), && \mathcal{J}_{71}(s,t) = \mathcal{J}_{41}(s,-s-t),\\
&\mathcal{J}_{57}(s,t) = \mathcal{J}_{27}(s,-s-t), && \mathcal{J}_{72}(s,t) = \mathcal{J}_{42}(s,-s-t).
\end{aligned}
$$

Appendix C

Canonical MIs for $q\bar{q} \to \gamma\gamma$

C.1 PLA canonical MIs

$$
\begin{aligned}
f_1^{\text{PLA}} &= \epsilon^2 J_1,\\
f_2^{\text{PLA}} &= \epsilon^2 y J_2(y),\\
f_3^{\text{PLA}} &= \epsilon^2 \sqrt{-4+y}\sqrt{y} J_3(y),\\
f_4^{\text{PLA}} &= \epsilon^2 \sqrt{-4+y}\sqrt{y} J_4(y) + \epsilon^2 \sqrt{-4+y}\sqrt{y} J_5(y)/2,\\
f_5^{\text{PLA}} &= \epsilon^2 y J_5(y),\\
f_6^{\text{PLA}} &= \epsilon^2 \sqrt{-4+z}\sqrt{z} J_4(z) + \epsilon^2 \sqrt{-4+z}\sqrt{z} J_5(z)/2,\\
f_7^{\text{PLA}} &= \epsilon^2 z J_5(z),\\
f_8^{\text{PLA}} &= \epsilon^2 \sqrt{-4+y} y^{3/2} J_6(y),\\
f_9^{\text{PLA}} &= \epsilon^3 y J_7(y),\\
f_{10}^{\text{PLA}} &= \epsilon^2 y J_8(y),\\
f_{11}^{\text{PLA}} &= \epsilon^2 z J_8(z),\\
f_{12}^{\text{PLA}} &= \epsilon^3 y J_9(y),\\
f_{13}^{\text{PLA}} &= -1/2(\epsilon^3 \sqrt{-4-y}\sqrt{y} J_1)/(1+2\epsilon) + \epsilon^2 \sqrt{-4-y} y^{3/2} J_{10}(y),\\
f_{14}^{\text{PLA}} &= \epsilon^3 \sqrt{-4+y}\sqrt{y} J_{11}(y) + \epsilon^3 \sqrt{-4+y}\sqrt{y} J_{12}(y)/2 + \epsilon^2 \sqrt{-4+y}\sqrt{y} J_{13}(y),\\
f_{15}^{\text{PLA}} &= \epsilon^3 y J_{11}(y),\\
f_{16}^{\text{PLA}} &= \epsilon^3 y J_{12}(y),\\
f_{17}^{\text{PLA}} &= (1-2\epsilon)\epsilon^3 y J_{14}(y),\\
f_{18}^{\text{PLA}} &= \epsilon^3 y^2 J_{15}(y),\\
f_{19}^{\text{PLA}} &= \epsilon^4 y J_{16}(y),\\
f_{20}^{\text{PLA}} &= -(\epsilon^3 y \sqrt{-4+z}\sqrt{z} J_{22}(y,z)),\\
f_{21}^{\text{PLA}} &= -(\epsilon^2 y J_5(z))/2 + \epsilon^3 y J_{23}(y,z),\\
f_{22}^{\text{PLA}} &= \epsilon^4 (y+z) J_{24}(y,z),\\
f_{23}^{\text{PLA}} &= \epsilon^3 \sqrt{y}\sqrt{z}\sqrt{yz-4(y+z)} J_{25}(y,z),\\
f_{24}^{\text{PLA}} &= \epsilon^3 \sqrt{y}\sqrt{y+yz^2-2z(y+2z)} J_{26}(y,z),
\end{aligned}
$$

$$
\begin{aligned}
f_{25}^{\mathrm{PLA}} &= \epsilon^3\sqrt{y}\sqrt{z}\sqrt{yz-4(y+z)}J_{26}(y,z)+\epsilon^2\sqrt{y}\sqrt{z}\sqrt{yz-4(y+z)}J_{27}(y,z),\\
f_{26}^{\mathrm{PLA}} &= \epsilon^3 yJ_{28}(y,z),\\
f_{27}^{\mathrm{PLA}} &= \epsilon^4\sqrt{-4+y}y^(3/2)J_{18}(y),\\
f_{28}^{\mathrm{PLA}} &= \epsilon^4 yzJ_{29}(y,z),\\
f_{29}^{\mathrm{PLA}} &= \epsilon^4 y^(3/2)\sqrt{z}\sqrt{yz-4(y+z)}J_{35}(y,z),\\
f_{30}^{\mathrm{PLA}} &= (\epsilon^3\sqrt{-4+y}\sqrt{y}(y+2z)J_{25}(y,z))/2-\epsilon^3\sqrt{-4+y}\sqrt{y}(y+2z)J_{26}(y,z)\\
&\quad-\epsilon^2\sqrt{-4+y}\sqrt{y}(y+2z)J_{27}(y,z)+\epsilon^4\sqrt{-4+y}y^{3/2}J_{36}(y,z),\\
f_{31}^{\mathrm{PLA}} &= \epsilon^4y^2J_{35}(y,z)-\epsilon^4y^2J_{37}(y,z),\\
f_{32}^{\mathrm{PLA}} &= 2\epsilon^4(y+z)J_{14}(y)-\epsilon^3yzJ_{15}(y)-2\epsilon^4zJ_{16}(y)+\epsilon^4y(y+z)J_{18}(y)+\epsilon^4yJ_{24}(y,z)\\
&\quad-(\epsilon^3y(y+2z)J_{25}(y,z))/4+(\epsilon^3y(y+2z)J_{26}(y,z))/2+(\epsilon^2y(y+2z)J_{27}(y,z))/2\\
&\quad+\epsilon^4yzJ_{35}(y,z)-(\epsilon^4(-2+y)yJ_{36}(y,z))/2-\epsilon^4yzJ_{37}(y,z)-\epsilon^4yJ_{38}(y,z).
\end{aligned}
$$

C.2 NPL canonical MIs

$$
\begin{aligned}
f_1^{\mathrm{NPL}} &= \epsilon^2\mathcal{J}_1,\\
f_2^{\mathrm{NPL}} &= \epsilon^2 y\mathcal{J}_2(y),\\
f_3^{\mathrm{NPL}} &= \frac{1}{2}\mathcal{J}_5(y)\sqrt{y-4}\sqrt{y}\epsilon^2+\mathcal{J}_4(y)\sqrt{y-4}\sqrt{y}\epsilon^2,\\
f_4^{\mathrm{NPL}} &= \epsilon^2 y\mathcal{J}_5(y),\\
f_5^{\mathrm{NPL}} &= \frac{1}{2}\mathcal{J}_5(z)\sqrt{z-4}\sqrt{z}\epsilon^2+\mathcal{J}_4(z)\sqrt{z-4}\sqrt{z}\epsilon^2,\\
f_6^{\mathrm{NPL}} &= \epsilon^2 z\mathcal{J}_5(z),\\
f_7^{\mathrm{NPL}} &= \frac{1}{2}\mathcal{J}_5(w)\sqrt{-y-z-4}\sqrt{-y-z}\epsilon^2+\mathcal{J}_4(w)\sqrt{-y-z-4}\sqrt{-y-z}\epsilon^2,\\
f_8^{\mathrm{NPL}} &= -\epsilon^2(y+z)\mathcal{J}_5(w),\\
f_9^{\mathrm{NPL}} &= \epsilon^2 y\mathcal{J}_8(y),\\
f_{10}^{\mathrm{NPL}} &= \epsilon^2 z\mathcal{J}_8(z),\\
f_{11}^{\mathrm{NPL}} &= -\epsilon^2(y+z)\mathcal{J}_8(w),\\
f_{12}^{\mathrm{NPL}} &= \epsilon^3 y\mathcal{J}_9(y),\\
f_{13}^{\mathrm{NPL}} &= \epsilon^2\sqrt{-y-4}y^{3/2}\mathcal{J}_{10}(y)-\frac{\epsilon^4\sqrt{-y-4}y^{3/2}\mathcal{J}_1}{4y\epsilon^2+2y\epsilon},\\
f_{14}^{\mathrm{NPL}} &= \epsilon^4 y\mathcal{J}_{16}(y),\\
f_{15}^{\mathrm{NPL}} &= \epsilon^4 y\mathcal{J}_{17}(y),\\
f_{16}^{\mathrm{NPL}} &= -\epsilon^3 y\sqrt{z-4}\sqrt{z}\mathcal{J}_{22}(y,z,w),\\
f_{17}^{\mathrm{NPL}} &= \epsilon^3 y\mathcal{J}_{23}(y,z,w)-\frac{1}{2}\epsilon^2 y\mathcal{J}_5(z),\\
f_{18}^{\mathrm{NPL}} &= -\epsilon^3 y\sqrt{-y-z-4}\sqrt{-y-z}\mathcal{J}_{22}(y,w,z),\\
f_{19}^{\mathrm{NPL}} &= y\mathcal{J}_{23}(y,w,z)\epsilon^3-\frac{1}{2}y\mathcal{J}_5(w)\epsilon^2,\\
f_{20}^{\mathrm{NPL}} &= \epsilon^4(y+z)\mathcal{J}_{24}(y,z,w),
\end{aligned}
$$

$$
\begin{aligned}
f_{21}^{\text{NPL}} &= \epsilon^3\sqrt{y}\sqrt{z}\sqrt{yz-4(y+z)}\mathcal{J}_{25}(y,z,w),\\
f_{22}^{\text{NPL}} &= -\epsilon^4 z\mathcal{J}_{24}(y,w,z),\\
f_{23}^{\text{NPL}} &= \epsilon^3\sqrt{y}\sqrt{-y-z}\sqrt{4z-y(y+z)}\mathcal{J}_{25}(y,w,z),\\
f_{24}^{\text{NPL}} &= \epsilon^4 yz\mathcal{J}_{29}(y,z,w),\\
f_{25}^{\text{NPL}} &= -\epsilon^4 y(y+z)\mathcal{J}_{29}(y,w,z),\\
f_{26}^{\text{NPL}} &= \epsilon^4 y\mathcal{J}_{30}(y,z,w),\\
f_{27}^{\text{NPL}} &= -y^2\sqrt{z-4}\sqrt{z}\left(\frac{\sqrt{z-4}}{2\epsilon^2\left(\epsilon y-\epsilon^2 y\right)z^{3/2}}-\frac{3z\epsilon-6\epsilon+3}{\epsilon^2\sqrt{z-4}\sqrt{z}\left(2\epsilon^2 yz-2\epsilon^3 yz\right)}\right)\mathcal{J}_5(z)\epsilon^7\\
&\quad+\frac{1}{z}\left(y^2(y+z)\left(\frac{\sqrt{-y-z-4}}{2\epsilon^2\left(\epsilon y-\epsilon^2 y\right)\sqrt{-y-z}(y+z)}\right.\right.\\
&\quad\left.\left.-\frac{3((y+z)\epsilon+2\epsilon-1)}{2(\epsilon-1)\epsilon^4 y\sqrt{-y-z-4}\sqrt{-y-z}(y+z)}\right)\mathcal{J}_5(w)\sqrt{-y-z-4}\sqrt{-y-z}\epsilon^7\right)\\
&\quad+\frac{y^2(-2z\epsilon-4\epsilon+2z+2)\mathcal{J}_8(z)\epsilon^5}{\epsilon^2 yz-\epsilon^3 yz}+\frac{y^2(-y-z-4)\mathcal{J}_4(w)\epsilon^5}{\left(\epsilon y-\epsilon^2 y\right)z}-\frac{y^2(z-4)\mathcal{J}_4(z)\epsilon^5}{\left(\epsilon y-\epsilon^2 y\right)z}\\
&\quad-\frac{y^2\mathcal{J}_{32}(y,z,w)\epsilon^3}{z}-\frac{y(y+z)\left(\frac{4\epsilon-2}{(\epsilon-1)(y+z)}-2\right)\mathcal{J}_8(w)\epsilon^3}{z},\\
f_{28}^{\text{NPL}} &= \epsilon^3\sqrt{-y-z}\sqrt{z}\sqrt{4y-z(y+z)}\mathcal{J}_{31}(y,z,w),\\
f_{29}^{\text{NPL}} &= \epsilon^4\sqrt{y}\sqrt{-y-z}\sqrt{z}\mathcal{J}_{33}(y,z,w),\\
f_{30}^{\text{NPL}} &= -\frac{1}{4}y^2\mathcal{J}_{25}(y,z,w)\epsilon^3+\frac{1}{4}(-4\epsilon-1)y(y+z)\mathcal{J}_{33}(y,z,w)\epsilon^3-y(y+z)\mathcal{J}_{34}(y,z,w)\epsilon^3\\
&\quad+\frac{1}{4}(-y-z)(y+z)\mathcal{J}_{31}(y,z,w),\\
f_{31}^{\text{NPL}} &= \epsilon^4 y^2\mathcal{J}_{19}(y),\\
f_{32}^{\text{NPL}} &= \frac{\epsilon^4 y^2(y+16)\mathcal{J}_{20}(y)}{4\epsilon+2},\\
f_{33}^{\text{NPL}} &= \epsilon^4 y^3\mathcal{J}_{39}(y,z,w),\\
f_{34}^{\text{NPL}} &= \epsilon^4 y^2\mathcal{J}_{40}(y,z,w),\\
f_{35}^{\text{NPL}} &= \epsilon^4 y^4\mathcal{J}_{41}(y,z,w),\\
f_{36}^{\text{NPL}} &= \epsilon^4 y\mathcal{J}_{42}(y,z,w).
\end{aligned}
$$

Appendix D

RV - RR contributions to diphoton production

D.0.1 Real-Virtual contributions to diphoton production

We consider the computation of the Real-Virtual contributions to diphoton production in association with an emission of real radiation. We have two different channels, i.e. $q\overline{q} \to \gamma\gamma g$ and $qg \to \gamma\gamma q$. Here we discuss the computation of the interference between the one-loop in the $q\overline{q}$-channel (Fig. D.0.1) and the tree-level with the emission of one gluon in Fig. D.0.2. The qg-channel can be obtained directly from crossing. The diagrams in this Appendix are drawn using `FeynArts` [231].

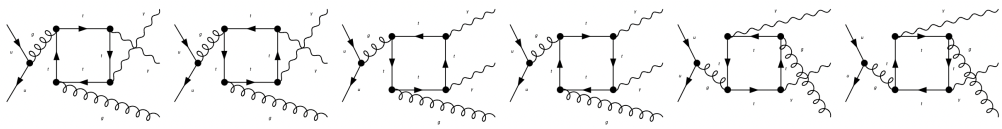

Figure D.0.1. One-loop diagrams for $q\overline{q} \to \gamma\gamma g$ with top quark loop.

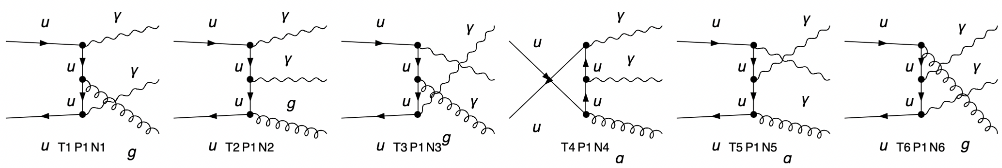

Figure D.0.2. Tree-level diagrams for $q\overline{q} \to \gamma\gamma g$.

At the partonic level:

$$q(p_1) + \overline{q}(p_2) \to g(p_3) + \gamma(p_4) + \gamma(p_5)\,, \tag{0.1}$$

where all the external particles are on-shell, i.e. $p_i^2 = 0$, and there is a heavy quark with mass m_t running in the loop.

The kinematics for this process is described by the following set of Mandelstam invariants:

$$\begin{aligned}
&(p_1+p_2)^2 = s_{12}, \quad (p_1-p_3)^2 = s_{13}, \quad (p_1-p_4)^2 = s_{14}, \quad (p_1-p_5)^2 = s_{15},\\
&(p_2-p_3)^2 = s_{23}, \quad (p_2-p_4)^2 = s_{24}, \quad (p_2-p_5)^2 = s_{25},\\
&(p_3+p_4)^2 = -s_{12}-s_{13}-s_{14}-s_{23}-s_{24}, \quad (p_3+p_5)^2 = s_{12}+s_{14}+s_{24}.
\end{aligned} \tag{0.2}$$

The diagrams in Fig. D.0.1 are described by the following scalar integral families:

TopoA

$$\begin{aligned} &D_1 = k^2 - m_t^2, \quad D_2 = (k - p_1 - p_2)^2 - m_t^2, \quad D_3 = (k - p_1 - p_2 + p_4)^2 - m_t^2, \\ &D_4 = (k - p_3)^2 - m_t^2, \quad D_5 = (k - p_1)^2 - m_t^2, \end{aligned} \tag{0.3}$$

TopoB

$$\begin{aligned} &D_1 = k^2 - m_t^2, \quad D_2 = (k - p_1 - p_2)^2 - m_t^2, \quad D_3 = (k - p_3 - p_4)^2 - m_t^2, \\ &D_4 = (k - p_3)^2 - m_t^2, \quad D_5 = (k - p_1)^2 - m_t^2, \end{aligned} \tag{0.4}$$

TopoC

$$\begin{aligned} &D_1 = k^2 - m_t^2, \quad D_2 = (k - p_1 - p_2)^2 - m_t^2, \quad D_3 = (k - p_1 - p_2 + p_4)^2 - m_t^2, \\ &D_4 = (k - p_1 - p_2 + p_3 + p_4)^2 - m_t^2, \quad D_5 = (k - p_1)^2 - m_t^2. \end{aligned} \tag{0.5}$$

These scalar integral families are defined as follows:

$$\mathcal{I}_{topo}(a_1, ..., a_9) = \int \frac{\mathcal{D}k}{D_1^{a_1} D_2^{a_2} D_3^{a_3} D_4^{a_4} D_5^{a_5}}\,, \tag{0.6}$$

where $topo \in \{\text{TopoA}, \text{TopoB}, \text{TopoC}\}$ labels the families and the scalar products $D_1, ..., D_5$ are given in eqs. (0.3), (0.4) and (0.5). The indices $a_1, ..., a_5$ are positive and the integration measure is defined as:

$$\mathcal{D}k = \frac{d^d k}{i\pi^{2-\epsilon}\Gamma(1+\epsilon)} \left(\frac{\mu^2}{m_t^2}\right)^{-\epsilon}. \tag{0.7}$$

We can reduce each integral related to these scalar integral families in terms of nine MIs for topology:

$$\begin{aligned} &I_{topo}(0,1,0,1,0), \quad I_{topo}(0,1,1,1,0), \quad I_{topo}(1,0,0,0,0), \\ &I_{topo}(1,0,1,0,0), \quad I_{topo}(1,0,1,1,0), \quad I_{topo}(1,1,0,0,0), \\ &I_{topo}(1,1,0,1,0), \quad I_{topo}(1,1,1,0,0), \quad I_{topo}(1,1,1,1,0), \end{aligned} \tag{0.8}$$

The amplitude is finite, not only in four dimensions, but also after integrating over the transverse momentum of the diphoton pair $p_T^{\gamma\gamma}$.

D.0.2 Double-Real contributions to diphoton production

We have calculated the double-real amplitudes associated with diphoton production in the context of the emission of two on-shell top quarks. There are two different channels, i.e. $q\bar{q} \to \gamma\gamma t\bar{t}$ and $gg \to \gamma\gamma t\bar{t}$, at the NNLO. This sub-process can be

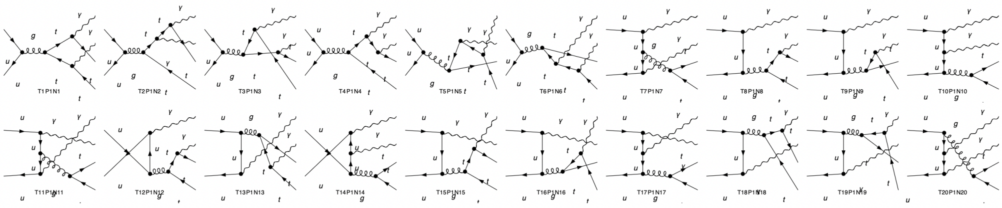

Figure D.0.3. Diagrams for $q\bar{q} \to \gamma\gamma t\bar{t}$.

effectively detected experimentally and then subtracted, but the experimental analyses do not perform such a subtraction [165], and therefore the most complete NNLO description of diphoton production must include this contribution. For the $q\bar{q}$ channel we have 20 diagrams contributing to the amplitude, shown in Fig. D.0.3. The NNLO contribution is given by the square modulus of the amplitude computed with these diagrams.

For the $gg \to \gamma\gamma t\bar{t}$ we have 30 diagrams contributing to the amplitude, represented in Fig. D.0.4. Also in this case the NNLO contribution is given by the square modulus

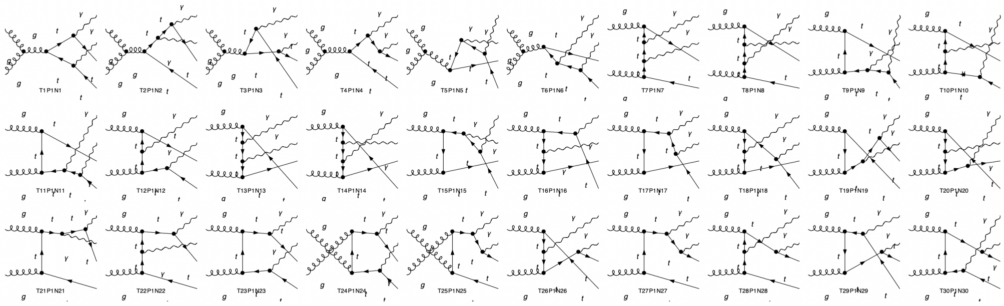

Figure D.0.4. Diagrams for $gg \to \gamma\gamma t\bar{t}$.

of the amplitude.

All the scattering amplitudes presented in this Appendix were cross-checked with the Openloops package [70].

Appendix E

MIs for $gg \to \gamma\gamma$

$$
\begin{aligned}
\mathcal{J}_{1} &= \mathcal{I}_{\mathrm{PLA}}(0,2,2,0,0,0,0,0,0), \\
\mathcal{J}_{2} &= \mathcal{I}_{\mathrm{PLA}}(2,2,0,0,0,1,0,0,0), \\
\mathcal{J}_{3} &= \mathcal{I}_{\mathrm{PLA}}(0,2,2,0,0,0,1,0,0), \\
\mathcal{J}_{4} &= \mathcal{I}_{\mathrm{PLA}}(0,2,2,0,0,1,0,0,0), \\
\mathcal{J}_{5} &= \mathcal{I}_{\mathrm{PLA}_{\sigma_{124}}}(0,2,2,0,0,0,1,0,0), \\
\mathcal{J}_{6} &= \mathcal{I}_{\mathrm{PLA}_{\sigma_{123}}}(0,2,2,0,0,0,1,0,0), \\
\mathcal{J}_{7} &= \mathcal{I}_{\mathrm{PLA}}(0,2,1,0,0,2,0,0,0), \\
\mathcal{J}_{8} &= \mathcal{I}_{\mathrm{PLA}_{\sigma_{12}}}(0,0,2,1,0,0,0,0,2), \\
\mathcal{J}_{9} &= \mathcal{I}_{\mathrm{PLA}_{\sigma_{12}}}(0,0,2,2,0,0,0,0,1), \\
\mathcal{J}_{10} &= \mathcal{I}_{\mathrm{PLA}}(0,0,2,1,0,0,0,0,2), \\
\mathcal{J}_{11} &= \mathcal{I}_{\mathrm{PLA}}(0,0,2,2,0,0,0,0,1), \\
\mathcal{J}_{12} &= \mathcal{I}_{\mathrm{PLA}}(0,1,2,1,0,0,1,0,0), \\
\mathcal{J}_{13} &= \mathcal{I}_{\mathrm{PLA}}(0,1,1,2,0,0,1,0,0), \\
\mathcal{J}_{14} &= \mathcal{I}_{\mathrm{PLA}}(0,2,2,1,0,0,1,0,0), \\
\mathcal{J}_{15} &= \mathcal{I}_{\mathrm{PLA}_{\sigma_{124}}}(0,1,2,1,0,0,1,0,0), \\
\mathcal{J}_{16} &= \mathcal{I}_{\mathrm{PLA}_{\sigma_{124}}}(0,1,1,2,0,0,1,0,0), \\
\mathcal{J}_{17} &= \mathcal{I}_{\mathrm{PLA}_{\sigma_{124}}}(0,2,2,1,0,0,1,0,0), \\
\mathcal{J}_{18} &= \mathcal{I}_{\mathrm{PLA}_{\sigma_{123}}}(0,1,2,1,0,0,1,0,0), \\
\mathcal{J}_{19} &= \mathcal{I}_{\mathrm{PLA}_{\sigma_{123}}}(0,1,1,2,0,0,1,0,0), \\
\mathcal{J}_{20} &= \mathcal{I}_{\mathrm{PLA}_{\sigma_{123}}}(0,2,2,1,0,0,1,0,0), \\
\mathcal{J}_{21} &= \mathcal{I}_{\mathrm{PLA}}(2,2,0,0,0,1,1,0,0), \\
\mathcal{J}_{22} &= \mathcal{I}_{\mathrm{PLA}}(1,0,2,0,0,1,0,0,1), \\
\mathcal{J}_{23} &= \mathcal{I}_{\mathrm{PLA}}(2,0,2,0,0,1,0,0,1), \\
\mathcal{J}_{24} &= \mathcal{I}_{\mathrm{PLA}}(0,1,3,0,0,1,0,0,1), \\
\mathcal{J}_{25} &= \mathcal{I}_{\mathrm{PLA}_{\sigma_{12}}}(0,1,3,1,0,0,0,0,1), \\
\mathcal{J}_{26} &= \mathcal{I}_{\mathrm{PLA}}(0,1,3,1,0,0,0,0,1), \\
\mathcal{J}_{27} &= \mathcal{I}_{\mathrm{PLA}}(0,1,2,0,0,0,1,0,1), \\
\mathcal{J}_{28} &= \mathcal{I}_{\mathrm{PLA}_{\sigma_{124}}}(0,1,2,0,0,0,1,0,1), \\
\mathcal{J}_{29} &= \mathcal{I}_{\mathrm{PLA}_{\sigma_{123}}}(0,1,2,0,0,0,1,0,1), \\
\mathcal{J}_{30} &= \mathcal{I}_{\mathrm{PLC}}(2,2,0,0,0,1,1,0,0), \\
\mathcal{J}_{31} &= \mathcal{I}_{\mathrm{PLC}}(0,1,1,0,1,1,0,1,0), \\
\mathcal{J}_{32} &= \mathcal{I}_{\mathrm{PLC}}(0,0,0,2,2,0,0,1,1), \\
\mathcal{J}_{33} &= \mathcal{I}_{\mathrm{PLA}}(1,1,1,0,0,1,1,0,0), \\
\mathcal{J}_{34} &= \mathcal{I}_{\mathrm{PLA}}(1,0,2,1,0,1,0,0,1), \\
\mathcal{J}_{35} &= \mathcal{I}_{\mathrm{PLA}}(1,0,2,1,0,1,0,-1,1), \\
\mathcal{J}_{36} &= \mathcal{I}_{\mathrm{PLA}_{\sigma_{12}}}(1,0,2,1,0,1,0,0,1), \\
\mathcal{J}_{37} &= \mathcal{I}_{\mathrm{PLA}_{\sigma_{12}}}(1,0,2,1,0,1,0,-1,1), \\
\mathcal{J}_{38} &= \mathcal{I}_{\mathrm{PLA}}(1,1,1,0,0,1,0,0,1), \\
\mathcal{J}_{39} &= \mathcal{I}_{\mathrm{PLA}_{\sigma_{123}}}(0,1,1,1,0,1,0,0,1), \\
\mathcal{J}_{40} &= \mathcal{I}_{\mathrm{PLA}_{\sigma_{123}}}(0,1,2,1,0,1,0,0,1), \\
\mathcal{J}_{41} &= \mathcal{I}_{\mathrm{PLA}}(0,1,1,1,0,1,0,0,1), \\
\mathcal{J}_{42} &= \mathcal{I}_{\mathrm{PLA}}(0,1,2,1,0,1,0,0,1), \\
\mathcal{J}_{43} &= \mathcal{I}_{\mathrm{PLA}_{\sigma_{12}}}(0,1,1,1,0,1,0,0,1), \\
\mathcal{J}_{44} &= \mathcal{I}_{\mathrm{PLA}_{\sigma_{12}}}(0,1,2,1,0,1,0,0,1), \\
\mathcal{J}_{45} &= \mathcal{I}_{\mathrm{PLA}}(0,1,2,1,0,0,1,0,1), \\
\mathcal{J}_{46} &= \mathcal{I}_{\mathrm{PLA}}(0,1,3,1,0,0,1,0,1), \\
\mathcal{J}_{47} &= \mathcal{I}_{\mathrm{PLA}}(0,1,2,1,-1,0,1,0,1), \\
\mathcal{J}_{48} &= \mathcal{I}_{\mathrm{PLA}_{\sigma_{12}}}(0,1,2,1,0,0,1,0,1), \\
\mathcal{J}_{49} &= \mathcal{I}_{\mathrm{PLA}_{\sigma_{12}}}(0,1,3,1,0,0,1,0,1), \\
\mathcal{J}_{50} &= \mathcal{I}_{\mathrm{PLA}_{\sigma_{12}}}(0,1,2,1,-1,0,1,0,1), \\
\mathcal{J}_{51} &= \mathcal{I}_{\mathrm{PLA}_{\sigma_{123}}}(0,1,2,1,0,0,1,0,1), \\
\mathcal{J}_{52} &= \mathcal{I}_{\mathrm{PLA}_{\sigma_{123}}}(0,1,3,1,0,0,1,0,1), \\
\mathcal{J}_{53} &= \mathcal{I}_{\mathrm{PLA}_{\sigma_{123}}}(0,1,2,1,-1,0,1,0,1), \\
\mathcal{J}_{54} &= \mathcal{I}_{\mathrm{PLA}_{\sigma_{124}}}(0,1,2,1,0,0,1,0,1), \\
\mathcal{J}_{55} &= \mathcal{I}_{\mathrm{PLA}_{\sigma_{124}}}(0,1,3,1,0,0,1,0,1), \\
\mathcal{J}_{56} &= \mathcal{I}_{\mathrm{PLA}_{\sigma_{124}}}(0,1,2,1,-1,0,1,0,1), \\
\mathcal{J}_{57} &= \mathcal{I}_{\mathrm{PLA}_{\sigma_{1234}}}(0,1,2,1,0,0,1,0,1), \\
\mathcal{J}_{58} &= \mathcal{I}_{\mathrm{PLA}_{\sigma_{1234}}}(0,1,3,1,0,0,1,0,1),
\end{aligned}
$$

$\mathcal{J}_{59} = \mathcal{I}_{\mathrm{PLA}_{\sigma_{1234}}}(0,1,2,1,-1,0,1,0,1)$,
$\mathcal{J}_{60} = \mathcal{I}_{\mathrm{PLA}_{\sigma_{1243}}}(0,1,2,1,0,0,1,0,1)$,
$\mathcal{J}_{61} = \mathcal{I}_{\mathrm{PLA}_{\sigma_{1243}}}(0,1,3,1,0,0,1,0,1)$,
$\mathcal{J}_{62} = \mathcal{I}_{\mathrm{PLA}_{\sigma_{1243}}}(0,1,2,1,-1,0,1,0,1)$,
$\mathcal{J}_{63} = \mathcal{I}_{\mathrm{PLA}}(2,1,0,0,0,1,1,0,1)$,
$\mathcal{J}_{64} = \mathcal{I}_{\mathrm{PLC}}(1,1,1,0,1,1,0,0,0)$,
$\mathcal{J}_{65} = \mathcal{I}_{\mathrm{PLC}}(1,1,1,0,1,2,0,0,0)$,
$\mathcal{J}_{66} = \mathcal{I}_{\mathrm{PLC}_{\sigma_{12}}}(0,1,1,1,1,0,0,1,0)$,
$\mathcal{J}_{67} = \mathcal{I}_{\mathrm{PLC}_{\sigma_{12}}}(0,1,1,1,1,0,0,2,0)$,
$\mathcal{J}_{68} = \mathcal{I}_{\mathrm{PLC}}(0,1,1,1,1,0,0,1,0)$,
$\mathcal{J}_{69} = \mathcal{I}_{\mathrm{PLC}}(0,1,1,1,1,0,0,2,0)$,
$\mathcal{J}_{70} = \mathcal{I}_{\mathrm{PLC}}(0,1,1,1,1,1,0,0,0)$,
$\mathcal{J}_{71} = \mathcal{I}_{\mathrm{PLC}_{\sigma_{12}}}(1,1,1,0,1,0,0,1,0)$,
$\mathcal{J}_{72} = \mathcal{I}_{\mathrm{PLC}}(1,1,1,0,1,0,0,1,0)$,
$\mathcal{J}_{73} = \mathcal{I}_{\mathrm{PLC}}(1,2,0,1,0,1,1,0,0)$,
$\mathcal{J}_{74} = \mathcal{I}_{\mathrm{PLC}_{\sigma_{12}}}(1,0,0,1,2,0,0,1,1)$,
$\mathcal{J}_{75} = \mathcal{I}_{\mathrm{PLC}}(1,0,0,1,2,0,0,1,1)$,
$\mathcal{J}_{76} = \mathcal{I}_{\mathrm{PLC}_{\sigma_{123}}}(1,2,0,1,0,1,0,1,0)$,
$\mathcal{J}_{77} = \mathcal{I}_{\mathrm{PLC}}(1,2,0,1,0,1,0,1,0)$,
$\mathcal{J}_{78} = \mathcal{I}_{\mathrm{PLC}_{\sigma_{12}}}(1,2,0,1,0,1,0,1,0)$,
$\mathcal{J}_{79} = \mathcal{I}_{\mathrm{PLC}}(0,1,2,0,1,1,0,1,0)$,
$\mathcal{J}_{80} = \mathcal{I}_{\mathrm{PLC}}(0,2,1,0,1,1,0,1,0)$,
$\mathcal{J}_{81} = \mathcal{I}_{\mathrm{PLC}_{\sigma_{12}}}(0,0,0,2,2,0,0,1,1)$,
$\mathcal{J}_{82} = \mathcal{I}_{\mathrm{PLC}_{\sigma_{12}}}(0,1,1,0,1,1,0,1,0)$,
$\mathcal{J}_{83} = \mathcal{I}_{\mathrm{PLC}_{\sigma_{12}}}(0,1,2,0,1,1,0,1,0)$,
$\mathcal{J}_{84} = \mathcal{I}_{\mathrm{PLC}_{\sigma_{12}}}(0,2,1,0,1,1,0,1,0)$,
$\mathcal{J}_{85} = \mathcal{I}_{\mathrm{PLC}_{\sigma_{123}}}(0,1,1,0,1,1,0,1,0)$,
$\mathcal{J}_{86} = \mathcal{I}_{\mathrm{PLC}_{\sigma_{123}}}(0,1,2,0,1,1,0,1,0)$,
$\mathcal{J}_{87} = \mathcal{I}_{\mathrm{PLC}_{\sigma_{123}}}(0,2,1,0,1,1,0,1,0)$,
$\mathcal{J}_{88} = \mathcal{I}_{\mathrm{PLA}}(1,1,1,0,0,1,1,0,1)$,
$\mathcal{J}_{89} = \mathcal{I}_{\mathrm{PLA}}(1,1,1,1,0,1,0,0,1)$,
$\mathcal{J}_{90} = \mathcal{I}_{\mathrm{PLA}_{\sigma_{12}}}(1,1,1,1,0,1,0,0,1)$,
$\mathcal{J}_{91} = \mathcal{I}_{\mathrm{PLC}}(1,1,0,1,1,1,1,0,0)$,
$\mathcal{J}_{92} = \mathcal{I}_{\mathrm{PLC}_{\sigma_{12}}}(1,1,0,1,1,0,0,1,1)$,
$\mathcal{J}_{93} = \mathcal{I}_{\mathrm{PLC}}(1,1,0,1,1,0,0,1,1)$,
$\mathcal{J}_{94} = \mathcal{I}_{\mathrm{PLC}}(1,1,1,0,1,1,0,1,0)$,
$\mathcal{J}_{95} = \mathcal{I}_{\mathrm{PLC}}(1,1,1,-1,1,1,0,1,0)$,
$\mathcal{J}_{96} = \mathcal{I}_{\mathrm{PLC}_{\sigma_{12}}}(1,1,1,0,1,1,0,1,0)$,
$\mathcal{J}_{97} = \mathcal{I}_{\mathrm{PLC}_{\sigma_{12}}}(1,1,1,-1,1,1,0,1,0)$,
$\mathcal{J}_{98} = \mathcal{I}_{\mathrm{PLC}_{\sigma_{123}}}(1,1,1,0,1,1,0,1,0)$,
$\mathcal{J}_{99} = \mathcal{I}_{\mathrm{PLC}_{\sigma_{123}}}(1,1,1,-1,1,1,0,1,0)$,
$\mathcal{J}_{100} = \mathcal{I}_{\mathrm{PLC}_{\sigma_{12}}}(0,1,1,1,1,1,0,1,0)$,
$\mathcal{J}_{101} = \mathcal{I}_{\mathrm{PLC}_{\sigma_{12}}}(-1,1,1,1,1,1,0,1,0)$,
$\mathcal{J}_{102} = \mathcal{I}_{\mathrm{PLC}}(0,1,1,1,1,1,0,1,0)$,
$\mathcal{J}_{103} = \mathcal{I}_{\mathrm{PLC}}(-1,1,1,1,1,1,0,1,0)$,
$\mathcal{J}_{104} = \mathcal{I}_{\mathrm{PLC}_{\sigma_{123}}}(0,1,1,1,1,1,0,1,0)$,
$\mathcal{J}_{105} = \mathcal{I}_{\mathrm{PLC}_{\sigma_{123}}}(-1,1,1,1,1,1,0,1,0)$,
$\mathcal{J}_{106} = \mathcal{I}_{\mathrm{NPA}}(1,1,1,1,0,0,1,1,0)$,
$\mathcal{J}_{107} = \mathcal{I}_{\mathrm{NPA}}(1,2,1,1,0,0,1,1,0)$,
$\mathcal{J}_{108} = \mathcal{I}_{\mathrm{NPA}_{\sigma_{124}}}(1,1,1,1,0,0,1,1,0)$,
$\mathcal{J}_{109} = \mathcal{I}_{\mathrm{NPA}_{\sigma_{124}}}(1,2,1,1,0,0,1,1,0)$,
$\mathcal{J}_{110} = \mathcal{I}_{\mathrm{NPA}_{\sigma_{123}}}(1,1,1,1,0,0,1,1,0)$,
$\mathcal{J}_{111} = \mathcal{I}_{\mathrm{NPA}_{\sigma_{123}}}(1,2,1,1,0,0,1,1,0)$,
$\mathcal{J}_{112} = \mathcal{I}_{\mathrm{NPA}}(1,1,1,0,0,1,1,1,0)$,
$\mathcal{J}_{113} = \mathcal{I}_{\mathrm{NPA}}(1,2,1,0,0,1,1,1,0)$,
$\mathcal{J}_{114} = \mathcal{I}_{\mathrm{NPB}}(1,1,1,0,0,1,1,1,0)$,
$\mathcal{J}_{115} = \mathcal{I}_{\mathrm{NPB}_{\sigma_{124}}}(1,1,1,0,0,1,1,1,0)$,
$\mathcal{J}_{116} = \mathcal{I}_{\mathrm{NPB}_{\sigma_{123}}}(1,1,1,0,0,1,1,1,0)$,
$\mathcal{J}_{117} = \mathcal{I}_{\mathrm{PLA}}(1,1,1,1,0,1,1,0,1)$,
$\mathcal{J}_{118} = \mathcal{I}_{\mathrm{PLA}}(1,1,1,1,-1,1,1,0,1)$,
$\mathcal{J}_{119} = \mathcal{I}_{\mathrm{PLA}}(1,1,1,1,0,1,1,-1,1)$,
$\mathcal{J}_{120} = \mathcal{I}_{\mathrm{PLA}}(1,1,1,1,-1,1,1,-1,1)$,
$\mathcal{J}_{121} = \mathcal{I}_{\mathrm{PLA}_{\sigma_{12}}}(1,1,1,1,0,1,1,0,1)$,
$\mathcal{J}_{122} = \mathcal{I}_{\mathrm{PLA}_{\sigma_{12}}}(1,1,1,1,-1,1,1,0,1)$,
$\mathcal{J}_{123} = \mathcal{I}_{\mathrm{PLA}_{\sigma_{12}}}(1,1,1,1,0,1,1,-1,1)$,
$\mathcal{J}_{124} = \mathcal{I}_{\mathrm{PLA}_{\sigma_{12}}}(1,1,1,1,-1,1,1,-1,1)$,
$\mathcal{J}_{125} = \mathcal{I}_{\mathrm{PLC}}(1,1,1,0,1,1,1,1,0)$,
$\mathcal{J}_{126} = \mathcal{I}_{\mathrm{PLC}}(1,1,1,-1,1,1,1,1,0)$,
$\mathcal{J}_{127} = \mathcal{I}_{\mathrm{PLC}}(1,1,1,-1,1,1,1,1,-1)$,
$\mathcal{J}_{128} = \mathcal{I}_{\mathrm{PLC}_{\sigma_{12}}}(1,1,1,0,1,1,1,1,0)$,
$\mathcal{J}_{129} = \mathcal{I}_{\mathrm{PLC}_{\sigma_{12}}}(1,1,1,-1,1,1,1,1,0)$,
$\mathcal{J}_{130} = \mathcal{I}_{\mathrm{PLC}_{\sigma_{12}}}(1,1,1,-1,1,1,1,1,-1)$,
$\mathcal{J}_{131} = \mathcal{I}_{\mathrm{PLC}_{\sigma_{123}}}(1,1,1,0,1,1,1,1,0)$,
$\mathcal{J}_{132} = \mathcal{I}_{\mathrm{PLC}_{\sigma_{123}}}(1,1,1,-1,1,1,1,1,0)$,
$\mathcal{J}_{133} = \mathcal{I}_{\mathrm{PLC}_{\sigma_{123}}}(1,1,1,-1,1,1,1,1,-1)$,
$\mathcal{J}_{134} = \mathcal{I}_{\mathrm{PLC}_{\sigma_{12}}}(0,1,1,1,1,1,0,1,1)$,
$\mathcal{J}_{135} = \mathcal{I}_{\mathrm{PLC}_{\sigma_{12}}}(-1,1,1,1,1,1,0,1,1)$,
$\mathcal{J}_{136} = \mathcal{I}_{\mathrm{PLC}_{\sigma_{12}}}(-1,1,1,1,1,1,-1,1,1)$,
$\mathcal{J}_{137} = \mathcal{I}_{\mathrm{PLC}}(0,1,1,1,1,1,0,1,1)$,
$\mathcal{J}_{138} = \mathcal{I}_{\mathrm{PLC}}(-1,1,1,1,1,1,0,1,1)$,
$\mathcal{J}_{139} = \mathcal{I}_{\mathrm{PLC}}(-1,1,1,1,1,1,-1,1,1)$,
$\mathcal{J}_{140} = \mathcal{I}_{\mathrm{PLC}_{\sigma_{123}}}(0,1,1,1,1,1,0,1,1)$,

$$\mathcal{J}_{141} = \mathcal{I}_{\mathrm{PLC}_{\sigma_{123}}}(-1,1,1,1,1,1,0,1,1),$$
$$\mathcal{J}_{142} = \mathcal{I}_{\mathrm{PLC}_{\sigma_{123}}}(-1,1,1,1,1,1,-1,1,1),$$
$$\mathcal{J}_{143} = \mathcal{I}_{\mathrm{NPA}}(1,1,1,1,0,1,1,1,-1),$$
$$\mathcal{J}_{144} = \mathcal{I}_{\mathrm{NPA}}(1,2,1,1,0,1,1,1,-1),$$
$$\mathcal{J}_{145} = \mathcal{I}_{\mathrm{NPA}}(1,1,1,1,0,1,1,1,-2),$$
$$\mathcal{J}_{146} = \mathcal{I}_{\mathrm{NPA}}(1,1,1,1,0,1,1,1,0),$$
$$\mathcal{J}_{147} = \mathcal{I}_{\mathrm{NPB}}(1,1,1,1,0,1,1,1,0),$$
$$\mathcal{J}_{148} = \mathcal{I}_{\mathrm{NPB}}(1,1,1,1,0,1,1,1,-1),$$
$$\mathcal{J}_{149} = \mathcal{I}_{\mathrm{NPB}}(1,1,1,1,-1,1,1,1,0),$$
$$\mathcal{J}_{150} = \mathcal{I}_{\mathrm{NPB}}(1,1,1,1,0,1,1,1,-2),$$
$$\mathcal{J}_{151} = \mathcal{I}_{\mathrm{NPB}}(1,1,1,1,-1,1,1,1,-1),$$
$$\mathcal{J}_{152} = \mathcal{I}_{\mathrm{NPB}_{\sigma_{124}}}(1,1,1,1,0,1,1,1,0),$$
$$\mathcal{J}_{153} = \mathcal{I}_{\mathrm{NPB}_{\sigma_{124}}}(1,1,1,1,0,1,1,1,-1),$$
$$\mathcal{J}_{154} = \mathcal{I}_{\mathrm{NPB}_{\sigma_{124}}}(1,1,1,1,-1,1,1,1,0),$$
$$\mathcal{J}_{155} = \mathcal{I}_{\mathrm{NPB}_{\sigma_{124}}}(1,1,1,1,0,1,1,1,-2),$$
$$\mathcal{J}_{156} = \mathcal{I}_{\mathrm{NPB}_{\sigma_{124}}}(1,1,1,1,-1,1,1,1,-1),$$
$$\mathcal{J}_{157} = \mathcal{I}_{\mathrm{NPB}_{\sigma_{123}}}(1,1,1,1,0,1,1,1,0),$$
$$\mathcal{J}_{158} = \mathcal{I}_{\mathrm{NPB}_{\sigma_{123}}}(1,1,1,1,0,1,1,1,-1),$$
$$\mathcal{J}_{159} = \mathcal{I}_{\mathrm{NPB}_{\sigma_{123}}}(1,1,1,1,-1,1,1,1,0),$$
$$\mathcal{J}_{160} = \mathcal{I}_{\mathrm{NPB}_{\sigma_{123}}}(1,1,1,1,0,1,1,1,-2),$$
$$\mathcal{J}_{161} = \mathcal{I}_{\mathrm{NPB}_{\sigma_{123}}}(1,1,1,1,-1,1,1,1,-1).$$

Appendix F

Letters

In this Appendix, we provide the explicit expression of the different types of letters that appear in the integration kernels of the iterated integrals. To simplify the notation, we will use G for $G(s,t,m_t^2)$ and ϖ_0 for $\varpi_0(s,m_t^2)$.

F.1 Algebraic letters

$$
\begin{aligned}
A_1 &= \frac{s - r_1}{s + r_1}, \\
A_2 &= \frac{s - r_4}{s + r_4}, \\
A_3 &= \frac{t - r_2}{t + r_2}, \\
A_4 &= \frac{-s - t - r_3}{-s - t + r_3}, \\
A_5 &= \frac{s(-4m_t^2 - s - t) - r_3 r_4}{s(-4m_t^2 - s - t) + r_3 r_4}, \\
A_6 &= \frac{s(-4m_t^2 + t) - r_2 r_4}{s(-4m_t^2 + t) + r_2 r_4}, \\
A_7 &= \frac{st - r_7}{st + r_7}, \\
A_8 &= \frac{s(-s - t) - r_8}{s(-s - t) + r_8}, \\
A_9 &= \frac{(-s - t)t - r_9}{(-s - t)t + r_9}, \\
A_{10} &= \frac{s(-4m_t^2 + s)t - r_1 r_7}{s(-4m_t^2 + s)t + r_1 r_7}, \\
A_{11} &= \frac{s(-4m_t^2 + s)(-s - t) - r_1 r_8}{s(-4m_t^2 + s)(-s - t) + r_1 r_8}, \\
A_{12} &= \frac{st(-4m_t^2 + t) - r_2 r_7}{st(-4m_t^2 + t) + r_2 r_7}, \\
A_{13} &= \frac{(-s - t)t(-4m_t^2 + t) - r_2 r_9}{(-s - t)t(-4m_t^2 + t) + r_2 r_9},
\end{aligned}
$$

$$
\begin{aligned}
A_{14} &= \frac{s(-s-t)(-4m_t^2-s-t)-r_3r_8}{s(-s-t)(-4m_t^2-s-t)+r_3r_8},\\
A_{15} &= \frac{(-s-t)(-4m_t^2-s-t)t-r_3r_9}{(-s-t)(-4m_t^2-s-t)t+r_3r_9},\\
A_{16} &= \frac{-s(-4m_t^2+s)(-s-t)t-r_7r_8}{-s(-4m_t^2+s)(-s-t)t+r_7r_8},\\
A_{17} &= \frac{-s(-s-t)(-4m_t^2-s-t)t-r_8r_9}{-s(-s-t)(-4m_t^2-s-t)t+r_8r_9},\\
A_{18} &= \frac{-s(-s-t)t(-4m_t^2+t)-r_7r_9}{-s(-s-t)t(-4m_t^2+t)+r_7r_9},\\
A_{19} &= \frac{m_t^2s+(-s-t)(s+2t)-r_{10}}{m_t^2s+(-s-t)(s+2t)+r_{10}},\\
A_{20} &= \frac{m_t^2s+(-s-2t)t-r_{11}}{m_t^2s+(-s-2t)t+r_{11}},\\
A_{21} &= \frac{m_t^2(-s-t)+(s-t)t-r_{12}}{m_t^2(-s-t)+(s-t)t+r_{12}},\\
A_{22} &= \frac{s(-2s-t)+m_t^2t-r_{13}}{s(-2s-t)+m_t^2t+r_{13}},\\
A_{23} &= \frac{m_t^2(-s-t)+s(-s+t)-r_{14}}{m_t^2(-s-t)+s(-s+t)+r_{14}},\\
A_{24} &= \frac{m_t^2t+(-s-t)(2s+t)-r_{15}}{m_t^2t+(-s-t)(2s+t)+r_{15}},\\
A_{25} &= \frac{s(-s-t)+m_t^2(s+2t)-r_{10}}{s(-s-t)+m_t^2(s+2t)+r_{10}},\\
A_{26} &= \frac{m_t^2(-s-2t)+st-r_{11}}{m_t^2(-s-2t)+st+r_{11}},\\
A_{27} &= \frac{m_t^2(s-t)+(-s-t)t-r_{12}}{m_t^2(s-t)+(-s-t)t+r_{12}},\\
A_{28} &= \frac{m_t^2(-2s-t)+st-r_{13}}{m_t^2(-2s-t)+st+r_{13}},\\
A_{29} &= \frac{s(-s-t)+m_t^2(-s+t)-r_{14}}{s(-s-t)+m_t^2(-s+t)+r_{14}},\\
A_{30} &= \frac{(-s-t)t+m_t^2(2s+t)-r_{15}}{(-s-t)t+m_t^2(2s+t)+r_{15}},\\
A_{31} &= \frac{s(-m_t^2(-3s-4t)+s(-s-t))-r_1r_{10}}{s(-m_t^2(-3s-4t)+s(-s-t))+r_1r_{10}},\\
A_{32} &= \frac{s(st-m_t^2(s+4t))-r_1r_{11}}{s(st-m_t^2(s+4t))+r_1r_{11}},\\
A_{33} &= \frac{t(st-m_t^2(4s+t))-r_2r_{13}}{t(st-m_t^2(4s+t))+r_2r_{13}},\\
A_{34} &= \frac{t(-m_t^2(-4s-3t)+(-s-t)t)-r_2r_{15}}{t(-m_t^2(-4s-3t)+(-s-t)t)+r_2r_{15}},\\
A_{35} &= \frac{(-s-t)((-s-t)t-m_t^2(-s+3t))-r_3r_{12}}{(-s-t)((-s-t)t-m_t^2(-s+3t))+r_3r_{12}},
\end{aligned}
$$

$$
\begin{aligned}
A_{36} &= \frac{(s(-s-t)-m_t^2(3s-t))(-s-t)-r_3r_{14}}{(s(-s-t)-m_t^2(3s-t))(-s-t)+r_3r_{14}},\\
A_{37} &= \frac{s(-m_t^2(-s-4t)+s(-s-t))(-s-t)-r_8r_{10}}{s(-m_t^2(-s-4t)+s(-s-t))(-s-t)+r_8r_{10}},\\
A_{38} &= \frac{st(st-m_t^2(3s+4t))-r_7r_{11}}{st(st-m_t^2(3s+4t))+r_7r_{11}},\\
A_{39} &= \frac{(-s-t)t((-s-t)t-m_t^2(-3s+t))-r_9r_{12}}{(-s-t)t((-s-t)t-m_t^2(-3s+t))+r_9r_{12}},\\
A_{40} &= \frac{st(st-m_t^2(4s+3t))-r_7r_{13}}{st(st-m_t^2(4s+3t))+r_7r_{13}},\\
A_{41} &= \frac{s(-m_t^2(s-3t)+s(-s-t))(-s-t)-r_8r_{14}}{s(-m_t^2(s-3t)+s(-s-t))(-s-t)+r_8r_{14}},\\
A_{42} &= \frac{(-s-t)t(-m_t^2(-4s-t)+(-s-t)t)-r_9r_{15}}{(-s-t)t(-m_t^2(-4s-t)+(-s-t)t)+r_9r_{15}},\\
A_{43} &= \frac{st(4m_t^2(-s-t)+st)-2r_7r_{16}}{st(4m_t^2(-s-t)+st)+2r_7r_{16}},\\
A_{44} &= \frac{s(-s-t)(s(-s-t)+4m_t^2t)-2r_8r_{16}}{s(-s-t)(s(-s-t)+4m_t^2t)+2r_8r_{16}},\\
A_{45} &= \frac{(-s-t)t(4m_t^2s+(-s-t)t)-2r_9r_{16}}{(-s-t)t(4m_t^2s+(-s-t)t)+2r_9r_{16}}.
\end{aligned}
$$

F.2 Rational letters

$$
\begin{aligned}
&R_1 = s,\\
&R_2 = t,\\
&R_3 = -s-t,\\
&R_4 = -4m_t^2+s,\\
&R_5 = 4m_t^2+s,\\
&R_6 = -4m_t^2+t,\\
&R_7 = -4m_t^2-s-t,\\
&R_8 = 4m_t^2s+(-s-t)t,\\
&R_9 = s(-s-t)+4m_t^2t,\\
&R_{10} = 4m_t^2(-s-t)+st,\\
&R_{11} = 16m_t^2+s.
\end{aligned}
$$

F.3 Modular letters

$$
\begin{aligned}
M_1^s &= -\frac{1}{s^2(16^2+s)\varpi_0^2}\,, & M_1^t &= 0\,, & M_1^{2} &= \frac{1}{s^2\,(16^2+s)\,\varpi_0^2}\,,\\
M_2^s &= \varpi_0\,, & M_2^t &= 0\,, & M_2^{2} &= -\frac{s\varpi_0}{2}\,,\\
M_3^s &= -\frac{r_4\varpi_0}{4^2+s}\,, & M_3^t &= 0\,, & M_3^{2} &= \frac{r_4 s\varpi_0}{2\,(4^2+s)}\,,
\end{aligned}
$$

$$M_4^s = -\frac{(8^2+s)^2\varpi_0^2}{16^2+s}\,, \qquad M_4^t = 0\,, \quad M_4^{2} = \frac{s\left(8^2+s\right)^2\varpi_0^2}{{}^2\left(16^2+s\right)}\,.$$

F.4 Elliptic letters

$$\begin{aligned}
E_1^s &= \frac{4G}{s^2\varpi_0^2(16m_t^2+s)} + \frac{2r_9}{s\varpi_0(s+t)(4m_t^2 s - t(s+t))}\,,\\
E_1^t &= \frac{2r_9}{t\varpi_0(s+t)(t(s+t)-4m_t^2 s)}\,,\\
E_1^{m_t^2} &= \frac{-4G}{m_t^2 s(16m_t^2+s)\varpi_0^2},\\
E_2^s &= -\frac{2G^2}{s^2\varpi_0^2(16m_t^2+s)} + \frac{2Gr_9}{s\varpi_0(s+t)(t(s+t)-4m_t^2 s)} + \frac{8m_t^2-t}{8m_t^2 s - 2t(s+t)}\,,\\
E_2^t &= -\frac{2Gr_9}{t\varpi_0(s+t)(t(s+t)-4m_t^2 s)} - \frac{s+2t}{8m_t^2 s - 2t(s+t)}\,,\\
E_2^{m_t^2} &= \frac{2G^2}{m_t^2 s(16m_t^2+s)\varpi_0^2},\\
E_3^s &= \frac{4G(s+3t)}{s(s+t)} + \frac{2r_9\varpi_0(16m_t^2+s)}{(s+t)(4m_t^2 s - t(s+t))}\,,\\
E_3^t &= G\left(-\frac{8}{s+t} - \frac{8}{t}\right) + \frac{2r_9 s\varpi_0(16m_t^2+s)}{t(s+t)(t(s+t)-4m_t^2 s)}\,,\\
E_3^{m_t^2} &= \frac{4G}{m_t^2}\,,\\
E_4^s &= \frac{r_9\varpi_0}{2(t(s+t)-4m_t^2 s)} - \frac{G}{s+t}\,,\\
E_4^t &= \frac{Gs}{t(s+t)}\,,\\
E_4^{m_t^2} &= \frac{s\varpi_0 r_9}{2m_t^2\left(4m_t^2 s - t(s+t)\right)}\,,\\
E_5^s &= \frac{\varpi_0(4m_t^2 s - t(8m_t^2+s))}{8m_t^2 s - 2t(s+t)} - \frac{Gr_9 t}{s(s+t)(t(s+t)-4m_t^2 s)}\,,\\
E_5^t &= \frac{Gr_9(s+2t)}{t(s+t)(t(s+t)-4m_t^2 s)} + \frac{s\varpi_0(16m_t^2+s)}{8m_t^2 s - 2t(s+t)}\,,\\
E_5^{m_t^2} &= \frac{-2m_t^2 s(s+2t)\varpi_0 + Gr_9}{m_t^2\left(4m_t^2 s - t(s+t)\right)}\,,\\
E_6^s &= -\frac{2G^3}{s^2\varpi_0^2(16m_t^2+s)} + G\left(\frac{6m_t^2}{4m_t^2 s - t(s+t)} + \frac{1}{32m_t^2+2s} - \frac{2}{s+t} + \frac{2}{s}\right)\\
&\quad + \frac{3G^2 r_9}{s\varpi_0(s+t)(t(s+t)-4m_t^2 s)}\\
&\quad + \frac{r_9\varpi_0\left(64m_t^4 s + 16m_t^2(s-2t)(s+t) - 3st(s+t)\right)}{4(s+t)(t(s+t)-4m_t^2 s)^2}\,,\\
E_6^t &= -\frac{3G^2 r_9}{t\varpi_0(s+t)(t(s+t)-4m_t^2 s)} + G\left(-\frac{2}{s+t} - \frac{2}{t}\right) +\\
&\quad + \frac{r_9 s\varpi_0\left(-64m_t^4 s + 64m_t^2 t(s+t) + 3st(s+t)\right)}{4t(s+t)(t(s+t)-4m_t^2 s)^2}\,,
\end{aligned}$$

$$
\begin{aligned}
E_6^{m_t^2} &= \frac{(64m_t^2 s - 64m_t^2 t(s+t) - 3st(s+t))G}{2m_t^2(16m_t^2+s)\left(4m_t^2 s - t(s+t)\right)} \\
&\quad + \frac{2G^3}{(16m_t^2 s + m_t^2 s^2)\varpi_0^2} - \frac{4s(s+2t)\varpi_0 r_9}{\left(-4m_t^2 s + t(s+t)\right)^2}\,, \\
E_7^s &= \frac{4r_2\varpi_0(s+2t)}{t(s+t)-4m_t^2 s} - \frac{8Gr_2r_9}{t(s+t)(t(s+t)-4m_t^2 s)}\,, \\
E_7^t &= \frac{8Gr_9r_2\left(4m_t^2 s + t^2\right)}{t^2(4m_t^2-t)(s+t)(t(s+t)-4m_t^2 s)} + \frac{4r_2 s\varpi_0(16m_t^2+s)}{(4m_t^2-t)(4m_t^2 s - t(s+t))}\,, \\
E_7^{m_t^2} &= \frac{-8s(-2m_t^2(s-2t)+t(s+t))\varpi_0 r_2}{m_t^2(4m_t^2-t)\left(4m_t^2 s - t(s+t)\right)} \\
&\quad + \frac{8Gr_2r_9}{m_t^2(4m_t^2-t)\left(4m_t^2 s - t(s+t)\right)}\,, \\
E_8^s &= \frac{4r_3\varpi_0\left(-12m_t^2 s + 8m_t^2 t + 3st + 2t^2\right)}{(4m_t^2+s+t)(t(s+t)-4m_t^2 s)} \\
&\quad - \frac{32Gm_t^2 r_3 r_9}{(s+t)^2(4m_t^2+s+t)(t(s+t)-4m_t^2 s)}\,, \\
E_8^t &= \frac{8Gr_3r_9\left(4m_t^2 s + (s+t)^2\right)}{t(s+t)^2(4m_t^2+s+t)(t(s+t)-4m_t^2 s)} - \frac{4r_3 s\varpi_0(16m_t^2+s)}{(4m_t^2+s+t)(t(s+t)-4m_t^2 s)}\,, \\
E_8^{m_t^2} &= \frac{8s\left(t(s+t)-2m_t^2(3s+2t)\right)\varpi_0 r_3}{m_t^2\left(4m_t^2+s+t\right)\left(4m_t^2 s - t(s+t)\right)} \\
&\quad + \frac{8Gr_3r_9}{m_t^2\left(4m_t^2+s+t\right)\left(4m_t^2 s - t(s+t)\right)}\,, \\
E_9^s &= -\frac{4Gr_9r_8(4m_t^2(t-2s)+t(s+t))}{s(s+t)^2(s(s+t)-4m_t^2 t)(t(s+t)-4m_t^2 s)} \\
&\quad - \frac{2r_8\varpi_0\left(-64m_t^4 st + 4m_t^2\left(-4s^3-2s^2t+5st^2+2t^3\right)+st(s+t)(4s+3t)\right)}{s(s+t)(s(s+t)-4m_t^2 t)(t(s+t)-4m_t^2 s)}\,, \\
E_9^t &= \frac{2r_8 s\varpi_0(16m_t^2+s)(-4m_t^2+s+t)}{(s+t)(s(s+t)-4m_t^2 t)(t(s+t)-4m_t^2 s)} \\
&\quad - \frac{4Gr_8r_9(4m_t^2(s-2t)+s(s+t))}{t(s+t)^2(s(s+t)-4m_t^2 t)(t(s+t)-4m_t^2 s)}\,, \\
E_9^{m_t^2} &= \frac{2\left(-3st(s+t)+4m_t^2\left(4s^2+st-2t^2\right)\right)\varpi_0 r_8}{m_t^2\left(s^2-4m_t^2 t+st\right)\left(4m_t^2 s - t(s+t)\right)} \\
&\quad + \frac{4\left(4m_t^2-s-t\right)Gr_8r_9}{m_t^2\left(s+t\right)\left(s^2-4m_t^2 t+st\right)\left(4m_t^2 s - t(s+t)\right)}\,, \\
E_{10}^s &= -\frac{4Gr_9r_7(4m_t^2-t)(2s+t)}{st(s+t)(st-4m_t^2(s+t))(t(s+t)-4m_t^2 s)} \\
&\quad - \frac{2r_7\varpi_0\left(t^2(8m_t^2+3s)+2st(2m_t^2+s)-8m_t^2 s(8m_t^2+s)\right)}{s(4m_t^2(s+t)-st)(4m_t^2 s - t(s+t))}\,, \\
E_{10}^t &= \frac{4Gr_7r_9(12m_t^2 s + 8m_t^2 t - st)}{t^2(s+t)(st-4m_t^2(s+t))(t(s+t)-4m_t^2 s)} \\
&\quad - \frac{2r_7 s\varpi_0(16m_t^2+s)(4m_t^2+t)}{t(st-4m_t^2(s+t))(t(s+t)-4m_t^2 s)}\,, \\
E_{10}^{m_t^2} &= \frac{2\left(3st(s+t)-4m_t^2(s^2-5st-2t^2)\right)\varpi_0 r_7}{m_t^2\left(-st+4m_t^2(s+t)\right)\left(4m_t^2 s - t(s+t)\right)}
\end{aligned}
$$

$$
\begin{aligned}
&- \frac{4\left(4m_t^2+t\right)Gr_7r_9}{m_t^2t\left(-st+4m_t^2(s+t)\right)\left(4m_t^2s-t(s+t)\right)}\,, \\
E_{11}^{s} &= \frac{32Gr_9r_{16}}{s(s+t)^2(t(s+t)-4m_t^2s)} + \frac{16r_{16}\varpi_0(t(3s+2t)-16m_t^2s)}{s(s+t)(t(s+t)-4m_t^2s)}\,, \\
E_{11}^{t} &= \frac{16r_{16}s\varpi_0(16m_t^2+s)}{t(s+t)(t(s+t)-4m_t^2s)} - \frac{32Gr_9r_{16}(s+2t)}{t^2(s+t)^2(t(s+t)-4m_t^2s)}\,, \\
E_{11}^{m_t^2} &= \frac{16(s+2t)\varpi_0r_{16}}{m_t^2\left(4m_t^2s-t(s+t)\right)} \\
&- \frac{32Gr_9r_{16}}{m_t^2t\,(s+t)\left(4m_t^2s-t(s+t)\right)}\,, \\
E_{12}^{s} &= -\frac{2G^2}{s+t} + \frac{2Gr_9\varpi_0}{t(s+t)-4m_t^2s} + \frac{s^2\varpi_0^2(8m_t^2-t)}{8m_t^2s-2t(s+t)}\,, \\
E_{12}^{t} &= \frac{2G^2s}{st+t^2} + \frac{s^2\varpi_0^2(16m_t^2+s)}{8m_t^2s-2t(s+t)}\,, \\
E_{12}^{m_t^2} &= \frac{4s^2(s+2t)\varpi_0^2}{-4m_t^2s+t(s+t)} + \frac{2sG\varpi_0r_9}{m_t^2\left(4m_t^2s-t(s+t)\right)}\,, \\
E_{13}^{s} &= -\frac{4G^4}{s^2\varpi_0^2(16m_t^2+s)} + \frac{8G^3r_9}{s\varpi_0(s+t)(t(s+t)-4m_t^2s)} + \\
&+ G^2\left(\frac{24m_t^2}{4m_t^2s-t(s+t)} + \frac{2}{16m_t^2+s} - \frac{8}{s+t} + \frac{8}{s}\right) \\
&- \frac{2Gr_9\varpi_0\left(-64m_t^4s-16m_t^2(s-2t)(s+t)+3st(s+t)\right)}{(s+t)(t(s+t)-4m_t^2s)^2} \\
&- \frac{s\varpi_0^2\left(4096m_t^8s+2048m_t^6\left(s^2-4t^2\right)+128m_t^4s\left(s^2-3st-11t^2\right)\right)}{4(16m_t^2+s)(t(s+t)-4m_t^2s)^2} \\
&+ \frac{s\varpi_0^2\left(32m_t^2s^2t(s+2t)+st^2(s+t)^2\right)}{4(16m_t^2+s)(t(s+t)-4m_t^2s)^2}\,, \\
E_{13}^{t} &= -\frac{8G^3r_9}{t\varpi_0(s+t)(t(s+t)-4m_t^2s)} + G^2\left(-\frac{8}{s+t} - \frac{8}{t}\right) + \\
&+ \frac{2Gr_9s\varpi_0\left(-64m_t^4s+64m_t^2t(s+t)+3st(s+t)\right)}{t(s+t)(t(s+t)-4m_t^2s)^2} - \\
&\frac{8m_t^2s^2\varpi_0^2(16m_t^2+s)(s+2t)}{(t(s+t)-4m_t^2s)^2}\,, \\
E_{13}^{m_t^2} &= \frac{2\left(64m_t^2s-64m_t^2t(s+t)-3st(s+t)\right)G^2}{m_t^2(16m_t^2+s)\left(4m_t^2s-t(s+t)\right)} \\
&+ \frac{4G^4}{\left(16m_t^2s+m_t^2s^2\right)\varpi_0^2} \\
&+ \frac{s^2\left(4096m_t^4s+st^2(s+t)^2+2048m_t^3(s+2t)^2+128m_t^2s(s^2+5st+5t^2)\right)\varpi_0^2}{4m_t^2(16m_t^2+s)\left(-4m_t^2s+t(s+t)\right)^2} \\
&- \frac{32s(s+2t)G\varpi_0r_9}{\left(-4m_t^2s+t(s+t)\right)^2}\,.
\end{aligned}
$$

Bibliography

[1] Matteo Becchetti et al. “Full top-quark mass dependence in diphoton production at NNLO in QCD”. In: *Phys. Lett. B* 848 (2024), p. 138362. DOI: 10.1016/j.physletb.2023.138362. arXiv: 2308.10885 [hep-ph].

[2] Matteo Becchetti et al. “Two-loop form factors for diphoton production in quark annihilation channel with heavy quark mass dependence”. In: *JHEP* 12 (2023), p. 105. DOI: 10.1007/JHEP12(2023)105. arXiv: 2308.11412 [hep-ph].

[3] Federico Coro. “Full NNLO QCD corrections to diphoton production”. In: *PoS* EPS-HEP2023 (2024), p. 263. DOI: 10.22323/1.449.0263. arXiv: 2310.10458 [hep-ph].

[4] Federico Coro. “Photon pair production: full NNLO corrections in QCD with heavy quark mass dependence”. In: *PoS* LL2024 (2024), p. 041. DOI: 10.22323/1.467.0041.

[5] Peter W. Higgs. “Broken Symmetries and the Masses of Gauge Bosons”. In: *Phys. Rev. Lett.* 13 (1964). Ed. by J. C. Taylor, pp. 508–509. DOI: 10.1103/PhysRevLett.13.508.

[6] Peter W. Higgs. “Broken symmetries, massless particles and gauge fields”. In: *Phys. Lett.* 12 (1964), pp. 132–133. DOI: 10.1016/0031-9163(64)91136-9.

[7] F. Englert and R. Brout. “Broken Symmetry and the Mass of Gauge Vector Mesons”. In: *Phys. Rev. Lett.* 13 (1964). Ed. by J. C. Taylor, pp. 321–323. DOI: 10.1103/PhysRevLett.13.321.

[8] S. Abachi et al. “Observation of the top quark”. In: *Phys. Rev. Lett.* 74 (1995), pp. 2632–2637. DOI: 10.1103/PhysRevLett.74.2632. arXiv: hep-ex/9503003.

[9] Georges Aad et al. “Observation of a new particle in the search for the Standard Model Higgs boson with the ATLAS detector at the LHC”. In: *Phys. Lett. B* 716 (2012), pp. 1–29. DOI: 10.1016/j.physletb.2012.08.020. arXiv: 1207.7214 [hep-ex].

[10] Serguei Chatrchyan et al. “Observation of a New Boson at a Mass of 125 GeV with the CMS Experiment at the LHC”. In: *Phys. Lett. B* 716 (2012), pp. 30–61. DOI: 10.1016/j.physletb.2012.08.021. arXiv: 1207.7235 [hep-ex].

[11] H. David Politzer. “Asymptotic Freedom: An Approach to Strong Interactions”. In: *Phys. Rept.* 14 (1974), pp. 129–180. DOI: 10.1016/0370-1573(74)90014-3.

[12] H. David Politzer. "Reliable Perturbative Results for Strong Interactions?" In: *Phys. Rev. Lett.* 30 (1973). Ed. by J. C. Taylor, pp. 1346–1349. DOI: 10.1103/PhysRevLett.30.1346.

[13] David J. Gross and Frank Wilczek. "Ultraviolet Behavior of Nonabelian Gauge Theories". In: *Phys. Rev. Lett.* 30 (1973). Ed. by J. C. Taylor, pp. 1343–1346. DOI: 10.1103/PhysRevLett.30.1343.

[14] D. J. Gross and Frank Wilczek. "Asymptotically Free Gauge Theories - I". In: *Phys. Rev. D* 8 (1973), pp. 3633–3652. DOI: 10.1103/PhysRevD.8.3633.

[15] D. J. Gross and Frank Wilczek. "ASYMPTOTICALLY FREE GAUGE THEORIES. 2." In: *Phys. Rev. D* 9 (1974), pp. 980–993. DOI: 10.1103/PhysRevD.9.980.

[16] John C. Collins, Davison E. Soper, and George F. Sterman. "Factorization of Hard Processes in QCD". In: *Adv. Ser. Direct. High Energy Phys.* 5 (1989), pp. 1–91. DOI: 10.1142/9789814503266_0001. arXiv: hep-ph/0409313.

[17] J. Pumplin et al. "New generation of parton distributions with uncertainties from global QCD analysis". In: *JHEP* 07 (2002), p. 012. DOI: 10.1088/1126-6708/2002/07/012. arXiv: hep-ph/0201195.

[18] A. D. Martin et al. "Parton distributions for the LHC". In: *Eur. Phys. J. C* 63 (2009), pp. 189–285. DOI: 10.1140/epjc/s10052-009-1072-5. arXiv: 0901.0002 [hep-ph].

[19] Guido Altarelli and G. Parisi. "Asymptotic Freedom in Parton Language". In: *Nucl. Phys. B* 126 (1977), pp. 298–318. DOI: 10.1016/0550-3213(77)90384-4.

[20] Yuri L. Dokshitzer. "Calculation of the Structure Functions for Deep Inelastic Scattering and e+ e- Annihilation by Perturbation Theory in Quantum Chromodynamics." In: *Sov. Phys. JETP* 46 (1977), pp. 641–653.

[21] V. N. Gribov and L. N. Lipatov. "Deep inelastic e p scattering in perturbation theory". In: *Sov. J. Nucl. Phys.* 15 (1972), pp. 438–450.

[22] J. Andersen et al. "Les Houches 2023: Physics at TeV Colliders: Standard Model Working Group Report". In: *Physics of the TeV Scale and Beyond the Standard Model: Intensifying the Quest for New Physics*. June 2024. arXiv: 2406.00708 [hep-ph].

[23] F. Febres Cordero et al. "Two-loop master integrals for leading-color $pp \to t\bar{t}H$ amplitudes with a light-quark loop". In: *JHEP* 07 (2024), p. 084. DOI: 10.1007/JHEP07(2024)084. arXiv: 2312.08131 [hep-ph].

[24] Simon Badger, Hjalte Frellesvig, and Yang Zhang. "A Two-Loop Five-Gluon Helicity Amplitude in QCD". In: *JHEP* 12 (2013), p. 045. DOI: 10.1007/JHEP12(2013)045. arXiv: 1310.1051 [hep-ph].

[25] Simon Badger et al. "First look at two-loop five-gluon scattering in QCD". In: *Phys. Rev. Lett.* 120.9 (2018), p. 092001. DOI: 10.1103/PhysRevLett.120.092001. arXiv: 1712.02229 [hep-ph].

[26] Samuel Abreu et al. "Planar Two-Loop Five-Gluon Amplitudes from Numerical Unitarity". In: *Phys. Rev. D* 97.11 (2018), p. 116014. DOI: 10.1103/PhysRevD.97.116014. arXiv: 1712.03946 [hep-ph].

[27] Simon Badger et al. "Applications of integrand reduction to two-loop five-point scattering amplitudes in QCD". In: *PoS* LL2018 (2018), p. 006. DOI: 10.22323/1.303.0006. arXiv: 1807.09709 [hep-ph].

[28] S. Abreu et al. "Planar Two-Loop Five-Parton Amplitudes from Numerical Unitarity". In: *JHEP* 11 (2018), p. 116. DOI: 10.1007/JHEP11(2018)116. arXiv: 1809.09067 [hep-ph].

[29] Simon Badger et al. "Analytic helicity amplitudes for two-loop five-gluon scattering: the single-minus case". In: *JHEP* 01 (2019), p. 186. DOI: 10.1007/JHEP01(2019)186. arXiv: 1811.11699 [hep-ph].

[30] S. Abreu et al. "Analytic Form of Planar Two-Loop Five-Gluon Scattering Amplitudes in QCD". In: *Phys. Rev. Lett.* 122.8 (2019), p. 082002. DOI: 10.1103/PhysRevLett.122.082002. arXiv: 1812.04586 [hep-ph].

[31] S. Abreu et al. "Analytic Form of the Planar Two-Loop Five-Parton Scattering Amplitudes in QCD". In: *JHEP* 05 (2019), p. 084. DOI: 10.1007/JHEP05(2019)084. arXiv: 1904.00945 [hep-ph].

[32] S. Badger et al. "Analytic form of the full two-loop five-gluon all-plus helicity amplitude". In: *Phys. Rev. Lett.* 123.7 (2019), p. 071601. DOI: 10.1103/PhysRevLett.123.071601. arXiv: 1905.03733 [hep-ph].

[33] Simon Badger et al. "Two-loop amplitudes for $\mathcal{O}(\alpha_s^2)$ corrections to $W\gamma\gamma$ production at the LHC". In: (Sept. 2024). arXiv: 2409.08146 [hep-ph].

[34] Simon Badger et al. "Two-loop integrals for $t\bar{t}$+jet production at hadron colliders in the leading colour approximation". In: *JHEP* 07 (2024), p. 073. DOI: 10.1007/JHEP07(2024)073. arXiv: 2404.12325 [hep-ph].

[35] Simon Badger et al. "Isolated photon production in association with a jet pair through next-to-next-to-leading order in QCD". In: *JHEP* 10 (2023), p. 071. DOI: 10.1007/JHEP10(2023)071. arXiv: 2304.06682 [hep-ph].

[36] Simon Badger et al. "Two-loop master integrals for a planar topology contributing to pp $\to t\bar{t}j$". In: *JHEP* 01 (2023), p. 156. DOI: 10.1007/JHEP01(2023)156. arXiv: 2210.17477 [hep-ph].

[37] Simon Badger et al. "One-loop QCD helicity amplitudes for pp $\to t\bar{t}j$ to O(ε^2)". In: *JHEP* 06 (2022), p. 066. DOI: 10.1007/JHEP06(2022)066. arXiv: 2201.12188 [hep-ph].

[38] Simon Badger et al. "Two-loop leading-colour QCD helicity amplitudes for Higgs boson production in association with a bottom-quark pair at the LHC". In: *JHEP* 11 (2021), p. 012. DOI: 10.1007/JHEP11(2021)012. arXiv: 2107.14733 [hep-ph].

[39] Simon Badger et al. "Next-to-leading order QCD corrections to diphoton-plus-jet production through gluon fusion at the LHC". In: *Phys. Lett. B* 824 (2022), p. 136802. DOI: 10.1016/j.physletb.2021.136802. arXiv: 2109.12003 [hep-ph].

[40] Simon Badger et al. "Virtual QCD corrections to gluon-initiated diphoton plus jet production at hadron colliders". In: *JHEP* 11 (2021), p. 083. DOI: 10.1007/JHEP11(2021)083. arXiv: 2106.08664 [hep-ph].

[41] Simon Badger, Heribertus Bayu Hartanto, and Simone Zoia. "Two-Loop QCD Corrections to Wbb¯ Production at Hadron Colliders". In: *Phys. Rev. Lett.* 127.1 (2021), p. 012001. DOI: 10.1103/PhysRevLett.127.012001. arXiv: 2102.02516 [hep-ph].

[42] Gerard 't Hooft and M. J. G. Veltman. "Regularization and Renormalization of Gauge Fields". In: *Nucl. Phys. B* 44 (1972), pp. 189–213. DOI: 10.1016/0550-3213(72)90279-9.

[43] C. G. Bollini and J. J. Giambiagi. "Dimensional Renormalization: The Number of Dimensions as a Regularizing Parameter". In: *Nuovo Cim. B* 12 (1972), pp. 20–26. DOI: 10.1007/BF02895558.

[44] T. Kinoshita. "Mass singularities of Feynman amplitudes". In: *J. Math. Phys.* 3 (1962), pp. 650–677. DOI: 10.1063/1.1724268.

[45] T. D. Lee and M. Nauenberg. "Degenerate Systems and Mass Singularities". In: *Phys. Rev.* 133 (1964). Ed. by G. Feinberg, B1549–B1562. DOI: 10.1103/PhysRev.133.B1549.

[46] S. Catani and M. H. Seymour. "The Dipole formalism for the calculation of QCD jet cross-sections at next-to-leading order". In: *Phys. Lett. B* 378 (1996), pp. 287–301. DOI: 10.1016/0370-2693(96)00425-X. arXiv: hep-ph/9602277.

[47] S. Catani and M. H. Seymour. "A General algorithm for calculating jet cross-sections in NLO QCD". In: *Nucl. Phys. B* 485 (1997). [Erratum: Nucl.Phys.B 510, 503–504 (1998)], pp. 291–419. DOI: 10.1016/S0550-3213(96)00589-5. arXiv: hep-ph/9605323.

[48] S. Frixione, Z. Kunszt, and A. Signer. "Three jet cross-sections to next-to-leading order". In: *Nucl. Phys. B* 467 (1996), pp. 399–442. DOI: 10.1016/0550-3213(96)00110-1. arXiv: hep-ph/9512328.

[49] Gudrun Heinrich. "Collider Physics at the Precision Frontier". In: *Phys. Rept.* 922 (2021), pp. 1–69. DOI: 10.1016/j.physrep.2021.03.006. arXiv: 2009.00516 [hep-ph].

[50] Roberto Bonciani et al. "The q_T subtraction method for top quark production at hadron colliders". In: *Eur. Phys. J. C* 75.12 (2015), p. 581. DOI: 10.1140/epjc/s10052-015-3793-y. arXiv: 1508.03585 [hep-ph].

[51] S. Catani and M. H. Seymour. "QCD jet calculations in DIS based on the subtraction method and dipole formalism". In: *4th International Workshop on Deep Inelastic Scattering and Related Phenomena*. Sept. 1996, pp. 454–458. arXiv: hep-ph/9609237.

[52] A. Gehrmann-De Ridder, T. Gehrmann, and E. W. Nigel Glover. "Antenna subtraction at NNLO". In: *JHEP* 09 (2005), p. 056. DOI: 10.1088/1126-6708/2005/09/056. arXiv: hep-ph/0505111.

[53] A. Daleo, T. Gehrmann, and D. Maitre. "Antenna subtraction with hadronic initial states". In: *JHEP* 04 (2007), p. 016. DOI: 10.1088/1126-6708/2007/04/016. arXiv: hep-ph/0612257.

[54] James Currie, E. W. N. Glover, and Steven Wells. "Infrared Structure at NNLO Using Antenna Subtraction". In: *JHEP* 04 (2013), p. 066. DOI: 10.1007/JHEP04(2013)066. arXiv: 1301.4693 [hep-ph].

[55] Lance J. Dixon. “A brief introduction to modern amplitude methods”. In: *Theoretical Advanced Study Institute in Elementary Particle Physics: Particle Physics: The Higgs Boson and Beyond*. 2014, pp. 31–67. DOI: 10.5170/CERN-2014-008.31. arXiv: 1310.5353 [hep-ph].

[56] Lance J. Dixon. “Calculating scattering amplitudes efficiently”. In: *Theoretical Advanced Study Institute in Elementary Particle Physics (TASI 95): QCD and Beyond*. Jan. 1996, pp. 539–584. arXiv: hep-ph/9601359.

[57] Giovanni Ossola, Costas G. Papadopoulos, and Roberto Pittau. “Reducing full one-loop amplitudes to scalar integrals at the integrand level”. In: *Nucl. Phys. B* 763 (2007), pp. 147–169. DOI: 10.1016/j.nuclphysb.2006.11.012. arXiv: hep-ph/0609007.

[58] P. Mastrolia et al. “Optimizing the Reduction of One-Loop Amplitudes”. In: *JHEP* 06 (2008), p. 030. DOI: 10.1088/1126-6708/2008/06/030. arXiv: 0803.3964 [hep-ph].

[59] Tiziano Peraro. “Ninja: Automated Integrand Reduction via Laurent Expansion for One-Loop Amplitudes”. In: *Comput. Phys. Commun.* 185 (2014), pp. 2771–2797. DOI: 10.1016/j.cpc.2014.06.017. arXiv: 1403.1229 [hep-ph].

[60] Giovanni Ossola, Costas G. Papadopoulos, and Roberto Pittau. “CutTools: A Program implementing the OPP reduction method to compute one-loop amplitudes”. In: *JHEP* 03 (2008), p. 042. DOI: 10.1088/1126-6708/2008/03/042. arXiv: 0711.3596 [hep-ph].

[61] P. Mastrolia et al. “Scattering AMplitudes from Unitarity-based Reduction Algorithm at the Integrand-level”. In: *JHEP* 08 (2010), p. 080. DOI: 10.1007/JHEP08(2010)080. arXiv: 1006.0710 [hep-ph].

[62] Celine Degrande, Valentin Hirschi, and Olivier Mattelaer. “Automated Computation of One-Loop Amplitudes”. In: *Ann. Rev. Nucl. Part. Sci.* 68 (2018), pp. 291–312. DOI: 10.1146/annurev-nucl-101917-020959.

[63] C. F. Berger et al. “An Automated Implementation of On-Shell Methods for One-Loop Amplitudes”. In: *Phys. Rev. D* 78 (2008), p. 036003. DOI: 10.1103/PhysRevD.78.036003. arXiv: 0803.4180 [hep-ph].

[64] Gavin Cullen et al. “Automated One-Loop Calculations with GoSam”. In: *Eur. Phys. J. C* 72 (2012), p. 1889. DOI: 10.1140/epjc/s10052-012-1889-1. arXiv: 1111.2034 [hep-ph].

[65] Valentin Hirschi et al. “Automation of one-loop QCD corrections”. In: *JHEP* 05 (2011), p. 044. DOI: 10.1007/JHEP05(2011)044. arXiv: 1103.0621 [hep-ph].

[66] T. Hahn and M. Perez-Victoria. “Automatized one loop calculations in four-dimensions and D-dimensions”. In: *Comput. Phys. Commun.* 118 (1999), pp. 153–165. DOI: 10.1016/S0010-4655(98)00173-8. arXiv: hep-ph/9807565.

[67] Janusz Gluza et al. “Numerical Evaluation of Tensor Feynman Integrals in Euclidean Kinematics”. In: *Eur. Phys. J. C* 71 (2011), p. 1516. DOI: 10.1140/epjc/s10052-010-1516-y. arXiv: 1010.1667 [hep-ph].

[68] Thomas Hahn. “Automatic loop calculations with FeynArts, FormCalc, and LoopTools”. In: *Nucl. Phys. B Proc. Suppl.* 89 (2000), pp. 231–236. DOI: 10.1016/S0920-5632(00)00848-3. arXiv: hep-ph/0005029.

[69] R. Keith Ellis et al. "One-loop calculations in quantum field theory: from Feynman diagrams to unitarity cuts". In: *Phys. Rept.* 518 (2012), pp. 141–250. DOI: 10.1016/j.physrep.2012.01.008. arXiv: 1105.4319 [hep-ph].

[70] Federico Buccioni et al. "OpenLoops 2". In: *Eur. Phys. J. C* 79.10 (2019), p. 866. DOI: 10.1140/epjc/s10052-019-7306-2. arXiv: 1907.13071 [hep-ph].

[71] Federico Buccioni, Stefano Pozzorini, and Max Zoller. "On-the-fly reduction of open loops". In: *Eur. Phys. J. C* 78.1 (2018), p. 70. DOI: 10.1140/epjc/s10052-018-5562-1. arXiv: 1710.11452 [hep-ph].

[72] Stefano Carrazza, R. Keith Ellis, and Giulia Zanderighi. "QCDLoop: a comprehensive framework for one-loop scalar integrals". In: *Comput. Phys. Commun.* 209 (2016), pp. 134–143. DOI: 10.1016/j.cpc.2016.07.033. arXiv: 1605.03181 [hep-ph].

[73] Tiziano Peraro and Lorenzo Tancredi. "Physical projectors for multi-leg helicity amplitudes". In: *JHEP* 07 (2019), p. 114. DOI: 10.1007/JHEP07(2019)114. arXiv: 1906.03298 [hep-ph].

[74] Tiziano Peraro and Lorenzo Tancredi. "Tensor decomposition for bosonic and fermionic scattering amplitudes". In: *Phys. Rev. D* 103.5 (2021), p. 054042. DOI: 10.1103/PhysRevD.103.054042. arXiv: 2012.00820 [hep-ph].

[75] Piotr Bargiela et al. "Three-loop helicity amplitudes for diphoton production in gluon fusion". In: *JHEP* 02 (2022), p. 153. DOI: 10.1007/JHEP02(2022)153. arXiv: 2111.13595 [hep-ph].

[76] C. Gnendiger et al. "To d, or not to d: recent developments and comparisons of regularization schemes". In: *Eur. Phys. J. C* 77.7 (2017), p. 471. DOI: 10.1140/epjc/s10052-017-5023-2. arXiv: 1705.01827 [hep-ph].

[77] Vittorio Del Duca. *Scattering Amplitudes*. Lecture notes, ETH Zurich, Fall Semester 2020. 2020. URL: https://people.phys.ethz.ch/~delducav/SCATTERING_AMPLITUDES_HS20.pdf.

[78] R. Britto. *Lecture Notes on [Subject/Topic]*. https://www.maths.tcd.ie/~britto/lecture-notes.pdf. Accessed: [Access Date].

[79] Stefan Weinzierl. *Feynman Integrals. A Comprehensive Treatment for Students and Researchers*. UNITEXT for Physics. Springer, 2022. ISBN: 978-3-030-99557-7, 978-3-030-99560-7, 978-3-030-99558-4. DOI: 10.1007/978-3-030-99558-4. arXiv: 2201.03593 [hep-th].

[80] Samuel Abreu, Ruth Britto, and Claude Duhr. "The SAGEX review on scattering amplitudes Chapter 3: Mathematical structures in Feynman integrals". In: *J. Phys. A* 55.44 (2022), p. 443004. DOI: 10.1088/1751-8121/ac87de. arXiv: 2203.13014 [hep-th].

[81] Simon Badger et al. "Scattering Amplitudes in Quantum Field Theory". In: *Lect. Notes Phys.* 1021 (2024), pp. DOI: 10.1007/978-3-031-46987-9. arXiv: 2306.05976 [hep-th].

[82] K. G. Chetyrkin and F. V. Tkachov. "Integration by parts: The algorithm to calculate β-functions in 4 loops". In: *Nucl. Phys. B* 192 (1981), pp. 159–204. DOI: 10.1016/0550-3213(81)90199-1.

[83] A. V. Smirnov and A. V. Petukhov. "The Number of Master Integrals is Finite". In: *Lett. Math. Phys.* 97 (2011), pp. 37–44. DOI: 10.1007/s11005-010-0450-0. arXiv: 1004.4199 [hep-th].

[84] Thomas Bitoun et al. “Feynman integral relations from parametric annihilators”. In: *Lett. Math. Phys.* 109.3 (2019), pp. 497–564. DOI: 10.1007/s11005-018-1114-8. arXiv: 1712.09215 [hep-th].

[85] R. N. Lee. “Group structure of the integration-by-part identities and its application to the reduction of multiloop integrals”. In: *JHEP* 07 (2008), p. 031. DOI: 10.1088/1126-6708/2008/07/031. arXiv: 0804.3008 [hep-ph].

[86] T. Gehrmann and E. Remiddi. “Differential equations for two-loop four-point functions”. In: *Nucl. Phys. B* 580 (2000), pp. 485–518. DOI: 10.1016/S0550-3213(00)00223-6. arXiv: hep-ph/9912329.

[87] S. Laporta. “High-precision calculation of multiloop Feynman integrals by difference equations”. In: *Int. J. Mod. Phys. A* 15 (2000), pp. 5087–5159. DOI: 10.1142/S0217751X00002159. arXiv: hep-ph/0102033.

[88] Philipp Maierhöfer, Johann Usovitsch, and Peter Uwer. “Kira—A Feynman integral reduction program”. In: *Comput. Phys. Commun.* 230 (2018), pp. 99–112. DOI: 10.1016/j.cpc.2018.04.012. arXiv: 1705.05610 [hep-ph].

[89] Jonas Klappert et al. “Integral reduction with Kira 2.0 and finite field methods”. In: *Comput. Phys. Commun.* 266 (2021), p. 108024. DOI: 10.1016/j.cpc.2021.108024. arXiv: 2008.06494 [hep-ph].

[90] R. N. Lee. “Presenting LiteRed: a tool for the Loop InTEgrals REDuction”. In: (Dec. 2012). arXiv: 1212.2685 [hep-ph].

[91] Roman N. Lee. “LiteRed 1.4: a powerful tool for reduction of multiloop integrals”. In: *J. Phys. Conf. Ser.* 523 (2014). Ed. by Jianxiong Wang, p. 012059. DOI: 10.1088/1742-6596/523/1/012059. arXiv: 1310.1145 [hep-ph].

[92] C. Studerus. “Reduze – Feynman integral reduction in C++”. In: *Comput. Phys. Commun.* 181 (2010), pp. 1293–1300. DOI: 10.1016/j.cpc.2010.03.012. arXiv: 0912.2546 [physics.comp-ph].

[93] A. von Manteuffel and C. Studerus. “Reduze 2 - Distributed Feynman Integral Reduction”. In: (Jan. 2012). arXiv: 1201.4330 [hep-ph].

[94] Alexander V. Smirnov and Mao Zeng. “FIRE 6.5: Feynman integral reduction with new simplification library”. In: *Comput. Phys. Commun.* 302 (2024), p. 109261. DOI: 10.1016/j.cpc.2024.109261. arXiv: 2311.02370 [hep-ph].

[95] A. V. Smirnov. “Algorithm FIRE – Feynman Integral REduction”. In: *JHEP* 10 (2008), p. 107. DOI: 10.1088/1126-6708/2008/10/107. arXiv: 0807.3243 [hep-ph].

[96] Kuo-Tsai Chen. “Iterated path integrals”. In: *Bull. Am. Math. Soc.* 83 (1977), pp. 831–879. DOI: 10.1090/S0002-9904-1977-14320-6.

[97] Alexander B. Goncharov. “Multiple polylogarithms, cyclotomy and modular complexes”. In: *Math. Res. Lett.* 5 (1998), pp. 497–516. DOI: 10.4310/MRL.1998.v5.n4.a7. arXiv: 1105.2076 [math.AG].

[98] A. B. Goncharov. “Multiple polylogarithms and mixed Tate motives”. In: (Mar. 2001). arXiv: math/0103059.

[99] Alexander B. Goncharov et al. “Classical Polylogarithms for Amplitudes and Wilson Loops”. In: *Phys. Rev. Lett.* 105 (2010), p. 151605. DOI: 10.1103/PhysRevLett.105.151605. arXiv: 1006.5703 [hep-th].

[100] A. V. Kotikov. "Differential equations method: New technique for massive Feynman diagrams calculation". In: *Phys. Lett. B* 254 (1991), pp. 158–164. DOI: 10.1016/0370-2693(91)90413-K.

[101] Ettore Remiddi. "Differential equations for Feynman graph amplitudes". In: *Nuovo Cim. A* 110 (1997), pp. 1435–1452. DOI: 10.1007/BF03185566. arXiv: hep-th/9711188.

[102] Johannes M. Henn. "Multiloop integrals in dimensional regularization made simple". In: *Phys. Rev. Lett.* 110 (2013), p. 251601. DOI: 10.1103/PhysRevLett.110.251601. arXiv: 1304.1806 [hep-th].

[103] Johannes M. Henn. "Lectures on differential equations for Feynman integrals". In: *J. Phys. A* 48 (2015), p. 153001. DOI: 10.1088/1751-8113/48/15/153001. arXiv: 1412.2296 [hep-ph].

[104] L. Lewin. *Polylogarithms and Associated Functions*. New York: North-Holland, 1981.

[105] Claude Duhr. "Mathematical aspects of scattering amplitudes". In: *Theoretical Advanced Study Institute in Elementary Particle Physics: Journeys Through the Precision Frontier: Amplitudes for Colliders*. 2015, pp. 419–476. DOI: 10.1142/9789814678766_0010. arXiv: 1411.7538 [hep-ph].

[106] M. Waldschmidt. "Multiple Polylogarithms: An Introduction". In: *Number Theory and Discrete Mathematics*. Ed. by A. K. Agarwal et al. Basel: Birkhäuser Basel, 2002, pp. 1–12. ISBN: 978-3-0348-8223-1.

[107] Claude Duhr, Herbert Gangl, and John R. Rhodes. "From polygons and symbols to polylogarithmic functions". In: *JHEP* 10 (2012), p. 075. DOI: 10.1007/JHEP10(2012)075. arXiv: 1110.0458 [math-ph].

[108] Claude Duhr and Falko Dulat. "PolyLogTools — polylogs for the masses". In: *JHEP* 08 (2019), p. 135. DOI: 10.1007/JHEP08(2019)135. arXiv: 1904.07279 [hep-th].

[109] Nima Arkani-Hamed et al. "Local Integrals for Planar Scattering Amplitudes". In: *JHEP* 06 (2012), p. 125. DOI: 10.1007/JHEP06(2012)125. arXiv: 1012.6032 [hep-th].

[110] Johannes Broedel et al. "Elliptic Feynman integrals and pure functions". In: *JHEP* 01 (2019), p. 023. DOI: 10.1007/JHEP01(2019)023. arXiv: 1809.10698 [hep-th].

[111] Hjalte Frellesvig and Stefan Weinzierl. "On ε-factorised bases and pure Feynman integrals". In: *SciPost Phys.* 16.6 (2024), p. 150. DOI: 10.21468/SciPostPhys.16.6.150. arXiv: 2301.02264 [hep-th].

[112] Song He et al. "A study of Feynman integrals with uniform transcendental weights and their symbology". In: *JHEP* 10 (2022), p. 165. DOI: 10.1007/JHEP10(2022)165. arXiv: 2206.04609 [hep-th].

[113] Marco Abate and Francesca Tovena. *Geometria Differenziale*. Italian. Milano, Italy: McGraw-Hill, 2004.

[114] Francis C. S. Brown and Andrey Levin. *Multiple Elliptic Polylogarithms*. 2013. arXiv: 1110.6917 [math.NT]. URL: https://arxiv.org/abs/1110.6917.

[115] Johannes Broedel et al. "Elliptic polylogarithms and iterated integrals on elliptic curves. Part I: general formalism". In: *JHEP* 05 (2018), p. 093. DOI: 10.1007/JHEP05(2018)093. arXiv: 1712.07089 [hep-th].

[116] Johannes Broedel et al. "Elliptic polylogarithms and iterated integrals on elliptic curves II: an application to the sunrise integral". In: *Phys. Rev. D* 97.11 (2018), p. 116009. DOI: 10.1103/PhysRevD.97.116009. arXiv: 1712.07095 [hep-ph].

[117] Matthias Wilhelm and Chi Zhang. "Symbology for elliptic multiple polylogarithms and the symbol prime". In: *JHEP* 01 (2023), p. 089. DOI: 10.1007/JHEP01(2023)089. arXiv: 2206.08378 [hep-th].

[118] Johannes Broedel et al. "Elliptic multiple zeta values and one-loop superstring amplitudes". In: *JHEP* 07 (2015), p. 112. DOI: 10.1007/JHEP07(2015)112. arXiv: 1412.5535 [hep-th].

[119] J. Ablinger et al. "Iterated Elliptic and Hypergeometric Integrals for Feynman Diagrams". In: *J. Math. Phys.* 59.6 (2018), p. 062305. DOI: 10.1063/1.4986417. arXiv: 1706.01299 [hep-th].

[120] Lennard Görges et al. "On a procedure to derive ϵ-factorised differential equations beyond polylogarithms". In: *JHEP* 07 (2023), p. 206. DOI: 10.1007/JHEP07(2023)206. arXiv: 2305.14090 [hep-th].

[121] Christoph Dlapa, Johannes M. Henn, and Fabian J. Wagner. "An algorithmic approach to finding canonical differential equations for elliptic Feynman integrals". In: *JHEP* 08 (2023), p. 120. DOI: 10.1007/JHEP08(2023)120. arXiv: 2211.16357 [hep-ph].

[122] Johannes Broedel et al. "Elliptic polylogarithms and Feynman parameter integrals". In: *JHEP* 05 (2019), p. 120. DOI: 10.1007/JHEP05(2019)120. arXiv: 1902.09971 [hep-ph].

[123] R. E. Cutkosky. "Singularities and discontinuities of Feynman amplitudes". In: *J. Math. Phys.* 1 (1960), pp. 429–433. DOI: 10.1063/1.1703676.

[124] Roman N. Lee and Andrei A. Pomeransky. "Critical points and number of master integrals". In: *JHEP* 11 (2013), p. 165. DOI: 10.1007/JHEP11(2013)165. arXiv: 1308.6676 [hep-ph].

[125] P. A. Baikov. "Explicit solutions of n loop vacuum integral recurrence relations". In: (Apr. 1996). arXiv: hep-ph/9604254.

[126] Hjalte Frellesvig and Costas G. Papadopoulos. "Cuts of Feynman Integrals in Baikov representation". In: *JHEP* 04 (2017), p. 083. DOI: 10.1007/JHEP04(2017)083. arXiv: 1701.07356 [hep-ph].

[127] Mark Harley, Francesco Moriello, and Robert M. Schabinger. "Baikov-Lee Representations Of Cut Feynman Integrals". In: *JHEP* 06 (2017), p. 049. DOI: 10.1007/JHEP06(2017)049. arXiv: 1705.03478 [hep-ph].

[128] Amedeo Primo and Lorenzo Tancredi. "On the maximal cut of Feynman integrals and the solution of their differential equations". In: *Nucl. Phys. B* 916 (2017), pp. 94–116. DOI: 10.1016/j.nuclphysb.2016.12.021. arXiv: 1610.08397 [hep-ph].

[129] Amedeo Primo and Lorenzo Tancredi. "Maximal cuts and differential equations for Feynman integrals. An application to the three-loop massive banana graph". In: *Nucl. Phys. B* 921 (2017), pp. 316–356. DOI: 10.1016/j.nuclphysb.2017.05.018. arXiv: 1704.05465 [hep-ph].

[130] Jorrit Bosma, Kasper J. Larsen, and Yang Zhang. “Differential equations for loop integrals in Baikov representation”. In: *Phys. Rev. D* 97.10 (2018), p. 105014. DOI: 10.1103/PhysRevD.97.105014. arXiv: 1712.03760 [hep-th].

[131] Jorrit Bosma, Mads Sogaard, and Yang Zhang. “Maximal Cuts in Arbitrary Dimension”. In: *JHEP* 08 (2017), p. 051. DOI: 10.1007/JHEP08(2017)051. arXiv: 1704.04255 [hep-th].

[132] Francesco Moriello. “Generalised power series expansions for the elliptic planar families of Higgs + jet production at two loops”. In: *JHEP* 01 (2020), p. 150. DOI: 10.1007/JHEP01(2020)150. arXiv: 1907.13234 [hep-ph].

[133] Martijn Hidding. “DiffExp, a Mathematica package for computing Feynman integrals in terms of one-dimensional series expansions”. In: *Comput. Phys. Commun.* 269 (2021), p. 108125. DOI: 10.1016/j.cpc.2021.108125. arXiv: 2006.05510 [hep-ph].

[134] Tommaso Armadillo et al. “Evaluation of Feynman integrals with arbitrary complex masses via series expansions”. In: *Comput. Phys. Commun.* 282 (2023), p. 108545. DOI: 10.1016/j.cpc.2022.108545. arXiv: 2205.03345 [hep-ph].

[135] S. Pozzorini and E. Remiddi. “Precise numerical evaluation of the two loop sunrise graph master integrals in the equal mass case”. In: *Comput. Phys. Commun.* 175 (2006), pp. 381–387. DOI: 10.1016/j.cpc.2006.05.005. arXiv: hep-ph/0505041.

[136] Kirill Melnikov, Lorenzo Tancredi, and Christopher Wever. “Two-loop amplitudes for $qg \to Hq$ and $q\bar{q} \to Hg$ mediated by a nearly massless quark”. In: *Phys. Rev. D* 95.5 (2017), p. 054012. DOI: 10.1103/PhysRevD.95.054012. arXiv: 1702.00426 [hep-ph].

[137] U. Aglietti et al. “The Two loop crossed ladder vertex diagram with two massive exchanges”. In: *Nucl. Phys. B* 789 (2008), pp. 45–83. DOI: 10.1016/j.nuclphysb.2007.07.019. arXiv: 0705.2616 [hep-ph].

[138] Kirill Melnikov, Lorenzo Tancredi, and Christopher Wever. “Two-loop $gg \to Hg$ amplitude mediated by a nearly massless quark”. In: *JHEP* 11 (2016), p. 104. DOI: 10.1007/JHEP11(2016)104. arXiv: 1610.03747 [hep-ph].

[139] Romain Mueller and Deniz Gizem Öztürk. “On the computation of finite bottom-quark mass effects in Higgs boson production”. In: *JHEP* 08 (2016), p. 055. DOI: 10.1007/JHEP08(2016)055. arXiv: 1512.08570 [hep-ph].

[140] Roberto Bonciani et al. “Analytical Method for Next-to-Leading-Order QCD Corrections to Double-Higgs Production”. In: *Phys. Rev. Lett.* 121.16 (2018), p. 162003. DOI: 10.1103/PhysRevLett.121.162003. arXiv: 1806.11564 [hep-ph].

[141] Bernhard Mistlberger. “Higgs boson production at hadron colliders at N^{3}LO in QCD”. In: *JHEP* 05 (2018), p. 028. DOI: 10.1007/JHEP05(2018)028. arXiv: 1802.00833 [hep-ph].

[142] Roman N. Lee, Alexander V. Smirnov, and Vladimir A. Smirnov. “Solving differential equations for Feynman integrals by expansions near singular points”. In: *JHEP* 03 (2018), p. 008. DOI: 10.1007/JHEP03(2018)008. arXiv: 1709.07525 [hep-ph].

[143] Roman N. Lee, Alexander V. Smirnov, and Vladimir A. Smirnov. "Evaluating 'elliptic' master integrals at special kinematic values: using differential equations and their solutions via expansions near singular points". In: *JHEP* 07 (2018), p. 102. DOI: 10.1007/JHEP07(2018)102. arXiv: 1805.00227 [hep-ph].

[144] Roberto Bonciani et al. "A Numerical Routine for the Crossed Vertex Diagram with a Massive-Particle Loop". In: *Comput. Phys. Commun.* 241 (2019), pp. 122–131. DOI: 10.1016/j.cpc.2019.03.014. arXiv: 1812.02698 [hep-ph].

[145] Robin Brüser, Simon Caron-Huot, and Johannes M. Henn. "Subleading Regge limit from a soft anomalous dimension". In: *JHEP* 04 (2018), p. 047. DOI: 10.1007/JHEP04(2018)047. arXiv: 1802.02524 [hep-th].

[146] Joshua Davies et al. "Double Higgs boson production at NLO in the high-energy limit: complete analytic results". In: *JHEP* 01 (2019), p. 176. DOI: 10.1007/JHEP01(2019)176. arXiv: 1811.05489 [hep-ph].

[147] Joshua Davies et al. "Double-Higgs boson production in the high-energy limit: planar master integrals". In: *JHEP* 03 (2018), p. 048. DOI: 10.1007/JHEP03(2018)048. arXiv: 1801.09696 [hep-ph].

[148] Charalampos Anastasiou et al. "Higgs Boson Gluon-Fusion Production in QCD at Three Loops". In: *Phys. Rev. Lett.* 114 (2015), p. 212001. DOI: 10.1103/PhysRevLett.114.212001. arXiv: 1503.06056 [hep-ph].

[149] Stefano Catani and Massimiliano Grazzini. "An NNLO subtraction formalism in hadron collisions and its application to Higgs boson production at the LHC". In: *Phys. Rev. Lett.* 98 (2007), p. 222002. DOI: 10.1103/PhysRevLett.98.222002. arXiv: hep-ph/0703012.

[150] Stefano Catani et al. "Universality of transverse-momentum resummation and hard factors at the NNLO". In: *Nucl. Phys. B* 881 (2014), pp. 414–443. DOI: 10.1016/j.nuclphysb.2014.02.011. arXiv: 1311.1654 [hep-ph].

[151] John C. Collins and Davison E. Soper. "Back-To-Back Jets in QCD". In: *Nucl. Phys. B* 193 (1981). [Erratum: Nucl.Phys.B 213, 545 (1983)], p. 381. DOI: 10.1016/0550-3213(81)90339-4.

[152] John C. Collins, Davison E. Soper, and George F. Sterman. "Transverse Momentum Distribution in Drell-Yan Pair and W and Z Boson Production". In: *Nucl. Phys. B* 250 (1985), pp. 199–224. DOI: 10.1016/0550-3213(85)90479-1.

[153] Giuseppe Bozzi et al. "Transverse-momentum resummation and the spectrum of the Higgs boson at the LHC". In: *Nucl. Phys. B* 737 (2006), pp. 73–120. DOI: 10.1016/j.nuclphysb.2005.12.022. arXiv: hep-ph/0508068.

[154] Stefano Camarda, Leandro Cieri, and Giancarlo Ferrera. "Drell–Yan lepton-pair production: qT resummation at N4LL accuracy". In: *Phys. Lett. B* 845 (2023), p. 138125. DOI: 10.1016/j.physletb.2023.138125. arXiv: 2303.12781 [hep-ph].

[155] O. V. Tarasov, A. A. Vladimirov, and A. Yu. Zharkov. "The Gell-Mann-Low Function of QCD in the Three Loop Approximation". In: *Phys. Lett. B* 93 (1980), pp. 429–432. DOI: 10.1016/0370-2693(80)90358-5.

[156] S. A. Larin and J. A. M. Vermaseren. "The Three loop QCD Beta function and anomalous dimensions". In: *Phys. Lett. B* 303 (1993), pp. 334–336. DOI: 10.1016/0370-2693(93)91441-O. arXiv: hep-ph/9302208.

[157] T. van Ritbergen, J. A. M. Vermaseren, and S. A. Larin. "The Four loop beta function in quantum chromodynamics". In: *Phys. Lett. B* 400 (1997), pp. 379–384. DOI: 10.1016/S0370-2693(97)00370-5. arXiv: hep-ph/9701390.

[158] F. Herzog et al. "The five-loop beta function of Yang-Mills theory with fermions". In: *JHEP* 02 (2017), p. 090. DOI: 10.1007/JHEP02(2017)090. arXiv: 1701.01404 [hep-ph].

[159] Leandro Cieri et al. "Higgs boson production at the LHC using the q_T subtraction formalism at N^{3}LO QCD". In: *JHEP* 02 (2019), p. 096. DOI: 10.1007/JHEP02(2019)096. arXiv: 1807.11501 [hep-ph].

[160] Daniel de Florian and Massimiliano Grazzini. "The Structure of large logarithmic corrections at small transverse momentum in hadronic collisions". In: *Nucl. Phys. B* 616 (2001), pp. 247–285. DOI: 10.1016/S0550-3213(01)00460-6. arXiv: hep-ph/0108273.

[161] Thomas Becher and Matthias Neubert. "Factorization and NNLL Resummation for Higgs Production with a Jet Veto". In: *JHEP* 07 (2012), p. 108. DOI: 10.1007/JHEP07(2012)108. arXiv: 1205.3806 [hep-ph].

[162] Wojciech Bizon et al. "Momentum-space resummation for transverse observables and the Higgs $p_\perp$ at N^{3}LL+NNLO". In: *JHEP* 02 (2018), p. 108. DOI: 10.1007/JHEP02(2018)108. arXiv: 1705.09127 [hep-ph].

[163] Stefano Catani. "The Singular behavior of QCD amplitudes at two loop order". In: *Phys. Lett. B* 427 (1998), pp. 161–171. DOI: 10.1016/S0370-2693(98)00332-3. arXiv: hep-ph/9802439.

[164] Stefano Catani et al. "Diphoton production at hadron colliders: a fully-differential QCD calculation at NNLO". In: *Phys. Rev. Lett.* 108 (2012). [Erratum: Phys.Rev.Lett. 117, 089901 (2016)], p. 072001. DOI: 10.1103/PhysRevLett.108.072001. arXiv: 1110.2375 [hep-ph].

[165] Georges Aad et al. "Measurement of the production cross section of pairs of isolated photons in *pp* collisions at 13 TeV with the ATLAS detector". In: *JHEP* 11 (2021), p. 169. DOI: 10.1007/JHEP11(2021)169. arXiv: 2107.09330 [hep-ex].

[166] Morad Aaboud et al. "Measurements of integrated and differential cross sections for isolated photon pair production in *pp* collisions at $\sqrt{s} = 8$ TeV with the ATLAS detector". In: *Phys. Rev. D* 95.11 (2017), p. 112005. DOI: 10.1103/PhysRevD.95.112005. arXiv: 1704.03839 [hep-ex].

[167] Serguei Chatrchyan et al. "Measurement of differential cross sections for the production of a pair of isolated photons in pp collisions at $\sqrt{s} = 7$ TeV". In: *Eur. Phys. J. C* 74.11 (2014), p. 3129. DOI: 10.1140/epjc/s10052-014-3129-3. arXiv: 1405.7225 [hep-ex].

[168] Georges Aad et al. "Measurement of isolated-photon pair production in *pp* collisions at $\sqrt{s} = 7$ TeV with the ATLAS detector". In: *JHEP* 01 (2013), p. 086. DOI: 10.1007/JHEP01(2013)086. arXiv: 1211.1913 [hep-ex].

[169] Georges Aad et al. "Measurements of the Higgs boson inclusive and differential fiducial cross-sections in the diphoton decay channel with pp collisions at $\sqrt{s} = 13$ TeV with the ATLAS detector". In: *JHEP* 08 (2022), p. 027. DOI: 10.1007/JHEP08(2022)027. arXiv: 2202.00487 [hep-ex].

[170] Armen Tumasyan et al. "Measurement of the Higgs boson inclusive and differential fiducial production cross sections in the diphoton decay channel with pp collisions at $\sqrt{s} = 13$ TeV". In: *JHEP* 07 (2023), p. 091. DOI: 10.1007/JHEP07(2023)091. arXiv: 2208.12279 [hep-ex].

[171] Albert M Sirunyan et al. "Measurements of Higgs boson production cross sections and couplings in the diphoton decay channel at $\sqrt{\mathrm{s}} = 13$ TeV". In: *JHEP* 07 (2021), p. 027. DOI: 10.1007/JHEP07(2021)027. arXiv: 2103.06956 [hep-ex].

[172] Albert M Sirunyan et al. "A measurement of the Higgs boson mass in the diphoton decay channel". In: *Phys. Lett. B* 805 (2020), p. 135425. DOI: 10.1016/j.physletb.2020.135425. arXiv: 2002.06398 [hep-ex].

[173] Morad Aaboud et al. "Measurements of Higgs boson properties in the diphoton decay channel with 36 fb^{-1} of pp collision data at $\sqrt{s} = 13$ TeV with the ATLAS detector". In: *Phys. Rev. D* 98 (2018), p. 052005. DOI: 10.1103/PhysRevD.98.052005. arXiv: 1802.04146 [hep-ex].

[174] Vardan Khachatryan et al. "Observation of the Diphoton Decay of the Higgs Boson and Measurement of Its Properties". In: *Eur. Phys. J. C* 74.10 (2014), p. 3076. DOI: 10.1140/epjc/s10052-014-3076-z. arXiv: 1407.0558 [hep-ex].

[175] Georges Aad et al. "Measurement of Higgs boson production in the diphoton decay channel in pp collisions at center-of-mass energies of 7 and 8 TeV with the ATLAS detector". In: *Phys. Rev. D* 90.11 (2014), p. 112015. DOI: 10.1103/PhysRevD.90.112015. arXiv: 1408.7084 [hep-ex].

[176] Georges Aad et al. "Measurements of fiducial and differential cross sections for Higgs boson production in the diphoton decay channel at $\sqrt{s} = 8$ TeV with ATLAS". In: *JHEP* 09 (2014), p. 112. DOI: 10.1007/JHEP09(2014)112. arXiv: 1407.4222 [hep-ex].

[177] Georges Aad et al. "Search for periodic signals in the dielectron and diphoton invariant mass spectra using 139 fb^1 of pp collisions at $\sqrt{s} = 13$ TeV with the ATLAS detector". In: *JHEP* 10 (2023), p. 079. DOI: 10.1007/JHEP10(2023)079. arXiv: 2305.10894 [hep-ex].

[178] Georges Aad et al. "Search in diphoton and dielectron final states for displaced production of Higgs or Z bosons with the ATLAS detector in s=13 TeV pp collisions". In: *Phys. Rev. D* 108.1 (2023), p. 012012. DOI: 10.1103/PhysRevD.108.012012. arXiv: 2304.12885 [hep-ex].

[179] Georges Aad et al. "Search for boosted diphoton resonances in the 10 to 70 GeV mass range using 138 fb^1 of 13 TeV pp collisions with the ATLAS detector". In: *JHEP* 07 (2023), p. 155. DOI: 10.1007/JHEP07(2023)155. arXiv: 2211.04172 [hep-ex].

[180] Albert M Sirunyan et al. "Search for supersymmetry using Higgs boson to diphoton decays at $\sqrt{s} = 13$ TeV". In: *JHEP* 11 (2019), p. 109. DOI: 10.1007/JHEP11(2019)109. arXiv: 1908.08500 [hep-ex].

[181] Vardan Khachatryan et al. "Search for high-mass diphoton resonances in proton–proton collisions at 13 TeV and combination with 8 TeV search". In: *Phys. Lett. B* 767 (2017), pp. 147–170. DOI: 10.1016/j.physletb.2017.01.027. arXiv: 1609.02507 [hep-ex].

[182] Morad Aaboud et al. "Search for new phenomena in high-mass diphoton final states using 37 fb^{-1} of proton–proton collisions collected at $\sqrt{s} = 13$ TeV with the ATLAS detector". In: *Phys. Lett. B* 775 (2017), pp. 105–125. DOI: 10.1016/j.physletb.2017.10.039. arXiv: 1707.04147 [hep-ex].

[183] John M. Campbell et al. "Predictions for diphoton production at the LHC through NNLO in QCD". In: *JHEP* 07 (2016), p. 148. DOI: 10.1007/JHEP07(2016)148. arXiv: 1603.02663 [hep-ph].

[184] Stefano Catani et al. "Diphoton production at the LHC: a QCD study up to NNLO". In: *JHEP* 04 (2018), p. 142. DOI: 10.1007/JHEP04(2018)142. arXiv: 1802.02095 [hep-ph].

[185] Robin Schuermann et al. "NNLO Photon Production with Realistic Photon Isolation". In: *PoS* LL2022 (2022), p. 034. DOI: 10.22323/1.416.0034. arXiv: 2208.02669 [hep-ph].

[186] Z. Bern, A. De Freitas, and Lance J. Dixon. "Two loop amplitudes for gluon fusion into two photons". In: *JHEP* 09 (2001), p. 037. DOI: 10.1088/1126-6708/2001/09/037. arXiv: hep-ph/0109078.

[187] Fabrizio Caola et al. "Three-loop helicity amplitudes for quark-gluon scattering in QCD". In: *JHEP* 12 (2022), p. 082. DOI: 10.1007/JHEP12(2022)082. arXiv: 2207.03503 [hep-ph].

[188] Herschel A. Chawdhry et al. "Two-loop leading-color helicity amplitudes for three-photon production at the LHC". In: *JHEP* 06 (2021), p. 150. DOI: 10.1007/JHEP06(2021)150. arXiv: 2012.13553 [hep-ph].

[189] Bakul Agarwal et al. "Two-loop leading colour QCD corrections to $q\bar{q} \to \gamma\gamma g$ and $qg \to \gamma\gamma q$". In: *JHEP* 04 (2021), p. 201. DOI: 10.1007/JHEP04(2021)201. arXiv: 2102.01820 [hep-ph].

[190] Herschel A. Chawdhry et al. "Two-loop leading-colour QCD helicity amplitudes for two-photon plus jet production at the LHC". In: *JHEP* 07 (2021), p. 164. DOI: 10.1007/JHEP07(2021)164. arXiv: 2103.04319 [hep-ph].

[191] Bakul Agarwal et al. "Two-Loop Helicity Amplitudes for Diphoton Plus Jet Production in Full Color". In: *Phys. Rev. Lett.* 127.26 (2021), p. 262001. DOI: 10.1103/PhysRevLett.127.262001. arXiv: 2105.04585 [hep-ph].

[192] Herschel A. Chawdhry et al. "NNLO QCD corrections to diphoton production with an additional jet at the LHC". In: *JHEP* 09 (2021), p. 093. DOI: 10.1007/JHEP09(2021)093. arXiv: 2105.06940 [hep-ph].

[193] Mauro Chiesa et al. "Electroweak corrections to diphoton plus jets". In: *JHEP* 10 (2017), p. 181. DOI: 10.1007/JHEP10(2017)181. arXiv: 1706.09022 [hep-ph].

[194] Leandro Cieri and German Sborlini. "Exploring QED Effects to Diphoton Production at Hadron Colliders". In: *Symmetry* 13.6 (2021), p. 994. DOI: 10.3390/sym13060994.

[195] T. Binoth et al. "A Full next-to-leading order study of direct photon pair production in hadronic collisions". In: *Eur. Phys. J. C* 16 (2000), pp. 311–330. DOI: 10.1007/s100520050024. arXiv: hep-ph/9911340.

[196] C. Balazs et al. "Calculation of prompt diphoton production cross-sections at Tevatron and LHC energies". In: *Phys. Rev. D* 76 (2007), p. 013009. DOI: 10.1103/PhysRevD.76.013009. arXiv: 0704.0001 [hep-ph].

[197] Duane A. Dicus and Scott S. D. Willenbrock. "Photon Pair Production and the Intermediate Mass Higgs Boson". In: *Phys. Rev. D* 37 (1988), p. 1801. DOI: 10.1103/PhysRevD.37.1801.

[198] Zvi Bern, Lance J. Dixon, and Carl Schmidt. "Isolating a light Higgs boson from the diphoton background at the CERN LHC". In: *Phys. Rev. D* 66 (2002), p. 074018. DOI: 10.1103/PhysRevD.66.074018. arXiv: hep-ph/0206194.

[199] John M. Campbell, R. Keith Ellis, and Ciaran Williams. "Vector Boson Pair Production at the LHC". In: *JHEP* 07 (2011), p. 018. DOI: 10.1007/JHEP07(2011)018. arXiv: 1105.0020 [hep-ph].

[200] Leandro Cieri, Francesco Coradeschi, and Daniel de Florian. "Diphoton production at hadron colliders: transverse-momentum resummation at next-to-next-to-leading logarithmic accuracy". In: *JHEP* 06 (2015), p. 185. DOI: 10.1007/JHEP06(2015)185. arXiv: 1505.03162 [hep-ph].

[201] Thomas Becher and Tobias Neumann. "Fiducial q_T resummation of color-singlet processes at N^{3}LL+NNLO". In: *JHEP* 03 (2021), p. 199. DOI: 10.1007/JHEP03(2021)199. arXiv: 2009.11437 [hep-ph].

[202] Shashikant R. Dugad et al. "The top threshold effect in the $\gamma\gamma$ production at the LHC". In: *Eur. Phys. J. C* 78.9 (2018), p. 715. DOI: 10.1140/epjc/s10052-018-6188-z. arXiv: 1605.07360 [hep-ph].

[203] Sayaka Kawabata and Hiroshi Yokoya. "Top-quark mass from the diphoton mass spectrum". In: *Eur. Phys. J. C* 77.5 (2017), p. 323. DOI: 10.1140/epjc/s10052-017-4884-8. arXiv: 1607.00990 [hep-ph].

[204] Fabio Maltoni, Manoj K. Mandal, and Xiaoran Zhao. "Top-quark effects in diphoton production through gluon fusion at next-to-leading order in QCD". In: *Phys. Rev. D* 100.7 (2019), p. 071501. DOI: 10.1103/PhysRevD.100.071501. arXiv: 1812.08703 [hep-ph].

[205] Long Chen et al. "Photon pair production in gluon fusion: Top quark effects at NLO with threshold matching". In: *JHEP* 04 (2020), p. 115. DOI: 10.1007/JHEP04(2020)115. arXiv: 1911.09314 [hep-ph].

[206] Fabrizio Caola, Andreas Von Manteuffel, and Lorenzo Tancredi. "Diphoton Amplitudes in Three-Loop Quantum Chromodynamics". In: *Phys. Rev. Lett.* 126.11 (2021), p. 112004. DOI: 10.1103/PhysRevLett.126.112004. arXiv: 2011.13946 [hep-ph].

[207] Paulo Nogueira. "Automatic Feynman Graph Generation". In: *J. Comput. Phys.* 105 (1993), pp. 279–289. DOI: 10.1006/jcph.1993.1074.

[208] Matteo Becchetti and Roberto Bonciani. "Two-Loop Master Integrals for the Planar QCD Massive Corrections to Di-photon and Di-jet Hadro-production". In: *JHEP* 01 (2018), p. 048. DOI: 10.1007/JHEP01(2018)048. arXiv: 1712.02537 [hep-ph].

[209] E. W. Nigel Glover, C. Oleari, and M. E. Tejeda-Yeomans. "Two loop QCD corrections to gluon-gluon scattering". In: *Nucl. Phys. B* 605 (2001), pp. 467–485. DOI: 10.1016/S0550-3213(01)00210-3. arXiv: hep-ph/0102201.

[210] Andreas von Manteuffel and Lorenzo Tancredi. "A non-planar two-loop three-point function beyond multiple polylogarithms". In: *JHEP* 06 (2017), p. 127. DOI: 10.1007/JHEP06(2017)127. arXiv: 1701.05905 [hep-ph].

[211] Xiao Liu and Yan-Qing Ma. "AMFlow: A Mathematica package for Feynman integrals computation via auxiliary mass flow". In: *Comput. Phys. Commun.* 283 (2023), p. 108565. DOI: 10.1016/j.cpc.2022.108565. arXiv: 2201.11669 [hep-ph].

[212] Sergei N. Bernstein. "Sur l'ordre de la meilleure approximation des fonctions continues par des polynômes de degré donné". French. In: *Mémoires de l'Académie Royale de Belgique* 4 (1912). Prize Memoir, pp. 1–103.

[213] Isaac J. Schoenberg. "Contributions to the problem of approximation of equidistant data by analytic functions". In: *Quarterly of Applied Mathematics* 4.2 (1946), pp. 45–99.

[214] Carl de Boor. *A Practical Guide to Splines*. Springer-Verlag, 1978.

[215] Michael J.D. Powell. *Approximation Theory and Methods*. Cambridge University Press, 1981.

[216] Carl Runge. "Über empirische Funktionen und die Interpolation zwischen äquidistanten Ordinaten". German. In: *Zeitschrift für Mathematik und Physik* 46 (1901), pp. 224–243.

[217] John Backus et al. "The FORTRAN automatic coding system". In: *Proceedings of the Western Joint Computer Conference*. 1957, pp. 188–198.

[218] Taushif Ahmed et al. "Two-loop non-planar four-point topology with massive internal loop". In: *JHEP* 05 (2024), p. 064. DOI: 10.1007/JHEP05(2024)064. arXiv: 2402.07311 [hep-th].

[219] Stefan Weinzierl. "Modular transformations of elliptic Feynman integrals". In: *Nucl. Phys. B* 964 (2021), p. 115309. DOI: 10.1016/j.nuclphysb.2021.115309. arXiv: 2011.07311 [hep-th].

[220] Thomas Gehrmann et al. "Scale and isolation sensitivity of diphoton distributions at the LHC". In: *JHEP* 01 (2021), p. 108. DOI: 10.1007/JHEP01(2021)108. arXiv: 2009.11310 [hep-ph].

[221] Stefano Frixione. "Isolated photons in perturbative QCD". In: *Phys. Lett. B* 429 (1998), pp. 369–374. DOI: 10.1016/S0370-2693(98)00454-7. arXiv: hep-ph/9801442.

[222] Stefano Frixione and Werner Vogelsang. "Isolated photon production in polarized *pp* collisions". In: *Nucl. Phys. B* 568 (2000), pp. 60–92. DOI: 10.1016/S0550-3213(99)00575-1. arXiv: hep-ph/9908387.

[223] Richard D. Ball et al. "Parton distributions from high-precision collider data". In: *Eur. Phys. J. C* 77.10 (2017), p. 663. DOI: 10.1140/epjc/s10052-017-5199-5. arXiv: 1706.00428 [hep-ph].

[224] Andy Buckley et al. "LHAPDF6: parton density access in the LHC precision era". In: *Eur. Phys. J. C* 75 (2015), p. 132. DOI: 10.1140/epjc/s10052-015-3318-8. arXiv: 1412.7420 [hep-ph].

[225] Massimiliano Grazzini, Stefan Kallweit, and Marius Wiesemann. "Fully differential NNLO computations with MATRIX". In: *Eur. Phys. J. C* 78.7 (2018), p. 537. DOI: 10.1140/epjc/s10052-018-5771-7. arXiv: 1711.06631 [hep-ph].

[226] Stefano Camarda et al. "DYTurbo: Fast predictions for Drell-Yan processes". In: *Eur. Phys. J. C* 80.3 (2020). [Erratum: Eur.Phys.J.C 80, 440 (2020)], p. 251. DOI: 10.1140/epjc/s10052-020-7757-5. arXiv: 1910.07049 [hep-ph].

[227] Stefano Camarda, Leandro Cieri, and Giancarlo Ferrera. "Drell–Yan lepton-pair production: qT resummation at N3LL accuracy and fiducial cross sections at N3LO". In: *Phys. Rev. D* 104.11 (2021), p. L111503. DOI: 10.1103/PhysRevD.104.L111503. arXiv: 2103.04974 [hep-ph].

[228] David Bachman. *A Geometric Approach to Differential Forms*. 2012. arXiv: math/0306194 [math.GT]. URL: https://arxiv.org/abs/math/0306194.

[229] John M. Lee. *Introduction to Smooth Manifolds*. 2nd ed. Vol. 218. Graduate Texts in Mathematics. New York, NY: Springer, 2013. ISBN: 978-1461386156. DOI: 10.1007/978-1-4614-8476-2.

[230] Manfredo Perdigão do Carmo. *Differential Geometry of Curves and Surfaces*. Englewood Cliffs, NJ: Prentice-Hall, 1976. ISBN: 978-0132125895.

[231] Thomas Hahn. "Generating Feynman diagrams and amplitudes with FeynArts 3". In: *Comput. Phys. Commun.* 140 (2001), pp. 418–431. DOI: 10.1016/S0010-4655(01)00290-9. arXiv: hep-ph/0012260.